Joint Doctoral Thesis
by
Claudia Scatigno

AN INNOVATIVE MULTIDISCIPLINARY METHODOLOGY TO EVALUATE THE CONSERVATION STATE OF CULTURAL SITES AS A WHOLE: "CASA DI DIANA" (OSTIA ANTICA, ITALY)

Supervisors:
Dr. Maria Preite-Martinez
Ph.D. Nagore Prieto-Taboada

SAPIENZA
UNIVERSITÀ DI ROMA

Universidad del País Vasco
Euskal Herriko Unibertsitatea

Rome (Italy), February 2017

University of Rome "La Sapienza"

Department of Earth Sciences
Doctoral Programme in Earth Sciences
Curriculum in Environment and Cultural Heritage

University the Basque Country (UPV/EHU)

IBeA -Environmental Analytical Chemistry
Doctoral Programme in Scientific Cross-Disciplinary Approaches to Heritage and Landscape (SCAHL)

Joint Doctoral Thesis

AN INNOVATIVE MULTIDISCIPLINARY METHODOLOGY TO EVALUATE THE CONSERVATION STATE OF CULTURAL SITES AS A WHOLE: "CASA DI DIANA" (OSTIA ANTICA, ITALY)

Supervisors:
Dr. Maria Preite Martinez
Ph.D. Nagore Prieto-Taboada

TABLE OF CONTENTS

«Science is a way of life. Science is a perspective. Science is the process that takes us from confusion to understanding in a manner that's precise, predictive and reliable - a transformation, for those lucky enough to experience it, that is empowering and emotional»

Brian Greene

ACKNOWLEDGEMENTS

The author of this joint doctoral thesis is grateful to:

- University of Rome "La Sapienza", DST for her doctoral fellowship;
- University of Rome "La Sapienza" for the grants obtained for her study sojourns by LLP/EP (Lifelong Learning Programme/Erasmus Placement, academic year 2013-2014) and Erasmus+ (Student Mobility for Traineeship, academic year 2014-2015 and academic year 2015-2016);
- University of the Basque Country (UPV/EHU) for the grant for study sojourns by trainee researchers (six months) from foreign universities engaged in a jointly supervised doctoral thesis.

She also is also grateful for having had the possibility to work in the Ostia Antica archaeological area, during the past three years, in particular to the director Dr. Cinzia Morelli, all of her security company and the technical staff.

She would like to give a special thanks to the people that provided her with valuable support during these three years.

Special thanks go to Maria and Nagore, the supervisors, for believing in her and for their support in this work. In particular, to Nagore for her suggestions and her full dedication. Thanks to her, the author has learned a lot.

To Pr. Juan Manuel Madariaga, for giving the possibility of this jointly supervised doctoral thesis. From the first moment, he believed in her.

Special thanks go to Pr. Ettore Cardarelli, for his professional support during geophysics surveys, for starting this collaboration. The author is grateful to him for the time dedicated to her, for never saying "no", for working tirelessly. Above all, for his time spent teaching geophysics, a new science for the author. Surely, she has gotten to know a real professor but most of all, has acquired a friend.

To Sonia Ravera (Dep. of Di. B. T., University of Molise) for her contribution in the recognition of the biological species and Maria Teresa Lepone (Dep. of Physics, University of Rome "La Sapienza") for her suggestions regarding the lighting results. Both friends, they helped without any complaint.

To Aida Conte for her support in the petrographic-mineralogical study and the coffee breaks.

To Gianni Andreozzi, for his suggestions during these three years, and his diplomacy. He is a special director for this doctoral programme.

Franco Mazzei (Dep. of Chemistry and Drug Technologies, University of Rome "La Sapienza") for his economic effort in buying the CO and CO_2 sensors.

All the technical and human support provided by SGIker (UPV/EHU, MICINN, GV/EJ, ERDF and ESF) and by DST (University of Rome "La Sapienza") is also gratefully acknowledged.

The deepest thanks goes to Claudia Moricca, for the English revisions. Thank you so much, darling!

The author wishes to thank Pr. Fernando J. García-Diego (Dep. of Applied Physics, UPV), for humbly transmitting her his knowledge in the sensors' technology.

From here onward, the author wants to say "thank you" to her Spanish friends, in their language. A mis compañeros de Zamudio, por su calidez y compañerismo. Quisiera dar las gracias porque hicieron que mi larga estancia fuera lo menos pesada posible, pora considerarme una de ellos, come si fuera de la familia. Fue una experiencia increíble y he conocido personas muy especiales. En particular a Cristina, mi mejor amiga, a su ama por el Marmitako! Tambien a Hector, Iker, Maite, Leticia, Julene y Olivia, gracias a todos! A mis compañeros de Valencia. En particular quiero agradecer a Eliseo por su apoyo en la simulacion del aire.

She would like to give a special thanks to Sara and Rezarta, her friends.

Finally, the author has a great debt of gratitude towards her grandparents (who have passed away during the last two years) and in particular, her grandmother Enza, an extraordinary woman, very determined and resolute and her grandfather Antonio that used to say«*…sta come torre ferma, che non crolla già mai la cima per soffiar di venti*». She also would like to give a special thanks to her parents (the people who know her best) and her sister (and her wonderful sons), for their unconditional love and support. In particular, the author would like to express, in her own mother tongue, her personal gratitude:
Il mio grazie più intimo e profondo va a mio marito Claudio, per avere appoggiato e rispettato, senza mai esitare, il mio lavoro, pur sacrificando il nostro neo rapporto coniugale, vivendo in lontananza per lunghi mesi. Tu, rappresenti la prova più reale e viva che l'amore è indissolubile, guidato dalla Grazia del Signore. Ti amo.

SUMMARY

Archaeological sites, perceived as open museums, are particularly complicated to study because of the extensive number of environmental stressors affecting their conservation state. Diagnostic methodologies can easily omit some of them, causing irreparable and inestimable damages to these sites.

In this sense, multidisciplinary studies seem to constitute the most suitable approach to understand the decaying processes that occur. Up until now, these types of studies have been applied within local programmes, leading to loss of strategic output, risk of duplication and reduction in the international competitiveness of the research.

Therefore, in this Joint Doctoral Thesis, a new protocol for the preservation and accessibility of the archaeological sites, based on the synergic combination of physical, geological and analytical chemistry methodologies, is presented, in order to understand the sites as a whole. The project was born in 2012 within a multidisciplinary study on Ostia Antica *Mithraea*, as the result of my master degree. Successively, thanks to an international cooperation (Italy-Spain) and institutional effort (National and International Research centers and Departments) it was possible to combine different disciplines developing a new analytical approach. The final aim of this approach was assess the **conservation state** of the building under study, pointing out the areas most at risk, resolving important issues emerged during the investigation, and identifying the origin of the decay, suggesting also possible repair tools.

The diagnostic protocol consists in a dynamic model, developed as a pyramid that includes three steps or levels that can be summarised into **anamnesis** (the state of art, the macroscopic observation on both environment and materials), **analysis** (the development of a protocol that includes the investigation actions that lead to the identification of damage's sources) and a **conservation step** (the real state of conservation of the site under study). This last action also considers some suggestions for a future and global conservation and lays the "ad-hoc designing" to create a whole conservation plan. The final goal is the conservation, **safeguard and "usability" of open museums or cultural sites in general**, thanks to the protocol flexibility, organised in steps procedures. The base of the pyramid is built on an initial hypothesis based on the "content and container" axiom, the relationship between the environment and the materials.

In order to validate the proposed diagnostic protocol, the model has been implemented in a complex building, the "Casa di Diana" *Mithraeum*, a Roman masonry dated 130 CE, found in Ostia Antica (Italy), the port of the old city of

Rome, obtaining a well-developed pyramid. The rising damp represents the key between all the actions successively developed, both geophysical and chemical surveys, and is the result of a synergic interaction.

Thanks to the well-planned multi-analytical procedure, the results obtained point out towards the rising damp and acids gases as the main environmental stressors. It was possible to associate the rising damp to the presence of freshwater at shallow depth, which causes the preliminary hydration phase on bricks, and the attack of the wall-building materials by the atmospheric acid gases through dry deposition mechanism. Furthermore, the results obtained by non-destructive spectroscopic analyses have led to the hypothesis that the observed yellow bricks could date back to a different historic period, for instance Byzantine, which corresponds to the last period of utilization of this house, while the red bricks derive from the Roman period.

In addition to the new protocol, each methodology is characterised by several **novelty keys**, obtaining in this sense, 12 research articles published/reviewed on important international journals.

Some processes of this multidisciplinary study involve an important economic effort, but the present method allows making an objective decision, through a **solid analytical protocol**, which has an important value in the management of Cultural Heritage.

SOMMARIO

I siti archeologici, definiti come musei aperti, sono particolarmente complicati da studiare a causa dell'ampio numero di fattori di stress ambientali che influenzano la loro conservazione. Le metodologie diagnostiche possono facilmente non prendere in considerazione alcuni di questi fattori, causando così irreparabili e inestimabili danni a questo tipo di siti.

Gli studi multidisciplinari sembrano rappresentare l'approccio più adeguato per capire il meccanismo dei processi di degrado. Fino ad ora, però, tale approccio è stato applicato solo con programmi a livello locale, comportando così la perdita di azioni a livello strategico, il rischio di duplicazione e la riduzione della competitività della ricerca internazionale.

Pertanto, in questa Tesi di Dottorato in co-tutela, si presenta un nuovo protocollo per la conservazione e la fruizione dei siti archeologici, basato sulla combinazione sinergica delle metodologie fisiche, geologiche e chimiche, al fine di comprendere i musei aperti nella loro interezza. Il progetto nasce nel 2012, con uno studio multidisciplinare sui Mitrei di Ostia Antica, durante la mia tesi magistrale. Successivamente, grazie alla cooperazione internazionale (Italia-Spagna) e all'impegno di istituzioni (Centri di ricerca e Dipartimenti nazionali e internazionali), è stato possibile combinare differenti discipline, sviluppando un nuovo protocollo analitico. L'obiettivo è quello di valutare lo stato di conservazione dell'edificio in studio, individuando le aree a maggior rischio, risolvendo importanti questioni emerse durante la ricerca, e identificando l'origine del degrado, suggerendo anche possibili interventi conservativi.

Il protocollo diagnostico consiste in un modello dinamico piramidale, sviluppato su tre tappe o livelli, che si possono riassumere in **anamnesi** (lo stato dell'arte, l'osservazione macroscopica sia dell'ambiente che dei materiali), **analisi** (lo sviluppo stesso del protocollo che include tutte le azioni investigative che conducono all'identificazione delle sorgenti del degrado) e **conservazione** (l'attuale stato di conservazione del sito oggetto di studio). Quest'ultima, considera anche dei suggerimenti conservativi per la salvaguardia del sito, grazie alla creazione di un "piano ad hoc", gettando le basi per una futura e globale azione di tutela. L'obiettivo finale è la conservazione, la **salvaguardia e la fruibilità dei musei aperti o siti culturali in generale**, grazie alla flessibilità del protocollo, organizzato per livelli. La base della piramide è costruita su un'ipotesi iniziale basata sull'assioma "contenuto e contenitore", la relazione tra ambiente e materiali.

Al fine di validare tale protocollo, il modello è stato applicato ad una complessa struttura, il Mitreo della "Casa di Diana", una casa romana del 130 d.C. che si trova nell'area archeologica di Ostia Antica (Italia), l'antico porto della città di Roma, ottenendo una piramide completa e ben sviluppata. L'umidità di risalita capillare rappresenta la chiave dello sviluppo e del collegamento delle azioni successive, analisi geofisiche e chimiche, come risultato dell'interazione sinergica.

Grazie alla procedura analitica multidisciplinare ben sviluppata, i risultati ottenuti dimostrano come l'umidità di risalita e i gas acidi siano i principali fattori del degrado. È stato possibile inoltre associare l'umidità di risalita alla presenza di un acquifero presente a basse profondità che causa una preliminare azione d'idratazione dei mattoni e il successivo attacco dei gas acidi sulle mura dell'edificio attraverso il meccanismo di deposizione secca. Inoltre i resultati ottenuti dalle analisi spettroscopiche non distruttive hanno condotto all'ipotesi che i mattoni gialli potrebbero essere di un periodo storico differente, ad esempio Bizantino, che corrisponde all'ultimo periodo di utilizzazione della casa, mentre i rossi sono di derivazione Romana.

Oltre al protocollo in sé, ciascuna metodologia è caratterizzata da diverse **innovazioni**, che hanno portato alla stesura di 12 articoli scientifici pubblicati/in revisione su importanti riviste internazionali.

Alcune metodologie di questo studio multidisciplinare implicano un importante impegno economico, però si tratta di un metodo globale che permette di effettuare una decisione oggettiva, attraverso il **solido protocollo analitico**, azione importante nella gestione dei Beni Culturali.

RESUMEN

Los sitios arqueológicos, también definibles como museos abiertos, son particularmente complicados de estudiar debido a los numerosos estresores ambientales que condicionan su estado de conservación. Las metodologías de diagnóstico fácilmente pueden no tener en cuenta alguno de ellos, causando un daño irreparable y inestimable.

En este sentido, los estudios multidisciplinares parecen ser el enfoque más adecuado para entender los mecanismos de los procesos de deterioro. Sin embargo, hasta ahora, este tipo de estudios se han aplicado a nivel local, lo que conlleva un error estratégico, riesgo de duplicación y, por tanto, una reducción de la competitividad de la investigación internacional.

Por lo tanto, en esta Tesis Doctoral en cotutela, se presenta un nuevo protocolo para la preservación y accesibilidad de los sitios arqueológicos en base a la combinación sinérgica de metodologías físicas, geológicas y químicas, con el fin de entender los sitios arqueológicos como un todo. El proyecto nace en el 2012 con un estudio multidisciplinar sobre los Mitreos de Ostia Antica durante mi tesis de grado. Después, gracias a la cooperación internacional (Italia-España) y a el esfuerzo de la organización (Centros de investigación y departamentos nacionales y internacionales), fue posible combinar diferentes disciplinas y desarollar un nuevo enfoque analítico con el objetivo de evaluar el **estado de conservación** del edificio bajo estudio, señalando las zonas de mayor riesgo, resolviendo las cuestiones más importantes que emergieron durante la investigación, e identificando el origen de los deterioros, indicando también, posibles acciones reparadoras.

El protocolo diagnóstico consiste en un modelo dinámico, desarrollado como una pirámide que incluye tres etapas o niveles que se pueden resumir en la **anamnesis** (el estado del arte, la observación macroscópica tanto en el medio ambiente como en los materiales), el **análisis** (el desarrollo de un protocolo que incluye las acciones de investigación que conducen a la identificación de las fuentes de el daño) y la etapa de **conservación** (el estado real de conservación del sitio en estudio). Esta última acción, también considera, al menos parcialmente, un esbozo final de un plan de conservación y sentar las bases de un "diseño ad-hoc" para poder crear un plan de acción de conservación global. El objetivo final es la conservación, salvaguardar el sitio y aumentar la usabilidad de los museos abiertos o lugares culturales en general, gracias a un protocolo flexible, organizado por etapas. La base de la pirámide se apoya en la hipótesis inicial, el axioma del "contenido y contenedor", la relación entre el medio ambiente y los materiales.

Con el fin de validar este protocolo de diagnostico, el modelo ha sido desarrollado en un edificio complejo, el Mitreo de la "Casa di Diana", una casa Romana del 130 d.C., que se encuentra en el sitio de Ostia Antica (Italia), el puerto de la antigua ciudad de Roma, consiguiendo completar una pirámide totalmente desarrollada. La humedad ascendente representa la clave de unión entre todas las acciones que se desarrollan sucesivamente, tanto los estudios geofísicos y los químicos, resultado tener una interacción sinérgica.

Gracias al procedimiento analítico multidisciplinar bien planteado, los resultados obtenidos ponen de manifiesto como la humedad ascendente y los gases ácidos atmosféricos son los principales estresores ambientales que afectan al sitio. Fue posible asociar la humedad ascendente a la presencia de agua dulce que se encuentra a poca profundidad bajo la casa, que actúa en una fase inicial hidratando los ladrillos y favoreciendo el ataque posterior, mediante deposición seca, de los gases ácidos atmosféricos. Además, los resultados obtenidos mediante técnicas espectroscópicas no destructivas han llevado a la hipótesis de que los ladrillos de color amarillo podrían corresponder a un período histórico diferente, por ejemplo bizantino, que corresponde a la última etapa de utilización de esta casa, mientras que los ladrillos rojos derivan de la época romana.

Además del nuevo protocolo piramidal, cada metodología desarrollada presenta una **innovación** determinada, lo que ha favorecido que la presente tesis doctoral haya dado lugar a 12 artículos publicados/en revisión en importantes revistas internacionales.

Algunas metodologías de este estudio multidisciplinar implican un importante esfuerzo económico, pero el presente método global permite tomar una decisión objetiva sobre el estado de conservación de un sitio arqueológico, a través de un protocolo de análisis sólido, lo cual tiene un valor importante en una gestión del Patrimonio Cultural.

PROJECTS

The following projects, short-term scientific mission and accompanying action financially supported this Joint PhD work:

- ✓ *In-situ* inspections (Ostia Antica), international conference and scientific missions have been partially financially supported by fund of Department of Earth Science (University of Rome "La Sapienza"), Doctoral programme (academic year 2013-2016).
- ✓ The geophysical campaigns have been financially supported by the Ateneo Grant 2015 - University of Rome "La Sapienza".
- ✓ Laboratory activity performed in the University of the Basque Country (UPV/EHU) has been partially financially supported by the project DISILICA-1930 (ref. BIA2014-59124-P) funded by the Spanish Ministry of Economy and Competitiveness (MINECO) and the European Regional Development Fund (FEDER).
- ✓ The CFD study and the continuous monitoring by thermo-hygrometric probes have been partially financially supported by the projects HAR2013-47895-C2-1-P and HAR2013-47895-C2-2-P from Spanish Ministry of Economy and Competitiveness (MINECO).

Chapter 1 Introduction

Europe has a particularly rich and diversified Cultural Heritage, including buildings, monuments and objects of all sizes, characterised by a great variety of materials. Their conservation and safeguard represents an important economic effort but culturally, a fundamental need in its own right.

In particular, the Built Heritage, which represent the history and culture of a location and its communities [1], collect a wide variety of historical architectures (i.e. masonries, churches, castles and fortifications). These last represent, thanks to its historical-artistic value, a unique and irreplaceable expression of the human traces, which as the rest of Cultural Heritage, merits to be conserved. In this sense, stony building materials are often considered as being the most resistant building material, however they can suffer the impact of different weathering processes that can transform their original composition [2], due to direct exposure to environmental stressors (than can be either repetitive or persistent). Thus, its conservation is extremely necessary.

A large number of ancient structures characterises Italy, including Roman and religious examples. Among them, **open museums** represent a consistent group. They are the object of this PhD work, as they are set in a complicated scenario due to the numerous conservative problems that they face and because their preventive conservation is particularly complex due to the particular environmental features.

Particular climatic conditions, such as high thermo-hygrometric values and rapid fluctuations, atmospheric pollution, wind, rain, frozen-thawed, etc. are some of the factors that contribute to the natural decay of these materials, involving damage morphologies caused by infiltration water (rain, floods, melted snow), colonisation of microorganisms, cracking phenomena (wind erosion, soil's movement, particular hydro-geological setting). These sources of damage are the results of the synergic interaction of several factors. Establishing the correlation of these factors is the key to set-up a proper conservation plan. Therefore, these open sites often require **adequate monitoring tools** combined with solid analytical methodologies in order to carry out appropriated **strategies for scheduling routine maintenance and designing suitable layouts for their preservation**.

1.1 Open museums

The definition of "open museum" includes all historical structures, monuments (such as ancient palaces, churches, masonries, open-air exhibitions, etc.) which are not located in closed environments (libraries, museum) and, therefore, directly exposed to outdoors. Cultural Heritage sites are the more common example. They

are the clear expression of places where time (historical time) has stopped, but they continue to live as a memory. They represent a borderline case, set between the historical buildings destined to new life, changing their use (as the major part of Italian ancient building) and the ruins, vestiges, or those places left to themselves.

These sites, on one hand, thanks to their accessibility highly encourage the visitors to explore them (also due to the huge spaces). In this sense, it is enhanced the usability of the Goods, improving the knowledge on ancient cultures and civilizations (without any interactive and multimedia tour as vastly applied in scientific museums). However, the vastness of these open museums may constitute a threat for the management activities and, most of all, which are dependent on the environmental stressors.

Indeed, archaeological sites (and Built Heritage in general) suffer the macroclimatic conditions more than any other type of Cultural Heritage. Furthermore, natural calamities and anthropogenic activities often impacted them. The former includes landslides, earthquakes, floods, adverse weather and abrupt climate changes. However, more serious and increasing threats could be caused by wars, overexploitation (direct consequence of the brutal human activities), as well as urbanization and uncontrolled tourism. Consequently, monitoring/characterisation and preventive diagnosis are essential for the safeguarding and conservation of Cultural Heritage sites.

In Italy, there are many archaeological evidences of Roman houses. The best-known examples are Pompeii, Herculaneum and Ostia Antica. This PhD work takes into consideration the latter, in particular the "Caseggiato di Diana", or "Casa di Diana" building.

1.2 The archaeological site of Ostia Antica and the "Casa di Diana" building

The ancient town of Ostia, founded near the ancient mouth of the Tiber (river harbour), played the role of port to supply the city of Rome and it was built during the second half of the 4th century BCE (developed towards the end of the Republican Age and during all of the Imperial Age). With the end of the Roman Empire, Ostia slowly fell into decay and it was finally abandoned in the 9th century due to repeated invasions and sackings by Arabic pirates, including the Battle of Ostia, a naval battle in 849 between Christians and Saracens. The remaining inhabitants moved to Gregoriopolis (4th and 5th century CE).

These 800 years reflected on the building constructions, which present a very articulate sequence, highlighting *opus caementicium* as the real protagonist of the technological renovation of the Roman age [3].

The geomorphology around Ostia Antica differs from the one present during Roman times, because of the numerous changes in the course of the Tiber River and the related fluvial deposits. The choice of this area for the first *castrum* was laid for commercial and political reasons, including the leadership of the lower valley of the Tiber River. In fact, this waterway represented the main communication channel from the coast inland and *viceversa*. Thus, since the 2nd century CE, the colony of Ostia Antica turned into an important trade center. In this period, the primordial fortified built-up was replaced by numerous shops (*tabernae* and *horreae*) used for sale and storage of the goods, respectively [4].

Sixteen *Mithraea* (only one of which is set in a *hypogeum*, the "Terme di Mitra" *Hypogeum* – **Fig. 1f**) have been found in the archaeological complex of Ostia Antica (**Fig. 1**). Very few structures, like the "Pareti Dipinte" *Mithraeum*, the "Menandro" *Mithraeum* or the "Sette sfere" *Mithraeum* (**Fig. 1a, b, c** respectively), were found in relatively good state of conservation thanks to the presence of protective structures built (roofs) in modern days. Most of the other, *Mithraea* are completely exposed to macroclimate (**Fig. 1d, e**).

The structures have various levels of protection in form of roofs, fences, and screens and, in recent times, a range of conservation treatments aimed at prolonging their life and improving legibility [5, 6].

Figure 1. Ostia Antica *Mithraea*. **a**) "Pareti dipinte" *Mithraeum*; **b**) "Menandro" *Mithraeum*; **c**) "Sette sfere" *Mithraeum*; **d**) "Presso la Porta Romana" *Mithraeum*; **e**) Terme di Mitra" *Hypogeum*.

However, until now, conservative actions (apart from direct and punctual recovery actions carried out by restoration equips) has been not applied. In recent years, several group of researchers (mostly coming from University centers) have been making efforts to study the area but in an independent way (each in the own sector without any contact among them). This recent interest has born after the latest events which have affected the archaeological site when, as a consequence of recent flows, on main newspapers was emerged its bad conservation state becoming object of debate.

Leaving aside the management of the archaeological site, if the assumption that the value of a Good is proportional to how much it is enjoyed (term linked to the usability concept), the possibility of preserving historical buildings is strictly connected to their use, mainly for tourism. According to the summary tables released by the Directorate-General Budget of "Ministero dei beni e delle attività culturali e del turismo" (MiBACT), Ostia Antica is the 16th most visited archaeological site in Italy, with an average turnout of 332.190 visitors in 2014 (Museums, Monuments and Archaeological Areas state-owned) [7]. Therefore, the maintenance of the site is more than justified.

Focusing on the Roman house under study, the building object of this PhD work, named "Casa di Diana" (Region I, Insula III), is located at a distance of 3 km from the Tyrrhenian sea, 250 m from the Tiber River and 4 km from the Fiumicino International airport. It was built in the central area of Ostia Antica (Rome, Italy) around 130 CE, remaining in use until the early fourth century (**Fig. 2**).

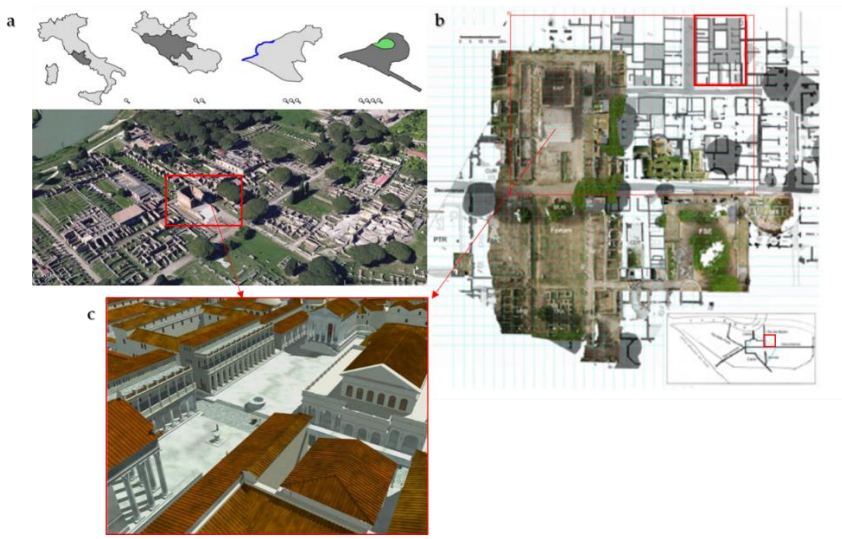

Figure 2. Ostia Antica archaeological site. **a**) Aerial photo (by Google map), which shows the Tyrrhenian Sea and Tiber River proximity; **b**) Orthophotography (by [8]); **c**) 3D reconstruction model by Ostia Superintendence (Jan Theo Bakker 2001). The red box and circle indicate the "Casa di Diana" building and the surrounding area.

The building is a 40 x 22 m rectangular masonry structure with 60 cm wide load bearing walls and two main corridors. The house originally had five floors, where the ground floor hosted shops and the upper floors apartments. Nowadays, only the ground floor and traces of the projecting part of the continuous balcony of the first floor still survive (**Fig. 3**). In the past, the house has used an advanced hydraulic system linked with the inner fountain, supplied by lead pipes from the street to the courtyard. It stands out as an example of aristocratic luxury adapted to the architecture of an *insula*. The masonry has its own brick made well having a depth of 4.20 m, located between the *latrina* and the courtyard, from which it was possible to draw water from an external tank, adjacent to the house.

Figure 3. Principal entrance to the "Casa di Diana".

A two-room apartment (*pre-Mithraeum* and *Mithraeum*) at the NE corner of the house (**Fig. 4**) represents a sanctuary consecrated to the Indo-European god Mithra, whose cult expanded rapidly in the 1st-century Roman Empire. These two rooms remain as in the past, with dark rooms, shadows, wet and cold, an altar illuminated by a natural spotlight, everything set to recreate a particular atmosphere for the tauroctony: the killing of the bull (**Fig. 5**).

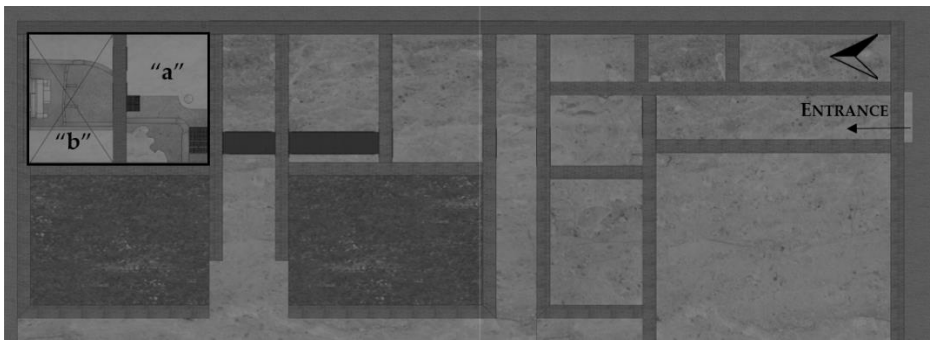

Figure 4. The "Casa di Diana" plan where the *Mithraeum* and *pre-Mithraeum*, located in the northeast. Black squares marked the two rooms. "a" and "b" indicate the *pre-Mithraeum* and *Mithraeum* room, respectively.

Regarding to the building materials, the entire house is mainly composed of bricks and pozzolanic mortar aligned with the *opus caementicium* technique (inner mortar and two outer bricklayers).

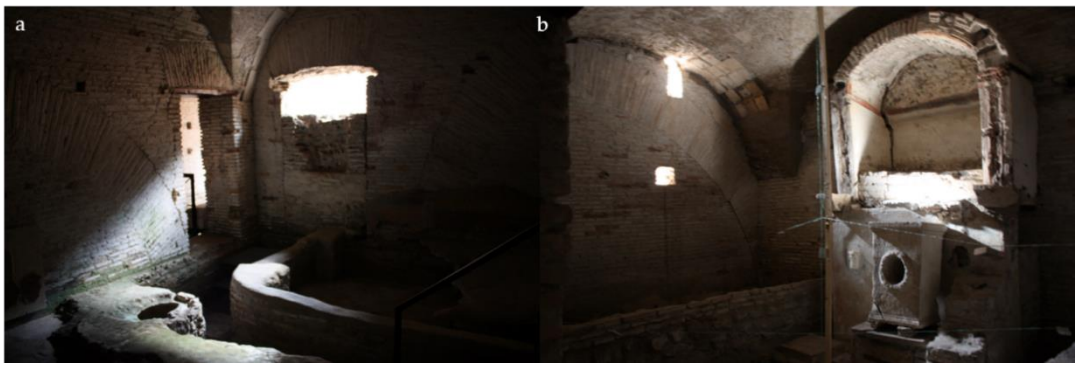

Figure 5. Rooms illuminated by natural spotlight. **a**) *Pre-Mithraeum*; **b**) *Mithraeum*.

Other kinds of materials (marbles, limestones, plaster, travertine and pumices) were used for the decoration of the rooms. Apart from the altar, other furniture, such as a *dolium*, an earthenware vase or container used during the sacred rite, and the *podia*, seats for the Romans that assisted the sacrificial ritual, were also conserved inside.

Focusing on the bricks, it is possible to identify two typologies: red and yellow. The red bricks, which are present in a greater amount than the yellow bricks, present a high resistance upon performing on-site drillings [9].
Moreover, the yellow bricks have a powdery (pulverisation) aspect and the loss of material is evident, especially in the corners of the masonry.
The walls show a retraction for the consumption of mortar joints, a material more permeable than bricks that have a typical morphology of degradation by exfoliation, delamination, cracking or chipping.
Where the continuity of brick and mortar is respected, a veil alters chromatically the appearance of the walls, giving a whitish appearance to brick and mortar surfaces (opacifying) making more difficult the reading of the wall structure (**Fig. 6, a-d**).

Figure 6. State of conservation of building materials: (**a-d**) consumption of mortar joints; (**a-d**) exfoliation, delamination, cracking or chipping; (**a-c**, **e**) mattifying veil and efflorescences; (**e-f**) biological growth.

The building materials are affected also by biological growth (**Fig. 6, e-f),** especially in the *pre-Mithraeum* [10] and in particular on the south wall and on the west transect (central area of the communication trench). Finally, crystallization of soluble salts, visible in the form of efflorescences affects bricks and mortars (**Fig. 6e**) [9].

1.3 Multidisciplinary approach

The nature of the decay products depends both on the origin, nature and influence rate of the environmental stressors affecting the item at the same time, confusing the damage's source/origin. Assets are being lost, or are at risk, through natural processes of decay (sometimes accelerated by poor environmental control), environmental disasters (sometimes exacerbated by human activity), the direct effects of enhanced public access (without commensurate conservation measures), conservation/preservation procedures without long-term validation, or simple negligence. The surrounding environment has a great influence in the acceleration of the natural ageing of materials. The stressors, which can be studied, controlled and, in the best case, eradicated, represent a phenomenon rather repetitive or persistent, depending on the site location and the properties of the materials.

The research required to alleviate this huge class of problems and, at the same time, make progress in the study of Built Heritage is the **multidisciplinary**. This demands the expertise of people directly involved with the Cultural Heritage (i.e. art historians, archaeologists, curators, conservators), as well as scientists. The conservation strategies are not usually developed as a result of a joint work involving professionals of different areas. Although the field of Built Heritage

science is vast and complex, it is possible to develop projects in order to design adequate conservation and prevention strategies. In fact, the European Commission is promoting actively the integration of the **multidisciplinary** concept in the projects of Cultural Heritage field. This is because, until now, Cultural Heritage projects have been developed in the last decades, in general, as local programmes, leading to a loss of strategic output, risk of duplication and reduction in the international competitiveness of research [11]. For all of this, the development of a systematic methodology to approach interventions on ancient materials is required.

Chapter 2 Objectives

The enormous quantity of inadequate interventions in historical buildings, with unidirectional systematic resources, applied in particular on archaeological sites, requiring the development of a diagnostic protocol through an interdisciplinary methodology, in order to ensure the conservation and safeguard of artworks.

In this sense and taking into account that this PhD work has been developed under several projects (listed in "**Projects**", **p. 15**) the final goal, or the general objective, is:

- **"ad-hoc designing conservation, safeguard and usability measures of sites (open museum and Build Heritage in general). "**

Moreover, the specific objective of this joint doctoral thesis is:

- **"a complete diagnostic protocol developing, organised in step procedures using multidisciplinary methodology, validating it on the "Casa di Diana" *Mithraeum*, with the aim to assess its conservation state, pointing out the areas most at risk and in this sense suggesting possible repair tools."**

Chapter 3 Instrumental and analytical methodology

This section describes the developed measurements' system, as well as the methodologies followed for each one disciplinary sector.

The section regarding environmental sensors (**Chapter 3.1**) includes the entire instrument used for both indoor and groundwater monitoring by environmental physic and geophysical surveys (electric and seismic). These environmental analyses are addressed to monitor, characterise and assess the environmental stressors (indoor), as well as the hydro-geological setting of the area (enclosed in the "Casa di Diana" building), in order to reveal the anomalies/peculiarities that surround it. Specifically, thanks to the use of dataloggers, probes and devices, it was possible to examine a "vertical section". An approach from top to bottom approach, including atmosphere (emissions, wind speed and direction and all the rest of the environmental parameters – T, RH, E, Qair and AQ), hydrosphere (groundwater contamination) and the lithosphere (bedrock geology, composition, soil parameters) that overlapped, giving a global overview in terms of sciences of the total environment.

The instruments used for this study came from by different Institutes and University Departments, nationally and internationally. The latter refers to the Department of Applied Physics and the Department of Construction Engineering and Civil Engineering Projects of Valencia (Spain).

The second part (**Chapter 3.2**) refers to the analytical chemistry section, in particular to all those analytical techniques (some validated in other archaeological sites) that have enabled the materials 'characterisation. This work was performed using different analytical techniques in order to respond to various issues (*in-situ* and laboratory characterisation). The majority of them were performed at the University of the Basque Country (Spain), Department of Analytical Chemistry, where this PhD work was carried out as a joint Doctoral Thesis.

3.1 Environmental sensors (Dataloggers, probes and devices)

Regarding the environment monitoring, according to the environmental parameter analysed the following sensors were employed and classified.

3.1.1 Micro-environmental analysis (multiparametric study)

3.1.1.1 Instrumentation

a. Dataloggers[1]

- Ta, RH, CO and CO_2 sensor **(Delta Ohm HD 37AB17D**[2]**, Fig. 7a)**. They are commercial instruments (according to ASHRAE and IMC regulations), suitable to research and monitor the AQ in internal environments. RH measurement is obtained with a sensor of capacitive type. NTC type sensor measured T with high precision. The sensor for CO measurement consists of an electrochemical cell with two electrodes, suitable to detect the presence of carbon monoxide in residential and industrial environments. CO_2 measurement is obtained with the special infrared sensor (NDIR technology) that, thanks to the use of a double filter and a special measurement technology, guarantees precise and constant measurements over time. The presence of a protection membrane through which is given off the air to check, protects the sensor from dust and atmospheric agents. The instrument is provided with a B type 2.0 USB communication interface. The connection to the PC (data download – prior driver installation **DeltaLog13**) is possible by cable (CP22). Technical features: 1 sample every 60 seconds (measure frequency and logging interval used); the range of measure is 5-98 % (RH); ± 0.2° C+ 0.15° C of the measurement, ± 2.5%, ± 3 ppm + 3% of the measurement, ± 50 ppm + 3% of the measurement (accuracy for T, RH, CO and CO_2 respectively).
- Ta, RH (**EBI 20- TH1, Fig. 7b**). Temperature-humidity logger with an internal sensor. NTC type sensor measured T with high precision. The RH is an indication of the degree of saturation related to the current Ta. A Universal Serial Bus (USB - **Winlog.x software**) connected the interface to the PC. Technical features: 1 sample every 5 minutes (measure frequency and logging interval used); the range of measure is 0-100% (RH); ± 0.5° C, ± 3% (10-30% interval) (accuracy T and RH respectively).
- Ta, RH (**Lascar EL-USB-2, Fig. 7b**). Stand-alone datalogger; at the touch of a button, use the on-board display to cycle between the current, T_{min} and T_{max} logs seen during the session for both T and RH. Easily set-up the logger and view downloaded data by plugging the

[1] The wide variety of instruments used (to measure the same parameter) derives from different monitoring campaigns during the last three years. Thanks to the establishment of several collaborations, the sensors and devices were changed. Furthermore, it is important to underline that some parameters (E, CO and CO_2) required complementary equipment. For each technical property, the most suitable sensor was chosen based on the specific study.

[2] The instrument was obtained by Pr. Matteo Vitali (Department of Public Health and infectious diseases, University of Rome "Sapienza").

unit into a PC's USB port and using the free **EasyLog software** provided. Technical features: 1 sample every 5 minutes (measure frequency and logging interval used); the range of measure is 0-100% (RH); 0.55° C, 0.5% (accuracy T and RH respectively).

- Ta, RH, E (**Data loggers HOBO® U12, Fig. 7c**), CO and CO_2 (**Vaisala GMW86P**). The latter is an infrared (IR) gas analyser for measuring CO_2 concentration based on the measure of the absorbed IR radiation deriving from the air diffused into the instrument and compared to the reference adsorption radiation, without the gas. Technical features: 1 sample every 5 minutes (measure frequency and logging interval used); the range of measure is 5-95% (RH); ± 2.5-3.5% accuracy (depending of measure logging), while for T is 0.35° C. The data were previous treated using the **HOBO ware Pro version 3.7.2 software** (Onset Computer Corporation© 2002-2015).
- Ta, TIR (**Testo 810 infrared thermometer, Fig. 7d**). The datalogger measures the T on two channels. On one hand, being an infrared thermometer, it can perform non-contact surface temperature measurements of the object being analysed; on the other hand, it can measure the Ta using its additionally integrated NTC sensor. Technical features: 1 sample every 0.5 s (measure frequency and logging interval used); ± 0.5° C NTC, ± 0.2° C TIR (accuracy).

Figure 7. Dataloggers. **a)** Ta, RH, CO and CO_2 (HD37AB17D); **b**) Ta, RH (EBI 20- TH1, white – right side) and ta, RH (Lascar EL-USB-2, grey- left side); **c)** Ta, RH, E (HOBO® U12, left side) and CO and CO_2 (Vaisala GMW86P, right side); **d**) Ta, TIR (Testo 810 infrared thermometer).

b. Probes

- T, RH probes[3] (**Fig. 8a**) that contain an 8-pin small-outline integrated circuit (SOIC), (model **DS2438** - Maxim Integrated Products, Inc., Sunnyvale, CA, USA) that incorporates a direct-to-digital T sensor with an accuracy of ±2° C, as well as an analogue-to-digital voltage converter, which measures the output voltage of a RH sensor (**HIH-**

[3]The construction of these probes was personally performed in collaboration with the Department of Applied Physics of Universitat Politècnica de València. All the other environmental sensors are commercial products.

4000, Honeywell International, Inc., Minneapolis, MN, USA). Since each DS2438 contains a unique silicon serial number, multiple DS2438s can exist on the same data bus. This allows simultaneous used of multiple sensors in the system with only one data line (1-wire communication protocol). The RH sensors were calibrated in the laboratory with a saturated solution of salt, as explained elsewhere [12, 13]. As specified by the manufacturer, the voltage output of the RH sensors is proportional to voltage supplied, thus the exact voltage supply was measured for each RH sensor once all probes and connections were installed and the calibration curves of each sensor were applied. Three electric wires come out from each probe: one wire for + 5 V DC for power supply, one for ground and another for data transfer.

- Tc (**Fig. 8b**). Multimeter (**PM 2521 Philips).** In this study, a **PT100 probe** was used (1.0 + 0.2° C accuracy, 0 -100° C range).
- Mc (**Fig. 8c**). GE Protimeter Surveymaster Moisture Meter (**SM BLD5360**). A moisture meter that combines the conventional two-pin inspection method with a non-invasive radio frequency technique. The Search Mode uses the same colour coded LED scale as the Measure mode, identifying degrees of dampness below the surface. The instrument employs radio frequency emissions (RFE) to measure moisture through most wall coverings. The two-pin Measure Mode discriminates different levels of humidity by means of green, yellow and red LEDs (dry, humid and wet surface). The range is 0-999 relative (non-invasive) and 7% to 99% (pin measurement). The depth of moisture is non-invasive up to 3/4 in (19 mm) and pin up to 1/2 in (12.7 mm).

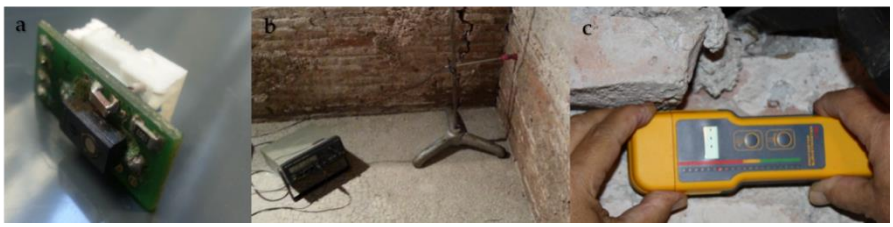

Figure 8. Probes. **a)** T, RH probes (DS2438- HIH-4000); **b**) Tc (PM 2521 Philips); **c**) Mc (SM BLD5360).

c. Devices

- E. Light artificial control. **SpectroVIS® Spectrophotometer** by Vernier Software & Technology (**Fig. 9a**). It is a portable and affordable visible light spectrophotometer with fluorescence capabilities. Measures wavelengths from 380 nm to 950 nm. The device was utilized to collect the spectrum of artificial lamps in order to measure

their emissions.

- Va, Ta, ΔP. Multi-sensor device[4] (**Fig. 9b**). The system consists in a portable PC (Pentium III, 64 Mb RAM) and a National Instrument Corporation (Austin, TX, USA) DAQCARD 6024E data acquisition card with 16 analogue inputs and a maximum sampling rate of 200 kS/s. Its absolute accuracy at full scale is 10.568 mV. As 16 channels are less that those needed, a central multiplexor data collection module was designed. The multiplexing modules are able to concentrate 8 signals into a single channel. Therefore, the system extended the 16 channels of the acquisition card to a maximum of 128 signals. To reduce interference, all information is sent in current mode instead of voltage mode. The card also had 8 digital input-output channels, which are used to control multiplexing units.
  In this work, we describe a system adapted to operate with 24 Va sensors, 24 T sensors, two ΔP modules and 7 multiplexers. Data was acquired in the PC by using specifically develop software, based on the National Instruments Corporation LavVIEW 8.2 platform (National Instrument, LabVIEW). The software is able to acquire and monitor signals from sensors, as well as to control the multiplexing and de-multiplexing functions. Material, circuit and calibration for each one parameter are described in [14].
- Va. Ultrasonic anemometer (**3D S83100** -Thies Clima, Ammonit GmbH, Germany) (**Fig. 9c**). It serves for the measurement of the wind direction and the wind velocity from all spatial directions. All calculations are carried out by a high-capacity digital-signal-processor (DSP) within the propagation time of the ultrasonic signals with an accuracy basis of 32 bit. Technical features: ≤ 5 m/s: ± 0.2 m/s; > 5 m/s: ± 2% of meas. Value (accuracy wind speed), ± 2 with wind speed > 1 m/s < 50 m/s (accuracy wind direction); ± 0.5 K (accuracy T).

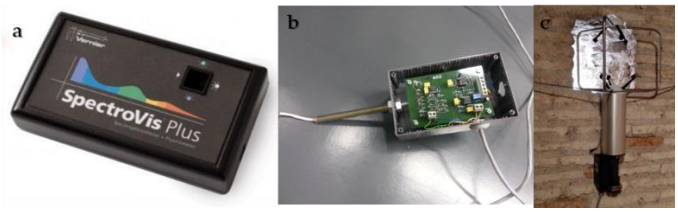

Figure 9. Devices. **a**) E. Light artificial control (SpectroVIS® Spectrophotometer); **b**) Va, Ta, ΔP (Multi-sensor device); **c**) Va (anemometer, 3D S83100).

[4] These devices were designed and built by PhD Eliseo Bustamante Garcia. Department of Construction Engineering and Civil Engineering Projects (Valencia, Spain).

3.1.2 Macro-environmental analysis (hydro-geological setting and foundation study)

3.1.2.1 Instrumentation

a. Probes

- Sound water velocity. (**MONITOR SVP** Sound Velocity Profiler[5] Valeport - **Fig. 10a**). It is a digital time of flight sound velocity sensor and synchronised sampling technique to suit small boat or shallow water applications. It uses the concept of distributed processing, where each sensor has its own microprocessor controlling sampling and calibration of readings. Each of these is then controlled by a central processor, which issues global commands and handles all the data. This means that all data are sampled at precisely the same instant, giving superior quality profile data. Technical features: 1 sample every 1 minute (measure frequency and logging interval used); ± 0.02 m/s, ± 0.01° C, ± 0.1% (accuracy sound velocity, T and RH respectively).
- **Georesistivimeter** (**IRIS Syscal Pro, Fig. 10b**). 48-channel with 24/48 copper plates (10x10 cm) for internal surveys, 48 stainless steel states, for external surveys, both using as electrodes. Customized sequence: dipole-dipole. ERT (2D and 3D) dataset are inverted with the VEMI algorithm - Versatile interface for Electrical Modelling and Inversion [15] built within the EIDORS environment [16]. This algorithm is able to perform both 2D and 3D inversion, by solving the forward problem with a finite element approximation of Poisson's equation governing the physical problem, while inversion is carried out using a Gauss-Newton formulation. The code can incorporate the finite length of the electrodes (non-negligible for archaeological applications) and it is possible to add a priori information to the inversion process. In this particular case, no preliminary assumption was made due to the scarce amount of information available on the study area.
- **Geode seismograph** (**GeometricsInc. Company**, **Fig. 10c**). 24-channels, utilizing a sampling rate of 31.5 μs. Data were acquired using 11 shot points produced by a 2 kg hammer source and 23 piezoelectric accelerometers with a cut-off frequency of 4.5 kHz. These data are inverted using the linear travel time interpolation (LTI) method for ray-tracing in the forward kernel and the iterative

[5] Instrument obtained from the National Research Council, Institute for Environmental Engineering and Geosciences CNR-IGAG (measured conduct by Alessandro Bosman Ph.D.).

bi-conjugate 203 gradient algorithm for travel time inversion [17]. The resolution of the inverted images is improved through the staggered grid technique [18], where inversion is computed 7 times for each direction, starting from an initial cell size of 0.48 x 0.2 m, leading to a final refined mesh of 2499 cells.

Figure 10. a) Sound water velocity (MONITOR SVP - Valeport); **b**) Georesistivimeter (IRIS Syscal Pro); **c**) Seismograph (Geometrics Geode, yellow box + piezoelectric accelerometers, black electrodes).

3.1.3 Software used

- The long-term monitoring at frequencies higher than 1 data point/day generates large volumes of data that are difficult to store, manage and analyse. In this sense, these data matrices were inserted into the "**Burrito**" software [19]. Such software is developed with Delphi using the Object Pascal language and Firebird as database engine. Firebird and Delphi are both developed by the same company (Borland, currently a subsidiary of Micro Focus), favouring compatibility, compared to other open source software, like PostgreSQL or MySQL. Firebird is an open source software; therefore, there is no need to pay a license fee for its download, use or the development of commercial programs. It works on MS Windows systems (XP, Vista and Windows 7) in 32 and 64 bit versions. It could possibly work on Linux with a Windows emulator, but this option has not been tested. It does not consume excessive system resources, and works perfectly well on a PC equipped with Windows XP and 500 MB of RAM. The DB is a single *.FDB file that can store millions of data points. Currently we manage a DB of over 37 million records and a size of 10.5 GB.
- **ANSYS FLUENT 6.2** (Fluent Inc., Lebanon, NH, USA). It is the most-powerful commercial computational fluid dynamics (CFD) software tool available. Fluent includes well-validated physical modelling capabilities to deliver fast, accurate results across the widest range of CFD and multi-physics applications.

3.2 Analytical techniques

The analytical techniques described below were performed on the mainly wall-building materials (brick). Some exceptions include mortar and travertine, which were analysed and characterised by SEM and isotopic analysis.

3.2.1 Petrographic and mineralogical characterisation (elemental and molecular)

3.2.1.1 Instrumentation

- Petrographic observations were performed by **Olympus Optical BX60** equipped with a MegaPixel Firewire - Vitana Corporation (PL-A6xx Capture 3.1) camera (**Fig. 11a**).
- The identification of both major and minor mineral phases was performed by X-ray powder diffraction (XRD) using a **Siemens D500 X-ray Powder Diffractometer**[6] equipped with a Cu Kα radiation source with λ=1.54056 Å and by **Philips PANalytical X'Pert PRO diffractometer**[7] using Cu$K\alpha$ radiation (n=1.5418 Å), operating at 40 kV and 40 mA at a step size of 0.0260°. The programme used for qualitative analyses is **WinPLOTR** Programme (CDIFX UMR6226 Rennes/ILL Grenoble) (**Fig. 11b**).

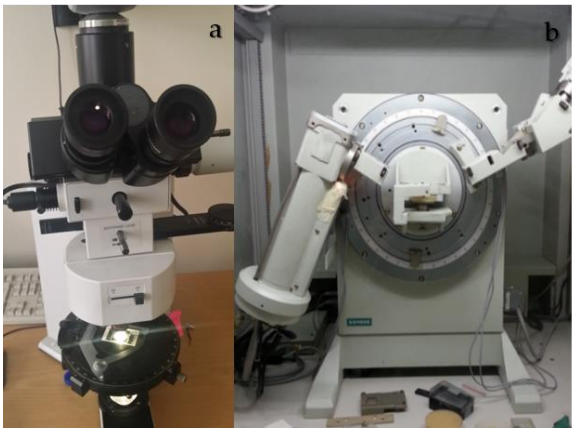

Figure 11. a) Olympus Optical BX60 microscope; **b**) Siemens D500 X-ray Powder Diffractometer.

- In order to observe the surface morphology and composition of the mortars (microstructural and chemical characterisation) was used the **FEI-Quanta 400–EDAX**[8] scanning electron microscope (**Fig. 12**) – SEM (microanalysis system by EDAX Genesis).

[6] Department of Earth Sciences University of Rome "La Sapienza", X-powered diffraction Laboratory (Stefano Stellino).

[7] LASPEA laboratory of the Research Services (SIGER, UPV/EHU).

[8] Performed by Marco Albano (Laboratory of Scanning Electron Microscope -S.E.M, Department of Earth Sciences University of Rome "La Sapienza").

Figure 12. FEI-Quanta 400–EDAX scanning electron microscope.

3.2.1.2 Sample preparation for petrographic analysis

- Thin-section[9] (microscopic preparation).

  After the sample has been impregnated and hardened, the same procedure as for rock fragments is followed, but possible heating has to be monitored by means of lubrication during the cutting and polishing processes, in which only oil can be used, since water could dissolve the soluble salts and perhaps lead to the swelling of certain clays. Firstly, the piece of soil included in the plastic block has to be cut with a diamond cut-off saw to obtain a flat surface with the required size of the microscopic preparation. After a flat surface is obtained, it is polished to eliminate the traces of cutting and to obtain a flat surface that is as smooth as possible. The polished surface is glued onto a glass microscope slide with a colourless and isotropic cementing agent (**Fig. 13**). After the piece of soil has been stuck to the microscope slide, it is cut to obtain the thinnest slice possible. The sample is trimmed until it reaches a thickness of about 30 microns. One this is achieved, the sample is carefully cleaned and covered with a slide cover, which has to be glued with a similar cement to the one used to stick the sample to the slide.

[9] Personally performed in Laboratory of rock crushing and thin-section under the supervision of the Laboratory Technician. Department of Earth Sciences University of Rome "La Sapienza".

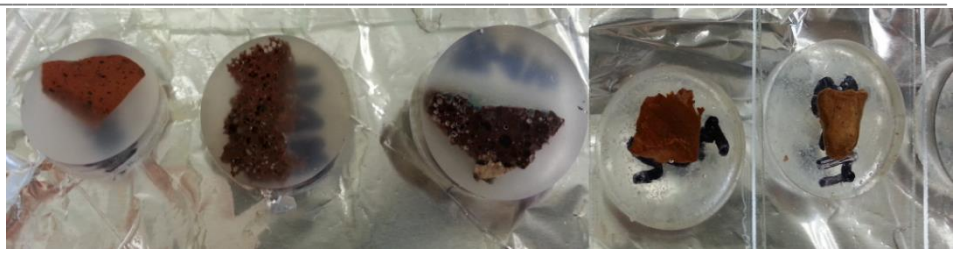

Figure 13. Mounting phase.

- Powered sample for XRD
  All the samples were crushed in an agate mortar and dried in a drying cabinet (60° C) until constant weight was obtained (24h).
- The cross-section specimens for SEM were prepared using standard metallographic techniques[10], by coating with a conductive metal, such as carbon, gold, or palladium in either a sputter or an evaporative coater. In our specific case the coating substance was graphite.

3.2.2 Isotopic analysis of water samples

3.2.2.1 Instrumentation

- Isotopic analysis of oxygen and carbon was performed with a by **Finnigan Delta Plus mass spectrometer**[11] DUAL INLET and triple collector. The chosen samples are 1 Travertine sample (analysis on the CO_2 carbonate extracted) and 7 water samples (analysis on the O_2 extracted) and manipulated by **Isodat NT Software.**

  - The gaseous sample to be analysed is fed into the ion source via the inlet system. In the ion source, ions are generated in a high vacuum by the impact of electrons. The ions are then accelerated to energies of up to 3 keV and focused by electrostatic lenses to form a beam. The ion beam exits the ion source into the magnetic field through a slit with a fixed width of 0.2 mm. It enters the magnetic field boundary at an angle of 26.5° and traverses the 90° magnetic sector field. Part of the ion beam exits at the same angle of 26.5°.
  - Regarding the water samples (n.4), the δO^{18} (SMOW) final value was obtained inserting some information: tot volume of the ampoule (Variable value according the ampoule used for each one sample) in which the analyser is contained, the ml of analyser (3 ml), the T conditions during the experiment (21.1° C), pressure value, standard values, etc.., into the electronic sheet (excel).

[10] Performed by Marco Albano (Laboratory of Scanning Electron Microscope -S.E.M, Department of Earth Sciences, Sciences University of Rome "La Sapienza").

[11] Dr. Mauro Brilli (IGAG CNR -Montelibretti, Rome) conducted the stable isotopes analysis with mass spectrometer.

3.2.2.2 Sample preparation for isotopic analysis

- O_2 extraction from water samples[12] (isotopic analysis of oxygen). The procedure was conducted following the equilibrium method modified by [20].
- CO_2 extraction from travertine (isotopic analysis of oxygen and carbon). The procedure was conducted following the method of [21].

3.2.3 Chemical analysis (non-destructive and destructive)

3.2.3.1 Elemental characterisation (*in-situ* and laboratory analysis) by X-ray fluorescence spectroscopy. It is an analysis technique for rapid and simple determination of the elemental composition of a material.

In this PhD work a **handheld ED-XRF** (**X-MET5100, Oxford Instrument, UK, Fig. 14a**) and **μ-EDXRF** (in the laboratory, it provides the possibility to focus on the desired measured point) by a **TORNADO M4 X-ray spectrometer (Bruker Nano, Berlin, Germany, Fig. 14b)**, was used (**Fig. 14**). The energy dispersive X-ray spectroscopy (EDS) allows to survey the light elements (in the chamber under vacuum).

The first spectrometer combines Oxford Instruments Ground-breaking Silicon Drift Detector (SDD) with a powerful Rh 45kV X-ray tube and an energetic resolution of 150 eV (for Mn Kα at – 20° C), allowing to acquire spectra with a resolution of 20 eV. It analyses light elements such as silicon and phosphorus from copper, nickel and steel alloys without the need for vacuum or helium attachments. The instrument is also equipped with a Personal Digital Assistant (PDA) that allows an easier management of the instrument and the storage process of the results. In order to improve the limit of detection, the measurements were acquired for 100 seconds (real time). The spectra obtained were transferred from the PDA to the computer in .txt format and were transformed into binary files in order to be treated with the **EZData (ChemiLab, USA) program**.

The second instrument implements two Rh tubes mounted on a mechanical collimator and on a poly-cap optic, respectively. In order to ensure the representativeness of the whole sample, the analyses were performed using the mechanical collimator set-up. Thus, the lateral resolution achieved was of 1 mm. The X-ray tube worked at 50 kV and 700 μA during the measurements, and 300 seconds (live time) were considered for each spectral acquisition. The detection of the fluorescence radiation was performed using an XFlash® silicon drift detector with 30 mm^2 sensitive area and an energy resolution of 145 eV for Mn-Kα. The

[12] Personally performed under the supervision of Dr. M. Preite-Martinez, Department of Earth Sciences, University of Rome "La Sapienza".

measurements were acquired under vacuum (20 mbar). To achieve the vacuum, a diaphragm pump MV 10 N VARIO-B (Vaccubrand, Germany) was used. The spectral data acquisition and treatment was performed using the **M4 TORNADO software** (Bruker Nano GmbH, Germany). Both instruments belonging to the laboratories of the IBeA research group[13].

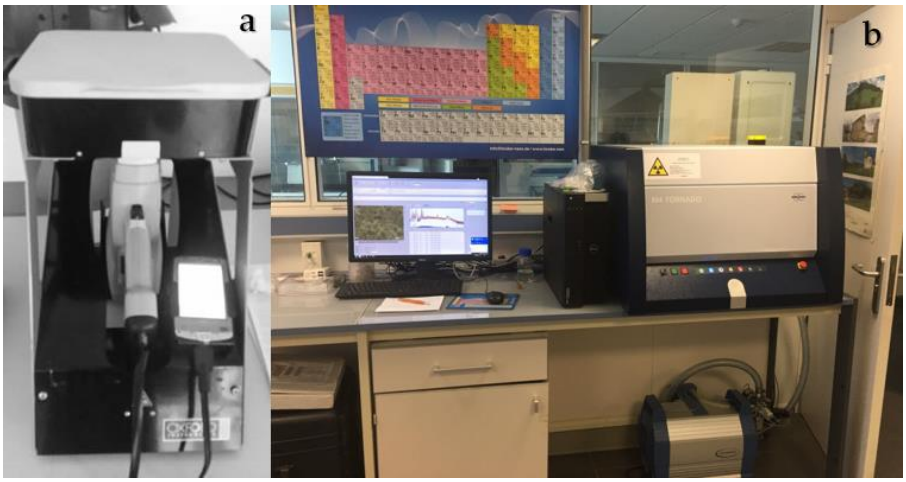

Figure 14. a) X-MET5100 spectrometer (Oxford Instrument, UK); **b**) TORNADO M4 X-ray spectrometer (Bruker Nano, Berlin, Germany).

3.2.3.2 Molecular characterisation (*in-situ* analysis and laboratory analysis).
Among the vibrational spectroscopic techniques (that provide very suitable and valuable results regarding the molecular composition) **Raman spectroscopy** was chosen. The instruments used were **innoRam™** (**B&WTEKINC, Newark, EEUU**) and dispersive Raman microprobe **RA100** (**Ranishaw, Gloucestershire, UK**) portable spectrometers, both belonging to the laboratories of the IBeA research group[14]. The former, provided with a CleanLaze® technology 785 nm excitation laser (< 300 mW laser output laser) was used (**Fig. 15a**). The instrument implements a controller of the laser power (a scale from 0 to 100% of the total power). It also includes a two-dimensional charge coupled device (CCD) to detect the dispersed Raman signal, which is Thermoelectrically Cooled (TC) to - 20° C, in order to maximize the dynamic range by reducing dark current. A back-thinned CCD is used to obtain 90% quantum efficiency by collecting incoming photons at wavelengths that would not pass through a front illuminated CCD. A spectral resolution (FWHM) of 3.4 cm^{-1} can be achieved with a double pass transmission optic. The spectral range is of 65-2500 cm^{-1}. The instrument is provided with a probe based on optic fibre (1.5 m length).

[13] Department of Analytical Chemistry, University of the Basque Country (Spain).
[14] Department of Analytical Chemistry, University of the Basque Country (Spain).

The working distance is 5.90 mm and the measured spot size in each case was 85 μm. Spectral acquisition was performed using the **BWSpec™ 3.26 software** (B&WTEKINC) and data treatment was performed using **OMNIC 7.2 and GRAMS/AI 7.02 software**.

The second portable spectrometer (**Fig. 15b**) is provided with the same excitation laser and detector as the first spectrometer (diode laser and Peltier cooled). The nominal laser power is 150 mW at the source. Neutral filters allow it to work at 1% (5 mW at source, 1 mW at the sample), 10% (50 mW at the source, 10 mW at the sample) or 100% (150 mW at the source, 30 mW at the sample) of the total power. The control of power was used in order to avoid thermal decomposition. For the measurements, long-distance lenses of 20x and 50x (laser focus on approximately 10-200 μm spots, depending on the lens used) were employed.

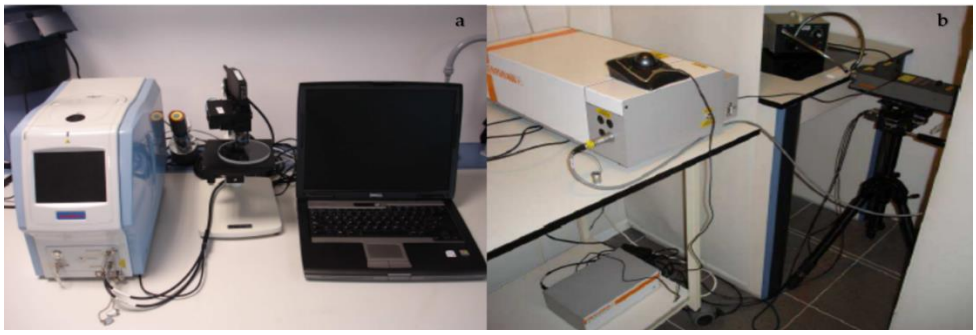

Figure 15. Portable Raman spectrometers. **a**) InnoRam™ (left side), laboratory stage connected to a video-camera (middle part); **b**) Raman Renishaw RA100, at the right side the micrometric stage.

The microprobe has a TV micro-camera, which allows to focus the different grains of the matrix, and positioning is controlled by a micrometric stage (**Fig. 16b**). The instrument was calibrated daily using the 520 cm^{-1} silicon Raman peak. The spectra were collected with a resolution of 1 cm^{-1} and they were taken in the 200-2500 cm^{-1} spectral range. The integration time and accumulation scans were set depending on the spectral response for each sample (higher or lower signal-to-noise ratio). Sometimes, photo-bleaching was applied to overcome the arousal of florescence phenomena in some samples. All the spectra obtained were acquired with the Renishaw **WIRE 3.2 software**.

Both instruments belonging to the laboratories of the IBeA research group[15].

3.2.3.3 Anions and cations quantification (aqueous sample obtained after extracting[16] the soluble salts form the solid material samples). The building

[15] Department of Analytical Chemistry, University of the Basque Country (Spain).

suffers from the effect of soluble salts crystallisation. In this sense, **ion chromatography (IC)** was used with the aim to evaluate the soluble salts content of bricks, suffering of different phenomena (infiltration water, acid pollutants depositions, etc.). Cations and anions involved in each soluble salt type were quantified by means of a **Dionex ICS 2500** ion chromatograph connected to a conductimetric detector (ED50 Dionex) with post-column suppression (Dionex Corporation, Sunnyvaley, California, USA) (**Fig. 16**). An IonPac AS23 (4×250 mm) column and IonPac AG23 (4×50 mm) pre-column from Dionex were used for the separation of anions. The quantification of cations was conducted using an IonPac CS12A (4×250 mm) column and an IonPac CG-12A (4×50 mm) pre-column from Dionex. The chromatographic conditions used in the anion quantification were 5 mM Na_2CO_3/0.8 mM $NaHCO_3$, 25 mA and 1 ml/min as mobile phase, suppression current and flow, respectively. In the case of cations, 20 mM CH_4SO_3 as mobile phase, 59 mA of suppression current and 1 ml/min flow were used. Prior to the analysis, the samples were passed through 0.45 μm nylon syringe filters and brought to a final volume.

The system is coupled with an auto-sampler AS40 from Dionex. The acquisition and data-handling was performed using the **Chromaleon 6.60-SPla software** (Dionex Corporation). The instrument belonging to the laboratories of the IBeA research group[17].

Figure 16. Dionex ICS 2500-ED50 ion chromatograph.

3.2.3.4 Sample preparation for IC analysis

The brick samples were subjected to a pre-treatment before extraction (ultrasound-assisted procedure). The scrapped samples were crushed in an agate mortar in order to obtain a fine powder (**Fig. 17a**). After that, the

[16] Ultrasound-assisted extraction, alternative to the obsolete Italian 13/83 NORMAL recommendation and actual UNI 11087 Italian standard method to extract the soluble salts [187].

[17] Department of Analytical Chemistry, University of the Basque Country (Spain).

samples were dried on a heater at 60°C until constant weight (24h). At this point, the samples were ready to undergo the extraction procedure. Lastly, an ultrasound bath for 45 min was performed, using 100 ml of deionized water (milli-Q quality) and 100 mg sample (**Fig. 17b**). This pre-treatment was replicated four times for each sample analysed. The solutions after extraction was filtered through a 0.45 μm syringe filter to obtain the final solution ready for quantification (**Fig. 17c**).

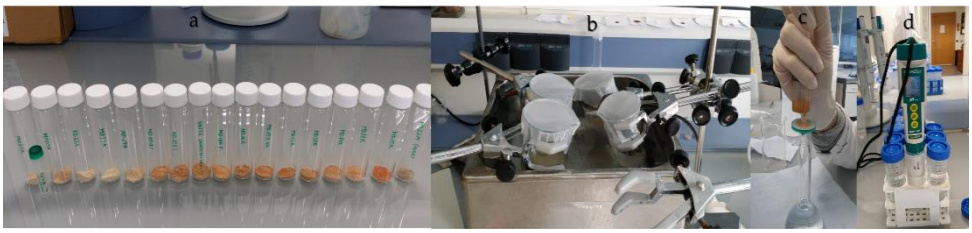

Figure 17. Brick samples treatment before ionic quantification analysis. **a**) samples crushed by agate mortar; **b**) ultrasound bath; **c**) filtration; **d**) pH measurements of solutions.

In order to estimate the carbonate concentration, the pH values of the extracted soluble salts were measured. Thus, the pH measurements were conducted and replicated three times, with **SOILSTIK pH meter item#2105**(Spectrum Technologies, Inc.) (**Fig. 17d**).

3.2.3.5 Thermodynamic software used

Two software were used to model the thermodynamic calculation of soluble salts.

- ✓ To predict the probable formation of decay compounds and soluble salts crystallisation under specific conditions of T and RH, the ECOS-**RUNSALT 1.8** (a version of ECOS, Environmental Control of Salts) software was used. This software is based on Pitzer's theory of electrolyte solutions. The software is able to predict the minerals that can exist in equilibrium at a certain T and RH. The software implements a database of salts that can crystallise in porous materials (stone, mortar, bricks, etc.). The electronegativity (sum of anions and cations, must be the same in units of ion equivalents Kg^{-1}) was checked before using the software. Successively, the data coming from the environmental monitoring was inserted in the software. However, the program has several restrictions correlated to the input of data, as anions like carbonates and cations like ammonium and barium are not considered by it. Furthermore, in some occasions, the prediction of gypsum crystallisation might cause problems, since the program is unable to calculate the crystallisation of other salts in its presence, and gypsum

must therefore be removed from the system. Finally, the program runs only within a certain thermo-hygrometric range. In particular, it does not allow maximum values of relative humidity (RH_{max}) exceeding 98%. Due to these restrictions, the model could be applied only to some of restricted cases, as a consequence of the abundant presence of calcium in the materials under study. Due to these restrictions, it was used in combined with the thermodynamic software (described below).

- ✓ **MEDUSA-Hydra** software (v. 2010). It does not consider the environmental conditions nor predicts chemical equilibria in dissolution, but is complementary to the other fills the gap left by the other program.

Apart from the use of analytical techniques to obtain experimental results from the samples, numerical data were also treated using chemometric tools (multivariate statistics), for both environmental and chemical analyses. The programs used for this purpose were:

- ✓ **Unscramble** X version 9.2 (chemometric software package - Camo, Woodbridge, NJ, USA) package (cross validation method and Singular Value Decomposition algorithm), to perform the Principal Component Analysis (PCA)
- ✓ **OriginPro** version 8.5.1 (OriginLab© Massachusetts, USA), for statistical data treatment.

Chapter 4 Proposed general methodology: the pyramid model. Initial hypothesis

To understand the deterioration processes originated by the effect of different environmental stressors on Built Heritage and to obtain reliable information regarding them, it is essential to design a **diagnostic protocol**. The latter must be successively validated, as any other procedure, in order to establish a solid methodology that could be applied in a more general context.

Taking into account that open museums represent extremely sensitive places, due to the presence of multiple environmental stressors in a complex scenario, the proposed protocol must consider all the factors in order to produce a useful model.

This PhD work revolves around an innovative diagnostic idea, using a pyramidal model **(Fig. 18**) because no sustainable system can evolve (development on vertical profile) without a multidisciplinary knowledge of a complex issue and without addressing all the targets as a whole.

The protocol created is based on an approach (dynamic model) that includes three main steps or levels that can be summarised into: (1) **anamnesis** (the state of art and the macroscopic observation on both environment and materials), (2) **analysis** (the development of a protocol that includes the investigation actions that lead to the identification of damage's sources) and (3) **conservation** (the evaluation of the conservation state of the site under study). This last action also considers some suggestions for a future and global conservation and lays the "ad-hoc designing" to create a whole conservation plan. The final goal is the conservation, **safeguard and usability of open museums or cultural sites in general**, thanks to the flexible protocol flexibility, organised in steps procedures, depending on the requirements during the growth of the pyramid.

In detail, the basic knowledge to achieve is represented by two different blocks, interconnected with each other: the environmental and the materials' characterisation (blue and red boxes, respectively). Moreover, a third block (purple boxes) appears as an interface between such blocks, considering the study of both aspects at the same time.

The methodologies to employ for the study of these blocks can be rather different considering each scientific area. The challenge is to combine these areas in a way that could be possible to develop new complementary methods, to achieve the targets and preserving, wherever possible, the studied materials. In a few words: a multidisciplinary approach.

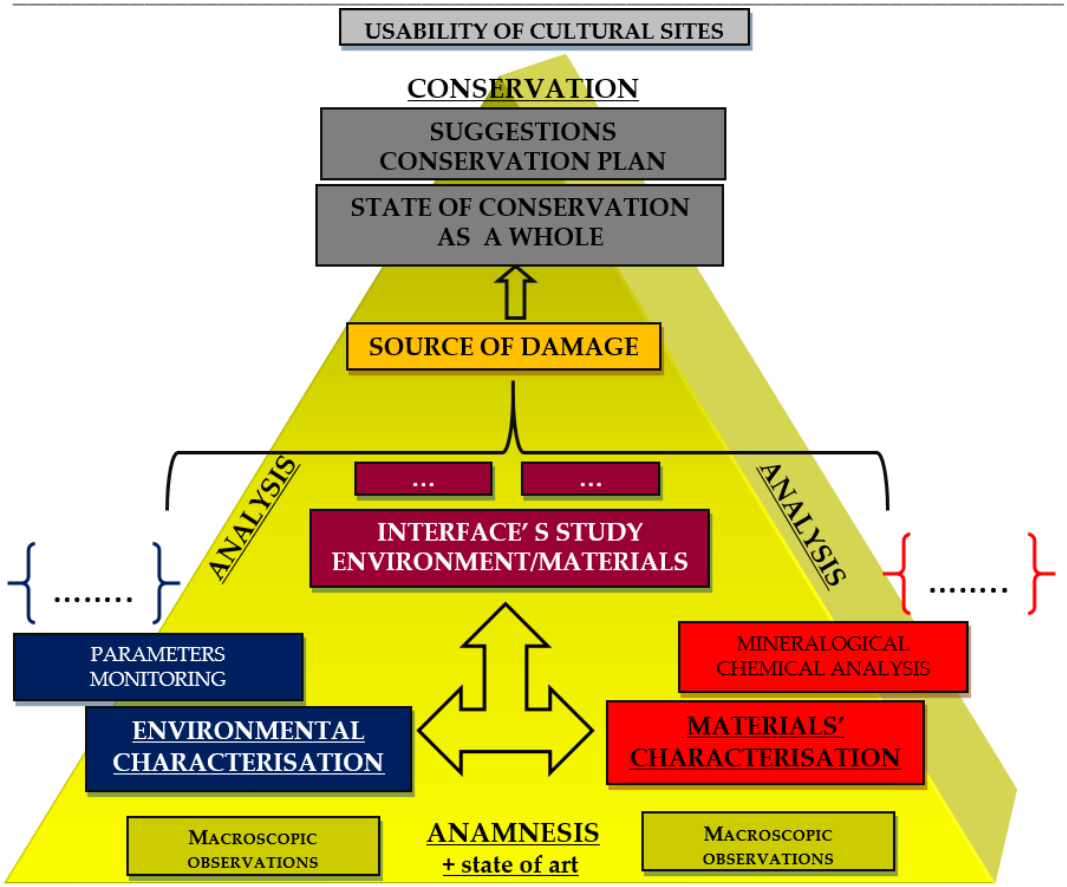

Figure 18. Pyramidal model of the proposed diagnostic protocol to develop.

Before performing any analysis on Built Heritage items, the place (microenvironment) in which the materials are kept must be taken into consideration. The **relationship between content and container, "system" and "environment"**, is on the basis of this approach.

Relationships between causes (stressors) and effects (damages) are often characterized by non-linear and dynamic behaviours, including the presence of thresholds. Non-linear systems are those in which outputs do not change proportionally to inputs. One of the main problems is the difficulty of providing meaningful quantifications of inputs and, in particular, outputs. Besides, outputs can present themselves in different territories and at different scales (from micro to macro). The system is clearly multicomponent, involving a range of interlinked chemical, physical, and biological processes. Furthermore, there are different causes of non-linearity, and many sources may be correlated, some of which are hard to categorize. After all, categorisation is indispensable to archive, study and resolve the causes of the damage (**decaying products → damage source → conservative action**).

Thus, in order to slow down the degradation of the ancient materials, a good knowledge of the relationship between environment and building materials behaviour is required, and it is the main objective of a good analytical study. For this purpose, a multidisciplinary approach carried out using different analytical techniques is needed for determine the chemical, physical, and mechanical properties of the original materials and establish the decaying processes that they are subjected to.

However, despite the decay "hotspots" occurring spontaneously, the probabilistic prediction would be more appropriate in the same cases. The key for an effective assessment and management of risk is to be able to recognise the most plausible explanation under different circumstances and to develop appropriate predictive strategies. Of course, a systemic development should be planned, or a process-oriented learning approach to explore the environmentally feasible development, viable now and sustainable in the future.

In this sense, the pyramid will fill up, according to the requirement and the results coming from the three basic boxes to understand the sources of damage (yellow box) and the conservation state of the archaeological site (grey boxes).

Thus, a new global protocol for the preservation and accessibility of archaeological sites based on a multidisciplinary approach by the combination of physical, geophysical, geochemistry and analytical methodologies will be developed throughout the present PhD work, to lay the foundations to propose a useful conservative plan.

Chapter 5 Environment parameters analysis

Historic buildings have a complex bond with the environment they are set in, being constantly influenced by external factors. Buildings interact with their surroundings in various ways. In the context of archaeological sites, the buildings kept inside, fully or partially protected by roofs (original or not) or by other structures that enclosing it, are subjected to a different microclimate. The orientation of masonries, the confinement of walls or their direct exposition to the macroclimate, the type of soil on which the foundations were laid, the feature of the same frameworks, the position of buildings (far or close to the coast/urban city, main wind direction, etc.), are only some of the factors that contribute to generate several microclimates inside a single macroclimate.

For that reason, the climatic control is crucial as a part of preventive conservation and it can be defined as an indirect action to increase the life expectancy of cultural objects and sites, which requires the assessment of the deterioration agents and the environmental context.

There are many microclimatic parameters for assessing the environmental condition. Temperature (T), relative humidity (RH), illuminance (E), air turbulence or air flow (Qa) and air quality (AQ, CO and CO_2 mainly) are the environmental parameters usually adopted by several monitoring systems (short-term or long-term) and technical devices (remote control with wireless sensors network, stations or smart-home, micro electro mechanical systems, or specially-designed sensors), with the aim to assess the spatial–temporal variations of these multiple parameters.

Among field measurements, continuous data monitoring is usually adopted for identification of buildings' response to weather and seasonal changes. Real time monitoring easily allows the reproduction of the structural characteristics of the building and represents an efficient monitoring to evaluate the local climate changes. Nowadays, many systems are adopted: WSN monitoring (wireless sensor network) [22] by dataloggers or i-Button sensors [23, 24] both supported by software designed as open source[19, 22], implemented strategies for a rapid, accurate and low-cost intelligent monitoring. In this sense, continuous monitoring represents the procedure most widely adopted in the preventive conservation of ancient buildings, such as the acquisition of a basic knowledge of an indoor environment.

5.1 Indoor monitoring (T, RH)

Amongst the main environmental parameters, the thermo-hygrometric (T, RH) features represent an indispensable tool to define some of the main properties

about the indoor environment, individuating the eventual influence from the outdoor environment.

In the last years, some microclimatic monitoring studies have been conducted in archaeological sites [13, 25, 26] with the objective to propose corrective measures, helpful in improving the preventive conservation plan for the sites. In this context, only some corrective actions are required to the safeguard of historical masonry structures with minimum intervention and a complete respect of the original construction [26, 27]. In this sense, monitoring studies of T and RH have been carried out in different Italian sites and statistical tools have been employed for exploratory purposes [13, 28, 29].

Additionally, simulating the behaviour of thermo-hygrometric parameters are valuable tools [27, 30, 31]. In particular, the relationship between input perturbations (e.g., seasonal changes, number of visitors) and output response variables (e.g., changes in temperature and humidity rate) must be determined via an environmental investigation based on real time control of T and RH [32].

Taking all of this into account, a carefully planned microclimatic study, involving multipoint continuous measurements, was carried out in the building under study.

Article 1

A microclimate study on hypogea environments of ancient roman building. Article published in Science of the Total Environment 566–567 (2016) 298–305.

Science of the Total Environment 566–567 (2016) 298–305

Contents lists available at ScienceDirect

Science of the Total Environment

journal homepage: www.elsevier.com/locate/scitotenv

A microclimate study on *hypogea* environments of ancient roman building

C. Scatigno [a,*], S. Gaudenzi [b], M.P. Sammartino [c], G. Visco [c]

[a] Department of Earth Science, University of Rome "La Sapienza", Piazzale Aldo Moro 5, 00185 Rome, Italy
[b] INAF/IAPS, Via Fosso del Cavaliere 100, 00133 Rome, Italy
[c] Department of Chemistry, University of Rome "La Sapienza", Piazzale Aldo Moro 5, 00185 Rome, Italy

HIGHLIGHTS

- A monitoring (T- RH) of a *Mithraeum* and *Hypogeum* was performed in Ostia Antica
- Multivariate statistical and PCA techniques were applied to evaluate the environments
- Study on semi-confined and underground environments in view of conservation

GRAPHICAL ABSTRACT

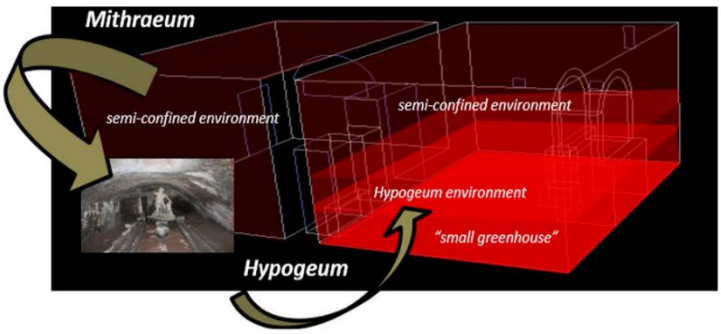

ARTICLE INFO

Article history:
Received 3 March 2016
Received in revised form 24 April 2016
Accepted 8 May 2016
Available online xxxx

Editor: D. Barcelo

Keywords:
Thermo-hygrometric parameters
Indoor monitoring
Mithraeum
Hypogeum
Multivariate statistic and chemometric analyses
Preventive conservation

ABSTRACT

Roman *hypogea*, vernacular settlements or crypts, are underground places characterised by specific and unique challenges (RH < 90% and almost constant temperature throughout the whole year) related to their relative isolation from the outdoor environment. These sites often require adequate monitoring tools providing complete environmental information in order to carry out appropriate strategies for scheduling routine maintenance and designing suitable layouts for their preservation.

In this work we present the results of a carefully planned thermo-hygrometric monitoring campaign conducted in a peculiar Roman building (130 CE), the "Casa di Diana" *Mithraeum*, sited in Ostia Antica (archaeological site, Rome-Italy), with the aim of characterising the indoor environment as the structure suffers of several conservation problems (biocolonisation, efflorescences, evaporating and condensing cycle for wall-building materials).

The campaign involving multipoint continuous measurement was carefully planned to better describe this micro-clime. In addition to underground environmental data available in literature, we have also performed, as a checkpoint control, a thermo-hygrometric monitoring campaign in the "Terme di Mitra" *Hypogeum*, a few meters from the "Casa di Diana".

The recorded data was analysed by multivariate statistical and chemometric analyses.

The results brought to light the presence of different microclimates (three areas) within a single *Mithraeum*: a room (*pre-Mithraeum*) and an area (*Mithraeum*: 2–4 m) present a thermo-hygrometric environmental behaviour

Abbreviations: T, temperature; RH, relative humidity; T_{dm}/RH_{dm}, average daily temperature/relative humidity; T_{min}/T_{max}, minimum and maximum temperature.

* Corresponding author.
E-mail address: claudia.scatigno@uniroma1.it (C. Scatigno).

http://dx.doi.org/10.1016/j.scitotenv.2016.05.050
0048-9697/

in accordance with a semi-confined environment, another area (*Mithraeum*: 1–2 m) behaves accordingly with underground environments (although it cannot be described as such), and the last area (*Mithraeum*: 0–1 m) where was recording RH values close to saturation (96–99%), associated with non-ventilated areas where the rising damp is "held" and not dispersed, describing an own micro-clime, comparable to a "small greenhouse". This study has allowed to identify some critical areas in view of planning future conservation solutions, without exporting the artefacts kept inside.

1. Introduction

Hypogea literally means "underground". It usually refers to an underground temple or tomb. The later Christians built underground shrines, crypts and tombs, which they called catacombs.

Thermo-hygrometric studies conducted in several *hypogea* (St. Calisto's and Priscilla's Catacombs and St. Marco, Marcelliano and Damaso, in Rome-Italy) recorded high values of relative humidity ≥95%, and temperature values typically range between 15 and 18 °C (Albertano and Urzi, 1999; Albertano and Bellezza, 2001; Cuzman et al., 2014). These studies were conducted focusing only on microbiological phenomena. In general, Roman *hypogea* are characterised by high relative humidity (≤90%), almost constant temperature throughout the year, and extremely low photon fluxes (Albertano and Urzi, 1999; Cardinale and Ruggiero, 2002; Compagnone et al., 1999; Cuzman et al., 2014). Roman *hypogea* are located in archaeological sites, where the preventive conservation is particularly complex due to the particular thermo-hygrometric features. Their conservative problems were concerned mainly the salt crystallization due to capillary rising (Casti, 2016) and biodeteriogenic presence caused by favourable microclimatic conditions (Cuzman et al., 2014). The preservation of *hypogea* is characterised by specific and unique challenges related to their relative isolation from the outdoor environment (Cardinale and Ruggiero, 2002; Cardinale et al., 2010; Visco et al., 2012a, 2012b).

Because of the extreme features of such environments, *hypogea* are not usually destined to worship or museum purposes. Additionally, the artefacts or decorations, such as wall paintings, organic-nature objects or funerary furnishings made of heterogeneous materials, are often removed from their original location and placed in museum environments, more suitable for their conservations (Mandrioli et al., 2003).

In the last years, in the context of closed or buried archaeological sites, a monitoring study of temperature and relative humidity was carried out in an Italian *hypogeum* by employing statistical tools for exploratory purposes, mainly focusing on the instrument validation and data treatment (Visco et al., 2012a).

In this work, a thermo-hygrometric monitoring and data analysis methodology (multivariate statistical and chemometric analyses based on principal component analysis (PCA)) was applied to the "Casa di Diana" *Mithraeum* (130 CE — 4th century), a Roman building located in the "Ostia Antica" archaeological site (Rome, Italy), with the aim of characterising the indoor environment where several damages are visible. The structure presents several problems: the building materials are affected by biological growth (Scatigno et al., 2016a, 2016b), along with the crystallization of soluble salts visible in the form of efflorescence (Scatigno et al., 2014, 2016b), compromising the durability of these ancient materials. Recent studies applied on this particular case reveal how the relative humidity close to saturation encourages phenomena of efflorescence, sub-efflorescence and biological proliferation (Scatigno et al., 2016b). This monitoring campaign involves multipoint continuous measurements carefully planned to better describe the indoor environment.

The "Terme di Mitra" *Hypogeum* monitoring (involving one sensor) was also conducted in order to serve as a checkpoint control, in addition to the data available in literature, which do not include multipoint continuous measurements.

2. Methodology

2.1. The "Casa di Diana" Mithraeum

Sixteen *Mithraea* (of which only one is set in a *hypogeum*: the "Terme di Mitra" *Hypogeum*) have been found in the archaeological complex of Ostia Antica. The "Casa di Diana" *Mithraeum* is situated in the north-eastern corner of the homonymous house (Fig. 1a). The "Casa di Diana" name is derived from a ceramic tile, found in the courtyard, representing the goddess Diana. The *Mithraeum* (a place dedicated to the cult of the Persian god Mithra during the Roman times) consists of two adjacent rooms, the "*Mithraeum*" and "*pre-Mithraeum*", each of which measures approximately 27 m^2 (Fig. 1b). The "Casa di Diana", Region I, Insula III, is set between the "Lucrezio Menandro" *Mithraeum*, to the north, and the "Molini" tenement, to the east. This structure is mainly composed of bricks and pozzolanic mortar aligned with the "*opus caementicium*" technique and was built in the central area of Ostia Antica approximately in 130 CE, remaining in use until the early fourth century. The house was originally made up of a ground floor and four upper floors; today, only the ground floor and traces of the projecting part of the continuous balcony of the first floor survive (Fig. 1c).

The *Mithraeum* has seven openings, five on the west side, facing the "triclinium" (one window and the entrance door are located in the *pre-Mithraeum*, while the remaining three openings are located in the *Mithraeum* at different heights on the west wall) and two passage areas between the two rooms (Fig. 1b). The podiums of the "*Mithraeum*" and the "*pre-Mithraeum*" are raised approximately 0.60 m above the central area of the communication trench (Fig. 1b).

2.2. Data-loggers' description

Taking into consideration that no funding was available, we utilized all the sensors momentarily available in the department laboratories, in spite of their difference always compatible with a coherent monitoring. Therefore, the monitoring survey involved nineteen data-loggers measuring temperature (Ta) and relative humidity (RH), specifically HOBO® (accuracy ±0.4 °C, ±2.5%) and EBI 20 (Ebro, accuracy ±0.5 °C, ±3%) data-loggers.

Regarding the thermo-hygrometric monitoring at "Terme di Mitra" *Hypogeum* (a few meters from the "Casa di Diana" *Mithraeum*), a Lascar EL-USB-2 (accuracy ±0.5 °C, ±3%) was utilized.

The sensors were calibrated before and after the measurement survey by placing the instruments in a "microclimatic chamber" producing thermo-hygrometric conditions coherent with those expected in the "Casa di Diana". In this way, before starting the measurement campaign, we checked the sensors' rising time, accuracy, hysteresis, and coherence. The obtained results, both for the temperature and relative humidity, are consistent with the standard deviation values (SD) declared by the manufacturer.

2.3. Continuous monitoring campaign: recorded data and positioning sensors

Continuous measurements at sampling interval of 5 min (HOBO®, accuracy ±0.4 °C, ±2.5%; EBI 20 — Ebro, accuracy ±0.5 °C, ±3%)

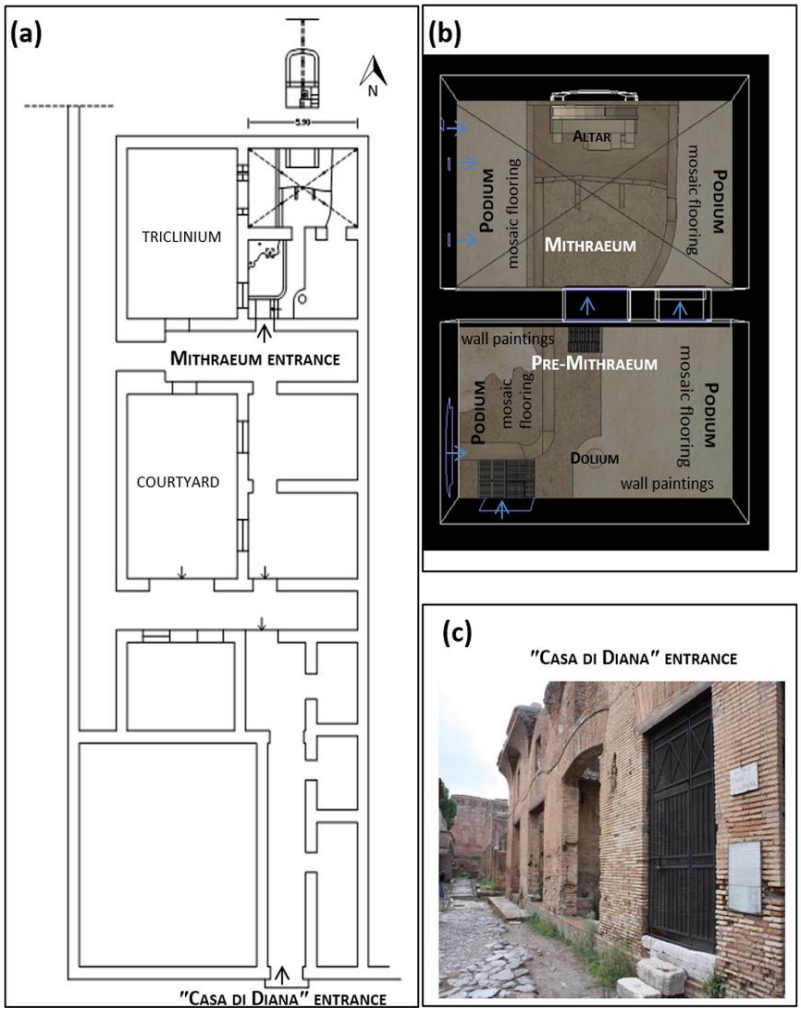

Fig. 1. Casa di Diana *Mithraeum*. (a) Plan of building. (b) *pre-Mithraeum* and *Mithraeum* rooms with the wall paintings, mosaic flooring and artwork (altar and *dolium*) kept inside.

were carried out in a period comprised between the 31st of July 2012 (summer) to the 15th of October 2012 (beginning of fall).

The survey was designed following the UNI 10969:2001 (Norma, 2002) and UNI 11131:2005 protocols, defining the modalities and principles of monitoring, elaboration and analysis of the microclimatic data as supporting actions for artefacts' preservation and, specifically, for measuring air humidity (Norma, 2005).

During a first phase, measurements were made along a grid of horizontal lines set at a height between 1.5 m and 5 m from the floor. Successively, we identified and selected the points to be used for continuous measurements on the basis of the results obtained in the first phase. A mixed sample design, involving both random and ad-hoc sampling, was adopted to cover the space of interest. As can be seen in Fig. 2, nineteen data-loggers were employed, one of which was placed in the "*triclinium*", a roofless room adjacent to the *Mithraeum* (HL green triangle), which reflects to some degree of the macro-environmental behaviour. The remaining data-loggers were appropriately placed in the *Mithraeum*, designing and implementing vertical (yellow triangles) and horizontal (red triangles) profiles (Fig. 2).

Thirteen data loggers were used along three profiles (two horizontal and one vertical axes):

- five data-loggers (E1, H8, H9, H10, H11) were placed along the vertical profile (at a distance between approximately 0.8 m and 1 m from each other) on a wooden pole at the centre of the room, almost at the same height as the vault (approximately 4 m);
- four sensors were placed on two horizontal axes (HA, HB, HC, HD, and HE, HF, HG, HH – approximately 2 m from each other), employing thin cords crossing the vertical profile at different heights (0.9 m apart from each other);
- The last six sensors were put in specific points that were considered to be of particular interest:

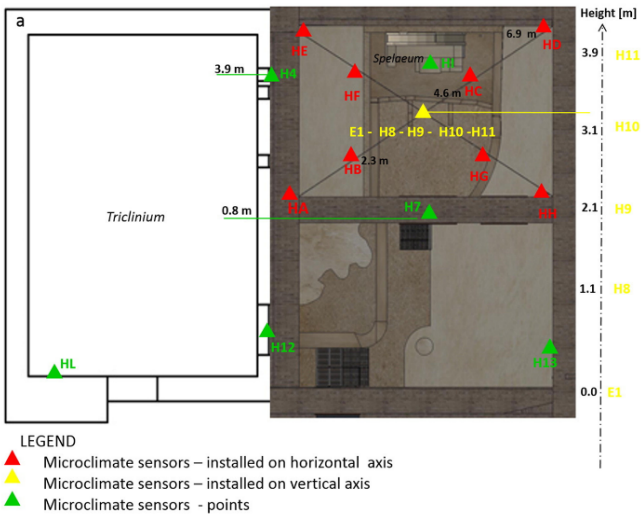

Fig. 2. Positioning of the sensors. The different colours of the triangles indicate the different typologies of placement of the sensors (point or installed on vertical and horizontal lines). The plan also indicates the heights and the distance between the data-loggers.

- one was placed in the *triclinium* (HL);
- two were placed in the *pre-Mithraeum* room on two different walls (SW, SE — one in front of the windows (H13) and the other inside the window (H12));
- one (HI) was placed inside the niche ("*spelaeum*");
- one (H4) was placed on the northwest wall at a height of approximately 3.9 m. It was placed close to a small opening, which is the only direct source of exchange with the outside environment, allowing the entrance of solar light at approximately 4 pm;
- the last one was located below the grid scale iron walkway (H7), an indirect source of exchange with the outdoors environments.

In order to compare microclimate and "macroclimatic" data, meteorological data was obtained from the "Ostia Pantanello" station (OPS) whose geographical coordinates (41°43′N, 12°21′E) are very close to those of the excavation of Ostia Antica (41°45′16.89″ N, 12°17′19.38″ E).

Regarding, the "Terme di Mitra" *Hypogeum*, the thermo-hygrometric data-logger was positioned at the south-east side of the complex at a height of approximately 1.5 m, a knot characterised by natural/spontaneous ventilation: the *hypogeum* is directly connected to the outdoors via three openings to other rooms (Fig. 1 — Supplementary Materials).

2.4. Data analysis

"Exploratory data analysis" (by run-sequence plots, box & whisker, scatter plot matrix) is usually performed in order to reveal possible correlations between the indoor and outdoor measured values, as well as to identify "spontaneous values", particularly important to describe particular environments like *hypogea* (Visco et al., 2012a).

In this work, aimed at characterising the data distribution and bringing out the behavioural characteristics of *mithraea* and *hypogea*, such as its dispersion or variability as well as areas particularly vulnerable (risk areas), representations as box-and-whisker, scatter plots, run time plots and histograms, are employed for the treatment of data concerning temperature and relative humidity.

Specifically, the preliminary analysis of the data obtained was carried out by means of box-and-whisker, where the variables (sensors) were plotted on the X-axis and the raw measured distribution was represented by the Y-axis. This powerful analytical tool shows (McGill et al., 1978) the median domain, the distribution, spread, skew and percentile values 5% and 95% (also outliers are show) by whiskers. This representation was being particularly significant because it revealed important results regarding the variable (sensors) distribution in the space (identifying the correlation with height and specific areas), pinpointing the areas characterised by a particularly high risk.

Successively, the scatter plot matrixes were designed, displaying all the possible Var-Var graphs (in our case: T/RH, RH/T) between all variables (sensors), starting from raw data, in order to enhance correlations as well as the distribution type of each variable on the vertical and diagonal. In our case, the distribution of all sensors' positions is displayed along the vertical profile, enhancing anomalies such as thermic inversions occurring in this particular area (centre of room). Such representation also highlights the air and humidity movement represented in the form of dispersion clouds.

Subsequently, multi-curve run time plots were plotted with the purpose of highlighting the co-linearity of data, focusing only on the three sensors that presented a different trend, bringing out the similar behaviour (underground environments).

A histogram featuring nineteen bars is shown for each variable, roughly allowing the identification of the distribution form. For mathematical validation purposes, a Gaussian curve displaying the temperature data was plotted: the chosen bin size of 0.5 °C allowed to obtain a tri-modal distribution.

Data was treated with OriginPro 8.5.1 and HOBO ware Pro version 3.7.2 software (Onset Computer Corporation' 2002–2015).

Finally, the principal component analysis (PCA) - whose primary aim is determining, from the geometrical point of view, the most significant reference basis representing the experimental data and minimizing the noise, confirming, in this way, some particular areas - was performed. This was possible using the Unscrambler version 9.7 (chemometric software package — Camo, Woodbridge, NJ, USA) package (cross validation method).

3. Results and discussion

3.1. Distribution analyses

The first step of the data analysis consists in studying, the box-and-whisker representation (Fig. 3) in order to evaluate the average thermo-hygrometric behaviour within the time-frame taken into consideration and identifying the correlation between the sensors' position and the physical parameters, characterising the indoor environment. The temperature remains stable: 90% of the temperature sensors reveal a symmetrical T distribution; the 10th and the 90th percentile are found at the same distance from the median value (Fig. 3a). In contrast, RH shows a higher amplitude: 100% of the humidity sensors show an asymmetrical data distribution (Fig. 3b); for this parameter, the 10th and 90th percentile are found at different distances. Of particular interest are the T gradients visible along the vertical vector (along arrow up Ebro, H7, H8, H9, H10 and H11 — Fig. 3a) and along two horizontal vectors. Their difference in height can be observed between the two horizontal arrows: HA, HB, HC and HD (lower down), revealing a lower temperature in comparison to that measured by HE, HF, HG and HH (upper arrow). The latter show the largest interquartile range. The 3th green arrow (Fig. 3a) indicates the HI sensor positioning in the *spelaeum* (or newsstand), middle position between H10 and H11 sensors (approximately 3.5 m).

A separate case is represented by the three sensors TMH, E1 and H7, which present a peculiar thermo-hygrometric behaviour (indicated with grey arrows and grey circle respectively in the Figs. ab). A lower T_{min}, of about 17.7 °C, is reached in the *hypogeum*, with a T_m of 21.9 °C; these values are followed by H7 and E1 (18.3 °C, 18.8 °C respectively) with a T_m of 22 °C. Concerning the RH, the previously discussed sequence presents the opposite trend: E1, H7 and finally TMH with 96.7%, 94.5%, 90.7% (T_m values) respectively (also in the T_{min} and T_{max} values). This thermo-hygrometric sequence reflects (in the *Mithraeum* context) the different positioning of sensors: E1 is placed at ground level (directly on the ground), whereas H7 at approximately 0.8 m of height. The values recorded by these two sensors are consistent with those measured by TMH.

The box-and-whisker representation also highlights that the position of each sensor characterises the specific area in which it is set: the H12 and H13 data-loggers are placed in the *pre-Mithraeum*, respectively on the bigger window and in front of it, representing the intermediate thermic-hygrometric values (downhill and climbing) between the values recorded by the vertical and the horizontal sensors (Fig. 3a, b); E1 and H7 represent an area which is part of the *Mithraeum* (until 0.8 m layer); all the remaining sensors are found in the *Mithraeum*.

Finally, it is possible (as briefly mentioned before), thanks to this positioning sensors strategy, to identify the thermo-hygrometric behaviour of the environment with respect to altitude, from the *pre-Mithraeum* to the *Mithraeum*: the T reaches its maximum value (T_{max} 28.2 °C) in the *Mithraeum* room, at a height of approximately 4 m, in correspondence of H4/H11 (placed on the bigger window and the wooden pole at the centre of the room, respectively), then decreases (T_{max} 25.4 °C) in correspondence of E1 (placed at 0.0 m). The T increases linearly with altitude (vertical gradient) (Fig. 4): from the bottom towards the top, starting from 22 to 25 °C (1 m), reaching a range of 25–29/30 °C (4.1 m) along the vertical profile.

Regarding RH, reaching in correspondence of the corners of house — *Mithraeum* (HA, HD, HE, HH) (Fig. 3b), it appears that its behaviour follows a vertical profile, presenting particularly high values (up to 99.2%) in correspondence of the lowest area (H7, E1) (RH_{max}), in contrast with the average value of 96.7% (during the monitoring period).

As shown in Fig. 4, contrarily to T, RH decreases with height, reaching maximum values (<95%) in the lowest strata (0–1.1 m), in correspondence to the position of E1, defining a less pronounced "cloud" of dispersion, underlining its low position (it is placed on the ground, at the lowest point of the vertical pole).

To furtherly analyse the correlation (coherence) between three sensors (TMH, E1, H7) run time plots by multi-curve representation (daily average) were plotted for both T_a (Fig. 5a) and RH (Fig. 5b).

Concerning the T, a high co-linearity is visible: three sensors show the same the thermic behaviour. A slight change is observable during the summer time (in the first 30 days of July) for the TMH sensor: the footprint marks a little difference, in term of short-term fluctuations, but in term of $T_{min/max}$ values, TMH is more similar to H7 (in particular in the first 10 days of July) (Fig. 5a). E1 recorded values higher than the other two.

Considering RH, it is possible to observe the same co-linearity during the autumn (Fig. 5b): the hygrometric behaviour recorded by all three sensors is equal. Furthermore, it is evident that TMH sensor records lower RH values than the other two: approximately 10% less than E1, and similar to the H7 sensor (±5%).

A histogram representation was plotted (Fig. 6) in order to visualise the changes occurring during the transition from summer to fall.

Fig. 6a, showing a significant bimodal trend for the temperature, points out the imprint of two different seasons (i.e., the end of the summer and the beginning of the fall). Fig. 6b, concerning relative humidity,

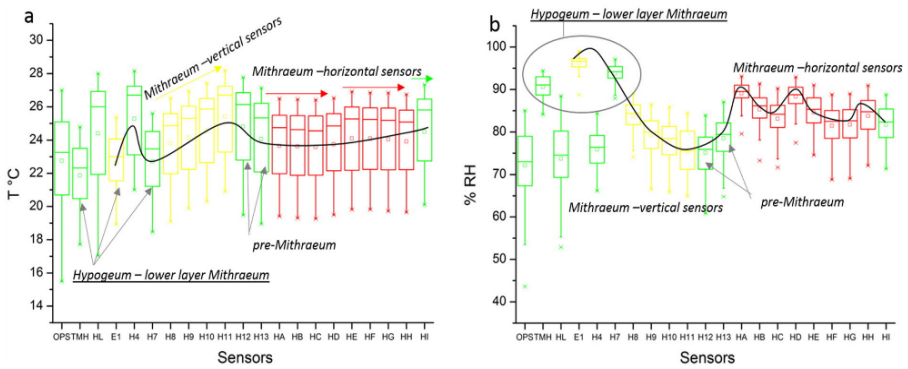

Fig. 3. Box-and-whisker. a) Temperature. The red horizontal arrows indicate the difference in height of positioning of the sensors along two lines (the 3rd green arrow indicates the third height represented by HL sensor, positioned in the *spelaeum*, between H10 and H11 sensors). The yellow arrow indicates the positioning of sensors along vertical line. b) Relative humidity. The circle indicates the TMH, E1 and H7 sensors. For both representations, the colour of the boxes is coherent with the typology of the sensors (point or positioning along horizontal and vertical lines). (For interpretation of the references to colour in this figure legend, the reader is referred to the web version of this article.)

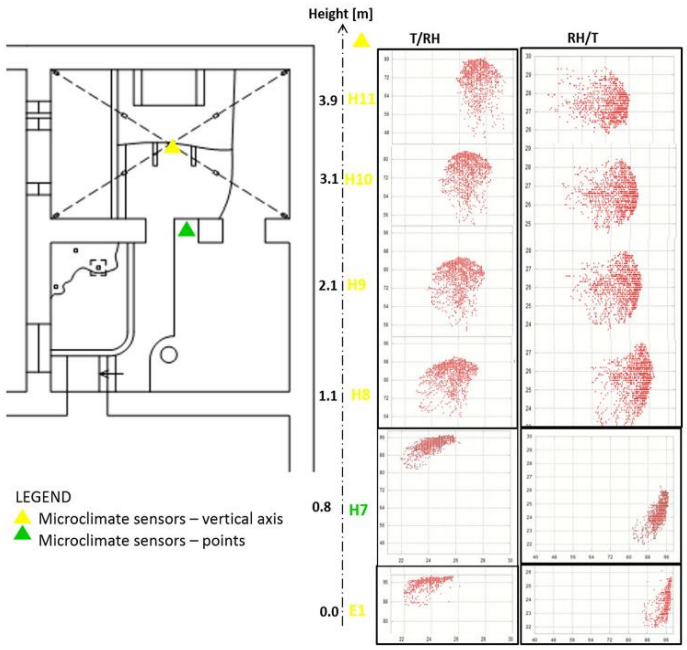

Fig. 4. Scatter plot (T/RH, RH/T) of microclimate sensors (vertical axis). The graph displays two variables for all sensors. Each scatter plot, illustrated on the right panel corresponds to a singular distribution.

thanks to a barely evident bimodality (the separation falls within the background noise) probably associated, rather than to a real change of regime, to the position of H7 (dark green) and E1 (light red) (see Fig. 2), reveals that the highest relative humidity values (96–99%) are present between 0.00 and 0.80 m from the ground, in the most humid and non-ventilated area (E1).

Moreover, concerning only the relative humidity data (Fig. 6b), each sensor outlines an individual Gaussian profile.

We performed a trial-and-error research to determine the Gaussian curve best fit to the temperature data: by utilising a bin size of 0.5 °C, we obtained a tri-modal distribution, as shown in Fig. 7 [Eq. n.1. Gaussian curve].

$$y = m_1 \frac{-(m_0-m_2)^2}{2m_3^2} + m_4 \frac{-(m_0-m_5)^2}{2m_6^2} + m_7 \frac{-(m_0-m_8)^2}{2m_9^2}$$

where m_2, m_5, and m_8 represent the average values of temperature and m_0, m_3, m_6, m_9 represent the standard deviation.

The tri-modality is coherent with a bi-modal trend due to the non-significant resolution between the m_2 and m_5 peaks: therefore, as can be seen in Fig. 7, the fit suggests two clear seasonal temperature profiles, fall (m_2, m_5) and summer (m_8).

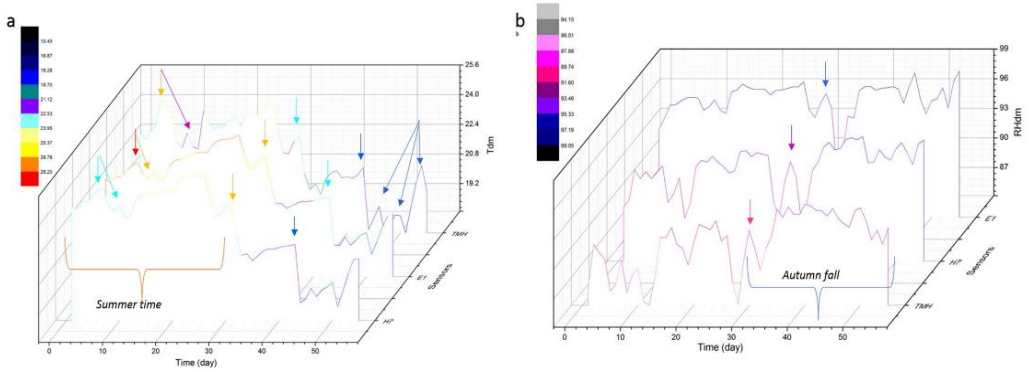

Fig. 5. Multi-curve run time plot for TMH, E1, H7 sensors. a) T_{dm} vs. day; b) RH_{dm} vs. day. The arrows indicate the co-linearity of the variables.

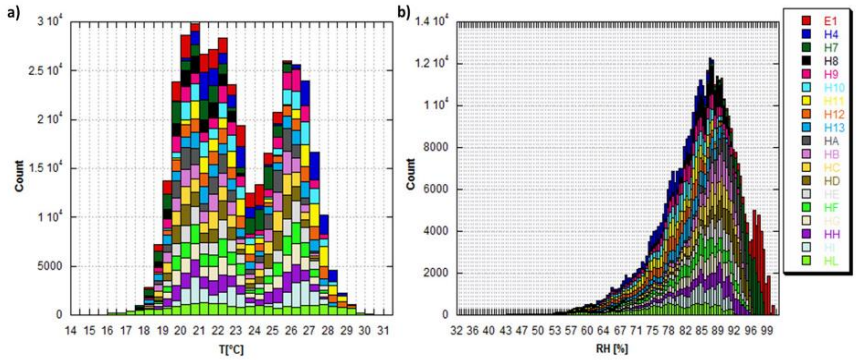

Fig. 6. Histogram, distribution for classes. (a) Temperature histogram, (b) Relative humidity histogram. The different colours correspond to different sensors, as shown in the two panels.

3.2. Principal component analysis (PCA)

In order to obtain further information about the variability of data related to RH (excluding data from meteorological station — OPS), chemometric analyses based on principal component analysis (PCA) were carried out using a cross validation method, after a previous auto scaling of the dataset.

At first sight, the PCA with two principal components explains 91% of the total variance (Fig. 8). The PC1, which explains the 83% of data variation, seems to be correlated with the height (between 0 and 4 m). There are clearly different clusters for the *Mithraeum*, correlated to the heights of the sensors and characterising different environments within the same room. The only exception concerns the sensors HA and HD which are positioned at corned walls at a height of 2.1 m. This deviation from the rest of the PCA results may derive from an accumulation of humidity in the corners, causing such data to be found in a cluster characteristic of lower heights. However, this phenomenon can be explained by focusing on the variability of the data (Fig. 3b): all of the sensors of a cluster feature similar data dispersion. This fact indicates that the PC1 is correlated both to the height and to the data variability.

Moving on to the analysis of the *pre-Mithraeum*, the data does not feature many differences caused by the height at which the sensors are positioned. This allows to consider the whole room as a unique, semi-confined, environment. This environment is characterised by air movements which correspond to the presence of the main entrance and several other openings (the windows). The PC1 value for this semi-confined room is similar to the that shown by the highest sensors of the *Mithraeum*, probably because such layer also behaves (2.1–4 m) as a semi-confined environment, thanks to the presence of the shared door connecting the rooms.

The third area under study, the *hypogeum*, has low values of PC1, despite of its height (1.5 m). This fact could be associated with its very low data dispersion (Fig. 3b). The position of the E1 sensor, with PC1 values lower that the *hypogeum* constitutes a remarkable case. Such features are not only caused by the height of the sensor, but also by its minor data variability, which reminds of the *hypogeum* behaviour.

Concerning the temperature data, the PCA was not able to give significant information.

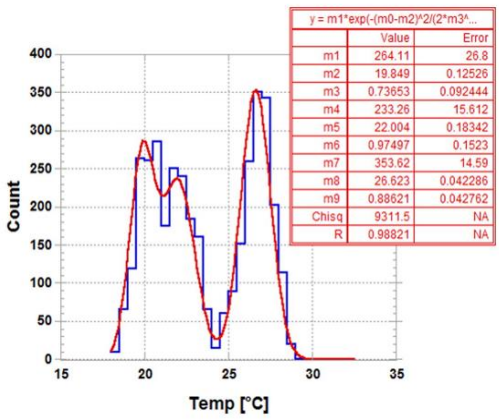

Fig. 7. Temperature of all sensors. Gaussian curve.

4. Conclusions

In this work we proposed a specific thermo-hygrometric monitoring campaign involving multipoint continuous measurement carefully planned to better describe the indoor environment of a particular *Mithraeum* (sited in Ostia Antica — Rome, Italy) identifying the critical areas, where the wall building materials and the artefacts or decorations (altar, mosaic floor, wall-paintings, ceramic object, pumices) are mostly at risk.

Data analysis brought to light the presence of different microclimates within a single *Mithraeum*.

The temperature kept stable (T_m 23 °C) throughout the monitoring campaign: 90% of the temperature sensors reveal a symmetrical T distribution and the daily temperature variations are not significant. Sensors placed at the same height but at a different distance from the openings show that the external climatic conditions have a minimal influence on the indoor climatic conditions, in contrast with what is expected of a semi-confined, rather behaving as *hypogea* environments, characterised by their relative thermic isolation from the outdoor environment (Visco et al., 2012a).

At the centre of the *Mithraeum* room, a vertical T increase from the ground level going up was observed, identifying an area of thermic inversion, a phenomenon which is particularly dangerous for the altar (made of different materials, pumice, pozzolanic mortar), which is also subjected to a thermic variation (resulting in mechanical changes) due to a great amplitude of T (22–29 °C) in only 4 m of height.

Relative humidity shows a higher amplitude of data: 100% of the humidity sensors show an asymmetrical data distribution. High values were recorded (RH_m 85.4%), considering both the *pre-Mithraeum* and the *Mithraeum*. Particularly high hygrometric values were recorded in specific areas of the *Mithraeum*. Increasing are visible in correspondence of the '*Mithraeum*' corners (RH_m 89.6%), particularly intense in

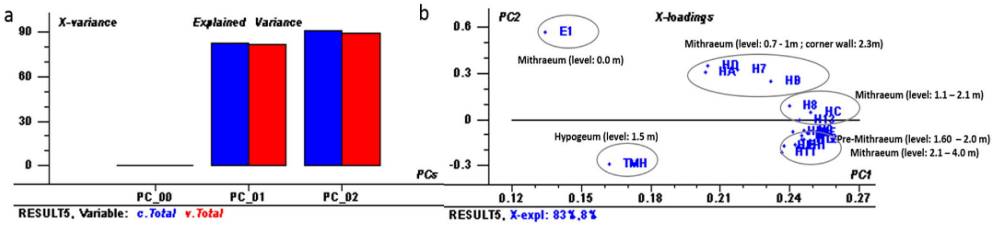

Fig. 8. PCA. a) Explained Variance (RH); b) X-loadings (RH).

correspondence of the lowest area (0–1.1 m), reaching values of 99.2% (RH_{max}). The average RH value recorded is of 95.6%, in accordance with the values typically recorded during *hypogea* studies (90–95%) (Albertano and Bellezza, 2001; Cuzman et al., 2014) and with those measured by TMH. This lowest area suffers of several conservative problems (biological growth and visible efflorescence salts) (Scatigno et al., 2016a, 2016b) due to rising damp (comes from under the floor).

The results brought to light the presence of different microclimates (three areas were distinguished) within a single *Mithraeum*: a room (*pre-Mithraeum*) and an area (2–4 m) with a thermo-hygrometric environmental behaviour in accordance with semi-confined environments, an area which presents a behaviour similar to underground environments (even though it is not a subterranean place), and a last area (lowest strata: 0–1.1 m) where the recorded relative humidity values were very close to saturation (96–99%), associated with the lack of ventilation area, causing the rising damp to be "held" rather than dispersed, inscribing a separate micro-clime, describable as a "small greenhouse".

This study has allowed to identify some critical areas in view of planning future conservation solutions, without the need to export the artefacts kept inside.

The results reveal that the environment studied is characterised by a very particular micro-environment, which requires a careful planning of solutions for its conservation.

Supplementary data to this article can be found online at http://dx.doi.org/10.1016/j.scitotenv.2016.05.050.

Acknowledgements

The authors thank the archaeological area of Ostia Antica, in particular the director Dr. Cinzia Morelli, the security company, and the technical staff (Drs. Paola Germoni, Flora Panariti, Orietta Mantovani) for the permission to work in this house. Claudia Scatigno is grateful to Dr. Filippo Ambrosino for his collaboration in using the Matwork programme for part of the data treatment, Claudia Moricca for the English revision of the manuscript and Nagore Prieto-Taboada for her help with the PCA results' discussion.

References

Albertano, P., Bellezza, S., 2001. Cytochemistry of cyanobacterial exopolymers in biofilms from Roman hypogea. Nova Hedwig. Beih. 123, 501–518.
Albertano, P., Urzì, C., 1999. Structural interactions among epilithic cyanobacteria and heterotrophic microorganisms in Roman hypogea. Microb. Ecol. 38, 244–252.
Cardinale, N., Ruggiero, F., 2002. A case study on the environmental measures techniques for the conservation in the vernacular settlements in Southern Italy. Build. Environ. 37, 405–414.
Cardinale, N., Rospi, G., Stazi, A., 2010. Energy and microclimatic performance of restored hypogeous buildings in south Italy: the "Sassi" district of Matera. Build. Environ. 45, 94–106.
Casti, M., 2016. Cristallizzazione del Solfato di Sodio in Calcari Biomicritici: L'uso di Inibitori per la Mitigazione del Degrado.
Compagnone, D., Di Carlo, V., Bruno, L., Albertano, P., Palleschi, G., 1999. Development of oxygen microsensors for monitoring cyanobacterial photosynthesis in Roman hypogea. Anal. Lett. 32, 213–222.
Cuzman, O.A., Tapete, D., Fratini, F., Mazzei, B., Riminesi, C., Tiano, P., 2014. Assessing and facing the biodeteriogenic presence developed in the Roman Catacombs of Santi Marco, Marcelliano e Damaso, Italy. Eur. J. Sci. Theol. 10, 185–197.
Mandrioli, P., Caneva, G., Sabbioni, C., 2003. Cultural heritage and aerobiology. In: Anonymous (Ed.), Methods and Measurement Techniques for Biodeterioration Monitoring. Springer.
McGill, R., Tukey, J.W., Larsen, W.A., 1978. Variations of box plots. Am. Stat. 32, 12–16.
Norma, U., 2002. UNI 10969:2001 Beni culturali. Principi Generali per la Scelta ed il Controllo del Microclima per la Conservazione dei beni cull'urali in Ambienti Interni.
Norma, U., 2005. UNI 11131:2005. Beni culturali – Misurazione in Campo Dell'umidità Dell'aria Sostituisce il Punto 13 Della NORMAL 5/83.
Scatigno, C., Sammartino, M.P., Gaudenzi, S., 2014. Non-invasive analysis of soluble salts. Preliminary Results on the Case Study of Casa di Diana Mithraeum (Achaeological Site of Ostia Antica – Italy).
Scatigno, C., Moricca, C., Tortolini, C., Favero, G., 2016a. The influence of environmental parameters in the biocolonization of the Mithraeum in the roman masonry of Casa di Diana (Ostia Antica, Italy). Environ. Sci. Pollut. Res.
Scatigno, C., Prieto-Taboada, N., Preite Martinez, M., Conte, A.M., García-Diego, F.J., Madariaga, J.M., 2016b. Analitycal techniques for the characterisation of historical building materials: case study "Casa di Diana" Mithraeum (archeological site in Ostia Antica, Italy). In: Wythers, M.C. (Ed.), Advances in Materials Science Research (New York).
Visco, G., Plattner, S.H., Fortini, P., Di Giovanni, S., Sammartino, M.P., 2012a. Microclimate monitoring in the Carcer Tullianum: temporal and spatial correlation and gradients evidenced by multivariate analysis; first campaign. Chem. Cent. J. 6, S11.
Visco, G., Plattner, S.H., Fortini, P., Sammartino, M.P., 2012b. Second campaign of microclimate monitoring in the carcer tullianum: temporal and spatial correlation and gradients evidenced by multivariate analysis. Chem. Cent. J. 6.

Thus, thanks to data processing techniques based on multivariate statistical and chemometric analyses, it was possible to bring to light the presence of different microclimates within a single *Mithraeum*, discrediting the only semi-confined environment behaviour and the identification of some critical areas (corners, centre of the *Mithraeum* room) where the wall-building materials and the artefacts or decorations are mostly at risk (altar) due to the presence of heterogeneous RH values, more uniform (defining a less pronounced "cloud" of dispersion) in the non-ventilated area.

In this sense, the presence of different microclimates (three areas were distinguished) in the same volume indicates that the two rooms are not behaving in the same way, despite the presence of the shared door connecting the rooms. In microclimatic terms, this connection is "unreal", as the air movement is not such as to enable the meshing among them. This is peculiar, as the rooms are only separated by a partition segment of about 1 m, compared with the 4 m of the entire wall, completely free.

Finally, another fact to take into consideration is the presence of several openings (windows and main door) which expose small areas to sunlight and outer air, especially from one window of significant dimensions (1.48x1.16m), set on the west side (*pre-Mithraeum* room). This last opening should be allowed a good air mixing. It is important to underline that no ventilation systems are found so, the ventilation is completely natural.

For all of these, the framework presents a very characteristic microclimate and a study on air turbulence could be helpful for identifying the "spontaneous values", disclosing the anomalies, particularly important for a complete safeguard of the place and of the visitors (an adequate air movement results in a good air quality) [33].

5.2 Indoor monitoring. Air turbulence study and Computational Fluid Dynamics (CFD) simulation[18]

Studies regarding the evaluation of indoor conditions of historical buildings [34] are in constant increase, to simulate the penetration, dispersion and deposition of particulate matter [35] (especially in terms of the adequacy of the natural microclimate [36-38]), to identify the suitability of a chosen indoor environment, equipped by HVAC (heating, ventilation and air conditioning)

[18] An adapted version was published in:
Preliminary data of CFD modelling to assess the ventilation in an archaeological building. 8th International Congress on Archaeology, Computer Graphics, Cultural Heritage and Innovation. Arqueològica 2.0 in Valencia (ES). ISBN: 1989-9947.

system or not (passive system). The final goal of studying the "optimal conditions" for the Good's Preservation. In particular, this evaluation is further complicated if the Goods to safeguard are archaeological sites, where (until now) systems to fully understand the real behaviour do not exist [37, 39], because they are not purely "closed systems".

In this sense, there are many environmental factors that contribute to the deterioration of heritage sites including wind action, groundwater, humidity, pollution, vibrations and seismic shocks [40]. Among them, the wind flow is one of the most aggressive factors, causing the erosion of monuments, especially those located in open areas. To investigate the wind structure over complex sites, field studies are often replaced by numerical studies, as full-scale measurements, which provide data on ventilation rate, Qa distribution and mean Va around and inside a building, reducing costs and proving to be less time-consuming.

Thus, in recent years, numerical studies, often called Computational Fluid Dynamics (CFD), have definitely become one of the most useful tools for studying the atmospheric wind environments, primarily thanks to the increasing power of new generations of computers. Furthermore, CFD simulations can provide information on all flow parameters in the entire modelling domain. CFD could also be a more cost-effective way in comparison to traditional wind tunnel studies, for the cases of wind flow investigations involving complex terrains, in absence of accurate physical models.

In bibliography, no three-dimensional CFD-based simulations with the successive validation have ever been performed to study the wind environment over a heritage site. There are some interesting cases where the wind environment is simulated over heritage sites like the Giza Plateau [41] or with particular attention to the Great Sphinx [42], adopting CFD simulation based only on literature survey over complex terrain, without field measurements. Consequently, for not restricting this study only to literature surveys over complex terrain, including implementation issues and guidelines for wind environment predictions (appropriate boundary conditions and the construction of an adequate and effective computational mesh) two campaigns of field measurements were also conducted to validate the simulation processed. One was carried out through 12 multiples sensors[19] (continuous measures per 4 days) and the other one through one 3D sensor[20] (per 1 day, placed in different points, covering the essentials area), in order to find a suitable instrumentation system to validate the simulations.

[19] Air velocity, air temperature and differential pressure.
[20] Anemometer.

In this context, a three dimensional (3D) CFD model and direct measurements for verification and validation (V&V) was developed to assess the ventilation issues (airflow patterns, air and Ta distribution and velocity) of this historic building, studying the airflows. In this sense, the influence of wind was assessed in terms of building material conservation (erosion and facilitation of evaporation processes) and the AQ (air exchange or Qa) was evaluated, with the final goal to find an appropriate solution, providing a proper microclimate, developing, in this way, a future global plan for conserving and protecting the site.

Taking all of these into account, the simulation phase was conducted with special attention (field measurements without 3D scanner and then converted into CAD format in order to be readable by the volume mesh generator), with the purpose of building an accurate geometrical model (objects/solids added to the whole volume/fluid). The building had different height levels deriving from the presence of structures like the altar (supported by a raised floor of 0.72 m) and "*podiae*" (about 0-0.70 m from the pedestrian level), seats for the Romans that assisted the sacrificial ritual of the killing of the bull. Due to this particular geometry and the novelty of CFD applied to build heritage of this complexity, the CFD simulation was created disregarding the lower strata. However, these lower strata were already characterised in a previous environmental work (**Chapter 5.2**), which defined them as a "small green house" or non-ventilated area. Therefore, a study on air turbulence would be considered completely unsuitable. Instead, a greater focus was placed on studying of the area of transit (connection area) where it is possible to predict, and later to validate, the velocity inlet and outlet.

Along with different CFD commercial software, the computational domain was built using the FLUENT 6.2 (Fluent Inc., Lebanon, NH, USA) software (already used for the study of ventilation in different types of buildings [43, 44]), in order to carry out all the simulations; while the geometry model and meshes were developed using a pre-processor Gambit v. 2.3 (Geometry and Mesh Building Intelligent Toolkit) of FLUENT [45]. No simplifications were performed, except from the roof. Actually, the two rooms present groined vaults, thus they were readapted to flat arches. Notwithstanding this last simplification, the computational mesh for this geometry was extremely complicated due to the diversity of dimensions of objects (altar) and other features like "boxes" (door, openings, arched window), building a different volume mesh for each one of them, obtaining a real reproduction. The main factor that affects the mesh near the wall surface is the roughness. A factor of 0.5 was taken into consideration in the model.

Specifically, the FLUENT software uses the Finite Element Method (FEM) to solve equations (a set of partial differential equations) of conservation for the different

quantities transported in the flow (mass, momentum, energy, water vapour concentration). These equations are the equation of continuity, the conservation of momentum (or Navier-Stokes Law – laminar regime) and the conservation of energy, that describe fluid flow, deducted for incompressible viscous Newton flow for both Cartesian and axisymmetric coordinates.
The Equation 1 integrates these equations in a single one.

$$\frac{\partial}{\partial t}(\rho\varphi) + div(\rho\vec{u}\varphi - \Gamma_{\varphi} grad\varphi) = S_{\varphi} \quad (1)$$

Where, ρ is the density of the fluid (air), φ is the variable of interest, t is the time, $\vec{u}$ is the velocity vector, $\Gamma\varphi$ is the diffusion coefficient of φ and $S\varphi$ is the source term of φ.

To investigate the development of the ventilation flow inside the rooms studied, considering a single volume (164 m^3), a time dependent simulation based on the turbulence model RANS (Reynolds Averaged Navier-Stokes) with standard k-ε (k turbulent kinetic energy and its dissipation rate ε - two equations model) turbulence model was performed. A large domain of computation was generated as a 3D full model of the two rooms. The 3D model did not take into account the lower strata (0 -0.70 cm from the pedestrian level), as previously said.

The CFD simulation requires a repetition of the solution of the fluid flow equations, starting from initial guess, until it converges. The flow variables are recalculated in each of the repetitions until the equations are solved up to a user-specified threshold. The termination criterion is usually based on the residuals of the corresponding equations. These residuals should tend to zero. In this case, the scaling of the residuals was done with the residuals after the first iteration, for a total of 8000 iterations. A reduction of the residuals of at least four orders (10^{-4}, convergence value) of magnitude, along the x, y and z velocity, was applied.

The mesh density was selected after four attempts in order to combine the solution accuracy with reduction of computational time, needed for convergence and to obtain a stabilisation of the results. The computational domain was discretized using a grid (0.05 m mesh spacing, 0.1 m for windows), mainly composed by tetrahedral elements, obtaining, in this sense, a very good quality of the mesh (2 mill., obtaining an accuracy of less than 3%). This form is in fact more suitable for our building.

The CFD software also requires some Boundary Conditions (BC) (air velocities - Va, pressures - P and Ta for inlets, outlets and for surface elements boundaries) to perform the CFD simulations. In this perspective, using suitable sensors, pressure and air velocity at the windows, doors and holes were measured, as well as the

temperatures at the walls, floor and air. Buoyancy plays an important role in the natural and mixed convective flow regimes [46], as in our case. All of the boundaries of the volume-meshes of the inner domains were marked as ''Interface-Boundary''. The flow was considered to be fully turbulent and incompressible. The wind environment over heritage sites is governed by the conservation laws of mass and momentum [41]. The flow is assumed to be three-dimensional, incompressible Newtonian fluid with constant density (1.225 kg/m^3) and constant viscosity (1.7894e-0.5 kg/m/s). However, Boussinesq assumes the turbulence stresses to be the product of the fluid strain and an eddy-viscosity.
The ground boundary conditions for the velocity are formulated based on the ''wall-function'' theory. These standard wall functions were modified for the specific roughness value.

Taking all of these into account, different BCs and meshes (line, surface and volume) were performed (**Figs. 19-21**).

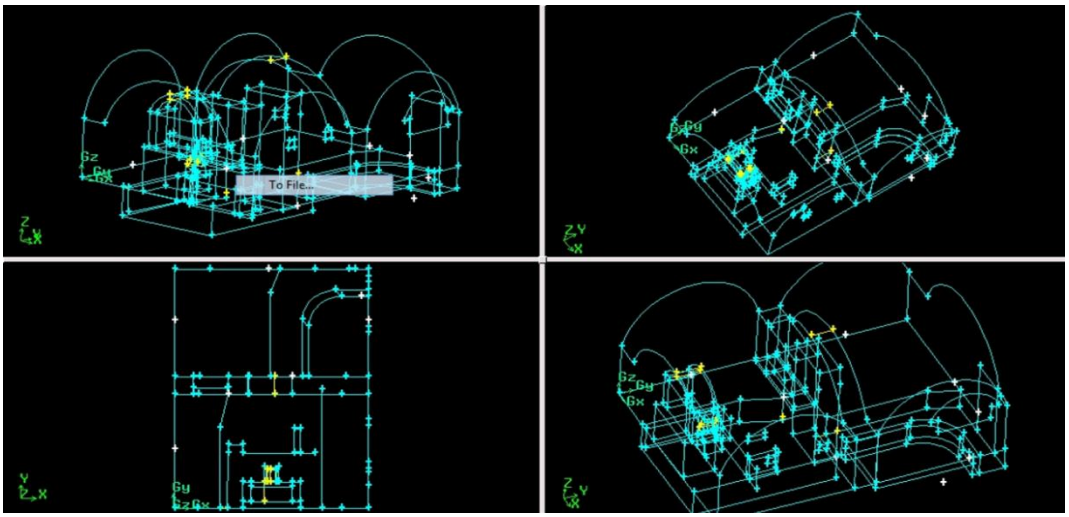

Figure 19. Screen graphic: phases (different point of views) of geometry building (point cloud), made by pre-processor Gambit.

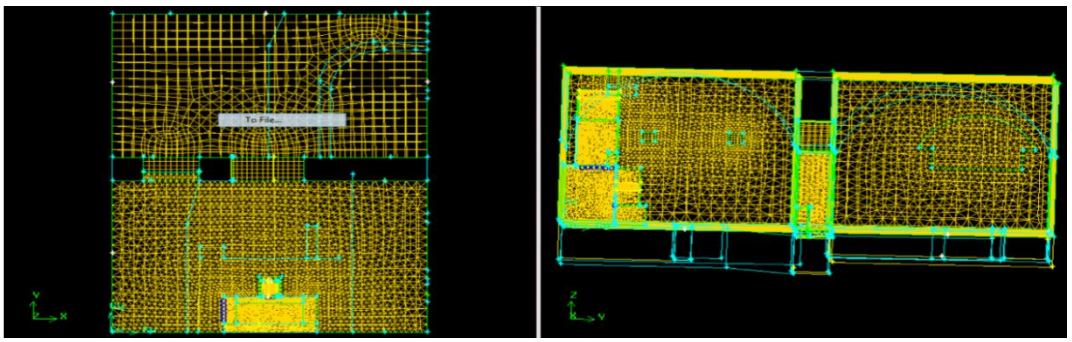

Figure 20. Screen graphic (different point of views): phases of geometry building (meshes) made by pre-processor Gambit.

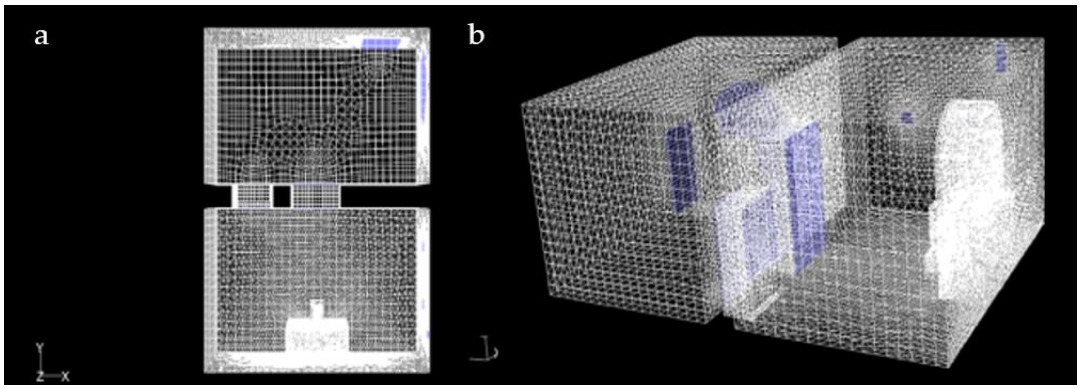

Figure 21. Mesh importation in FLUENT (computational domain). **a**) 3D slice representation (before meshing); **b**) 2D slice representation section plane (top view); **c**) 3D representation. The blue areas indicate the openings (main entrance, windows and openings).

Thereafter, CFD simulations were performed (exporting the mesh in FLUENT with a 3ddp- 3d double precision). Specifically, several simulations were carried out supposing that the Va[21] came from the main entrance and window (blue boxes, *pre-Mithraeum*, **Fig. 22**) with values of 0.24 m/s and 0.19 m/s (air inlet), respectively and an P outlet[22] from the three small openings (red boxes, *Mithraeum*, **Fig. 22**). With this initial hypothesis, a range of 0-4 m/s was considered as a maximum range (to appreciate some differences).

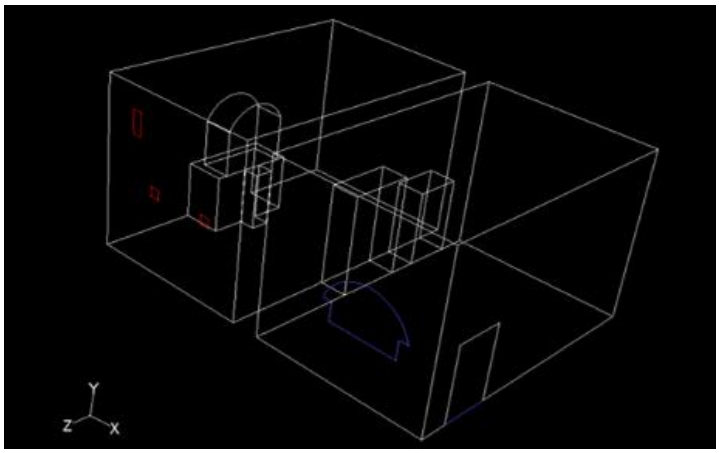

Figure 22. Starting model.

[21] That is of an expected Va in a direction perpendicular to each wall. In this sense, 0.24 m/s on north direction (from main door) and 0.19 m/s on east direction (from the window).
[22]101 325 Pa.

As can be seen on **Figure 23** (**a-f**), the Va expected (with a range 0-0.40 m/s) at 0.5 m above the ground run from 0 (corners) to 0.24 m/s in correspondence of the main entrance, central passage and the opening on the right side (**Fig. 23a**).
Gradually, as the level rises up to 1.5 m above the ground (**Fig. 23b**), the window, the upper part of the door (*pre-Mithraeum*) and the small openings (*pre-Mithraeum*) become the protagonists, achieving a Va expected of 0.20 m/s, 0.26 m/s and 0.40 m/s respectively (while the values for the central openings slightly decrease, 0.14-0.10m/s). When taking into account the plane at 2 m (**Fig. 23c**), the main entrance and the right connected area do not affect the model, while two small openings preserved their 0.40 m/s.

Considering the third opening, the uppermost, sited in the *Mithraeum* room, it is noticeable that the simulated Va of 0.40 m/s affects the left corner of north wall (**Fig. 23d**), where the altar is found. It is interesting to observe how the simulated Va (on vertical planes) focuses on the middle of volume (between the two rooms), with a velocity profile reaching 0.40 m/s only on left side, due to an opening set on the west side of *pre-Mithraeum*. In general, however, these communication areas presented a relatively low Va (max 0.08 m/s considering the vertical plan at 3 m, *pre-Mithraeum*, until 0.22 m/s considering the vertical plan at 5 m, *Mithraeum* - **Fig. 23e**). Thus, in terms of the vertical plan, the velocity profiles expand in the *Mithraeum* room. In contrast, while considering the horizontal plans, the lines are reducing, but only until 1 m from the ground (to 2 m the velocity contours become more intensive and with minor amplitude thanks to the small openings).

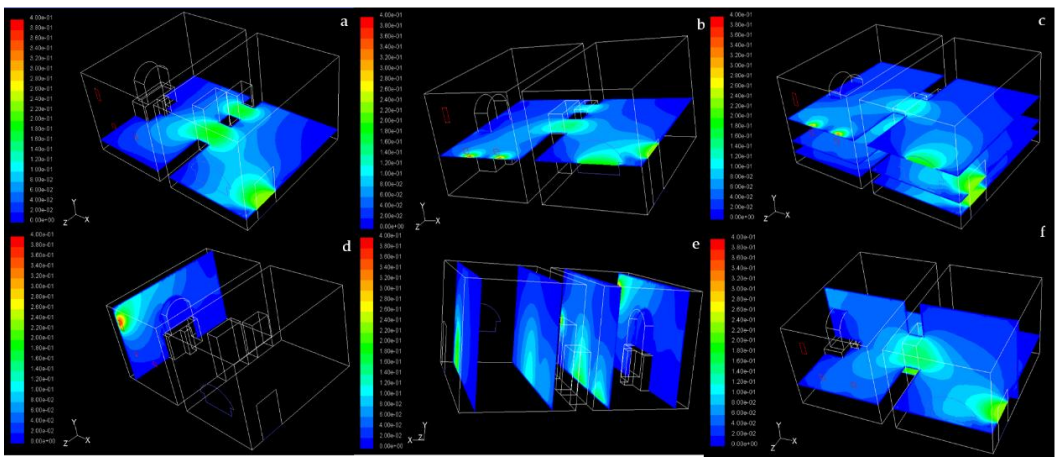

Figure 23. Velocity contours. **a**) Velocity contours (one horizontal plane) expected at 0.5 m above the ground; **b**) velocity contours (one horizontal plane) expected at 1.5 m above the ground; **c**) velocity contours in three horizontal plane at 0.5 m, 1 m and 2 m respectively; **d**) velocity contours (one vertical plane) at north wall (*Mithraeum*); **e**) velocity contours (4 vertical planes) expected at 0.5 m, 3 m, 5 m and 7.5 m, starting to the north wall of *Mithraeum* room, respectively; **f**) velocity contours in two floors (at 1 m – transverse plane, at 2.45 m - horizontal plane).

Simulating the Va near the walls (0.5 m), velocity contours were carried out, taking into account the walls on the east side (**Fig. 24**). Considering a range of 0-4 m/s, no significate differences are noticeable (**Fig. 24a**). The Va is zero.

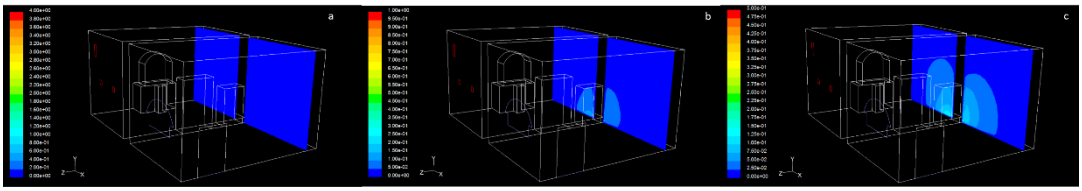

Figure 24. Air velocity contours. **a**) range of 0-4 m/s; **b**) range of 0-1 m/s; c) range of 0-0.5 m/s.

Changing the range (0-1 m/s), some differences can be pointed out (**Fig. 24b**). Only when a range of 0-0.5 m/s is considered, it is possible to observe a Va until 0.17 m/s (**Fig. 24c**).

In addition, trajectory simulations (path lines) were performed in the whole building (**Fig. 25**), in order to simulate flow direction and vortices. At first sight, the ability of the CFD simulations to predict airflow in archaeological site was clear. Some small vortices were found in correspondence with the altar (**Fig. 25a-d**), the only object (solid) input in the computation domain. In correspondence with the corners of walls, the wind speed is zero (as on evidence in the **Fig. 23**). It is possible to predict an air movement, with a curved shape (**Fig. 25a-d**), describing as U shape (considering both the horizontal plane – **Fig. 25a, d**, and the vertical plane – **Fig. 25b-d**).

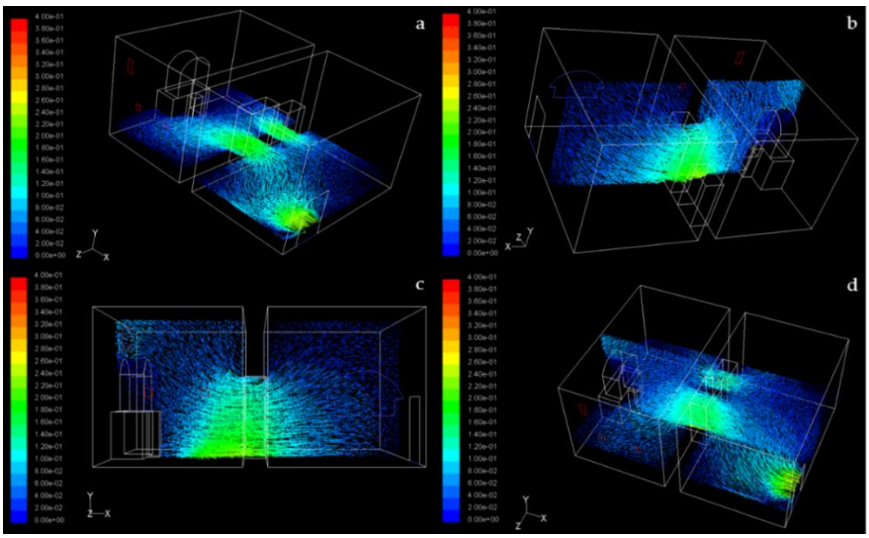

Figure 25. Path lines of the velocity magnitude expressed in m/s. **a**) Va at 0.5 m above the ground; **b**) Va simulation through the central area (vertical plane); **c**) Va simulation through the central area (vertical plane); **d**) Va simulation in two floors (at 1 m – transverse plane, at 2.45 m - horizontal plane).

Taking into account the experimental measures, in order to verify the model, direct measurements were performed. Specifically, two monitoring campaigns were conducted. The first one was carried out by positioning 12 multiple sensors devices [14] (**Fig. 26, Tab. 1**) that measure Va, Ta and ΔP. Plastic rods were appropriately positioned (from the 0.70 cm up to the ceiling –**Fig. 26b**). For each rod, 2 multiple sensors were fixed, except for the sensor positioned near the window (V29 – position n. 12). This first campaign was performed on the 26-29th of April 2014.

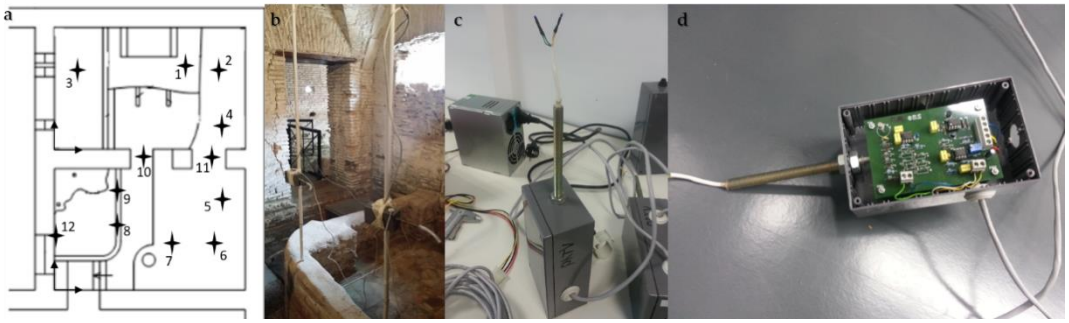

Figure 26. Positioning and technology of the multiple sensors. **a**) Plan of the measured points; **b**) *in-situ* positioning; **c**) multiple sensor (external view); **d**) technology sensor (interior view).

Table 1. Spatial coordinates.

POINT MEASURED	NAME SENSORS	SPATIAL COORDINATE		
		x (cm)	y (cm)	z (cm)
1	V11	417	246	282
	V12	417	246	100
2	V01	520	174	277
	V02	520	174	110
3	V09	9	242	282
	V10	0	242	174
4	V04	510	101	239
	V05	510	101	96
5	V17	500	315	241
	V18	500	315	78
6	V15	433	165	277
	V16	433	165	81
7	V13	305	160	287
	V14	305	160	77
8	V25	215	174	270
	V26	215	174	74
9	V27	227	274	260
	V28	227	274	83
10	V31	273	425	225
	V32	273	425	136
11	V06	447	431	142
	V08	447	431	87
12	V29	0	126	160

A second, more recent campaign (21st March of 2016), was carried out with one sensor (ultrasonic anemometer 3D -Thies Clima, Ammonit GmbH, Germany), which was moved in different points to map the area, considering the more ventilated areas (near to the openings: main entrance, windows – n. 3, 4, 8), the middle of the two rooms (within three central points – n. 1, 2, 7) and the central area (n. 5, 6), the shared "door" that connects the rooms (**Fig. 27, Tab. 2**).

The numerical results were obtained from a limited number of cases, i.e., these measured inputs were determined by the meteorology of the day of the field experiments, precisely in only one day with non-extreme meteorological conditions (21st March of 2016). Anyway, the model represents a good compromise with the real context, despite the Va not representing extreme conditions. Indeed, the previous monitoring campaign (**Chapter 5.1**) pointed out that the external climatic conditions have a minimal influence on the indoor environment (high thermic insolation from the macroclimate).

The simulation results were in agreement with the trends of Va and Ta of the experimental values measured during the two campaigns. The data treatment is still also under study. However, taking into account some of the first results, it was possible to highlight several important issues.

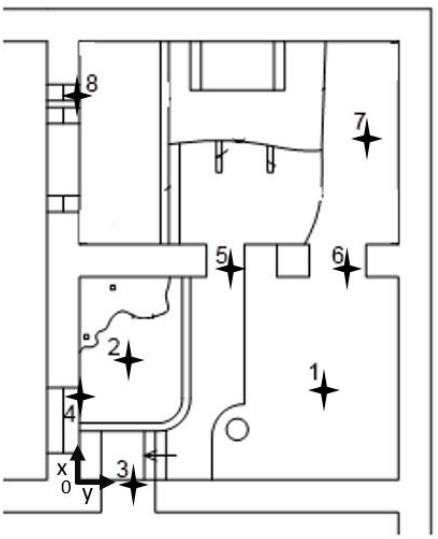

Figure 27. Positioning of the sensor.

Table 2. Spatial coordinate.

n. point measured	Spatial coordinate		
	x (cm)	y (cm)	z (cm)
1	490	170	138
2	84	224	138
3	0	100	138
4	110	0	165
5	280	403	138
6	402	475	138
7	667	510	138
8	647	0	221

A significant difference was found between two rooms. In particular, Va reach a zero value in a corner, pointing out the possibility of condensation phenomena. The wind speed presents different velocity contours. The air movement seems to follow a U shape. During the experiment, the Qa rates, which pass through the wholes, were small: no relevant wind gusts were detected during such day. As a consequence, no indoor air velocities changes appeared neither in direct measurements with sensors, nor in CFD results. Of course, seasonal changes and several wind gusts could also modify the nature of indoor microclimate of the monument. The next field measurements will be carried out in different seasons and in extreme meteorological conditions in order to compare the results.

In general, the data check confirms, with ± 10%, a good correspondence (model) between the numerical solutions and the data deriving from direct measurements, by both multiple and portable sensors. For this reason, the model proposed could be applied on similar cases, such as buildings characterised by different BC, to predict without direct measurements, the air movement in these ventilated spaces.

Within the results outcome, it is important to highlight that, at heights lower than 0.50 m, the wind speed is zero, thus, in the first of 1.2 m (also considering the *podia*'s structure), the air turbulence is absent and in the whole of volume is very low (0-0.4 m/s). This last issue indicates that good ventilation is not present and, by linking this to the previous thermo-hygrometric results, another important tool was brought to light.

Indeed, the low T recorded, the presence of levels of RH close to saturation and, finally, the lack of ventilation especially in the lower strata, together with natural lightning and artificial lightning (turned on occasionally), represent factors that encourage biological growth. The site under study presents an important affection of biological proliferation, with is not only an aesthetical problem. The biological proliferation induces aesthetic damages on surfaces (vegetative structures, coloured patches through biogenic pigments or patinas and crusts) but, more

importantly, a physical (abrasion, mechanical stresses to the mineral structure due to shrinking and swelling cycles of these colloidal biogenic slimes inside the pore system [47]) and chemical changes (solubilisation, new-reaction products). This is because the biological system functions like a "water pomp", which, through capillary transport, which "holds" the water (rising damp) in the lower strata, speeding up the deterioration of the stone and building materials. Actually, the materials in correspondence of major biological presence appear to be in an advanced state of damage. The consumption of mortar joints, more permeable than bricks, is evident, as well as a typical morphology of degradation by biological growth.

For all of that, the previous results were the key to understand the biological proliferation that suffer the studied building, but a deeper study on percent coverage and taxon composition was carried out, to identify the most affected areas, developing a targeted and effective solution to a problem.

5.3 Biological proliferation study. A new assessment method. A combination of Stage method and Braun-Blanquet scale[23]

Biodegradation is an action strictly linked to the presence of active organisms (biodeteriogens), and is not only unavoidable but represents a fundamental process of the Biosphere. When this process occurs on «valuable» objects, it is called biodeterioration.

The biodeterioration of Built Heritage is a worldwide phenomenon [48-51]. The building materials alteration by living organisms is usually indicative of an advanced state of deterioration, predetermined by chemical and physical processes [48], which lead to an increase of the surface area attacked (speed vegetative development). The phenomenon of biodeterioration in concurrence with other chemical and physical processes [48] is still a matter of controversy. A distinction between "active biofilms" (where microorganisms and humidity are present [47]) and complex biofilms is usually made in order to classify the level of harmfulness on buildings [51].

In this sense, modern conservation strategies highlight the need to know and understand the structure and function of complex microbial communities, which cause biodeterioration of materials that constitute our Cultural Heritage [52]. In fact, only once the active biological presence is investigated, classified and

[23] An adapted version was published in:
Scatigno, C., and S. Ravera. Characterisation of the biological proliferation on Roman masonry Case study: "Casa di Diana" *Mithraeum* (Ostia Antica, Rome – Italy). XXVIII National congress by SLI in Lanciano (IT). Not.Soc.Lich. Ital. 28:54 (2015). ISSN: 1121-9165.

isolated, it is possible to implement measures to stop and prevent this type of alteration, preferably without the chemical formulates with biocide action, safeguarding not only the environment [53] but also the Cultural Heritage, because many biocidal treatments have negative effects on the artefacts [54-56]. In addition, the removal of the microbial community may give a start to a new succession of microorganisms, which may be more damaging than the old population. Additionally, the inhibition of specific groups of microorganisms may favour the growth of others [57]. Thus, the study of the biological proliferation is crucial.

Different approaches have been adopted to isolate, identify and quantify such wide group of organisms [58-60]. Indices of taxonomic or phylogenetic diversity have a potential in the quantification of microbial diversity at a range of ranks, but the non-equivalence of ranks and representatives of the taxa detected have to be addressed. Furthermore, also identifying the species is important to classify the biological damage, which represents a principal tool in Built Heritage conservation, requiring, in this sense, as all harm categories, a set number. Additionally, it is important to find an appropriate method and the right techniques to quantify the biological proliferation evolution in time.

Taking all of these into account, this research's phase involves, on one hand, the calculation of the total biological coverage on the building's walls (to estimate microbial concentrations), in order to assess their actual or potential harms; on the other hand, the recognition of biological species by a punctual sampling, carried out as taxon composition.

Regarding the first step, the Stage method and readapted Braun-Blanquet system were used. The Stage method consists in an assignation of numeric values, by stages, according to the restoration actions to be implemented, in order to, successively, identify the type of biological colonisation found. This method is only used in the restoration field and, in practice, is an inverse process of scientific surveys. Depending on the conservation treatment to apply, it is possible to individuate the biological colonisation type (**Tab. 3**).

Table 3. Stage method.

<table>
<tr><th>Stage</th><th>Conservation treatment for biological colonisation</th><th colspan="2">Biological colonisation type</th></tr>
<tr><td>0</td><td>Not needed</td><td colspan="2">-</td></tr>
<tr><td>1</td><td>Superficial cleaning (mechanical suction)</td><td rowspan="3">Mosses, lichens and fungi</td><td>Shortly rooted</td></tr>
<tr><td>2</td><td>Deep cleaning (first chemical and after mechanical)</td><td rowspan="2">consolidated</td></tr>
<tr><td>3</td><td>Deep cleaning + consolidation</td></tr>
<tr><td>4</td><td>Deep cleaning + consolidation due to rupture</td><td colspan="2" rowspan="2">Superior plants</td></tr>
<tr><td>5</td><td>Deep cleaning + consolidation due to rupture by superior plants</td></tr>
</table>

The Braun-Blanquet is a cover-abundance scale system (density method) (**Tab. 4**) or technique of distinguishing units which can be named using the classification of plant communities according the Floristic School (Braun-Blanquet 1964). This technique is widely used to transform the initially generated value into others systems (OTV and Ord% scales quasi-metric) [61]. However, this system is only used in "Plant sociology", which allows utilising of plant communities as environmental indicators.

Table 4. Braun-Blanquet scale.

n.	Species coverage class [%]
+	Present, very scares cover
1	Well represented, < 5%,
2	Abundant, < 25%,
3	25-50%
4	50-75%
5	> 75%

In this work, this last method was readapted and combined with the first one (Stage method). Precisely, the values reported in **Table 4**, were not attributed to a single species (as request by original system) but with a general presence without any biological distinction. The abundance was not calculated in correlation to the number of individuals of each species, nor by the dominance or coverage of each species. The area occupied by all the species occupants was considered in term of percentage rates of the total area.

To combine the two methods, facilitating in this sense the percent coverage assigning a spatial number as instructed for both methodologies, a modular grid of 25x25 cm (quadrant value) was especially designed and mounted on the whole walls. Successively, in winter 2014, a number was assigned according to the Stage method (**Figs. 28-30, Tab. 3)**. The attribution was carried out using a scalpel[24], testing the conservation state of bricks.

As can be observed, the two rooms present a different behaviour. Differences can also be observed in terms of the walls orientation. The *Mithraeum* presents a maximum stage level of 2, focused on the lowest 0.25 m, suggesting a conservative treatment by deep cleaning both chemically and mechanically (**Fig. 28a-c, Tab. 3**) on only two walls (at east and north side). Indeed, these latter present a stage level of 1, focused on 0.50 m of height, defining a procedure linked to a superficial cleaning thanks to a superficial invasion of microorganisms (**Fig. 28a, c, Tab. 3**); while, the west wall presents the stage level of 2 in the first 0.50 m (**Fig. 28b, Tab. 3**).

[24] This operation has been made possible thanks to my knowledge as professional restorer.

Figure 28. Modular grid installation in *Mithraeum* room, with the Stage method values assignation. **a**) East wall; **b**) west wall; **c**) north wall.

Figure 29. Modular grid installation in *pre-Mithraeum* room, with the Stage method values assignation. **a**) East wall; **b**) west wall; **c**) south wall.

The situation changes in the *pre-Mithraeum*. The wall most affected is the exposed on the east side, where the biological proliferation covers almost the whole of wall (**Fig. 29a, Tab. 3**). Contrary, the two walls exposed to the west and south (**Fig. 29b-c, Tab. 3**) present a situation more similar to the walls belonging to the *Mithraeum* room, but with different damage level (until 0.75 cm) and stage level (until 4). It is important to underline that the east wall of *pre-Mithraeum* is the only one wall located in front of a window.

The *podia* (**Fig. 30**) represent a separate circumstance. The area most affected is concentrated on the lower strata of *pre-Mithraeum* room, in accordance with the main openings (main entrance and windows) and in the central area of the communication trench for visitors.

Figure 30. Modular grid installation in *pre-Mithraeum* room, with the Stage method values assignation. **a**) East wall; **b**) south wall; **b1**) south wall zoom.

As can be observed in **Figure 30**, the lower strata (belonging to the *podia*) are more affected by biological proliferation, where values until 5 were assigned. These structures are characterised by high values, suggesting very deep restoration actions such as cleansing and consolidation (values 3 and 4 respectively). The areas in question are, indeed, very damaged. In the corner of the south wall, the presence of a plant superior is clearly visible (value 5 – **Fig. 30b1**).

Leaving aside the Stage method assignation, the Braun-Blanquet scale was applied. A percentage value was attributed to each wall. A coverage of 30% (3 level- **Tab. 4**) was attributed to the walls belonging to the *Mithraeum* room. Regarding the *pre-Mithraeum*, a 40% (3 level- **Tab. 4**) was attributed to the west and south walls, while a value 90% was assigned to the east wall (5 level- **Tab. 4**). A 100% was ascribed to the *podia*.

Once an objective value is attributed to each wall, it is necessary to conduct some reflections. The Stage method (**Tab. 3**) indicates a biological colonisation type that is too general, indicating the presence of mosses, lichens and fungi for the first 4 stage levels (1-4), distinguishing only the first two, depending on whether the rooted invasion if superficial or deep/consolidated. Therefore, it is necessary to carry out a more detailed identification.

In this sense, an identification of taxa[25] was carried out. On a first inspection, four biological species (**Fig. 31**) were identified. These were cyanobacterias, green algaes, lichens and plants.

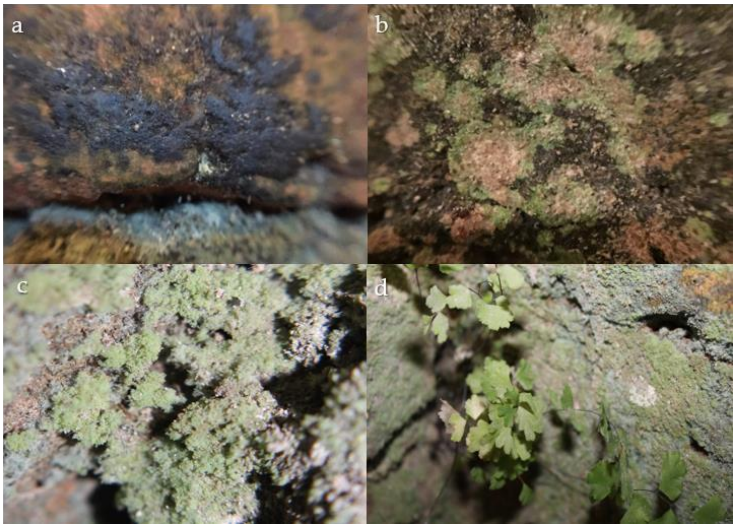

Figure 31. Taxon composition. **a**) Cyanobacteria. *Chroococcus* sp. (V_5H_5); **b**) Green algae. *Desmococcus* sp. (V_5H_6); **c**) Lichens. *Leprocaulon microscopicum* (Vill.) Gams. (V_7H_2); **d**) Plant. The letters V and H, enclosed in brackets, indicate a preliminary assignation to attribute the species according the box belonged (previous 25x25 grid). Specifically, V indicates the vector and H the height of each quadrant.

Specifically, the "fruticose" lichen, *Leprocaulon microscopicum*, was found in most of the lichens surveyed, as well as *Chroococcus* and *Desmococcus*, cyanobacteria and green algae, respectively.

[25] The recognition of the biological species was conducted by Dr. Sonia Ravera, Department of Di.B.T., University of Molise (IT).

Once identified and evaluated the level of biological proliferation on the studied site, it is important to study the environmental parameters associated to their proliferation in order to try to stop it. This is because, the microbiota on buildings represents a complex ecosystem which develops in different ways, depending on environmental condition [47]. Temperature, humidity, rain, sun exposure, air pollutants are only some of the climatic factors that can establish good conditions for the development of several organisms on the surfaces.

In this sense, T affects the rate of all the process occurring in microorganism and may help to determine the type of production, as well as high values of RH favour microbial activity. Light is another harmful tool, together with the air pollutions, which accelerates the microorganism process. The carbon dioxide (CO_2) is another fundamental parameter, directly linked with the microbial activity that has also implications in terms of AQ. Actually, this gas is an important AQ parameter because it is a contaminant and according to its concentration[26] is considered as a pollutant. Beyond the anthropogenic origin, CO_2 can be emitted by the biological apparatus, which can generate an increment in concentration during the night. The lack of air ventilation leads to think of a possible poor exchange of air (also during the day). Therefore, the AQ of the building is compromised, not only in terms of the eventual materials' carbonation [62] but above all as far as the usability of the site. In this sense, the evaluation of the concentration of CO_2 is an important indicator not only of the indoor environmental conditions in buildings [24] but also of the conservation state of historical buildings [62].

Taking all of this into account, a quality control of the environmental parameters associated to biological proliferation (T, RH, E, CO and CO_2) was carry out, in order to evaluate their impact (bioactivity emissions), by the monitoring of the CO_2 production.

[26] It is normally presents with 700 mg/m^3 (390 ppm)[221]. In indoor environments, its concentrations are greater. Although numerous norms [222, 223] that regulated it, distinguishing along residential [222] and for both residential and not [223], does not exist limits, standards but it talking about "acceptability". For last one [223] (our case), taking about three parameters: the differential concentration CO_2 (difference between the indoor and outdoor concentration Cind-Cout), the airflow (Qa) specification occupant or per unit area (Qs) and the number of spare parts/hour (n.). The German 's approach [224] considers > 1000 ppm (1800 mg/m^3) as harmless, between 1800-3.600 ppm as elevated and >3.600 ppm as unacceptable. Considering a lacking air system control, value > 1000 ppm are prejudicial. Furthermore are others norms, of others country ([225, 225]) that lower drastically those values. According the ASHRAE (taking into account in this thesis), establishes value of 1000 ppm as "action level" [226]. It is important to take into account also the exposition range.

Article 2

The influence of environmental parameters in the biocolonization of a Mithraeum in the roman masonry of Casa di Diana (Ostia Antica, Italy). Article published in Environmental Science and Pollution Research 23 (2016)13403-13412.

Environ Sci Pollut Res (2016) 23:13403–13412
DOI 10.1007/s11356-016-6548-x

RESEARCH ARTICLE

The influence of environmental parameters in the biocolonization of the Mithraeum in the roman masonry of casa di Diana (Ostia Antica, Italy)

C. Scatigno[1] · C. Moricca[2] · C. Tortolini[3] · G. Favero[3]

Received: 14 January 2016 / Accepted: 22 March 2016 / Published online: 30 March 2016

Abstract The microclimatic parameters (Ta, RH, E, and CO_2) reflect the indoor quality of the environment. Their relationship, connected with the design of the building, can facilitate the growth of photo/heterotrophic organisms and therefore facilitate the increase of the relative CO_2 production. Taking this into account, the impact of biological proliferation in a historical building is discussed for the *Mithraeum* of "Casa di Diana" in the archaeological site of Ostia Antica, which is subjected to guided tours. In this work, for the first time, we propose a study on biological monitoring to evaluate the contribution of bioactivity to air quality, with the objective to increase the comfort of visitors and to open the site for more than one day per week, suggesting possible tools providing a good compromise between building conservation and human comfort. In the sense, it has been possible to distinguish the contribution of the plants from the one deriving from humans: high values of carbon dioxide have been recorded during the night and its scarce removal during the day (air flow). The window present is not sufficient to eliminate the CO_2, involving concentrations of CO_2 relatively high in comparison to the proposed limits and guidelines defined by law. The obtained results strongly encouraged the elimination of flora in order to increase the comfort of visitors and to open the house for more than one day per week. Although, this process involves an important economic effort, the present study allows making an objective decision which has an important value in a cultural heritage management.

Keywords Microclimatic parameters · Roman masonry · Air quality · Natural and artificial light · Air flow · Human comfort and well-being

Responsible editor: Michel Sablier

✉ C. Scatigno
claudia.scatigno@uniroma1.it

[1] Department of Earth Science, Sapienza University of Rome, Piazzale Aldo Moro 5, 00185 Rome, Italy

[2] HERCULES Laboratory, University of Evora, Palacio do Vimioso, Largo Marques de Marialva 8, 7000-809 Evora, Portugal

[3] Department of Chemistry and Drug Technologies, Sapienza University of Rome, Piazzale Aldo Moro 5, 00185 Rome, Italy

Introduction

The possibility of preserving historical buildings is strictly connected to their use, mainly for tourism. Therefore, the evaluation of the concentration of carbon dioxide (CO_2) is an important indicator not only of the indoor environmental conditions in buildings (Varas-Muriel et al. 2014) but also of the conservation state of historical buildings. In the sense, the works found in literature distinguish two different themes: the biological proliferation and the relative damage on the stone materials (Ascaso et al. 2002, Ascaso et al. 1998, de los Ríos et al. 2009, Guiamet et al. 2012, Mohammadi and Krumbein 2008, Schabereiter-Gurtner et al. 2002). Specifically, the CO_2 parameter control is focused on several issues: the excretion of organic acid from the photosynthetic apparatus (Adamo and Violante 2000, Lee and Parsons 1999), the increase in chemical dissolution and frost wedging of rock surfaces caused by the water holding capacity of some species (Bjelland and Thorseth 2002), the damage caused by chromatic alteration (Barone et al. 2008). However, the control of indoor CO_2 concentration is also related to human studies were never conducted to evaluate the CO_2 contribution deriving from biological colonization, ranging from bacteria to more complex

organisms, such as plants (Dragovich and Grose 1990, Ferdyn-Grygierek 2014, Varas-Muriel et al. 2014).

In the subterranean environments, such as hypogea or indoor environments located in levels lower than the normal pedestrian levels, the proliferation of phototrophic microorganisms is often a consequence of the installation of artificial light for touristic purposes (Borderie et al. 2015). Leaving out the artificial light contribution, in an environment with natural light, aeration and ventilation decrease gradually, while relative humidity (RH) normally increases, the number of species is reduced, leaving only selected and adapted species, belonging mainly to heterotrophs (Cennamo et al. 2016). The type of substrate also affects microbial diversity. On stone, an inorganic material hostile to microbial growth, the early microbial pioneers are autotrophic organisms (Miller et al. 2012). In indoor environments, the most important photosynthetic communities are the primary producers (Cyanobacteria, often together with a few green algae) (Borderie et al. 2015, Urzí and Albertano 2001) due to their photosynthetic capacity and nitrogen fixation, making the organic matter and nitrogen bioavailable to the entire community, especially to heterotrophic microorganism (Borderie et al. 2015). The species composition is influenced by light conditions and humidity. In hypogeal environments, species of the genre *Chroococcus* are found (Urzí and Albertano 2001). Rare and not recent works conducted on environmental measurements underline the importance of the microclimatic parameters in correlation to a specific composition and distribution of biological organisms (Ariño and Saiz-Jimenez 1996). Furthermore, no studies have been performed on the biological carbon dioxide emission, in particular on indoor monuments.

Taking this into account, in this work, for the first time, we present a study for the CO_2 monitoring to evaluate the bioactivity contribution and the air quality of the *Mithraeum* of the Insula of Diana, sited in Ostia Antica (Italy), in order to increase the comfort of visitors and to open the house for more than one day per week with security for this archaeological site and to know the usefulness of the elimination of biological apparatus.

Materials and methods

Site description

The "Casa di Diana" is a complex building, comprised of several rooms, including a *Mithraeum*, situated in the northeast corner of the ground floor. It is a place dedicated to the Roman cult of the god Mithra (130 A.D.) and is comprised of two inter-communicating rooms (connected by two central openings) of about 24 m^2 total (Mithraeum and pre-Mithraeum).

The building, made of bricks and pozzolanic mortar aligned with the "*opus caementicium*" technique, has been the object of a multidisciplinary study starting from 2012 (Gaudenzi et al. 2012, Scatigno et al. 2016).

The framework presents a very characteristic microclimate: a similar behavior to a hypogeum, despite being structurally comparable to a semi-confined environment and being defined as such (Scatigno et al. 2016). For this reason, the inner and outer walls are subjected to different exposure to the macroclimate. The two inter-communicating rooms also present two different levels: on the sides of the communication trench, there are two *podiae*—seats for the Romans that assisted the sacrificial ritual of the killing the bull—which are about seventy centimeters above the pedestrian level. No

Fig. 1 *Pre-Mithraeum*. **a** main entrance to the *pre-Mithraeum* (door and window on the west and south wall); **b** detail of biological proliferation (communication trench)

Environ Sci Pollut Res (2016) 23:13403–13412

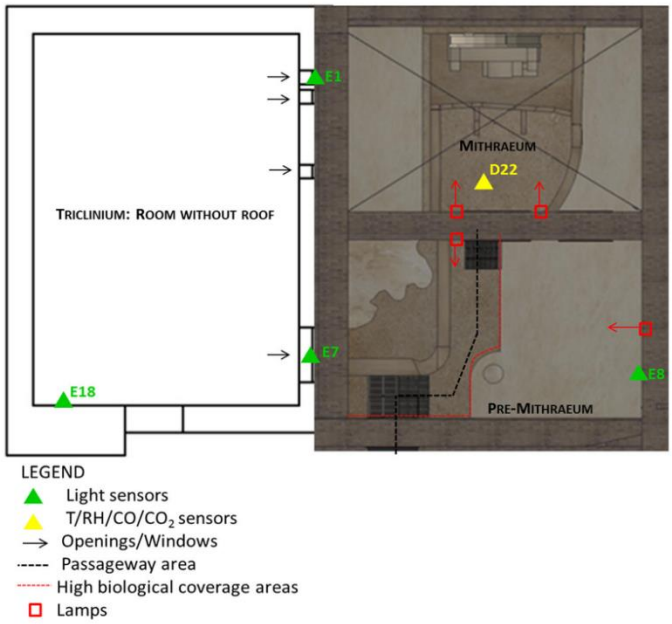

Fig. 2 Positioning sensors. The legend lists *four black arrows* which indicate the openings and windows present; the *dotted red line* represents the high biological coverage areas (south wall and the east transept: central area of the communication trench), the *dotted red line* represents the passageway area and the *red boxes* indicate the lamps. The lamp orientation is shown with *red arrows*, showing the direction correctly

ventilation systems are found, thus the ventilation is natural and comes from several openings. The two rooms are covered by a roof and are therefore protected against the rain. However, due to the openings, small areas are directly exposed to sunlight and outer air. In particular, the mostly ventilated room is the *pre-Mithraeum*, characterized by several openings such as the semi-circular window on the west wall and the main entrance to the *pre-Mithraeum* on the south (Fig. 1a, b). This window, of significant dimensions (1.48 × 1.16 m), along with the main entrance (the feature connecting the *Mithraeum* with the other environments), are the distinguishing factors of the two rooms, otherwise identical: the two rooms are specular, both in terms of volume and spatial distribution. Both rooms are equipped with incandescence lamps that are switched on only during the guided tours (once per week). Natural and artificial lighting, air flow, combined with a moisture content that reaches values of over 90 % and water flux (Scatigno et al. 2015) favor the biological attack (Sanchez-Moral et al. 2005).

Preliminary studies and data treatment

Two preliminary monitoring campaigns were conducted. For the first campaign, a light monitoring from the 7/30/12 to the 10/15/12 was performed in order to detect the daily indoor light contribution, as well as the working of the lamps (*pre-Mithraeum* and *Mithraeum*). It was conducted placing four light sensors (HOBO® U12-012–"E#"): one (E18) in the "*triclinium*" (Fig. 2a), a roofless neighboring room to *pre-Mithraeum* and *Mithraeum*, to evaluate the outdoor light daily contribution, two (E1, E7) on the openings/windows (Fig. 2), whereas the last one (E8) was placed in front of the biggest window (Fig. 2).

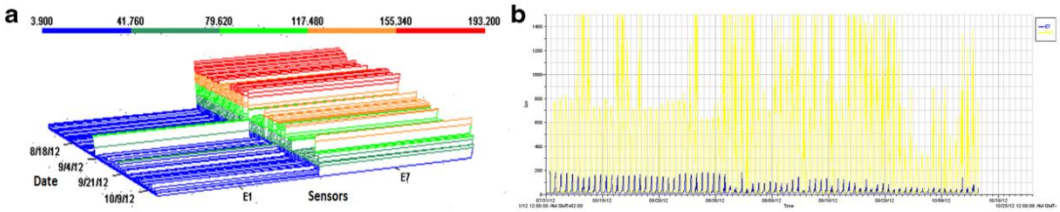

Fig. 3 Matrix plot (**a**) and time series plot (**b**) of the trend Illuminance: E1 vs. E7

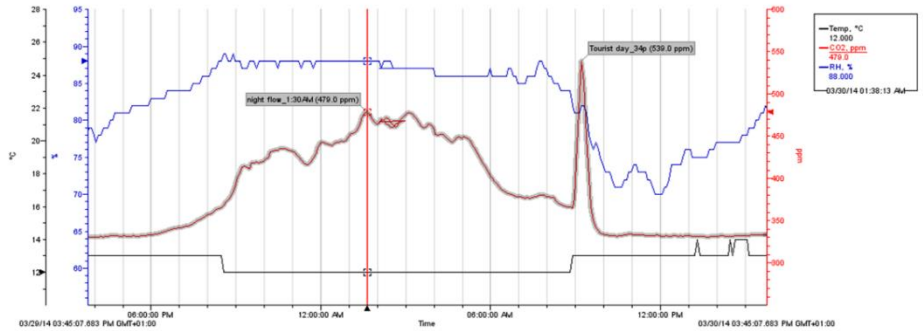

Fig. 4 Time series plot. The CO_2 parameter and the carbon dioxide cycles contribution are highlighted (daily, night and tourist day). In the figure, one day at the end of March was taken into consideration (3/29-3/30), with guided tours. During on the night of the 29th of March, the CO_2 contribute was of 422 ppm (average). During the 30th of March, before the guided tour, the CO_2 contribution was of 337 ppm. The CO_2 contribution during the guided tour of the 3/30 was of 539 ppm. It is a medium-high turnoff tourist day (34 people).

For the second campaign, a thermo-hygrometric and air quality monitoring (CO and CO_2) from the 3/26/2014 to the 9/16/2014 was performed to evaluate the average behavior of the indoor environment (*pre-Mithraeum*). The monitoring was conducted by means of a multi-parametric data-logger (DeltaOhm HD 37AB17D—"D22") set appropriately in the *Mithraeum* room (Fig. 2).

The obtained preliminary light data treatments have shown that the more illuminated room is the *pre-Mithraeum*; in contrast, the *Mithraeum* is dark: the intensity values recorded by the first sensor (E7) are significantly higher than those recorded by the second one (E1) (Fig. 3a). Furthermore, the light sensor E7 (*pre-Mithraeum*) shows the same trend as the E18 sensor (*triclinium*), reflecting the macroclimate behavior (Fig. 3b).

As far as the CO_2 is concerned, a night-day cyclic contribution was highlighted: the release of CO_2 was recorded in the time frame between 7 p.m. and 10 a.m., reaching peaks of 470 ppm. During the night flow, the T decreases of 1 ±0.4 °C and the RH increases consecutively (from 78 % to 89±2.5 %) (Fig. 4).

It is important to underline that the *Mithraeum* is not interested by the growth of vegetation, so these night emissions come from the *pre-Mithraeum*. Under such circumstances, another, more complex, monitoring campaign (from April 2015 to October 2015) was performed focusing on *pre-Mithraeum*.

New campaign procedure: biological proliferation characterization and monitoring campaign

A study on biofilm was conducted in the *pre-Mithraeum* in order to identify the areas most affected by biological proliferation. To assure the significance of the data collected, a reasoned non-probabilistic sampling design has been implemented. In this sense, Cyanobacteria, green algae and lichens were isolated and classified taxonomically (Fig. 5a–e), identifying the areas more affected by biological attack, corresponding to the maximum height (from the base up to 75 cm) reached by the microbial communities. In most of the lichens surveyed, "*fruticose*" lichen, *Leprocaulon microscopicum*, was found (Fig. 5e) (Scatigno and Ravera 2015). The space

Fig. 5 Biofilm. **a** Biological proliferation path cross; **b** plant; **c** green Algae, *Desmococcus* sp.; **d** Cyanobacteria. *Chroococcus* sp.; **e** lichen, *Leprocaulon microscopicum* (Vill.) Gams

Environ Sci Pollut Res (2016) 23:13403–13412

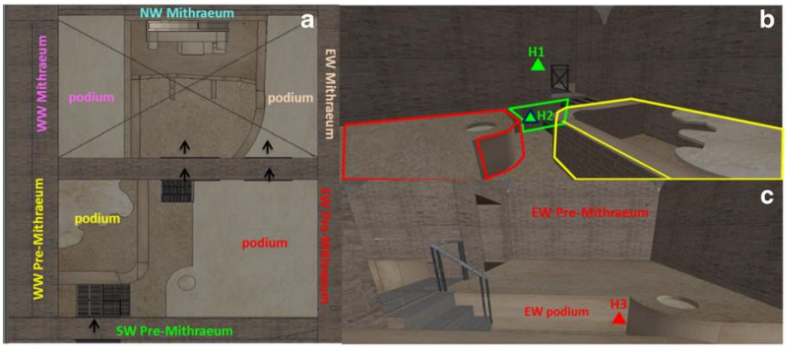

Fig. 6 Positioning sensors. **a** *pre-Mithraeum* and *Mithraeum* plan; **b**, **c** sensor placement in the *pre-Mithraeum*: H1 and H2 (**b**); H3 (**c**)

mostly interested by the growth of vegetation is concentrated in the lowest area of the *podiae*, which also corresponds to the path crossed by visitors (Fig. 5a). Three areas (25 × 25 cm) were selected. The three different organisms are found in all of them, but in variable concentrations. In general, the coverage of the areas is between 81–100 % (Scatigno and Ravera 2015).

In correspondence of these areas, a long term monitoring campaign (4/8/2015-10/20/2015) was performed placed three HOBO® U12 Temp/RH/Light/External Data loggers (H1, H2 and H3) (accuracy: ±0.4 °C from 0 to 50 °C, ±2.5 % from 10 to 90 % RH to a maximum of ± 3.5 %; range of measure: 20 to 70 °C, 5 to 95 % RH, 1 to 3000 (lumens/ft^2) at different heights (Fig. 6), along with Vaisala GMW86P (accuracy: 20–30 °C ± (30 ppm + 3 % of reading), 10–20 °C, 30–40 °C ± (35 ppm + 3.7 % of reading), 0–10 °C, 40–50 °C ± (40 ppm + 4.8 % of reading, range of measure: 0 to 2000 ppm) transmitters for CO_2. The infrared (IR) instrument for measuring CO_2 concentration is an infrared gas analyzer based on the measure of the absorbed IR radiation deriving from the air diffused into the instrument and compared to the reference adsorption radiation, without the gas. The HOBO ware Pro version 3.7.2 software (Onset Computer Corporation© 2002–2015) was used. A continuous measurement program has been selected to highlight both the hourly and daily variations of the parameters. The chosen logging frequency was of 5 min. This setting has been selected as it represents a high frequency, in contrast to the hourly measurement usually set (Loupa et al. 2006), which allows to observe the variations that may occur in short periods of time. Such choice is particularly recommended for this study, considering that guided tours usually include only a few minutes inside the *Mithraeum*.

Besides, in this campaign, to evaluate the lighting technology and the biofilm growth and to complement also the light monitoring campaign, other measurements have been performed. A SpectroVis® Plus Spectrophotometer by Vernier Software & Technology was employed.

Results and discussion

CO_2 measurements

As far as the CO_2 is concerned and thanks to long time monitoring design, it has been possible to distinguish the contribution of the plants from the one deriving from humans. In

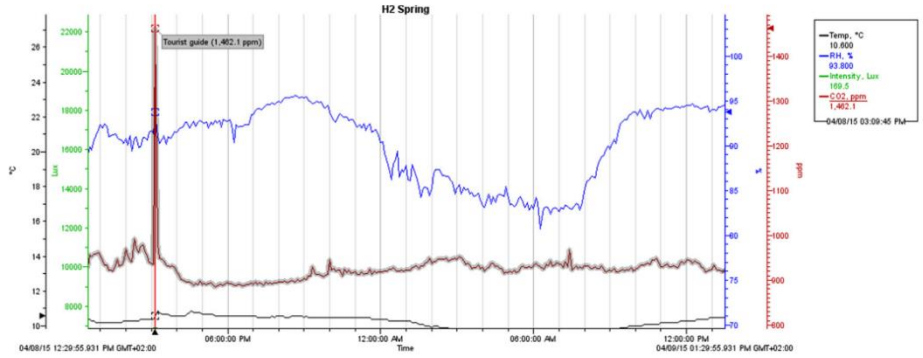

Fig. 7 The CO_2 trend of a high turnout day is highlighted (4/8/15 at 3 PM)

this way, between the spring and fall of 2015, 28 guided tours were recorded, with an average human contribution of 951 ppm and a turnout of about 30 people. The most crowded period, which covers about 50 % of the guided tours of the entire monitoring campaign, is the spring (977 ppm). During the month of August, the tours were not held, as the "Casa di Diana" and all the other domus were closed to the public. Two guided tours had a great influence on the average value, one in June and one in October, due to the high number of visitors, as it usually happens (Varas-Muriel et al. 2014). Unfortunately, the exact number of tourists that visit the site is unknown: during the guided tours, in addition to the official list, other people join without having booked the visit, and therefore their presence is not recorded. High values of CO_2 have been recorded during the daylight hours in correspondence with people's entrance (reaching a value of 1462 ppm—the maximum value detected by the sensor H2—with a turnoff of 50 people); the CO_2 increased significantly due to breathing (Fig. 7). The CO_2 contribution seems therefore to largely derive from humans. Taking into consideration a medium

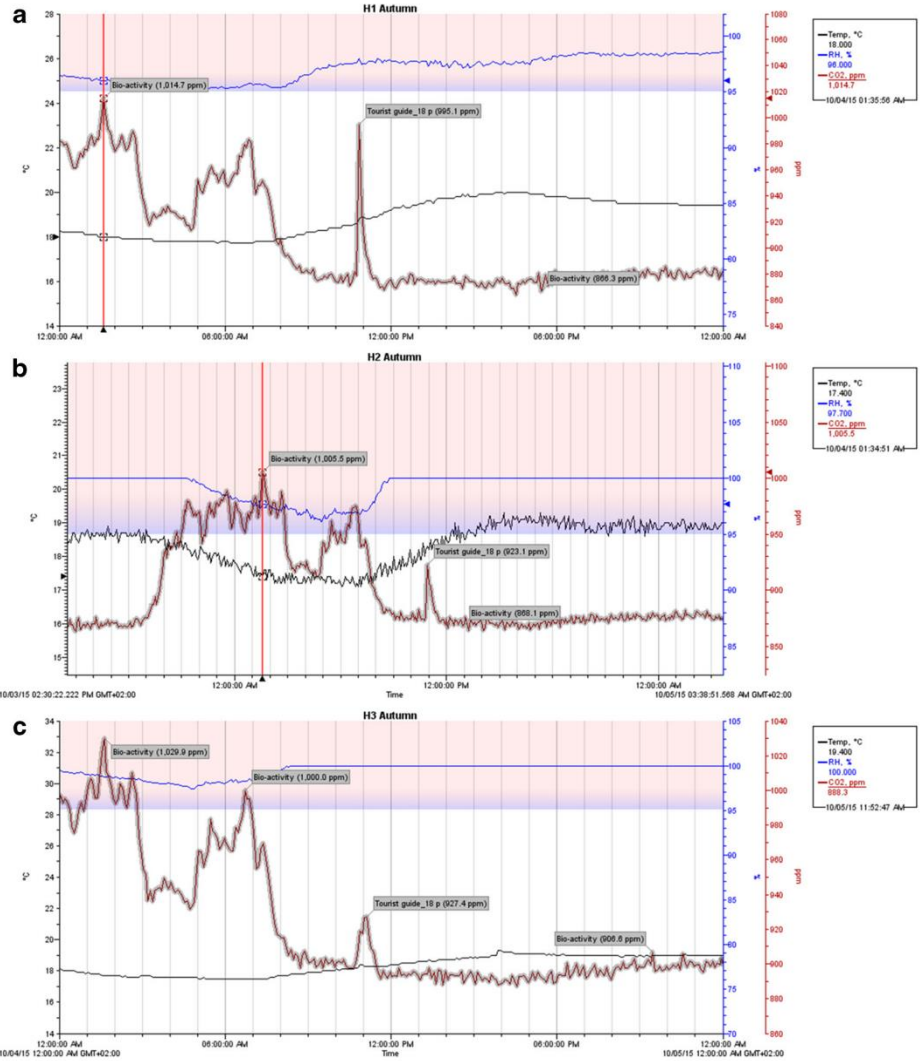

Fig. 8 On evidence cyclic emission from biologicals apparatus and one tourist guide contribute with a turnout of 18 people. **a** H1 trend; **b** H2 trend; **c** H3 trend. The *colored area* indicates humidity values higher than 95 % RH

Environ Sci Pollut Res (2016) 23:13403–13412

turnout (of approximately 18 people), the contribution of bioactivity is evident: the characteristic behavior of the three sensors remains (H1 sensors records about 70 ppm more than the other two sensors, set at a lower level) but the CO_2 contribution during the night is significant (Fig. 8a–c).

Every night, from 7:00 p.m. to 10:00 a.m., when the site is closed to the public, peaks of CO_2 between 1163 ppm (max value recorded by H2 sensor) and 1356 ppm (max value recorded by H1 sensor) are recorded. As seen in Fig. 8, during the night, the CO_2 footprint has a specific shape, which is the same for all three sensors: two increases framed by 2-h decreases (from 2 to 5 a.m.). During the bioactivity, RH and T decrease slightly: the RH starts from the saturation level and drops to a value very close to saturation (≥95 %).

Another observation can be made regarding the lack of daily variations of the thermo-hygrometric parameters: the parameters of temperature (*T*) and relative humidity environment do not undergo any significant change. The penetration of external air in the room, the impact of sunshine through the window and the heat and moisture released by people, do not seem to influence the thermo-hygrometric state of the environment. This is caused by the fact that these environmental parameters, RH in particular, are very critic: despite the *Mithraeum* being a semi-confined environment and featuring openings exits, the environment does not constitute a macroclimate. Before reaching a turnout of about 30 visitors, T and RH show no substantive changes: the values fall inside the measuring error of the instrument (Fig. 9).

Natural light measurements

Natural light, that is an important source of illumination, is difficult to control because of its variability (Mayorga Pinilla et al. 2016). Disregarding the problems related to the conservation of materials (thermal fluctuations, ΔT), (according to UNI10829:1999, illuminance is not considered relevant for brick and mortar), the solar irradiation plays a fundamental role in the preliminary proliferation processes. On the other hand, the advantages of using natural lighting in architecture are widely accepted: it is considered as a potential passive strategy for reducing buildings' energy consumption and improving the visual comfort without any expensive operational cost and installation (Fasi and Budaiwi 2015).

The natural light is represented by incident solar radiation (direct sunlight) coming mainly from the window and it contributes to the heat gain.

Throughout the measuring campaign, every day in the afternoon, a beam of natural light coming from the window situated in front of *podiae*, illuminates all the sensors. The intensity values and the hour of occurrence change by season. During the autumn, around 4 p.m., the sensors record values ranging from 17 to 19.000 lx (max values), reaching values of 32.000 lx recorded by H3 sensor (the lowest position), where the beam of natural light stays longer. During this time frame, the *T* rises and the UR decreases: + 5 °C (± 0.4 °C), +10 % (± 2.5 %) (Fig. 10). This event, repeated every year, assumes an important and significant role in the mechanical stress occurring in the material building, also as far as the biological proliferation is concerned.

Artificial light measurements

Artificial light is clearly connected with the pattern of biological growth (green biofilm—phototrophic microorganisms and photosynthetic bacteria) (Albertano and Bellezza 2001).

The microorganisms are more concentrated on the west side of the studied environment. Some microbial studies on bacterial and fungal deterioration reveal that this environmental exposition is the preferred orientation of development and the area's growth potential can be, instead, sheltered or not from sun irradiation and rain (Cappitelli et al. 2007). Moreover, the development of photosynthetic organisms is favored by the high humidity of such environments (RH >90 %) and a constant temperature throughout the year (our

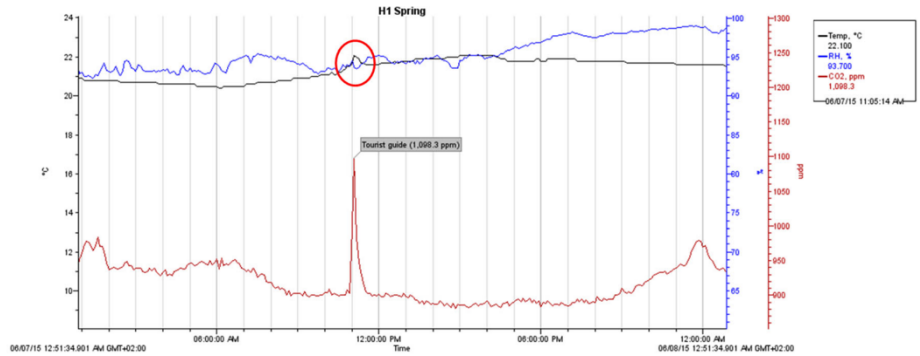

Fig. 9 T and RH changes in correspondence of a tourist guide (turnout: 30 people)

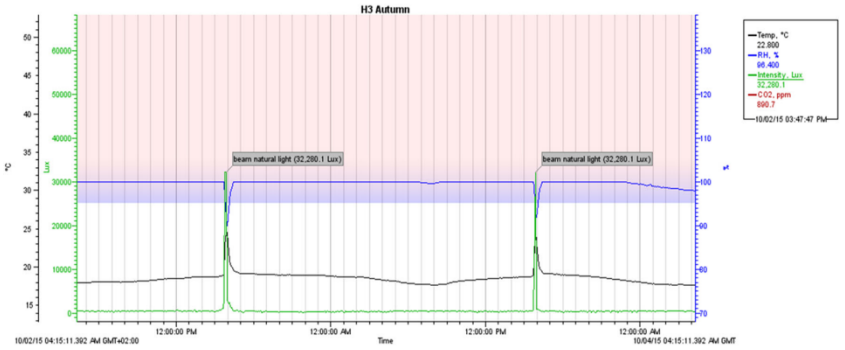

Fig. 10 The illuminance trend (H3 sensor) highlights the peaks at 3:47 PM. The *colored area* indicates humidity values higher than 95 % RH

specific case) (Scatigno et al. 2016), but it is mainly caused by the more or less prolonged lighting periods that are necessary to provide visitors with a convenient illumination of the sites (Compagnone et al. 1999). In the "Casa di Diana" *Mithraeum*, lights are usually switched on for a few minutes during the guided tours.

Studies conducted on several works of art in underground environments explain their relationship with the microbial communities, establishing specific and consequential processes of colonization: the primary producers are the first to develop as they are able to use extremely low photon fluxes to perform photosynthesis (Sanchez-Moral et al. 2005). They are followed by the heterotrophic populations of bacteria and fungi, which grow thanks to the organic matter produced by the phototrophs. These microbial communities are, therefore, characterized by an oxygen production that takes place during the light periods via photosynthetic activity, while maximum oxygen consumption occurs in the dark due to the respiratory metabolism of both auto- and heterotrophic microorganisms (Compagnone et al. 1999). The metabolic activity of microorganisms results also in the bio-mineralization of these types of substrates (Urzí and Albertano 2001).

The obtained results demonstrate that no temperature shift has been observed upon switching on the lamps. This is probably caused by the placement of the sensors (the measure is taken only in the point where the sensor is set) in relation to the orientation of the lamps. The temperature recorded does not increase significantly when people pass along the corridor (human corporal heat), although this moment also corresponds to switching on the lamps.

Furthermore, the emission spectra amply demonstrate the inadequacies of the lamps in terms of abundant IR contribution (near and far infrared) (Fig. 11). This results in a strong heat-up of the material's surface.

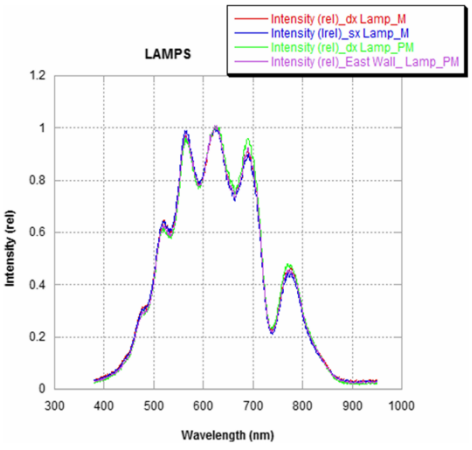

Fig. 11 Intensity (rel.) *vs.* wavelength (nm)

Conclusions (possible tools for human comfort)

At the entrance and in the artificially illuminated areas, phototrophic microorganisms (Cyanobacteria) are very abundant and are distributed in patches of green biofilm over a great extension of the material surface. For this reason, a future action for the removal of these microorganisms should be taken into consideration. The mechanical and chemical interventions are only a temporary remedy, so the natural light must be controlled through the installation of filters on the windows, in order to create less favorable conditions for the biological proliferation.

As far as the artificial lighting is concerned, substituting the halogen lamps with LED (i.e., light-emitting diodes or, alternatively, fluorescent compact lamps with low thermal infrared emissions, lamp technology equipped with appropriate emission spectra), which would provide a good compromise between conservation and human comfort, is recommended.

High CO_2 concentrations (750 ppm) acidify the water vapor (Bencs et al. 2007, Bonazza et al. 2009, Camuffo 2014, Vuerich et al. 2008).

In addition to the factors previously considered, high levels of RH (rising damp, presence of probably seeping water) induce surface condensation: temperature sensors installed in previous monitoring campaigns and different materials indicate that the temperature of rock and mortars was always lower than air temperature, subsequently inducing water condensation on the surfaces of the material surfaces, as well as efflorescence and subefflorescence (Scatigno et al. 2014, Scatigno et al. 2016).

The cyclic production of carbon dioxide during the night (CO_2 exchange that easily accumulates in lowest strata) and its scarce removal during day (air flow), involve concentrations of CO_2 relatively high in comparison to the suggested limits and guidelines defined by law (Standard 2001, UNE-EN 13779 2008, y Certificación, Asociación Española de Normalización 2008).

Natural ventilation would encourage the elimination of CO_2 (Varas-Muriel et al. 2014) but the windows are not sufficiently big to perform such task. It is suggested to optimize the HVAC (Heating, ventilation and air conditioning) system.

Besides, is it necessary to periodically check the results, identifying and achieving the optimal conditions for the conservation of the environment.

Summarizing the obtained results, among other minor actions, is strongly encouraged the elimination of biological apparatus, in order to increase the comfort of visitors and to open the house for more than one day per week (the "Casa di Diana, " set within such archaeological site, is subjected to guided tours only on Sunday) with security for this archaeological site. Although, this process involves an important economic effort, the present study allows making an objective decision which has an important value in a cultural heritage management.

Acknowledgments The authors would like to thank the staff of the archaeological area of Ostia Antica, especially the director Dr. Cinzia Morelli, the security company, and the technical staff (Drs. Paola Germoni, Flora Panariti, Orietta Mantovani) for the permission to work in this house.

Claudia Scatigno is grateful to Pr. Sonia Ravera (Department of Di. B. T., University of Molise) for her contribution in the recognition of the biological species and PhD Maria Teresa Lepone (Department of Physics, Sapienza University of Rome) for her suggestions regarding the lighting results. The authors also thank Pr. Franco Mazzei (Department of Chemistry and Drug Technologies, Sapienza University of Rome) for his contribution in the project realization.

References

Adamo P, Violante P (2000) Weathering of rocks and neogenesis of minerals associated with lichen activity. Appl Clay Sci. doi:10.1016/S0169-1317(99)00056-3

Albertano P, Bellezza S (2001) Cytochemistry of cyanobacterial exopolymers in biofilms from Roman hypogea. Nova Hedwigia Beiheft

Ariño X, Saiz-Jimenez C (1996) Colonization and deterioration processes in Roman mortars by cyanobacteria, algae and lichens. Aerobiologia

Ascaso C, Wierzchos J, Souza-Egipsy V, RiA de l, Rodrigues JD (2002) In situ evaluation of the biodeteriorating action of microorganisms and the effects of biocides on carbonate rock of the Jeronimos Monastery (Lisbon). Int Biodeterior Biodegrad

Ascaso C, Wierzchos J, Castello R (1998) Study of the biogenic weathering of calcareous litharenite stones caused by lichen and endolithic microorganisms. Int Biodeterior Biodegrad. doi:10.1016/S0964-8305(98)00043-2

Barone G, La Russa MF, Giudice AL, Mazzoleni P, Pezzino A (2008) The Cathedral of S. Giorgio in Ragusa Ibla (Italy): characterization of construction materials and their chromatic alteration. Environ Geol

Bencs L, Spolnik Z, Limpens-Neilen D, Schellen HL, Jütte BAHG, Van Grieken R (2007) Comparison of hot-air and low-radiant pew heating systems on the distribution and transport of gaseous air pollutants in the mountain church of Rocca Pietore from artwork conservation points of view. Journal of Cultural Heritage. doi:10.1016/j.culher.2007.05.001

Bjelland T, Thorseth IH (2002) Comparative studies of the lichen–rock interface of four lichens in Vingen, western Norway. Chem Geol

Bonazza A, Messina P, Sabbioni C, Grossi CM, Brimblecombe P (2009) Mapping the impact of climate change on surface recession of carbonate buildings in Europe. Sci Total Environ

Borderie F, Alaoui-Sossé B, Aleya L (2015) Heritage materials and biofouling mitigation through UV-C irradiation in show caves: state-of-the-art practices and future challenges. Environmental Science and Pollution Research

Camuffo D (2014) Microclimate for cultural heritage: conservation, restoration, and maintenance of indoor and outdoor monuments: second edition. In: Microclimate for cultural heritage: conservation, restoration, and maintenance of indoor and outdoor monuments: second edition., pp 1–526

Cappitelli F, Principi P, Pedrazzani R, Toniolo L, Sorlini C (2007) Bacterial and fungal deterioration of the Milan Cathedral marble treated with protective synthetic resins. Sci Total Environ. doi:10.1016/j.scitotenv.2007.06.022

Cennamo P, Montuori N, Trojsi G, Fatigati G, Moretti A (2016) Biofilms in churches built in grottoes. Sci Total Environ. doi:10.1016/j.scitotenv.2015.11.048

Compagnone D, Di Carlo V, Bruno L, Albertano P, Palleschi G (1999) Development of oxygen microsensors for monitoring cyanobacterial photosynthesis in Roman hypogea. Anal Lett

De los Rios A, del Cura CB, García MÁ, Rico VJ, Galván V, Ascaso C (2009) Deteriorating effects of lichen and microbial colonization of carbonate building rocks in the Romanesque churches of Segovia (Spain). Sci Total Environ

Dragovich D, Grose J (1990) Impact of tourists on carbon dioxide levels at Jenolan Caves, Australia: an examination of microclimatic constraints on tourist cave management. Geoforum. doi:10.1016/0016-7185(90)90009-U

Fasi MA, Budaiwi IM (2015) Energy performance of windows in office buildings considering daylight integration and visual comfort in hot climates. Energy Build. doi:10.1016/j.enbuild.2015.09.024

Ferdyn-Grygierek J (2014) Indoor environment quality in the museum building and its effect on heating and cooling demand. Energy Build. doi:10.1016/j.enbuild.2014.09.014

Gaudenzi S, Preite Martinez M, Bernardini ML, Imperi F, De Bianchi S, Guiso M, Sammartino MP, Sclavi S, Visco G, Vitali M, Protano C, Ferro D, Siani AM, Congiu A, Stellino S, Polcaro F, Ranieri M, Barbera MR, Pellegrino A, Panariti F, Mantovani O, Marano A, Sangiorgio M, Sammartino MP, Mola M, Avranovich Clerici E,

Ceccarelli C, Creddo A, Di Luca G, Meoni M, Rosciardi V, Carnevale F, Jankowski F, Lupo E, Monaco M, Scatigno C, Egidi B, Avranovic Clerici E, Gramaccioni C (2012) Studio multidisciplinare sui mitrei di ostia Antica

Guiamet PS, Rosato V, de Saravia SG, García AM, Moreno DA (2012) Biofouling of crypts of historical and architectural interest at La Plata Cemetery (Argentina). Journal of Cultural Heritage

Lee M, Parsons I (1999) Biomechanical and biochemical weathering of lichen-encrusted granite: textural controls on organic–mineral interactions and deposition of silica-rich layers. Chem Geol

Loupa G, Charpantidou E, Kioutsioukis I, Rapsomanikis S (2006) Indoor microclimate, ozone and nitrogen oxides in two medieval churches in Cyprus. Atmos Environ. doi:10.1016/j.atmosenv.2006.07.015

Mayorga Pinilla S, Vázquez Moliní D, Alvarez Fernández-Balbuena A, Hernández Raboso G, Herráez JA, Azcutia M, García Botella A (2016) Advanced daylighting evaluation applied to cultural heritage buildings and museums: Application to the cloister of Santa Maria El Paular. Renewable Energy. doi:10.1016/j.renene.2015.07.011

Miller AZ, Sanmartín P, Pereira-Pardo L, Dionísio A, Saiz-Jimenez C, Macedo MF, Prieto B (2012) Bioreceptivity of building stones: a review. Sci Total Environ. doi:10.1016/j.scitotenv.2012.03.026

Mohammadi P, Krumbein WE (2008) Biodeterioration of ancient stone materials from the Persepolis monuments (Iran). Aerobiologia

Sanchez-Moral S, Luque L, Cuezva S, Soler V, Benavente D, Laiz L, Gonzalez JM, Saiz-Jimenez C (2005) Deterioration of building materials in Roman catacombs: the influence of visitors. Sci Total Environ. doi:10.1016/j.scitotenv.2004.12.080

Scatigno C, Cardarelli E, De Donno G, Oliveti I, Preite Martinez M (2015) Geophysics and geochemistry methodologies: application and techniques to structural evaluation of a roman masonry (archaeological site in Ostia Antica)

Scatigno C, Ravera S (2015) Characterisation of the biological proliferation on Roman masonry. Case study: "Casa di Diana" Mithraeum (Ostia Antica, Rome – Italy)

Scatigno C, Sammartino MP, Gaudenzi S (2014) Non-invasive analysis of soluble salts. Preliminary results on the case study of Casa di Diana Mithraeum (Achaeological site of Ostia Antica - Italy)

Scatigno C, Prieto-Taboada N, Preite Martinez M, Conte AM, García-Diego FJ, Madariaga JM (2016) Analitycal techniques for the characterisation of historical building materials: case study "Casa di Diana" Mithraeum (Archeological site in Ostia Antica, Italy). In: Wythers MC (ed) Advances in Materials Science Research, Nova Science Publishers, Inc. edn, New York

Schabereiter-Gurtner C, Saiz-Jimenez C, Piñar G, Lubitz W, Rölleke S (2002) Altamira cave Paleolithic paintings harbor partly unknown bacterial communities. FEMS Microbiol Lett

Standard A (2001) Standard 62-2001. Ventilation for acceptable indoor air quality. American Society of Heating. Refrigeration and Air Conditioning Engineers, Atlanta

UNE-EN 13779 (2008) Ventilation for non-residential buildings—performance requirements for ventilation and room-conditioning systems

Urzì C, Albertano P (2001) Studying phototrophic and heterotrophic microbial communities on stone monuments. Meth Enzymol. doi:10.1016/S0076-6879(01)36600-4

Varas-Muriel MJ, Fort R, Martínez-Garrido MI, Zornoza-Indart A, López-Arce P (2014) Fluctuations in the indoor environment in Spanish rural churches and their effects on heritage conservation: hygro-thermal and CO2 conditions monitoring. Build Environ. doi:10.1016/j.buildenv.2014.08.010

Vuerich E, Malaspina F, Barazutti M, Georgiadis T, Nardino M (2008) Indoor measurements of microclimate variables and ozone in the church of San Vincenzo (Monastery of Bassano Romano—Italy): a pilot study. Microchemical Journal

y Certificación, Asociación Española de Normalización (2008) Ventilación de los edificios no residenciales–Requisitos de prestaciones de sistemas de ventilación y acondicionamiento de recintos UNE-EN 13779: 2008. AENOR, España

5.4 Effect of the environment on the materials. The relationship between them

In a complex system, where the indoor (environment) is not suitable for materials' safeguard, like the case under study, the objects (container) can respond to the solicitations, speeding up their decay. This is because, there is an undeniable inter-relationship between content and container, or between "environment" and "system".

The degree of this synergic connection, for each stimulus (input) there is a solicitation (output), depends on the starting point of each one of them. In other words, the materials will respond to environmental stressors according to their nature and to the conservation state in which they are found. It is impossible to go back in time, but each sphere can be studied and characterised.

Before evaluating the output, the direct effect on building materials, there is another step of the protocol that needs to be implemented, the third block (**Chapter 4**, **Fig. 18** - purple boxes), a hybrid between environmental characterisation and material characterisation, or the thermo-hygrometric surface state of building materials. In practice, that is the study on what is happening in the environment-system interface.

Indeed, among the results, there is one particularly relevant, which expresses the strongly risk of evaporation and condensation processes of the building materials (bricks and mortars), as the recorded values of RH are close to saturation and there is no air movement near to the walls. A successive step is required to understand what happens directly on materials' surface. This step perfectly combines the environmental characterisation with the materials' characterisation.

In the study of the environmental monitoring, it is very difficult to obtain efficient information concerning the effect that a particular microclimate (characterised by parameters with critical levels) can generate on building materials.

In this sense, an innovative seasonal measurement method was applied, taking into account two different single points measurements (brick and mortar) on several multipoint, to identify anomalies and areas at risk of evaporation–condensation phenomena. These measurements were directly carried out in the surface of the building materials.

Article 3

Evaporation and condensation phenomena on Roman wall-building of a *hypogeum* environment by a discrete monitoring. Article submitted to Construction and Building Materials. Ms. Ref. No.: CONBUILDMAT-D-16-03967.

EVAPORATION AND CONDENSATION PHENOMENA ON ROMAN WALL-BUILDING OF A*HYPOGEUM* ENVIRONMENT BY A DISCRETE MONITORING

C. Scatigno[1*], F. J. García-Diego[2-3], P. Merello[4]

[1*]Department of Earth Science, University of Rome "La Sapienza", Piazzale Aldo Moro 5, 00185, Rome, Italy. Phone: + 39 0649914156, Fax: (+39) 064454729
[2]Department of Applied Physics, Universitat Politècnica de València, Av. de los Naranjos s/n, Valencia 46022
[3]Centro de Tecnologías Físicas, Universitat Politècnica de València, Av. de los Naranjos s/n, Valencia 46022
[4]Accounting Department, Universitat de València, Avd. Tarongers s/n, 46000 Valencia, Spain
*Corresponding author, email: claudia.scatigno@uniroma1.it

Abstract
Nowadays, the procedures and instruments for measuring temperature of the air and of materials' surface, with the aim to evaluate the conservation status of ancient buildings, are regulated and vastly used (EN 15758 - EN 16242).
In this work, a monitoring system based, on a punctual and manual multipoint measurement and on innovative mapping survey, was applied in a Roman masonry in order to evaluate the thermo-hygrometric status of the wall-building materials and the evaporation and condensing risk.
The approach was based on contact measurements of the materials 'surface, as well as the air temperature close to surface, by means of different handheld instruments, performed during specific periods of the calendar year.
Results brought to light some particularly critical areas and highlighted different properties of materials.
A PCA and multivariate statistical procedure show the potential of this methodology, identifying the best practice in terms of cost and time efficiency.

Keywords thermo-hygrometric measurements; discrete monitoring; evaporation and condensation phenomena; multivariate statistical method.

Highlights

- A particular discrete monitoring together with a detailed mapping of measurements, was employed to investigate evaporation and condensation phenomena
- Thermo-hygrometric characterisation of Roman building materials (brick and mortar)
- A strategy, consists of a fixed number of measures repeated in selected days, was built to correlate the indoor environment (10 cm far to walls) to the materials

ABBREVIATIONS
T: temperature; Ta: air temperature (NTC); TIR: infrared ray temperature (superficial temperature: Ts); Tc: contact temperature; RH: relative humidity; RHCond: relative humidity measured by conductive method; RHRF: relative humidity measured by radio frequency method; T_m: average temperature; RH_m: average relative humidity

1 INTRODUCTION

Nowadays, wide ranges of techniques, destructive and non-destructive, direct and indirect, for thermo-hygrometric buildings' investigation are available. To characterise structures affected by capillary rise, condensation, rainwater infiltration [1], to evaluate the technology

building performance (energetic balance) as well as to understand the thermal footprints of historical buildings or its historical evolution [2].

The evaluation of the performance of building materials, by temperature and surface humidity measurements, plays an important role in the identification of the materials' properties, such as thermal insulation and conductivity. These properties depend from the nature of the material, the influencing temperature range and the material moisture content [3-5]. This practice is commonly used to estimate the energy efficiency and durability of residential buildings, often equipped with ventilations systems (HVAC equipment) [6, 7], buildings located in sites with harsh climatic conditions, evaluating the thickness and type of the construction material used and its ability to delay heat transfer over a period of time.

In preventive conservation of ancient buildings, thermo-hygrometric surface measurements represent an important tool to evaluate the possible evaporation–condensation cycles.

The procedures and instruments for measuring air and objects' surface temperatures are regulated by a European Norm (EN 15758) [8], as well as the procedure for measuring humidity of the air and moisture exchanges between air and cultural property (EN 16242) [9].

In this work, a new monitoring approach is presented, based on local and spot measurements performed in a sufficient number of areas (walls), representing different climatic zones in the building. This method is performed with handheld instruments to individuate behavioural differences between mortar and bricks. The seasonal measurement method takes into account two different single points measurements (brick and mortar) on several points, previously mapped on the walls, individuating anomalies and risk areas characterised by evaporation–condensation phenomena.

The data treatment was performed with PCA (Principal Component Analysis) and other multivariate statistical analysis (Box & Whisker, Scatter Plot) individuating it as an efficient procedure. The multipoint measurements procedure allows understanding the potentiality of the method, identifying the best practice, in terms of cost and time efficiency (time data treatment).

2 MATERIALS AND METHOD

2.1 Site description. "Casa di Diana" building.

The "Casa di Diana" Region I, Insula III, it is a roman building (130 CE), part of the famous archaeological site of Ostia Antica, found at 23 km from the centre of Rome. The building, comprised of "*tabernae*" and "*cenacula*", presents a very characteristic microclimate, especially inside two intercommunicating rooms (*Mithraeum* and *pre-Mithraeum*), at North East of the house, which, in the second half of the third century, were appointed to host a sacrificial rite[10]. The principal building materials are bricks and pozzolanic mortar, aligned with the "*opus caementicium*" technique. The two rooms are characterised by different heights due to the presence of "*podiae*" at the sides [10].

2.2 Discrete monitoring

2.2.1 Sensors technology

Three different instruments obtaining relative humidity and temperature measurements performed the discrete monitoring. The moisture meter, Protimeter Surveymaster (SM BLD5360), a

dual-purpose tool, allows the evaluation of the moisture conditions (electromagnetic method) both on the surface and under the surface layer, through the electrodes "deep wall" needle. This moisture meter combines the conventional two-pin inspection method with a non-invasive radio frequency technique. The Search Mode uses the same colour coded LED scale as the Measure mode, identifying degrees of dampness below the surface. The instrument employs radio frequency emissions (RFE) to measure moisture through most wall coverings. The two-pin Measure Mode discriminates different levels of humidity by means of green, yellow and red LEDs (dry, humid and wet surface). The dampness measured is quantified on an LCD display to one decimal digit in terms of % wood moisture equivalent (%WME). The range is 0-999 relative (non-invasive) and % to 99% WME (pin measurement). The depth of moisture is non-invasive up to 3/4 in (19 mm) and pin up to 1/2 in (12.7 mm). The multimeter PM 2521 Philips (PT100 probe, accuracy 1.0 + 0.2°C, range 0-100°C) allows to measure Tc, whereas the thermometer TESTO 810 (2-channel) allows "contact" or superficial (IR with laser sighting) and air temperature measurements (NTC), respectively. Furthermore, unlike for other instruments, the instrument response of temperature measurement with PT100, is low (order of seconds or fractions of seconds), so the probe was modified to have a stable measurement: a bell-shaped suction pad was applied to stabilise the measure. After preliminary testing, the measure appeared settled after 10 minutes, choosing this value as the measuring time.

2.2.2 Multi-point measurements

A non-probabilistic, reasoned statistical sampling was applied in order to evaluate the wall-building's thermo-hygrometric state along the vertical profile of walls (**Fig.1**). For each wall (six walls and six *podia*), three vectors were created (except for the northern wall due to the inaccessibility of access for the altar presence); for each vector 6 points (3 points for bricks and 3 for mortars), set at different heights (**Figs. a-b**), were identified (**Fig. 1b**). Other six vectors were implemented (24 measurements: 12 for bricks and 12 for mortars) in order to establish the thermo-hygrometric state of the lower level represented by the *podia*. Two measures were carried out for each vector at two different levels: level 0 (pedestrian level) and level 1 (maximum height of *podium* varying from0.23 cm (west wall *pre-Mithraeum podium*) to 0.85cm (East wall *pre-Mithraeum podium*) (**Fig.2b**), resulting in a total of 792 measurements. In this way, it was possible to obtain the materials' thermo-hygrometric state along the entire vertical profile (from 0 to 4.92 m). In particular, the area of the *podia* represents the area with the most conflictive areas in terms of conservative problems related to rising damp [12-13].

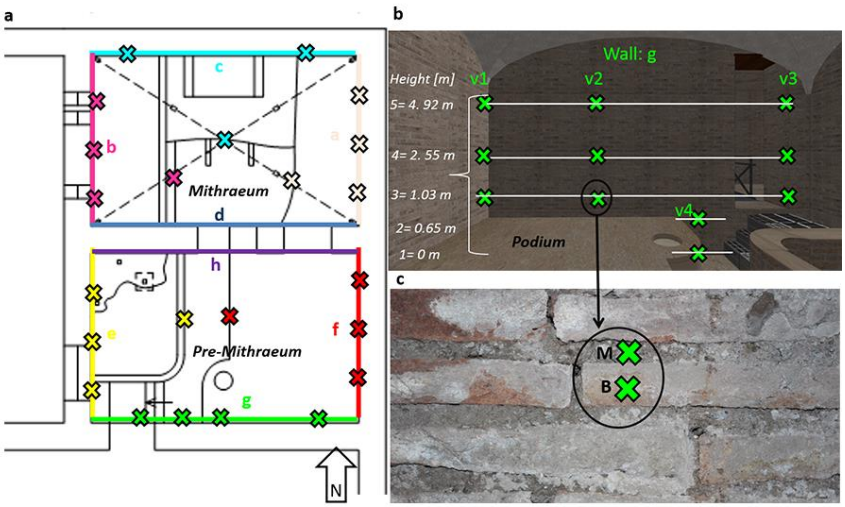

Figure 1. a) Multi- point measurements (*crosses*); **b**) South wall *pre-Mithraeum* (*green crosses*) was represented like the example above. A letter (a-f) was attributed to each wall (w). For each wall, four vectors (1-4) were assigned: from left to right; the n. 4 represents the podium's vector (pedestrian level = 0). Each measure is double (one cross represents 2 measurements); **c**) The arrow indicates the double measure: each measure (*cross*) indicates a measure on brick (B) and mortar (M); a colour was assigned to each wall, in order to facilitate its identification (and its orientation).

2.2.3 Recorded data

The measurements cover from spring 2014 to spring 2015 (**Tab. 1**), starting from the equinox or solstice for each season. Specifically, each acquisition data point takes one week approximately, due to the high number of points (**Tab. 1**), obtaining a matrix of 3290 values (22 points/wall x 6 variables x 5 monitoring campaigns).

Table 1. Measuring period.

Year	Season	Date
2014	Spring	03/26/2014-04/02/2014
2014	Summer	06/17/2014-06/20/2014
2014	Autumn	09/16/2014-09/19/2014
2014	Winter	12/15/2015-12/19/2015
2015	Spring	04/07/2015-04/08/2015

2.3 Data analysis

The data collected from each methodology was analysed with different techniques in order to bring out the conservation status of wall-building materials, the behavioural characteristics of the air near the building materials, thus revealing areas especially at high risk.

"Exploratory Data Analyses" (by Run-Sequence plots, Box & Whisker, Scatter Plot) were usually performed in order to identify any correlation between the variables (measured values) and the samples (instrument, rooms, mortar and brick).

In this work, we used a methodological sequence, starting from PCA and involving successively Box & Whisker, 3D scatter plots and representations.

Firstly, the Principal Component Analysis (PCA) - whose primary aim is determining, from the geometrical point of view, the most significant reference basis, representing the experimental data and minimizing the noise, confirming, in this way, some particular areas - was performed. The dataset was input into using the cross validation method and the SVD (Singular Value Decomposition) as algorithm. Moreover, the PCA analysis was

applied to highlight the performance of the instrument (confronting the differences between physical systems behind the instrument), individuating some materials' properties in terms of thermic capacity. This was possible using the Unscrambler version 9.7 (chemometric software package - Camo, Woodbridge, NJ, USA) package (cross validation method). Successively, the Box-and-Whisker representation, where the variables (sensors) plotted on the X-axis and the raw measured distribution represented by the Y-axis, was applied. This analytical tool shows the median domain, the distribution, spread, skew and percentile values 5% and 95% (also outliers are show) by whiskers [14, 15]. This representation has proven to be particularly significant, as it revealed important results regarding the distribution of variables (sensors) in space (seasons), pinpointing the thermic condition of the air and the contact temperature (identifying the possibility of evaporation and condensation phenomena). Finally, the 3D Scatter Bi-Plot was designed, displaying the parameters RH and T against all variables (sensors), starting from raw data, in order to enhance correlations, as well as the difference between mortar and brick in the areas and times analysed.

The data set was analysed using OriginPro 8.5.1 software.

3 RESULTS AND DISCUSSION

3.1 Principal Component Analysis (PCA)

Introducing the data obtained from of the all the measured points, a preliminary data treatment with the technology of the instrument used was tested. The obtained PCA explains 58% of the total variance with three principal components for T (the PC3 does not improve the separation) (**Fig. 2a**), and 72% of the total variance with three principal components for RH (**Fig. 2b**).

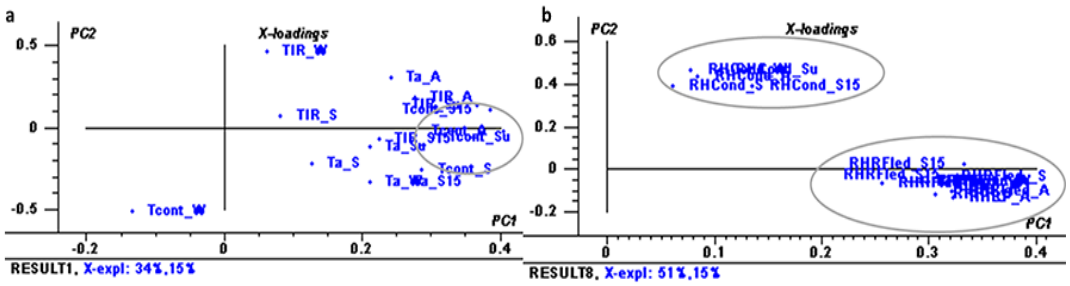

Figure 2. PCA Loadings. **a**) Temperature PC1-PC2; **b**) Relative Humidity PC1-PC2. The cluster was observed in the first three PCA although the figure only seems the first two.

In **Figure 2**, loadings representations (covariance/correlation between the original variables and the unit-scaled components) are shown, highlighting differences between the main clusters. Concerning T (**Fig. 2a**), no significant groupings were found, but it was possible to point out that the air T (recorded by two system Ta-NTC and Ts-IR) had more variability than the contact-measures of materials, except for those obtained during winter. This indicates that the surface material temperature keeps stable (thermic capacity).

For that concerns RH (**Fig. 2b**), two clear clusters were found: the moisture content is different between the surface (RHcond) and the interior of the material (19 mm), as detected by radiofrequency instrument. There was no significant correlation

between the two-radiofrequency measurements. This is important in terms of accuracy. The two modalities of data stored (RH% and led-red) are the same.

Considering the PC3 (PC1-PC3 and PC2-PC3 give a same contribute to the model), PC1-PC3 reveal that the superficial moisture content has a certain variability (above all in the spring and summer seasons) than the interior of the material (**Fig. 3**).

A successive PCA analysis was performed, evaluating the thermo-hygrometric state of each wall (**Fig. 4a-f**). Regarding the vector, no significant differences were found, with the exception of the podia (vector 4, dashed circle), due to their particular position: the *podia* (seats for the Romans that assisted the sacrificial ritual of the killing the bull) are about seventy centimetres above the pedestrian level. They represent a non-ventilated area, with the highest relative humidity values, mostly interested by the growth of vegetation, due to the likely presence of groundwater, seepage [10, 11]. Height (PC2) has proven to cause significant correlation between the values registered. A specific trend in accordance with the height was observed: a unique direction from bottom to top was manifested (**Fig. 4, black arrows**), except for the wall "d" (**Fig. 4d**). This exception, similarly to the *podia* case, can be sufficiently justified by the orientation of the building and the windows height and position, in accordance with the illumination studies conducted in this place [11] : the wall "d" represents a single confined wall, more protected from rapid exchanges with the outdoor environment.

Considering the *podia* (Ta values), three clusters were formed according to the room appurtenance (**Fig. 5**). The walls "b, f and a" show more variability.

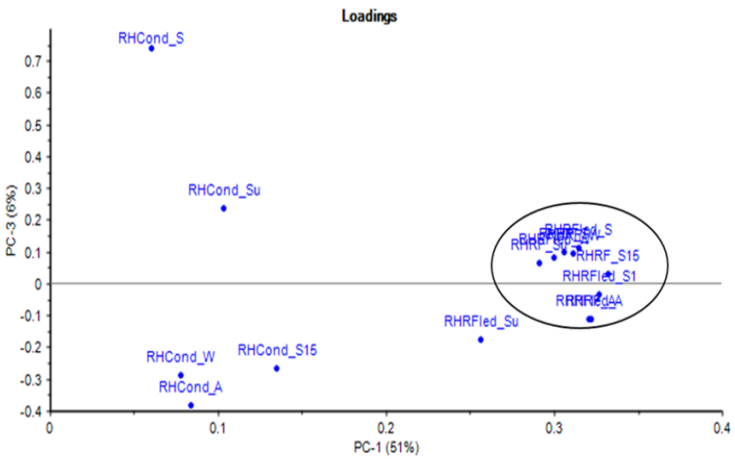

Figure 3. PC3 Loadings.

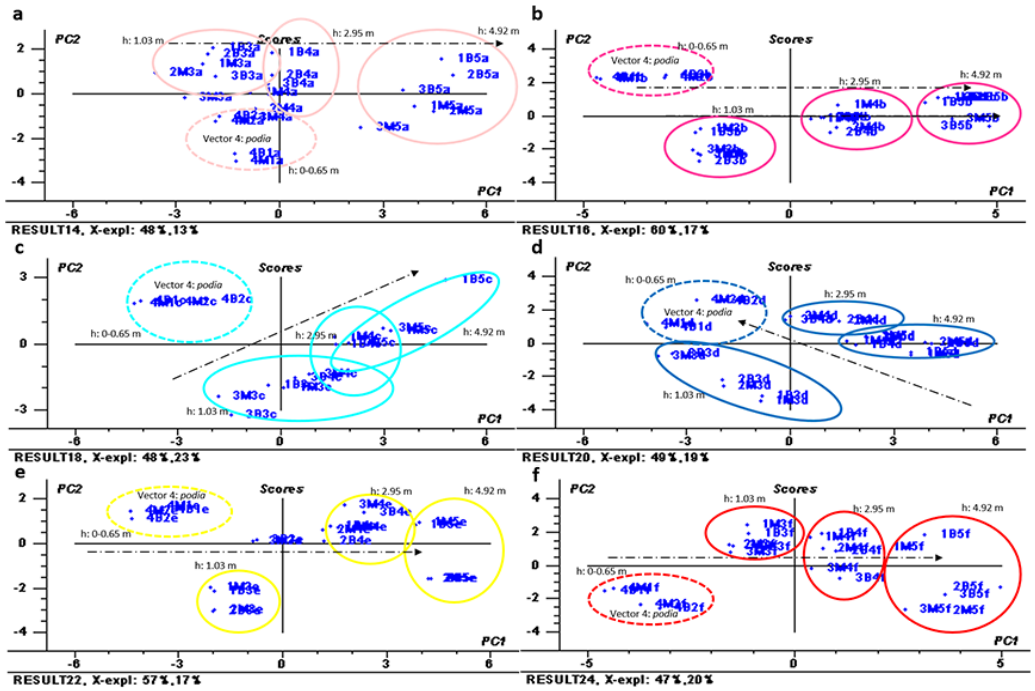

Figure 4. PCA Scores. **a**) wall "a" (*Mithraeum*); **b**) wall "b" (*Mithraeum*); **c**) wall "c" (*Mithraeum*); **d**) wall "d" (*pre- Mithraeum*); **e**) wall "e" (*pre- Mithraeum*); **f**) wall "f" (*pre-Mithraeum*). The circles (colour legend as– Fig.1) indicate the different heights (points measured). The black arrows indicate the progressive trend (bottom-up).

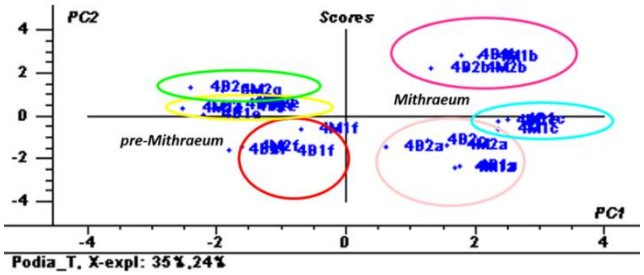

Figure 5. PCA Scores *podia*.

3.2 Box-Whiskers and Scatter Plot

Regarding the air temperature (Ta), it is higher than contact temperature (Tc) measured for both brick and mortar (**Fig. 6**), especially during the winter, where the variability is more accentuated, as evaporation and condensation processes are favoured. During summer and autumn, the gap is smaller (T keeps more stable for both). During autumn, the recorded values (Tc) are more stable (thermal capacity).

To identify the differences (T, RH) eventually presented between brick and mortar during the seasons, 3D scatter analysis was performed (**Fig. 7 a-e**). Concerning Tc, no significant differences were found (in the range of the instrumental error: ± 0.5-1°C) in the area above the *podia*, which is generally more stable.

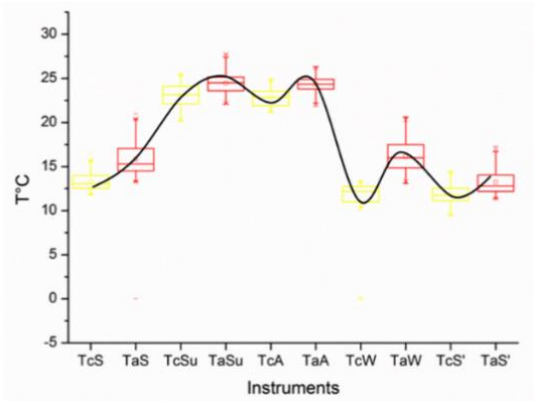

Figure 6. T_m during seasons. Tc vs. Ta

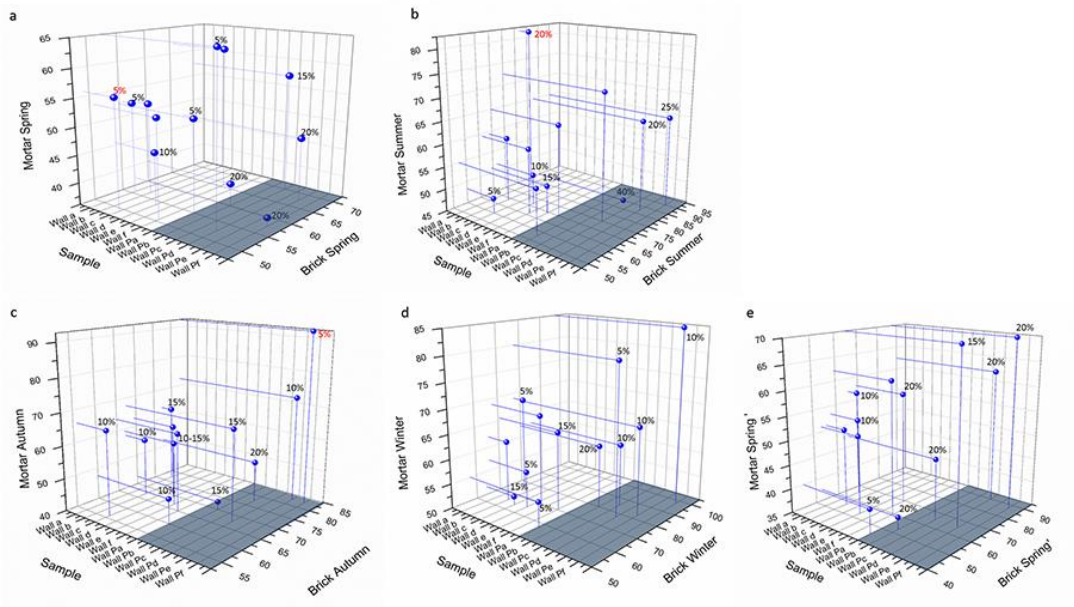

Figure 7. 3D Scatter. RH average (mortar vs. brick). **a**) Spring;**b**) summer;**c**) sutumn;**d**) winter;**e**) Spring' (Spring 2015). The *podia* areas are represented by blue rectangles.The values associated to every point are show next to it. The red values indicate the cases in which the RH percentage of mortar is higher than that of the bricks.

Regarding RH_m, in general, the bricks are characterised by a higher humidity than the mortar (with the exception of rare cases: red values in **Fig.7, a-c**). According the season, this difference changes (5-20%). Values around 20% are present in the wall "P" (*podia*).

4 CONCLUSIONS

The discrete monitoring, thought a detailed mapping of measurements and the employment of different instruments (physical principle), was built to study the building materials and to correlate the indoor environment (10 cm far to walls) to the materials, representing a full method.
The wall surface (with and without contact instruments) was investigated in order to

highlight the risk of particular phenomena, such as evaporation and condensation (responsible for damages like the salt efflorescences). This method employs a strategy that consists of a fixed number of measures repeated in selected days for one year. The outcomes of PCAs reveal that the materials' surface temperature (brick and mortar) keeps stable throughout the seasonal campaign, except in winter, where the Ta does not present major variations (the amplitude is minor). This reveals indirectly that the building materials have a good thermic capacity and the walls (with a thickness of 0.60 m) absorb homogeneously the heat, releasing it throughout time (Čáchová et al. 2014). During the winter, when the air (recorded by two system Ta-NTC and Ts-IR) is cold, the Tc is stable: Ts (IR) is in accordance with the Tc (clusters difference than the other measurements –**Fig. 3a**). The nature of materials has an important role in this sense, along with the microclimate. The influence of the outdoor environment (through the windows and several openings) is not thermally significant. Regarding RH, the instruments employed do not record any difference (conductive and radio frequency method), therefore the water content into pores from and through materials is the same (open porosity). Another important information given by PCA analysis, concerns the correlation of the walls' thermo-hygrometric state to the vectors (vertical profile: 0-5 m). No particular trend was found along the vector (expect for *podia* areas), but a very high correlation was detected along the vertical profile: a specific direction from bottom to top is evident. Assuming that the *podia*'s RH values are close to saturation and the temperature values are lower, it is possible to identify a specific trend: the RH values decrease with height (expect for the case of wall "d" where the trend is completely opposite), whilst the Tc of materials increased. The anomalous trend shown by wall "d" is due to the peculiarities of this wall: it is a single confined wall, more protected from rapid exchange with the outdoor environment. The particular thermos hygrometric behaviour of the microclimate reflects also on the material's behaviour, proving the interconnection between the system (environment) and the objects (material) kept inside. The Ta (NTC and IR method) of the podia walls have a different behaviour in the two rooms (*Mithraeum* and *pre-Mithraeum*), identifying a different microclimate. Box-Whiskers and 3D scatter plot reveal that the walls are thermally stable (with a small difference between Summer and Autumn) in the seasons except in the winter fall, when the building materials risk undergoing evaporation and condensation phenomena due to Ta being higher than Tc. In autumn the Tc is definitely more stable (thermal capacity). Regarding RHm, in general, the bricks are more humid than the mortar (except in rare cases).

The advantages have been widely discussed. The only disadvantage of the method is the manually procedure and the time spent to carry out the measurements, which can be considerably reduced by changing the PT100 probe.

ACKNOWLEDGEMENTS

The authors would like to thank the staff of the archaeological area of Ostia Antica for the permission to work in this house. This work is partially supported by the projects HAR2013-47895-C2-1-P and HAR2013-47895-C2-2-P from MINECO. Claudia Scatigno is grateful to Claudia Moricca for the English revision of the manuscript.

REFERENCES

[1] Sandrolini F, Franzoni E. An operative protocol for reliable measurements of moisture in porous materials of ancient buildings. Build Environ 2006; 41:1372-80.

[2] Grinzato E, Bison PG, Marinetti S. Monitoring of ancient buildings by the thermal method. J Cult Herit 2002; 3:21-9.

[3] Al-Homoud DMS. Performance characteristics and practical applications of common building thermal insulation materials. Build Environ 2005; 40:353-66.

[4] Korjenic A, Petránek V, Zach J, Hroudová J. Development and performance evaluation of natural thermalinsulation materials composed of renewable resources. Energy Build 2011; 43:2518-23.

[5] Singh MK, Mahapatra S, Atreya SK. Thermal performance study and evaluation of comfort temperatures in vernacular buildings of North-East India. Build Environ 2010; 45:320-9.

[6] Woloszyn M, Kalamees T, Olivier Abadie M, Steeman M, Sasic Kalagasidis A. The effect of combining a relative-humidity-sensitive ventilation system with the moisture-buffering capacity of materials on indoor climate and energy efficiency of buildings. Build Environ 2009; 44:515-24.

[7] Camuffo D, Van Grieken R, Busse H, Sturaro G, Valentino A, Bernardi A et al. Environmental monitoring in four European museums. Atmos Environ 2001;35: S127-40.

[8] European Committee for Standardisation (CEN). Conservation of cultural - property procedures and instruments for measuring temperatures of the air and the surface of objects, 2010.

[9] European Committee for Standardisation (CEN). Conservation of cultural heritage– procedures and instruments for measuring humidity in the air and moisture exchanges between air and cultural property. EN16242 2012.

[10] Scatigno C, Prieto-Taboada N, Preite Martinez M, Conte AM, García-Diego FJ, Madariaga JM. Analitycal techniques for the characterisation of historical building materials: Case study "Casa di Diana" Mithraeum (Archaeological site in Ostia Antica, Italy). In: Wythers MC, editor. Advances in Materials Science Research, New York; 2016.

[11] Scatigno C, Moricca C, Tortolini C, Favero G. The influence of environmental parameters in the biocolonization of the Mithraeum in the roman masonry of Casa di Diana (Ostia Antica, Italy). Environ Sci Pollut Res 2016.

[12] Scatigno C, Gaudenzi S, Sammartino M, Visco G. A microclimate study on hypogea environments of ancient roman building. Sci Total Environ 2016; 566:298-305.

[13] Scatigno C, Cardarelli E, De Donno G, Oliveti I, Preite Martinez M. Geophysics and geochemistry methodologies: application and techniques to structural evaluation of a roman masonry (archaeological site in Ostia Antica). 2015.

[14] McGill R, Tukey JW, Larsen WA. Variations of box plots. The American Statistician 1978; 32:12-6.

[15] Visco G, Plattner SH, Fortini P, Di Giovanni S, Sammartino MP. Microclimate monitoring in the Carcer Tullianum: temporal and spatial correlation and gradients evidenced by multivariate analysis; first campaign. Chem Cent J 2012;6: S11.

In order to validate the punctual monitoring system (direct measurement), a continuous monitoring system[27] was applied, based on air measures (T, RH) along the walls, thanks to appropriate small sensors (innovative technology). It is necessary to remark that this methodology is designed for the same aim of the direct measurement but is less time-consuming, because the measurements is done by sensors/probes. This approach consists of evaluating the air behaviour near the walls. Specifically, 29 probes, for a total of 58 thermo-hygrometric sensors (29 T probes + 29 RH probes) that are linked and positioned along the walls' surface. In this context, 28 probes are installed in the interior of the two rooms (**Fig. 32a**), and the last one is placed on the sill of a window as an outdoor climate control (**Fig. 32b**).

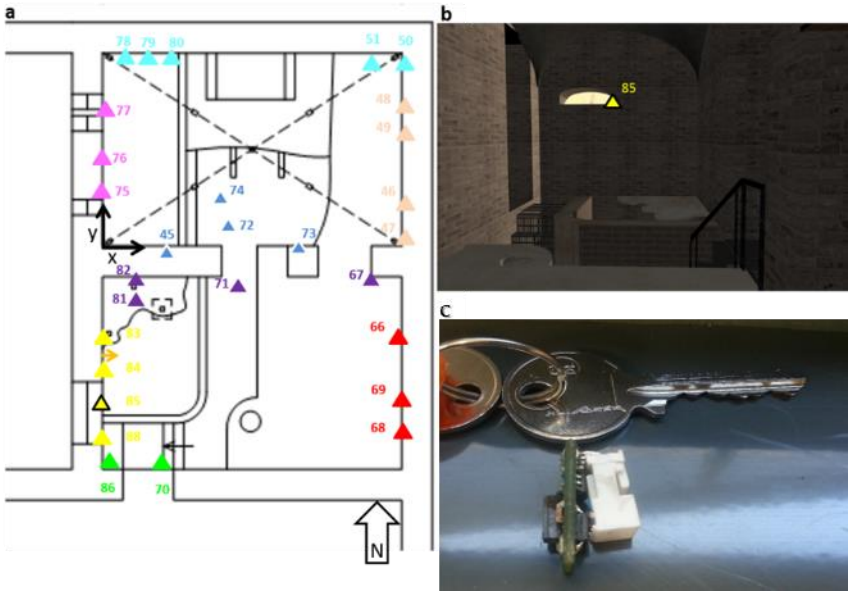

Figure 32. Positioning of the sensor. **a**) Positioning probes (numbered *triangles*); **b**) Probe n. 85 (*yellow triangle*), outdoor climate control; **c**) probe. Each one probe has a different colour due to wall belonging with a reference system (xy) to individuate the probe's position (coordinate allocation is expressed in the successive **Table 5**).

Table 5 describes the coordinate allocations (xyz) of the probes along the walls. X indicates the horizontal coordinate, y the distance of the walls surface and z indicates the height only for two probes (72, 73) that are not placed along the wall.

[27] An adapted version was published in:
Discrete and continuous monitoring to characterise The thermo-hygrometric state of wall-building materials in Ostia Antica archaeological site. Proceeding of the 8th International Congress on Archaeology, Computer Graphics, Cultural Heritage and Innovation. Arqueològica 2.0 in Valencia (ES). ISBN: 1989-9947.

Table 5. Probes description and coordinated allocation. Each one probe includes both T and RH sensors.

Reference system	Probe n.	x (cm)	y (cm)	z (cm)
Blue	45	70	102	0
	72	424	0	94
	73	400	80	116
	74	512	140	0
Pink	46	372	192	0
	47	372	89	0
	48	197	142	0
	49	196	304	0
Fuchsia	75	126	163	0
	76	176	302	0
	[◊]77	294	93	0
Azure	50	504	146	0
	51	425	201	0
	78	88	139	0
	79	174	148	0
	80	190	197	0
Green	70	226	217	0
	86	560	136	0
Yellow	83	330	90	0
	84	245	120	0
	85	164	204	0
	88	32	169	0
Red	66	7	70	0
	68	242	154	0
	69	205	280	0
Violet	67	532	164	0
	71	290	106	0
	[▫]81	84	-12	0
	82	86	80	0

[◊]Indicate that the RH sensor n. 77 are completely discarded, due to instrument anomalies, during the data recording.

[▫]Indicate that the T sensors 81-88 are not worked during the month of August.

The continuous monitoring campaign system began on the 29th of June 2014 and ended on the 21st of May 2015 including some erased dates (March was completely lost, due to technical problems). The system recorded data with a frequency of 60 data points per hour (1 data point per minute), recording a total of 43.200 data points per month (30 days × 24 h/day × 60 data points/h). Therefore, in this study, a data matrix of 401.760 (279 days × 24 h × 60 min) was obtained for each probe. The measurements were recorded in digital format by a microcontroller. All sensors were connected in parallel. Recorded data was downloaded to a pen drive.

Data was stored in the Burrito software [19]. Data analyses were carried out with the same chemometric tools and software of the previous discrete monitoring system, to better comparing the results of each method and, in this way, identifying the best procedure (time spending and costs).

The dataset was previously auto scaled. The model with two principal components (T), explaining the 100% of the total variance (**Fig. 33a**), and with two principal components (RH), explaining the 89% of the total variance (**Fig. 33b**), was selected to fit the data.

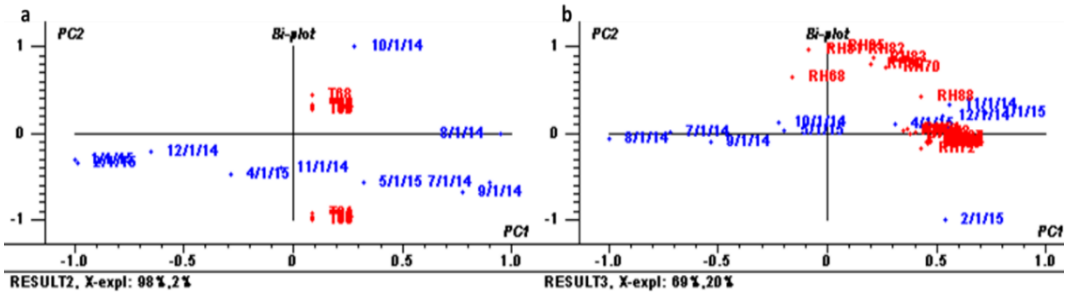

Figure 33. PCA Bi-plot (Scores-Loadings). **a**) Temperature (T_m) PC1-PC2; **b**) Relative Humidity (RH_m) PC1-PC2.

In **Figure 33** the monthly average for T (**Fig. 33a**) and RH (**Fig. 33b**) are shown. Taking into consideration the T (**Fig. 33a**), two clear groups are found: one is represented by 8 sensors (68, 81- 88) that were situated between the south west *pre-Mithraeum* wall and the north *pre-Mithraeum* wall (**Fig. 32a** – *yellow and orange triangles*). Those are the most ventilated areas due to the presence of the window and of the main entrance. All the remaining sensors (45 - 80) follow the same behaviour. No particular relationship between wall and season is found (except for October, that seems to have an own trend). Regarding RH (**Fig. 33b**), more variability of data is found, but two groups are clear: one group, more variable, is represented by sensors where were located in more ventilated areas. The sensors located along the more protected walls, away from the openings, windows and frontal walls to these, where the outdoor exchanges are frequent, represent the other one, more concise. There are no particular changes (amplitude) occurring during all the time. February represents a particular season, with a stand-alone behaviour.

To understand the thermo-hygrometric behaviour, a Multi-Curve plot was adopted (**Fig. 34**). In general, the Ta (T_{day_m}) remains stable between July and at the end of October (26.6° - 20.7° C). The winter season (17.7°- 3° C), presents greater amplitude than summer-autumn (**Fig. 34a**). Regarding RH (RH_{day_m}), it remains stable along the entire campaign with values between 84-99% (**Fig. 34b**). During the autumn-winter (October-February), the values are very close to

saturation (97-99%) (**Fig. 34b**). In both cases (T, RH), the sensors showed high co-linearity, showing the same thermo-hygrometric behaviour (considering the day mean values) (**Fig. 34**).

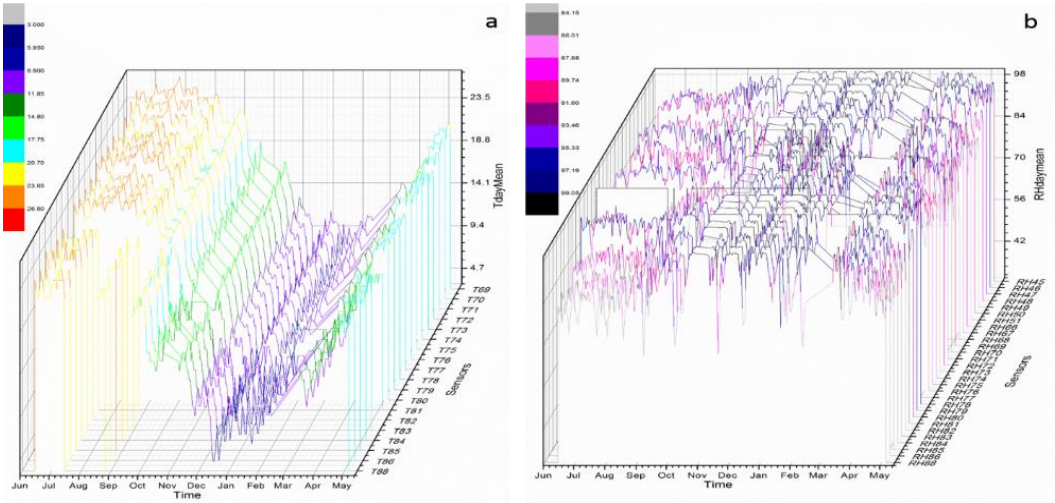

Figure 34. Multi-Curve Plot. **a**) $Tday_m$ vs. time; **b**) $RHday_m$ vs. time

Taking into account the walls' behaviour, the sensors were grouped according to the wall of belonging. Regarding T_{max} (**Fig. 35a**), Ta keeps stable along each wall (in accordance with median values). A particular case was represented by wall "e", which seems to present a minor variability (almost imperceptible) in comparison to the others boxes.

RH_{max} presents a greater variability: "a, c, d, f, h" have a smaller data variability than "b, e, g". The difference between those two groups are in accordance with the presence or absence of Qair, respectively. The first group (more data variability), is directly exposed to air flow, coming from the west side; on the contrary, the other group is represented by three wall that are not directly exposed to Qair directly, and these are the walls that feature openings (windows, openings and main entrance - door) (**Fig. 35c**).

Regarding T_{min} (**Fig. 35a**), it presents a higher amplitude than T_{max}, but the median values indicate that also Ta is stable. A particular case is represented by the walls "e" and "f", whose median values are decreasing. RH_{min} shows a higher variability (**Fig. 35b**). Walls "a, c, d, f, h" present higher RH values than "b, e, g".

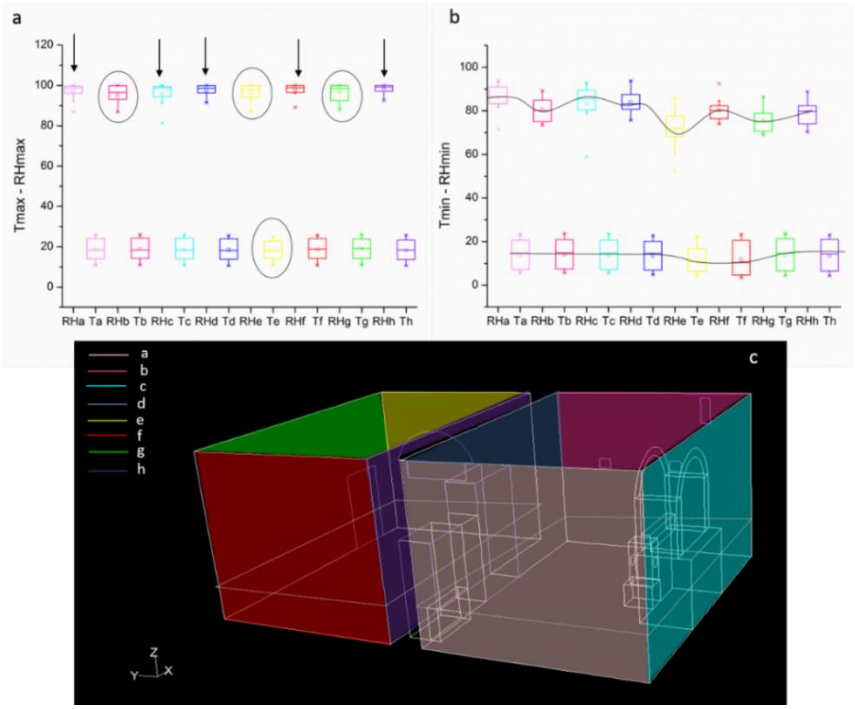

Figure 35. Box & Whisker. **a**) Box & Whisker T_{max} - RH_{max}; **b**) Box & Whisker T_{min} - RH_{min}; **c**) 3D representation. The colours are according with the wall belonging.

The outcomes of the PCA analysis reveal that the monthly Ta average presents significant differences within the rooms. The Ta closeness to the wall-building materials changes between the *pre-Mithraeum* and the *Mithraeum*, according to whether the walls are placed far or near from the window and the main entrance, indicating the most protected walls or those more exposed to air flow. A particular relationship between wall and season is found (except for October, that seems to have an own trend). Therefore, Ta retains stability in time. In addition, RHm values shows a variability in accordance with more ventilated on more protected areas and, in general, no particular changes occurred during the whole time span considered (highlighting the lack of influence of the macroclimate on the indoor environment).

The Multi-Curve Plot representation shows that, during the winter season, the Ta presents greater amplitude than during the summer-autumn season. In general, the temperature remains stable between July and the end of October (highlighting the lack of influence of the macroclimate).

Finally, the Box plot shows that Ta (max and min values) keeps stable along each wall (in accordance with median values), except for two walls of *pre-Mithraeum* (Ta_{min}): on average the walls to the west and east side are colder than the wall exposed to the south.

Regarding RH, the walls more exposed to airflow (window, openings and main door presence) present a higher variability. Specifically, RH_{max} on the walls to the southwest (*pre-Mithraeum*) and the wall sited to the west side (*Mithraeum*) is affected by climatic changes (macroclimate), as such walls are more exposed to air flow. In the RH_{min} values, the Ta close to wall-building has a higher humidity content (high RH values) than the pre-*Mithraeum*, as the room is more closed (more protected to air flow) than the second room.

Despite of the innovative probes technology, the continuous monitoring did not fulfil all the expectations it had raised. While on one hand, the procedure has allowed to identify the most humid walls, evaluating the air closest to the wall and the walls more protected from air flow and detecting differences within the single building (between *Mithraeum* and *pre-Mithraeum*), the procedure's disadvantages consist in the information obtained not being specific for materials characterisations (physical proprieties) and data treatment during the manipulation of data.

Therefore, despite being the practice more used for characterising indoor environment, and, notwithstanding its innovative technology (dimension of sensors - 0.5 cm, high memory of data storing - 10 years and more, high frequency of data recording - 1 minute), this last continuous monitoring campaigns, allow to characterise only the trends of physical parameters (T, RH), already investigated in the previous campaign (**Chapter 5.1**), identifying the episodes randomly. This practice is completely unnecessary in this building (particularly isolate microenvironment, not characterised by important fluctuations). Finally, even though the probes are collocated in the proximity of walls (about 2 cm), the system is not able to determine the thermo-hygrometric state of the building materials and, therefore, point out the risk of evaporation and condensation phenomena.

5.5 Conclusions

A complete indoor monitoring study, which has seen a specific and adequate succession of environmental parameters analyses by innovative methods (from the combined biological coverage system, the CFD model and its validation, the bioactivity discrete monitoring) has been carry out bringing to light fundamental environmental characteristics of the studied Roman building.

"Casa di Diana" *Mithraeum* was defined as a *hypogeum* environment, or underground place (even though it is not a subterranean place, but rest on a level of about 0.70 m lower than the rest of the house). Thus, due to some factors (wall thickness, not air circulation, building design) that contribute to generate a relative isolation from the outdoor environment, despite of its structural asset (the

confinement of walls or their direct exposition to the macroclimate), and different microclimates within a single volume. Moreover, the two intercommunicating rooms that compose the structure, are completely different (T, RH, Va, E, CO_2), although they are connected by two central openings (one of which of considerable dimensions). The rooms are specular (both in terms of volume and spatial distribution) but are distinguished by the presence of completely different microenvironments. These factors have a direct impact on building materials and on the AQ. The concentrations of CO_2 are relatively high (in comparison to the suggested limits and guidelines defined by law). The inputs deriving from the biological apparatus and from an inadequate air movement (air flow practically absent), making the environment uncomfortable also during the day, causing a poor AQ and a possible accelerate acidification, due to combined high RH values closed to saturation, on the wall-building material, above all for those sited at the lowest strata (*podia*). These last represents an aside from the rest of building, as well as the *pre-Mithraeum* room.

These results have been possible, as said briefly summarised above, thanks to continuous and discrete monitoring, characterised by novelty keys and by the possibility of applied to similar context or not necessary open museum.

Taking all of this into account, the information emerged in this chapter seems to have a precursor that lies behind the high RH values (close to saturation), in correspondence of the lowest area (0 -1.1m). In this sense, rising damp from the ground is a phenomenon that can be the responsible of it. In this sense, geophysical surveys are needed, not only for confirms the rising damp but also to try to understand better this particular microclimate.

Chapter 6 Geophysical surveys

Apart from its natural degradation, Built Heritage undergoes several decaying processes, due to the exposure to aggressive environmental conditions that threaten its durability and preservation [78]. One of the most harmful factors is moisture which, coming from the rain (infiltration) or by capillary (rising damp), provides, directly or indirectly, the required physic-chemical conditions for several decaying processes of porous materials [63, 79-81].

Moisture is the promoter of many decaying products. Freeze-thaw cycles, soluble salts crystallisation cycles, biological growth and chemical attack by acid rain, all dependent on the presence of high moisture values, are only some of the causes of wall rending deterioration [82-85]. In the case of rising damp, to understand and to recognise the role of this phenomenon, which damages the historical buildings, is fundamental to perform a detailed study on its nature, origin and movements across the subsoil/foundations, before penetrating the walls of the building. In this sense, it is possible to carry out development of conservation strategies and procedures focused on the safeguard of Cultural Heritage [25, 86, 87].

Additionally, understanding the inner geometry, the constructive materials and the degree of conservation is also a pivotal issue when the building under study is, as in this case, a historical masonry kept in an archaeological site, which undergoes accelerating degradation processes due to external stressors (i.e. the ravages of time, natural phenomena or human interventions).

In this sense, the application of non-destructive measurements can be an important tool in assessing the current state of an archaeological structure. In particular, geophysical techniques are the most popular because their speed and ease of execution. Furthermore, these techniques are, generally, cheaper than the invasive ones.

Geophysical methods have been applied worldwide during the last decades for archaeological purposes, in order to detect and characterize ancient structures [88]. Ground Penetrating Radar (GPR) has been employed for the detection of anomalies within the masonry components and analysing the rising damp phenomena [89]. Electrical Resistivity Tomography (ERT) can provide useful information about the hidden foundations and the surrounding geology, as long as non-invasive electrodes are used. This technique has been used on stone exposures [90] in an effort to understand the processes of stone weathering, to analyse the rising damp phenomenon and to assess the moisture content of historic walls [91]. Moreover, an estimation of the physical and mechanical parameters of the structural elements can be given by seismic tomography (ST),

focused on cracking-prone zones [17] or on the investigation of the foundation structure and ground materials of ancient buildings [92]. However, since it is not always possible to rate a single geophysical method as superior to all the others, the integration of different techniques can remove ambiguities in the interpretation of geophysical models and increase the degree of accuracy of the physical parameters [93].

Taking all of this into account, a sequence of geophysical surveys was carried out in order to assess the current conservation state of this Roman masonry. In particular, it was designed an experimental procedure, with a succession of several investigations, in order to establish the hydro-geological setting, understand the source and the movements of the rising damp that affects the walls-building and, consequently, to assess their state of conservation.

6.1 Hydro-geological setting

The ancient town of Ostia was located around 26 km far from Rome on the left bank of the mouth of the Tiber River (upper delta plain) and near the paleo-lagoon formed during the Holocene and built-up by the accumulation of sediments brought to the river. Furthermore, the hydro-geological complexes of Tiber delta are overlaid on plio-pleistocenic deposits from which depend the morphology and geometry, affecting recharge and flow distributions and the relationships with the neighbouring hydro-geological units [94]. The salt marshes have been exploited since antiquity with the use as saltworks. The ancient installations for salt production consisted of two distinct but connected basins and they continued until 1895 [4, 95].

Under this complex scenario, in view of the study of the rising damp, geophysical and geochemical techniques were performed in order to fulfil a physical and geometrical characterisation of subsoil with ERT lines (soil-structure interaction with ERT array), a reconstruction of the depth and the typology of the shallower aquifer (3D map). In particular, ERT was carried out taking advantage of the different resistivity values that the hydro-geological scenario of the area could show taking into account the existing aquifers due to both the near Tiber river (250 m far) and Tyrrhenian sea (3 km far). Moreover, geochemical analysis (soluble salts and stable isotopes, ^{18}O) were carried out to identify the origin of solutes, to isolate the main factors of the water source determining the isotopic content and to investigate the aquifer behaviour in terms of movements and distribution processes. All of these help in the interpretation of geophysical techniques, increasing the degree of accuracy. In this way, a new combined approach, based on non-invasive geophysical (ERT) and geochemical analyses, was designed.

Article 4

Geophysical and geochemical techniques to assess the origin of rising damp of a Roman building (Ostia Antica archaeological site). Article published in Microchemical Journal 129 (2016) 49-57.

Microchemical Journal 129 (2016) 49–57

Contents lists available at ScienceDirect

Microchemical Journal

journal homepage: www.elsevier.com/locate/microc

Geophysical and geochemical techniques to assess the origin of rising damp of a Roman building (Ostia Antica archaeological site)

E. Cardarelli [a], G. De Donno [a], C. Scatigno [b], I. Oliveti [a], M. Preite Martinez [b], N. Prieto-Taboada [c]

[a] University of Rome "Sapienza" - DICEA, Via Eudossiana 18, 00184 Rome, Italy
[b] University of Rome "Sapienza" - Department of Earth Science, Piazzale Aldo Moro 5, 00185 Rome, Italy
[c] University of the Basque Country (UPV/EHU), Department of Analytical Chemistry, Barrio Sarriena s/n, 48940 Leioa, Spain

ARTICLE INFO

Article history:
Received 21 April 2016
Received in revised form 27 May 2016
Accepted 3 June 2016
Available online 10 June 2016

Keywords:
Electrical resistivity tomography
Geochemistry
Ancient Roman masonry
Freshwater-salt water interface
Groundwater

ABSTRACT

A combined approach based on geophysical and geochemical analyses was carried out to determine the sources of rising damp in "Casa di Diana", a Roman building located in the Ostia Antica archaeological site (Rome, Italy). The studied building is characterized by high humidity values (closed to saturation, >90% RH) with significant efflorescence and sub-efflorescence phenomena on masonry walls.
Electrical Resistivity Tomography was performed both inside and outside the building to understand the geological setting, to estimate the freshwater-salt water interface, to locate building foundations and consequently, to evaluate the interaction between the structural elements and groundwater. On the other hand, local shallow groundwater was analysed for soluble salts and isotopic analysis ($\delta^{18}O$) to identify the origin of solutes, to isolate the main factors determining the isotopic content and to investigate the aquifer behaviour in terms of movement and distribution processes. The water samples were collected from one well and one tank sited inside and outside

The geophysical inverted models, were able to detect a freshwater aquifer at the shallower depths (2–5 m) in correspondence to the Roman foundation walls (extended at depth up to 8 m), while below (8–10 m from surface) the salt water presence is likely. The chemical analysis confirmed that groundwater is slightly mineralized even though the salt concentration can be compatible with an interaction with sea salts, maybe due to the depth of the foundation walls.
Therefore, the proposed approach is suitable for understanding the causal relationship between the observed phenomena, assessing the current degree of conservation of the archaeological site and consequently planning the recovery actions.

1. Introduction

Nowadays, built heritage undergoes several decaying processes, apart from their natural degradation, due to exposure to aggressive environmental conditions that threaten its durability and preservation [1,2].

In the archaeological context, the knowledge of the inner geometry, constructive materials and state of conservation of ancient buildings, is particularly important especially when the historical site is located in a complex geological scenario [3]. Therefore, in these cases the investigation methods should include both the evaluation of the subsoil (soil and groundwater) and of the masonry (wall, foundations) in order to plan solutions for building conservation and recovery.

In this sense, in the last two decades, the use of non-invasive by the ravages of time, human interventions or natural phenomena, has gained increasing interest due to several reasons: (i) the continuing improvement in survey equipment performance, automation and information resolution of sensors and devices; (ii) the advances in processing and imaging software; (iii) the non-destructive nature and the cost-effectiveness over traditional excavation.

Hence, the application of non-destructive testing methodologies (NDT) represents a helpful tool for evaluation the interaction between the structure and the subsoil without any damage on the masonry. Several geophysical methods were applied worldwide during last decades for archaeological purposes to detect and characterize ancient structures [4,5]. A useful review of geophysical and NDT methods for the assessment of masonry structures and a summary of their basic principles was found in some cases [6,7]. Some examples are present in literature about the application of Ground Penetrating Radar (GPR) for detecting anomalies within the masonry component [8] and analysing the rising dump phenomena [9], as well as for characterizing the interaction of the foundation structure and subsoil, occasionally in

E-mail address: claudia.scatigno@uniroma1.it (C. Scatigno).

http://dx.doi.org/10.1016/j.microc.2016.06.006
0026-265X/

Fig. 1. "Casa di Diana" building. a) Street view. b) External parietal walls. c) Internal parietal wall. d) Fountain courtyard remains.

3. Methods, data acquisition and processing

3.1. Electrical resistivity tomography (ERT)

Firstly, two 2D normal ERT lines (L1 and L2) were acquired along two sides of the building (Fig. 2a), using stainless steel electrodes (Fig. 2b) in order to retrieve a physical and geometrical characterization of subsoil, to reconstruct the depth and the typology of the shallower aquifer and to estimate the depth of the interface between salt and fresh water.

Then both 2D (L3 and L4) and a 3D array (L5) were performed inside the building (Fig. 2), using non-invasive copper square plates as electrodes, having a diameter of 10 cm (Fig. 2c), for evaluating the soil-structure interaction through the reconstruction of 2D and 3D high-resolution resistivity models. Thus, we can build a 3D map of the foundation of the building and of the subsoil with indication of possible anomalies in the groundwater circulation. The 3D survey was carried out with a U-shaped array where electrodes are placed alongside the L3 and L4 lines and partially in front of the building (Fig. 2), for a global investigated area of about 400 m^2. The dipole-dipole array was used as it combines consistent signal strength with good resolution and depth of investigation. Data were acquired by using the parameters in Table 1.

ERT dataset are inverted with the VEMI algorithm - *Versatile interface for Electrical Modelling and Inversion* [40,41], built within the EIDORS environment [42]. This algorithm is able to perform both 2D and 3D inversion, by solving the forward problem with a finite-element approximation of the Poisson's equation governing the physical problem [43–45] while inversion is carried out using a Gauss-Newton formulation [46]. The inversion is performed using the blocky inversion function [47], with cut-off factors set to 0.1 and 0.05 for the robust data and model constraints respectively. A priori information can be added by means of weights on the smoothness matrix (for enhancing anomalies elongated in the x- or in the z- direction) or by setting inequality constraints on the model (where we know the range of variation of the resistivity in the study area). In this particular case, we made no preliminary assumption on the soil layering.

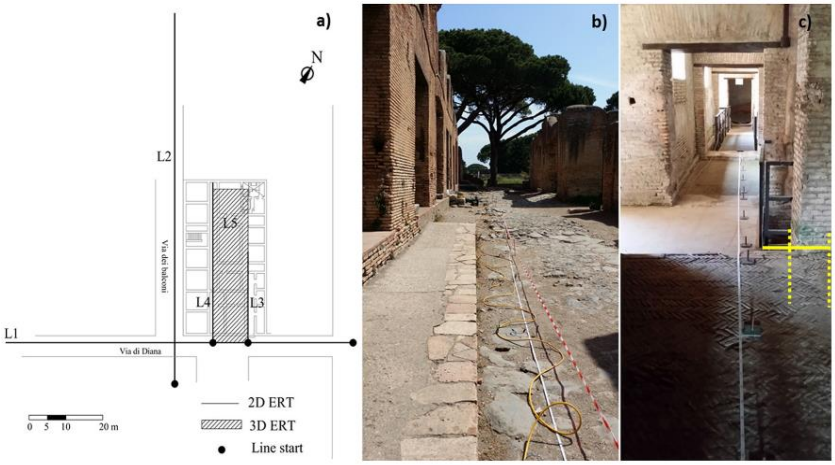

Fig. 2. Geophysical field data acquisition. a) Top view of the geophysical ERT investigation. b) External ERT lines with stainless steel electrodes. c) Internal ERT lines by using non-invasive 10 cm square copper plates. The well is located in correspondence to the dot line.

Table 1
Parameters for geophysical field data acquisition.

Technique	Acquisition details
Electrical Resistivity Tomography (ERT)	*Device*: Iris Syscal Pro 48-channel resistivimeter *Array*: Dipole-dipole (customized sequence) 2D lines, dipole-dipole 3D array *Number of lines*: four 2D lines (L1, L2, L3, L4) and one 3D array (L5) *Electrodes*: 24/48 copper plates (10 × 10 cm) for internal surveys, 48 stainless steel electrodes for external surveys *Electrodes spacing*: 2 m (L1, L2), 1 m (L3), 1.75 m (L4), 3 m (L5)

In addition to this, a water sample was collected from the well, its resistivity measured by using a simple four-electrode configuration on a cylindrical device [53], in order to evaluate the water type (fresh, salt or brackish) and to give an estimation of the aquifer porosity. In fact, the porosity of the shallow aquifer can be derived by using the Archie's law [54] as follows (Eq. (1)):

$$F = \frac{\rho}{\rho_w}, \quad F = a\phi^{-m} \tag{1}$$

where F is the formation factor, ρ and ρ_w the bulk and water resistivity respectively, a and m coefficients depending on tortuosity and cementation of the investigated medium and Φ the porosity.

3.2. Geochemical analysis of the water samples

Water samples were collected from the available water resources (well and tank), according to the non-invasive peculiarity of this work, with the purpose to study the well water composition and to support the 2D and 3D ERT survey performed inside the building. Ions (cations and anions) and $\delta^{18}O$ isotope analysis were conducted from these waters. After a direct inspection of the well, we deduced that it was built in brickwork, 4.20 m deep (water level at 2.7 m) and has a natural soil bottom floor. For this, a reasoned non-probabilistic sampling design has been implemented: to evaluate if a different ions and isotopic content (mixing processes) were present in the water volume and to control a possible connection with an aqueduct system, three samples were collected at different depths (W1, W2, W3 in Fig. 3a) in two different seasons. In fact, to obtain detailed information about groundwater flow paths and spring recharge areas and to better understand the above described hydrogeological setting, two water sampling campaigns were conducted in 2015 (summer and autumn), while one sample was collected from the external tank (T1 in Fig. 3b).

The quantification of the anions and cations present in the water samples was carried out by a Dionex ICS 2500 ionic chromatograph with a suppressed conductivity detector ED50. An IonPac AS23 (4 × 250 mm) column and IonPac AG23 (4 × 50 mm) precolumn were used for the separation of anions (fluoride, chloride, sulphate and nitrate). The quantification of cations (sodium, potassium and calcium) was conducted by using an IonPac CS12A (4 × 250 mm) column and IonPac CG-12A (4 × 50 mm) precolumn from Vertex. In the case of cations, 20 mM CH_4SO_3 as mobile phase, 75 mA of suppression current and 1 ml min^{-1} flow was used.

The oxygen isotopic composition was measured by means of the water-CO_2 equilibration technique [48]. Isotopic analyses were performed with a Finnigan Delta Plus mass spectrometer. The results are reported in d% units versus the international V-SMOW standard [49]. The standard deviations of the measurements were equal to approximately ±0.1 for $^{18}O/^{16}O$.

4. Results and discussion

4.1. Electrical resistivity tomography

The results of the geophysical investigations will be described in the following with reference to the two aims described above: detection and characterization of subsoil and study of the interaction between subsoil and building foundations.

Inverted models related to L1 (Fig. 4a) and L2 (Fig. 4b) lines performed outside the building have a similar behaviour in terms of layering and resistivity values. An high resistivity layer (>80–100 Ω m) having a variable thickness of 2–8 m, related to the Roman basalt pavement and to the 3D effect of building foundations [15], is superimposed to a very low resistivity zone (ρ < 1 Ω m) due to the salt water. As a matter of fact, the effective resistivity layering can be evaluated only on the line L2 at x > 40 m, where the survey has been

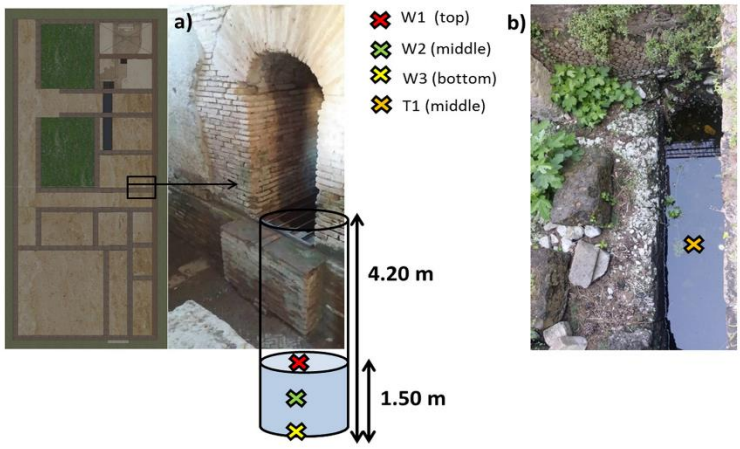

Fig. 3. Sampling design. a) Well. b) Tank.

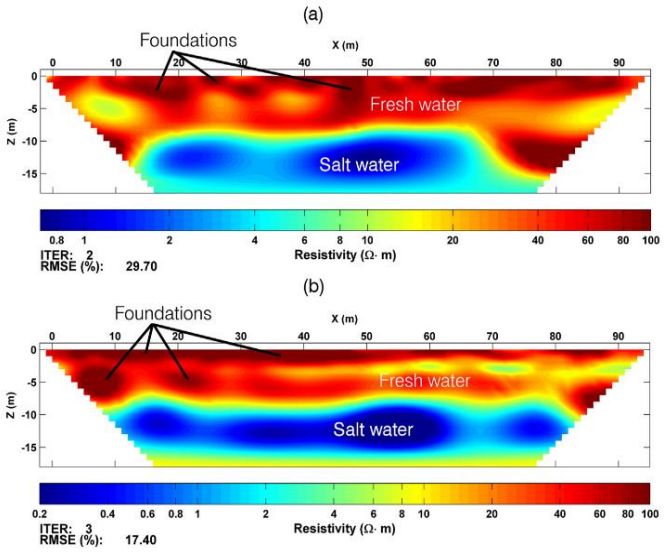

Fig. 4. Inverted models of 2D ERT. a) L1 line. b) L2 line.

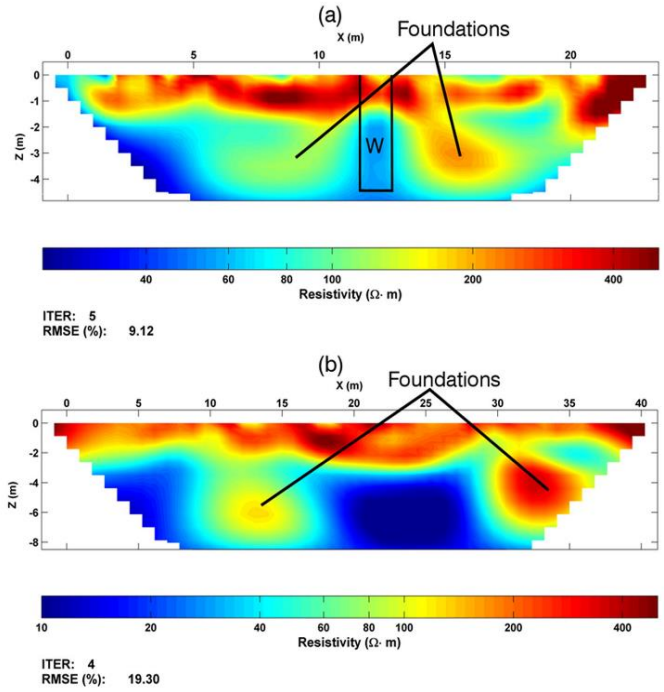

Fig. 5. Inverted models of 2D ERT. a) L3 line. Well is marked with "W". b) L4 line.

Table 2
Chemical composition of sampled waters (meq). W1–W3: water from well. T1: water from rainfall (outer tank). The HCO_3^- concentration is estimated.

Sample ID	Date	Na^+	K^+	Mg^{2+}	Ca^{2+}	Sr^{+2}	F^-	ClO_2^-	Cl^-	Br^-	NO_3^-	PO_4^{3-}	SO_4^{2-}	HCO_3^-
W1	11/1/15	3.1	1.1	0.71	1.0	n.d	0.02	n.d	2.7	0.001	0.16	n.d	0.33	2.7
W2	11/1/15	3.1	1.1	0.72	0.95	n.d	0.03	n.d	2.8	0.001	0.17	n.d	0.34	2.5
W3	5/7/15	2.7	1.1	0.76	1.1	0.003	0.03	n.d	2.8	0.003	0.20	0.40	0.33	1.8
T1	11/1/15	2.5	1.0	0.58	0.74	n.d	0.02	n.d	2.1	n.d	0.0004	n.d	0.23	2.5

can be visible ($r = 0.90$). Thus, it seems possible a marine water interaction in the well, since the total salts concentration in this sample (W3) is 0.049%, compatible with a freshwater/brackish water concentration. Moreover, the chlorine total concentration is 0.01%, lower compared with sea water. For all of that reasons, the soluble salts analysis reveals that the measured water seems to have some influence from the marine water, but its nature corresponds to freshwater/brackish water. Therefore, the rising damp has probably a marine salts contribution (paleo-lagoon origin).

The Chebotarev diagram [50] was used for visualization and classification of hydrochemical data (Fig. 7). One hydrogeochemical facies is observed: $K^+ > Ca^{2+}$: $HCO_3^- > SO_4^{=}$.

The "dominant" of K^+ among cations while among anions, HCO_3^- is "dominant", identifying a genetic classification of this type. Regarding the latter, the W3 sample has shown a slight increase ($HCO_3^- > SO_4^{=}$) in comparison to the others, indicating a little mineral weathering and favouring mineral dissolution [51].

With regard to isotopic analysis of the well samples, the $\delta^{18}O$ analyses exclude a supply/fed of sea water because the value is strongly negative (Table 3), indicating a contribution from an aquifer fed by the inner areas, less coastal waters (maybe the "Malafede" basin).

The water of the external tank has a fairly typical isotopic composition of local precipitation [52] with less salinity and the same order of enrichment in cations and anions with respect to the well. Finally, the origin of the above mentioned salts can be ascribed to marine aerosol (cyclic salts) for the tank, while for the well the salt enrichment is due to the influence of the salt deposits in the area [31] or to the interaction with the saline water.

5. Conclusions

The integration of geophysics and geochemical techniques allowed us to obtain a geometrical, physical and chemical characterization of the building and of the surrounding area and consequently to assess the causes of the rising damp affecting the archaeological structure.

Owing to 2D geo-electrical survey we are able to identify both the freshwater aquifer (piezometric level at about 2.5 m) and the salt water presence (resistivity values <1 Ω m from 8 to 10 m). The aquifer porosity, deduced from the Archie's law, where the water resistivity was measured in the laboratory and the bulk resistivity inferred from the ERT models, is pertinent to the in situ sand deposits.

The 3D survey performed inside the building detects two deep anomalous bodies, probably related to the "Casa di Diana" foundation walls. Although few information is present in literature about the foundations of these building, we can reasonably state that resistivity values higher than 80–100 Ω m could be ascribed to anthropic features (pavement, foundations), since the resistivity range of the geological formations (soil, freshwater and salt water), reconstructed with the external ERT lines, is limited from 0.1 to 80 Ω m.

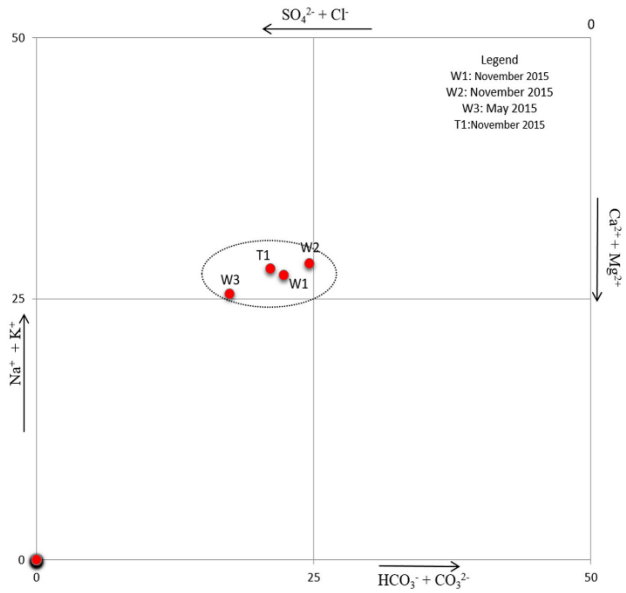

Fig. 7. Chebotarev diagram.

Table 3
Amount weighted mean oxygen values. (VSMOW: Vienna standard mean ocean water).

Sample ID	δ^{18} O‰ (V-SMOW)
W1	−6.6
W2	−6.7
T1	−5.7

Thanks to geochemical techniques, we identify the typology of the well water (paleo-lagoon "no local" water) where an interaction with the salt water (or with salt deposits). The salt concentration in the external tank should be due to marine aerosol (cyclic salts). The interaction between fresh and salt water could be enhanced by the presence of deep foundation walls up to 8 m that is the depth of the salt water in this area.

Therefore, the rising damp owns a marine salt contribution (paleo-lagoon origin) leading to the external evidences on the "Casa di Diana" building (material damages, efflorescence, etc.)

The results demonstrate that the analytical integration of geophysical and geochemical techniques can be an innovative tool for assessing the causal relationship between the observed evidenced and the occurring phenomena in order to assess the current degree of conservation of the archaeological site and consequently to plan the recovery actions.

Acknowledgements

The authors would like to thank the staff of the archaeological area of Ostia Antica, especially the director Dr. Cinzia Morelli, the security company, and the technical staff (Drs. Paola Germoni, Flora Panariti, Orietta Mantovani) for the permission to work in this house.

The geophysical campaign was financially supported by the Ateneo Grant 2015 - Sapienza University of Rome.

The work developed in the University of the Basque Country (UPV/EHU) has been partially supported by the project DISILICA-1930 (ref. BIA2014-59124-P) funded by the Spanish Ministry of Economy and Competitiveness (MINECO) and the European Regional Development Fund (FEDER).

References

[1] N. Prieto-Taboada, M. Maguregui, I. Martinez-Arkarazo, M. Olazabal, G. Arana, J. Madariaga, Spectroscopic evaluation of the environmental impact on black crusted modern mortars in urban–industrial areas, Anal. Bioanal. Chem. 399 (2011) 2949–2959.
[2] N. Prieto-Taboada, I. Ibarrondo, O. Gómez-Laserna, I. Martinez-Arkarazo, M. Olazabal, J. Madariaga, Buildings as repositories of hazardous pollutants of anthropogenic origin, J. Hazard. Mater. 248 (2013) 451–460.
[3] M.C. Laurenti, Le Coperture Delle Aree Archeologiche: Museo Aperto, Gangemi Editore spa, 2012.
[4] C. Gaffney, Detecting trends in the prediction of the buried past: a review of geophysical techniques in archaeology", Archaeometry 50 (2008) 313–336.
[5] D. Goodman, S. Piro, GPR Remote Sensing in Archaeology, Springer, 2013.
[6] R. Flint, P. Jackson, D. McCann, Geophysical imaging inside masonry structures, NDT E Int. 32 (1999) 469–479.
[7] D. McCann, M. Forde, Review of NDT methods in the assessment of concrete and masonry structures, NDT E Int. 34 (2001) 71–84.
[8] C. Maierhofer, S. Leipold, Radar investigation of masonry structures, NDT E Int. 34 (2001) 139–147.
[9] E. Gabrielli, C. Colla, Investigation of damp and salt distribution in outdoors full-scale masonry wall via wireless monitoring and radar testing, Key Eng. Mater. 624 (2014).
[10] E. Cardarelli, A. Godio, G. Morelli, L. Sambuelli, G. Santarato, L. Socco, Integrated geophysical surveys to investigate the Scarsella vault of St. John's baptistery in Florence, Lead. Edge 21 (2002) 467–470.
[11] G.N. Tsokas, N. Diamanti, P.I. Tsourlos, G. Vargemezis, A. Stampolidis, K.T. Raptis, Geophysical prospection at the Hamza Bey (Alkazar) monument Thessaloniki, Greece, Mediterr. Archaeol. Archaeometry 13 (2013) 9–20.
[12] N. Diamanti, G. Tsokas, P. Tsourlos, A. Vafidis, Integrated Interpretationof Geophysical Datainthe Archaeological Site of Europos (Northern Greece), Archaeol. Prospect. 12 (2005) 79–91.
[13] E. Cardarelli, R. De Nardis, Seismic refraction, isotropic anisotropic seismic tomography on an ancient monument (Antonino and Faustina temple AD 141), Geophys. Prospect. 49 (2001) 228–240.
[14] L. Polymenakos, S. Papamarinopoulos, A. Miltiadou, N. Charkiolakis, Investigation of the foundations of a Byzantine church by three-dimensional seismic tomography, J. Appl. Geophys. 57 (2005) 81–93.
[15] E. Cardarelli, G. Di Filippo, Integrated geophysical methods for the characterisation of an archaeological site (Massenzio Basilica—Roman forum, Rome, Italy), J. Appl. Geophys. 68 (2009) 508–521.
[16] O. Sass, Rock moisture measurements: techniques, results, and implications for weathering, Earth Surf. Process. Landf. 30 (2005) 359–374.
[17] L. Mol, P. Preston, The writing's in the wall: a review of new preliminary applications of electrical resistivity tomography within archaeology, Archaeometry 52 (2010) 1079–1095.
[18] O. Sass, H. Viles, Wetting and drying of masonry walls: 2D-resistivity monitoring of driving rain experiments on historic stonework in Oxford, UK, J. Appl. Geophys. 70 (2010) 72–83.
[19] V. Sousa, N. Almeida, I. Meireles, J. de Brito, Anomalies in wall renders: overview of the main causes of degradation, Int. J. Archit. Herit. 5 (2011) 198–218.
[20] F. Sandrolini, E. Franzoni, An operative protocol for reliable measurements of moisture in porous materials of ancient buildings, Build. Environ. 41 (2006) 1372–1380.
[21] E. Larsen, C. Nielsen, Decay of bricks due to salt, Mater. Struct. 23 (1990) 16–25.
[22] P.B. Lourenço, E. Luso, M.G. Almeida, Defects and moisture problems in buildings from historical city centres: a case study in Portugal, Build. Environ. 41 (2006) 223–234.
[23] L. Lambs, Correlation of conductivity and stable isotope 18O for the assessment of water origin in river system, Chem. Geol. 164 (2000) 161–170.
[24] M. Barbieri, T. Boschetti, M. Petitta, M. Tallini, Stable isotope (2H, 18 O and 87 Sr/86 Sr) and hydrochemistry monitoring for groundwater hydrodynamics analysis in a karst aquifer (Gran Sasso, Central Italy), Appl. Geochem. 20 (2005) 2063–2081.
[25] B. Andreo, C. Liñán, F. Carrasco, C. Jiménez de Cisneros, F. Caballero, J. Mudry, Influence of rainfall quantity on the isotopic composition (18O and 2H) of water in mountainous areas. Application for groundwater research in the Yunquera-Nieves karst aquifers (S Spain), Appl. Geochem. 19 (2004) 561–574.
[26] C. Scatigno, C. Moricca, C. Tortolini, G. Favero, The influence of environmental parameters in the biocolonization of the Mithraeum in the roman masonry of Casa di Diana (Ostia Antica, Italy), Environ. Sci. Pollut. Res. (2016).
[27] C. Vittori, I. Mazzini, F. Salomon, J. Goiran, S. Pannuzi, C. Rosa, A. Pellegrino, Palaeoenvironmental evolution of the ancient lagoon of Ostia Antica (Tiber delta, Italy), J. Archaeol. Sci. 54 (2015) 374–384.
[28] P. Santi, F. Antonelli, A. Renzulli, P. Pensabene, Leucite phonolite millstones from the Orvieto production centre: new data and insights into the Roman trade, Period. Mineral. 73 (2004) 57.
[29] P. Bellotti, C. Caputo, S. Ciccacci, D. De Rita, S. Donati, P. Fredi, R. Funiciello, G. La Monica, B. Landini, F. Marra, Fundaments for a geomorphological overview on Roma and its surroundings, Suppl. Geogr. Fis. Dinam. Quat. (1997) 105–121.
[30] F. Di Rita, A. Celant, D. Magri, Holocene environmental instability in the wetland north of the Tiber delta (Rome, Italy): sea-lake-man interactions, J. Paleolimnol. 44 (2010) 51–67.
[31] P. Bellotti, G. Calderoni, F. Di Rita, M. D'Orefice, C. D'amico, D. Esu, D. Magri, M.P. Martinez, P. Tortora, P. Valeri, The Tiber river delta plain (central Italy): coastal evolution and implications for the ancient Ostia Roman settlement, The Holocene 21 (2011) 1105–1116.
[32] G. Ciotoli, G. Etiope, F. Florindo, F. Marra, L. Ruggiero, P.E. Sauer, Sudden deep gas eruption nearby Rome's airport of Fiumicino, Geophys. Res. Lett. 40 (2013) 5632–5636.
[33] J. Carlut, G. Chazot, H. Dessales, É. Letellier, Trace element variations in an archeological carbonate deposit from the antique city of Ostia: environmental and archeological implications, Compt. Rendus Geosci. 341 (2009) 10–20.
[34] A.T. Hodge, Vitruvius, lead pipes and lead poisoning, Am. J. Archaeol. 85 (1981) 486–491.
[35] É. Bukowiecki, M. Bedello Tata II, Le acque e gli acquedotti nel territorio Ostiense e Portuense: ritrovamenti e ricerche recenti (MEFRA: Mélanges de l'École française de Rome), 118 (2006) 1000–1064.
[36] J. Adam, É. Bukowiecki, H. Dessales, J. Dubouloz, F. Zevi, Ostie, l'eau dans la ville, Châteaux d'eau et réseau d'adduction (CollÉFR, 402), 1 Vol., 2010.
[37] C. Scatigno, N. Prieto-Taboada, M. Preite Martinez, A.M. Conte, F.J. García-Diego, J.M. Madariaga, Analitycal techniques for the characterisation of historical building materials: Case study "Casa di Diana" Mithraeum (Archeological site in Ostia Antica, Italy), in: M.C. Wythers (Ed.), Advances in Materials Science Research, Nova Science Publishers, Inc., New York, 2016.
[38] F. Van Wonterghem, Mededelingen van het Nederlands Instituut te Rome, Antiquity (1996).
[39] W. Kloppmann, O. Rolland, E. Proust, A.T. Montech, Soluble salt sources in medieval porous limestone sculptures: a multi-isotope (N, O, S) approach, Sci. Total Environ. 470–471 (2014) 559–566.
[40] G. De Donno, 2D tomographic inversion of complex resistivity data on cylindrical models, Geophys. Prospect. 61 (2013) 586–601.
[41] G. De Donno, E. Cardarelli, A Flexible Interface for Tomographic Inversion of Real and Complex Resistivity Data in EIDORS, 2015.
[42] A. Adler, W.R. Lionheart, Uses and abuses of EIDORS: an extensible software base for EIT, Physiol. Meas. 27 (2006) S25.
[43] E. Cardarelli, F. Fischanger, 2D data modelling by electrical resistivity tomography for complex subsurface geology, Geophys. Prospect. 54 (2006) 121–133.
[44] A. Dey, H. Morrison, Resistivity modelling for arbitrarily shaped two-dimensional structures, Geophys. Prospect. 27 (1979) 106–136.
[45] A. Dey, H.F. Morrison, Resistivity modeling for arbitrarily shaped three-dimensional structures, Geophysics 44 (1979) 753–780.
[46] G. De Donno, E. Cardarelli, 3D complex resistivity tomography on cylindrical models using EIDORS, Near Surf. Geophys. 12 (2014) 587–598.
[47] R. Wolke, H. Schwetlick, Iteratively reweighted least squares: algorithms, convergence analysis, and numerical comparisons, SIAM J. Sci. Stat. Comput. 9 (1988) 907–921.
[48] S. Epstein, T. Mayeda, Variation of O 18 content of waters from natural sources, Geochim. Cosmochim. Acta 4 (1953) 213–224.
[49] H. Craig, Isotopic variations in meteoric waters, Science 133 (1961) 1702–1703.
[50] I. Chebotarev, Metamorphism of natural waters in the crust of weathering—1, Geochim. Cosmochim. Acta 8 (1955) 22–48.
[51] W. Stumm, J. Morgan, Aquatic chemistry, chemical equilibria and rates in natural waters, John Wiley & Sons (2012).
[52] A. Longinelli, E. Selmo, Isotopic composition of precipitation in Italy: a first overall map, J. Hydrol. 270 (2003) 75–88.
[53] E. Zimmermann, A. Kemna, J. Berwix, W. Glaas, H. Münch, J. Huisman, A high-accuracy impedance spectrometer for measuring sediments with low polarizability, Measurement Science and Technology 19 (2008) 105603.
[54] G.E. Archie, The electrical resistivity log as an aid in determining some reservoir characteristics, Transactions of the AIME 146 (1942) 54–62.
[55] A. Kaufman, G. Keller, Methods in Geochemistry and Geophysics (1983).

For all of these, it was remarkable the presence of three shallow sub-layers (1-basalt pavement, 2-freshwater shallow aquifer located within the sand alluvial deposits and 3-salt water) and the contribution of cyclic salts in the measured water samples (tank and well), which could indicate the interaction of the brick made structures (well and tanks) with the freshwater shallow aquifer but enriched with salts.

In order to solve these doubts, a simple *in-situ* sound velocity study was conducted at the beginning of September 2016[28] (per 1 day) by a probe set into the well that can validate the nature of the shallow aquifer according the sound velocity reference values. Unfortunately, the measures were not conducted in the outer and close tanks (others possible source of water), because in that day, they appeared to have dried out.

The measurements were carried out by the use of a probe (Monitor SVP v. 2c, Valeport, UK) introduced in the well. Sound velocity, P and T were recorded in the first 5 minutes of measure (sampling time of 1 minute at 1 Hz, disregarding the go down and climb measurements), giving values of sound velocity of 1472 m/s. Regarding the contribution of cyclic salts found in the previous work (**Article 4**), this result confirmed again that the measured water was freshwater (not saltwater). Really, the brackish water is characterized with values around 1485 m/s until 1495, while the surface Tyrrhenian Sea waters were 1509 and 1540 m/s in winter and summertime, respectively[29] (**Fig. 36**). Thus, the results obtained by sound velocity discredited that the measured water was affected by saline intrusion of the relative close Tyrrhenian Sea. What is more, the obtained results were compatible with the theory of John Cutnell (1998) [96], thus, the values are in the range of compatibility of the freshwater values. Therefore, the cyclic salts can be linked probably to the subsoil, where minerals and salts are circulating. It is important to remark that the subsoil is very rich in salts, this fact is evident due to the exploitations of salt marshes until 1895 [4, 95]. This salt enrichment depends on the water availability (weather changes). In this sense, during the drought period, the freshwater level decreases being a little been more enriched by soil mineralization (cyclic salts) but being always considered as freshwater. Contrary, during floods the freshwater shallow increases its level, reducing the salt content. It is important to underline that the archaeological site is affected by often floods so these level changes are usual in the area under study. Moreover, this sound velocity analysis also revealed significant water level changes in the well of about 0.40 m (**Fig. 36**), that is, a reduction of about 2 m in comparison with the previous

[28] Survey was conducted in collaboration with National Research Council, Institute for Environmental Engineering and Geosciences CNR-IGAG (Ph.D. Alessandro Bosman).
[29] Value generally influenced by only temperature parameter – thermocline.

work (2.4 m -**Article 4**). This level of the water observed, together with the detected in the tanks (zero, respect to that recognised in the previous work where were fill up – **Article 4**) revealed an important issue about the flow paths and recharge areas connected with the aquifer. For all of that, it was evident that the water measured in the well was not affected by the saline aquifer and the probably enrichment with salts was due to the interaction with the subsoil.

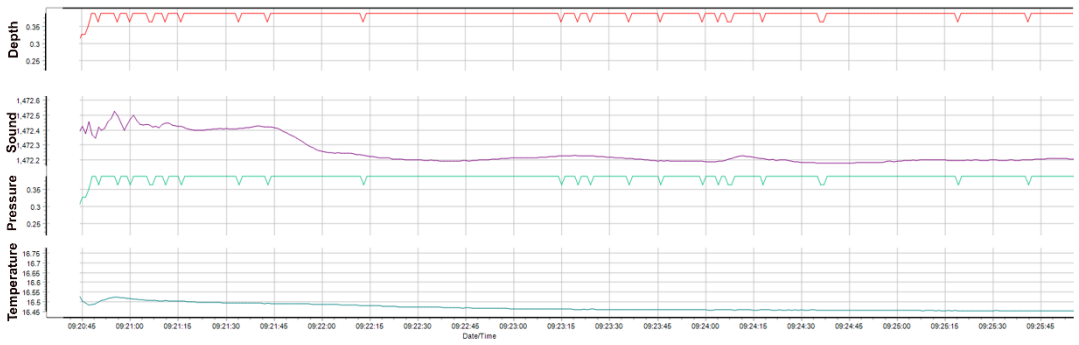

Figure 36. Sound water velocity trend. On the x axis is reported the time and on the y the measured parameters.

An ulterior evidence of the not-existent influence on the saline water aquifer in the freshwater aquifer derived by a hydrological and chemical investigations conducted in the surroundings of the site under study in the 2007 [94]. The researchers studied the water levels of the Tiber delta (sedimentary bodies' reconstruction) by the sampling on 120 wells located on the surroundings. These observations revealed the presence of salt-water intrusion and, therefore, a widespread contamination of the Tiber delta that constitutes a very high risk to water management [94]. In the **Figure 37** it is possible to observe that the saline intrusion in the "Canale della Fiumara Grande" that overreaches from the mouth and goes inwards with salinity high values (37 g/l). In the same vertical section, it was identified, as in the case of "Casa di Diana" (in the correspondence of about 38 g/l salinity values), two sub-layers of freshwater and salt water with a sub-horizontal trend (interface). Furthermore, the presence of significant hollows along the bed longitudinal profile, promotes the saline intrusion stagnation, which lasts for long times, despite the variability of the river system and the marine weather conditions (**Fig. 37**). For all of these, the study of 2007 was in accordance with the ERT results obtained in this PhD research work (**Article 4**), as can be seen in the **Figure 37**, with the identification on "Casa di Diana" (red circle) at 5 m of depth a section associable with "freshwater river" and below it, a salt-water intrusion. In the mentioned work, and despite of the variability of the river system according the weather conditions, the saline instruction is excluded (but not underestimated, groundwater vulnerability). Thus, the interface line between salt

and freshwater shown in the **Figure 37**, was also in accordance with the hypothesis made previously in this chapter of the coexistence of two distinct[30] masses of water (salt and freshwater) separated by a natural membrane (**Article 4**).

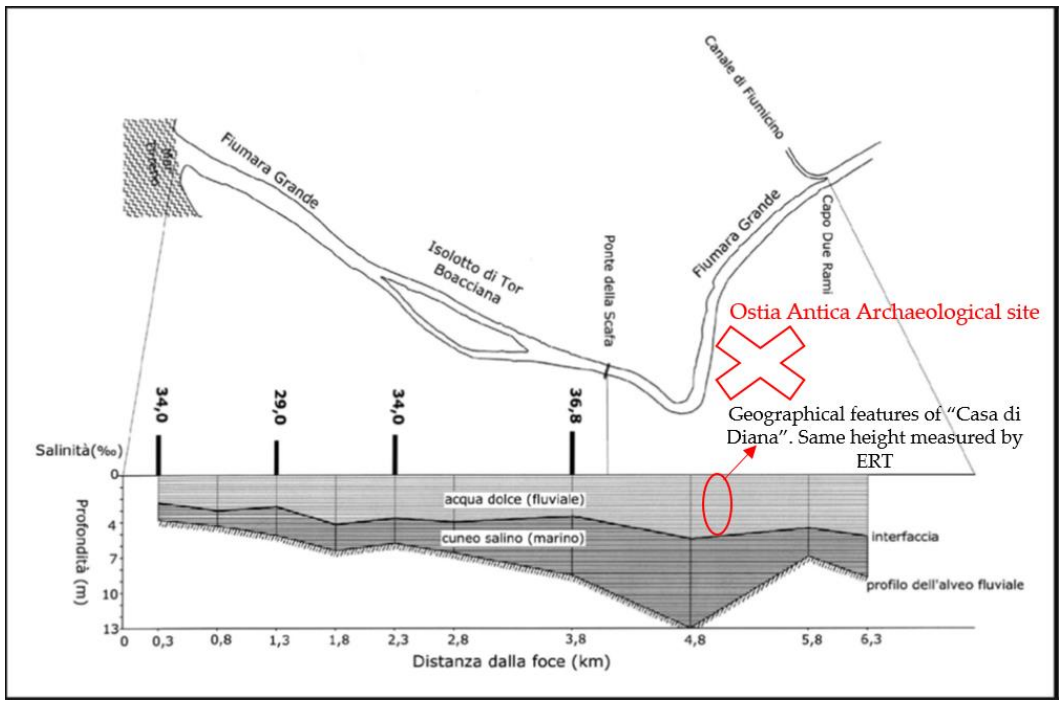

Figure 37. Schematic cross-section of the saline intrusion and the bathymetry along the median axis of the "Canale della Fiumara Grande", from Capo Due Rami to mouth [94]. The red cross and the circle red indicate the Ostia Antica site and "Casa di Diana" building (with the ERT measurements), respectively.

Once confirmed the independence of the saline and freshwater aquifers, it was necessary to understand if the water collected in the tanks and in the well comes from the freshwater aquifer. Regarding this probable interaction, it is important underline that the tanks, despite they being external to the structure, give the impression to be intercommunicated with the building by hidden connections. This direct intercommunication of these "hydraulic systems" is more than probable by macroscopic observations. For example, the bottoms of these structures seem covered by a non-cemented topsoil. Furthermore, it is probably that the well, in the antiquity, was deeper, probably, directly connected with the freshwater aquifer. Let us not forget that the well represented a source probably used to supply the masonry [97] thanks to channelling along the entire well and

[30] This fact does not impossible thinking of the complex Roman aqueducts systems, which knew the type of soil on which the foundations were laid, and obtaining a masonry or structure with an efficient hydraulics system.

conduits under raised floor, which are still visible. Furthermore, an ulterior water supplying was provided by a more complex hydraulic system. This last observation was supported by the presence of different parts of an antique hydraulic system (pipelines, connections, etc.) found and exhibit in the "Casa di Diana" that allowed the probably connection with the ancient aqueduct ("Malafede" basin – **Article 4**). For all of that, the connection of the well and tanks with the freshwater aquifer was probably. Therefore, the rising damp was supposed to be responsibility of this freshwater.

Finally, another aspect to focus is the way of the rising damp passes through the wall-building and reaches its phreatic level. This mechanism could promote the mineralization on building materials. For clarify this fact, the foundation walls' study could be useful and the previous work of the subsoil (**Chapter 6.1**) revealed two deep resistivity anomalies (with different thickness) which could fit with the building foundations. In this sense, other geophysical studies (ERT and ST) were conducted, pinpointing also the conservation state of wall-building.

6.2 Assessing the state of conservation of building through the combined used of electrical and seismic tomography[31]

Understanding the inner geometry, the construction materials and the degree of conservation of ancient buildings is a pivotal issue when Cultural Heritage undergoes degradation processes due to the ravages of time, human interventions or natural phenomena.

In this context, a perimeter walls at west side, adjacent the *Triclinium*, was taken into consideration, underscoring the cracking-prone zones, as well the movement of rising damp through the wall (area more at risk). In particular, ERT micro-electrodes and ST with accelerometers were carried out. Furthermore, 3D acquisition with stainless steel electrodes and non-invasive copper plates as electrodes was used outside and along the corridors of the whole building, respectively.

[31] An adapted version was published in:
Assessing the state of conservation of a masonry building through the combined used of electrical and seismic tomography. 22nd European Meeting of Environmental and Engineering Geophysics. Session: Archaeological Prospecting II. Near Surface Geoscience 2016 in Barcelona (ES). ISBN: 78-94-6882-155-2.

Article 5

Three-dimensional reconstruction of a masonry building through electrical and seismic tomography integrated by biological and environmental studies. Article under review in Near Surface Geophysics. Ms. Ref. No.: NSG-2016-1458.

THREE-DIMENSIONAL RECONSTRUCTION OF A MASONRY BUILDING THROUGH ELECTRICAL AND SEISMIC TOMOGRAPHY VALIDATED BY BIOLOGICAL AND ENVIRONMENTAL ANALYSIS

Ettore Cardarelli[1], Giorgio De Donno[1*], Ilaria Oliveti[1], Claudia Scatigno[2,3]

[1] "Sapienza" University of Rome - DICEA Via Eudossiana, 18 00184 Rome, Italy
[2] "Sapienza" University of Rome - DST P. le Aldo Moro 5 00185 Rome, Italy
[3] University the Basque Country, (UPV/EHU) - Department of Analytical Chemistry Barrio Sarriena s/n, 48940, Leioa, Spain.
*Corresponding author: giorgio.dedonno@uniroma1.it

Abstract
An integrated approach encompassing electrical resistivity, seismic tomography investigations and biological and environmental studies is presented in this work, aiming to assess the state of conservation of a Roman masonry building located in the Ostia Antica archaeological site (Rome, Italy), affected by rising damp and cracking phenomena.
A preliminary three-dimensional electrical survey was performed to detect the foundations and understand the range of variation of the resistivity at the study site. High-resolution electrical and seismic tomography lines were later acquired on an inner wall, prone to both rising damp and cracking. The combined use of electrical and seismic tomography allowed us to obtain a high-resolution map of the wall made in *opus caementicium*, where high resistivity and low P-wave velocity values can be associated to the presence of the inner mortar, while higher velocity and lower resistivity are due to the outer brick component.
These background values change under conditions of degradation, where an increase of resistivity in the bricks together with lower velocity values is related to the presence of fractures, while rising damp is marked by a strong resistivity decrease. Overall, the wall is undergoing a noteworthy degradation process, proven by the massive presence of fractures (low velocity and high resistivity zones) and a significant volume where rising damp is present (low resistivity zone). Biological analysis has validated the geophysical results, where the biological proliferation occurred from the pavement up to 0.75 m (lower strata where values of relative humidity close to saturation are recorded). This approach can be employed to reconstruct a three-dimensional model of masonry structures in order to plan recovery actions.

Keywords electrical resistivity tomography; seismic tomography; geochemistry; rising damp; biological and environmental analysis; Roman masonry

INTRODUCTION

Understanding the inner geometry, the constructive materials and the degree of conservation of ancient buildings is a pivotal issue when Cultural Heritage undergoes degradation processes due to the ravages of time, human interventions or natural phenomena. In this sense, the application of geophysical non-destructive testing can be an important tool for assessing the current state of an archaeological structure. Geophysical methods were applied worldwide during last decades for archaeological purposes in order to detect and characterize non-invasively ancient structures without any damage (Gaffney, 2008).
Ground Penetrating Radar (GPR) has been employed extensively for archaeological targets (Goodman and Piro, 2013). Through this method, a detailed image of the existent structures or important information about the location of buried bodies can be retrieved (Conyers, 2013).

Some successful applications have concerned the detection and characterisation of ancient structures (e.g. Orlando and Slob, 2009; Cataldo et al., 2012), the location of cavities and hidden objects in the shallow subsurface (e.g. Neubauer et al., 2002; Piro et al., 2003), the individuation of anomalous zones within ancient buildings and the evaluation of the current state of structures (e.g. Perez Gracia et al., 2013; Orlando et al., 2015). Although being a high-resolution technique, the GPR signal has the disadvantage of a lower depth of penetration in cases of conductive media (Daniels, 2009).

An estimation of the elastic parameters at low-strain of the structural elements can be given by seismic tomography, where lowvelocity zones are straightforward indicators of material weakness. Some et al., 2005).

Electrical Resistivity Tomography (ERT) can provide useful information about the hidden foundations and the surrounding geology and, as long as non-invasive electrodes are used, also about the structural elements. This technique was used on stone exposures (Sass, 2005) in an effort to understand the processes of stone weathering, for analysing the rising damp phenomenon and assessing the moisture content of historic walls (Mol and Preston, 2010) and to study a masonry wall (Tsourlos and Tsokas, 2011).

Since it is not always possible to rate a single geophysical method as superior to all the others, the integration of different techniques can remove ambiguities on interpretation of geophysical models and increase the degree of accuracy of the physical parameters (Cardarelli and Di Filippo, 2009; Tsokas et al., 2013). However only using geophysical techniques often cannot represent the best choice to investigate Cultural Heritage, in particular when we have to face a complex scenario in which different materials could give a similar geophysical response. In this sense, geophysical results should be supported and/or validated by other methods, concerning chemistry, geomatics, geotechnical or hydraulic engineering. Integrated approaches have been applied for archaeological prospection (e.g. Merello et al., 2013), pertaining to geomatics and geophysics (e.g. D'Aranno et al., 2016), geotechnical engineering and geophysics (e.g. Soupios et al., 2008; studies have been focused on the cracking-prone zones (e.g. Cardarelli and de Nardis, 2001) or on the investigation of the foundation structure and ground materials of ancient buildings (e.g. Polymenakos Westley et al., 2014) or, in presence of rising damp and cracking phenomena, geochemistry and geophysics (e.g. Cardarelli et al., 2016).

Rising damp is one of the main conservation problems affecting historical masonry structures and it is surely the most widespread phenomenon leading to moisture presence in building structures (Franzoni, 2014). Moisture plays a key role in the degradation of porous materials, being directly or indirectly responsible for several decay processes [86, 98]. This phenomenon is increased in coastal environments, which due to high levels of moisture and marine aerosol, represents the principal source of deterioration of buildings located close to the sea [85, 99].

In this regard, the integrated approach presented in this work encompasses the use of electrical and seismic tomography investigations validated by biological analysis, aiming to assess the current state of conservation of a Roman wall, with an application on a building located in the Ostia Antica archaeological site (Rome,

Italy), affected by rising damp on parietal walls and cracking in loadbearing walls. The experimental procedure has been divided into five main steps:

- establishment of the hydro-geological setting through 2D ERT investigations;
- detecting building foundations using 3D ERT with particular arrays;
- understanding the sources of the rising damp affecting the investigated wall, merging together results obtained at point i. and ii.;
- assessing the state of conservation of the wall with a combined use of 3D ERT and seismic tomography investigations;
- validation of results by biological and environmental analysis.

Owing to the above consideration, we discard the GPR technique because the masonry at this site is expected to be conductive due to the rising damp. In addition to this, since the depth of penetration is inversely proportional to the radiated frequency, GPR cannot be used for detecting deep foundations (as in this case).

MATERIAL AND METHODS

Site description

The investigated building, named "Casa di Diana", located at a distance of 3 km from the Tyrrhenian sea, 250 m from the Tiber River and 4 km from the Fiumicino International airport, was built in the central area of Ostia Antica (Rome, Italy) around 130 CE (**Fig. 1a**). The building is a 40 x 22 m rectangular masonry structure with 60 cm wide load bearing walls and two main corridors. The house originally had five floors, where the ground floor hosted shops while the upper floors apartments: nowadays only the ground floor and traces of the projecting part of the continuous balcony of the first floor still survive (**Fig. 1b**). In the past, the house used to have an advanced hydraulic system, in which the inner fountain, supplied by lead pipes from the street to the courtyard, stands out as an example of aristocratic luxury adapted to the architecture of an *insula*. The masonry has its own brick made well having a depth of 4.20 m, located between the *latrina* and the courtyard, from which it was possible to draw water and an external tank, adjacent to the house. A two-room apartment (*Mithraeum*)at NE corner of the house represents a sanctuary consecrated to the Indo-European god Mithra, whose cult expanded rapidly in the 1st-century Roman Empire. Regarding to the building materials, the entire house is mainly composed of bricks and pozzolanic mortar aligned with "*opus caementicium*" technique (inner mortar and two outer bricklayers). Two different types of bricks (red and yellow) can be detected, depending on the particular construction practices. The walls show a retraction for the consumption of mortar joints, a more permeable material than bricks and a typical morphology of degradation by exfoliation, delamination, cracking or chipping, as well as biological proliferation located in *Mithraeum room*. Where the continuity of brick and mortar is respected, a veil alters chromatically the appearance of the walls giving a whitish appearance to brick and mortar surfaces (mattifying veil) making difficult an easy reading of wall structure.

In previous work Cardarelli et al. (2016) established the hydro-geological setting of the archaeological site (point i. of the proposed procedure), assessing the origin of the rising damp occurring to the structural elements. Through geo-electrical investigations they detected a freshwater aquifer at a depth of 2.5 m (0 m a.s.l.),

within the *in-situ* sand deposits, while salt water is present from a depth of 8 m (-5.5. m a.s.l.). The depth of the salt water/fresh water interface is comparable to that recovered by Mikhalova et al. (2008). Thanks to geochemical analysis, they identified that the shallow water probably comes from Malafede basin with a marginal salt contribution due to the influence of the salt deposits in the area or to the interaction with the deeper saline water. Few information about the hidden foundations are available.

In this work we focus geophysical techniques on one of the perimetral wall of the *Triclinium* room, an adjacent room of the *Mithraeum*, without roof and located at the east side of house (**Figs. 1 c, d**). This wall (named in the following sections as *Triclinium* wall), 8.3 m wide, 1.8 m high and 0.7 m deep and embedded within a pre-existent arch, if compared with all the rest of inner walls, appears particularly damaged as confirmed by efflorescences and fractures directly visible on its surface. The whole *Mithraeum* is characterized by several damages (Scatigno et al., 2016a): the materials in an advanced state of damage with a massive biological presence are those of the *Mithraeum* face of the *Triclinium* wall.

Figure 1. a) "Casa di Diana" at the Ostia Antica archaeological site (indicated with a white rectangle) and location of the "*Triclinium*" wall (dashed line); **b**) street view (Via di Diana), **c**) outer face of the "*Triclinium"* wall located in the Triclinium room; **d**) inner face of the "*Triclinium*" wall located in the *Mithraeum* room.

The consumption of mortar joints, more permeable than bricks, is evident, as well as a typical morphology of degradation by biological growth. The biological proliferation induces aesthetic damages on surfaces (vegetative structures, coloured patches through biogenic pigments or patinas and crusts) but, more importantly, a physical (abrasion, mechanical stresses to the mineral structure due to shrinking and

swelling cycles of these colloidal biogenic slimes inside the pore system (Crispim and Gaylarde, 2005) and chemical (solubilisation, new-reaction products) changes.

Geophysical investigations

We performed a 3D ERT survey for detection of the foundations, while 3D ERT and two seismic tomography lines were acquired on the *Triclinium* wall (**Figs. 2, 3 and 4**).

Foundations

A 3D ERT array was applied both outside, along three sides of the building (**Fig. 2a**), and inside (alongside the corridors) using a 48-channel IRIS Instruments SyscalPro48, with a dipole-dipole configuration working on a combination of two different arrays (M-shaped and U-shaped in **Fig. 2a**).

The maximum values for the dipole separation *a* and the dipole separation factor *n* were set to 5 and 6 respectively, leading to 2512 apparent resistivity measurements. Stainless steel stakes (**Fig. 3a**) and 10 cm square copper plates (**Fig. 3b**) were employed as electrodes outside and inside the building respectively, with an electrode spacing of 3 m.

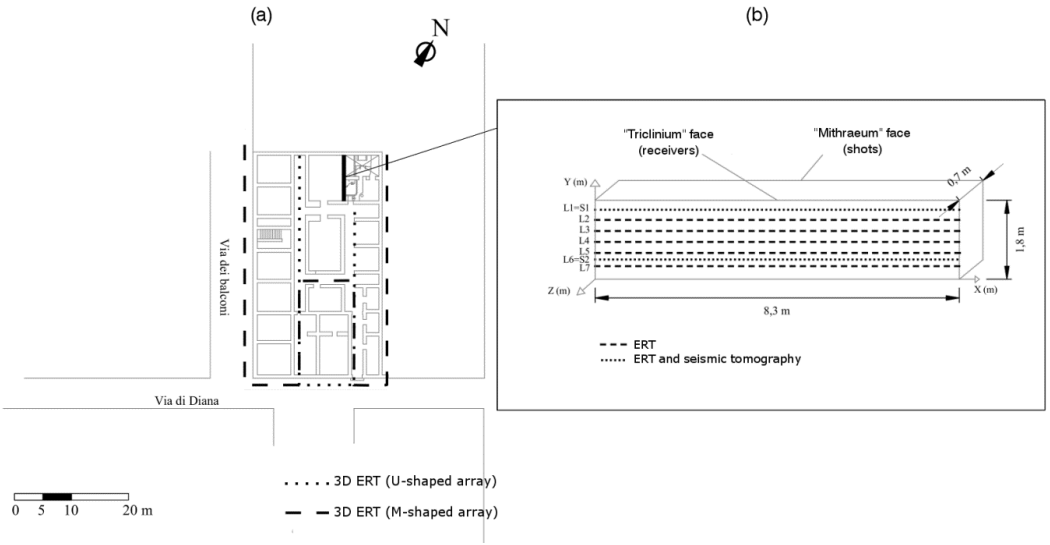

Figure 2. a) Plan of 3D electrical resistivity tomography investigation for detecting foundations (U-shaped, dotted line; M-shaped, dashed line); **b**) Location of electrical (dashed and dotted) and seismic tomography (dotted) lines at the "*Triclinium*" wall.

ERT dataset were inverted with the VEMI algorithm - Versatile interface for Electrical Modelling and Inversion (De Donno and Cardarelli, 2015), built within the EIDORS environment (Adler and Lionheart, 2006). This algorithm is able to perform both 2D and 3D inversion, by solving the forward problem with a finite element approximation of the Poisson's equation governing the physical problem while inversion is carried out using a Gauss-Newton formulation (De Donno 2013; De Donno and Cardarelli 2014). The code can incorporate the finite length of the electrodes (non-negligible for archaeological applications) and it is

possible to add a priori information to the inversion process. In this particular case we made no preliminary assumption, because of the few available information on the study area.

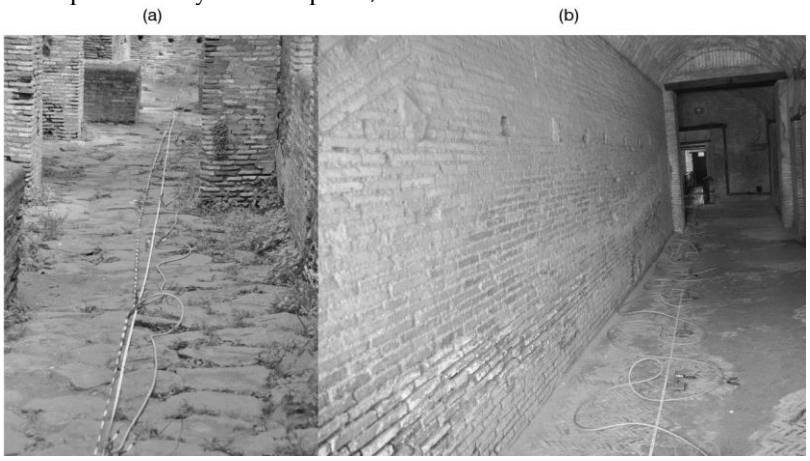

Figure 3. a) 3D ERT acquisition outside the building with stainless steel electrodes; **b**) non-invasive copper plates as electrodes used alongside corridors.

"Triclinium" wall

Electrical tomography profiles were acquired on the *Triclinium* wall along lines at different heights (**Fig. 2b**). ERT dataset consist of 7 lines acquired at 1.6, 1.35, 1.1, 0.85, 0.6, 0.45 and 0.3 m from the floor level (L1 to L7 in **Fig. 2b**), using 24 steel micro-electrodes (7 cm steel nails, diameter: 0.25 mm), spaced 0.35 m apart for each line, connected to the IRIS Syscal Pro (Fig. 4a). Dipole-dipole and Wenner-Schlumberger arrays were combined (3283 data points) in order to merge together the capability of resolving anomalies in the vertical (Wenner-Schlumberger) and horizontal (dipole-dipole) directions. Forward modelling and inversion was performed with VEMI replacing the Dirichlet boundary conditions, used for ground investigation, with a Neumann-type boundary condition due to the absence of current flow through the air-wall interface.

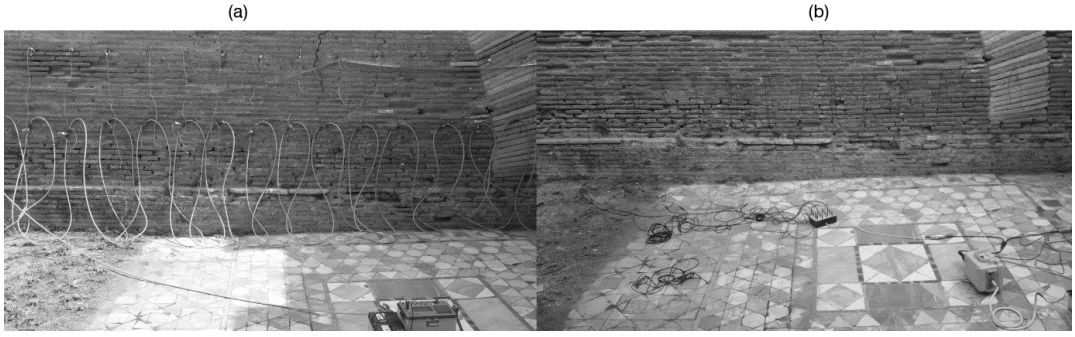

Figure 4. a) Electrical resistivity tomography at the "Triclinium" wall using micro-electrodes connected with the Syscal Pro system; **b**) Seismic tomography at the "Triclinium" wall with accelerometers connected with a 24-channel Geode seismograph.

Two seismic profiles were collected at 1.6 and 0.45 m from the floor (S1 and S2 in Fig. 2b, corresponding to L1 and L6), in order to validate the electrical models. Data were

acquired using 11 shot points (spacing =0.7 m) produced by a 2 kg hammer source and 23 piezoelectric accelerometers with a cut off frequency of 4.5 kHz, spaced 0.35 m apart, while traces were recorded by means of a 24-channels Geometrics Geode seismograph, utilizing a sampling rate of 31.5 μs (**Fig. 4b**). For each shot gather recorded for both seismic profiles, the first arrivals were manually picked and the travel times computed, as the difference between the shot instant and the first breaks of the P-wave. These data are inverted using the linear travel time interpolation (LTI) method for ray-tracing in the forward kernel (Cardarelli and Cerreto, 2002) and the iterative bi-conjugate gradient algorithm for travel time inversion (Cardarelli and de Nardis, 2001). The resolution of the inverted images was improved through the staggered grid technique (Cardarelli and Cerreto, 2015), where inversion was computed 7 times for each direction, starting from an initial cell size of 0.48x0.2 m, leading to a final refined mesh of 2499 cells.

Biological and environmental investigations

The validation of geophysical results has been performed by means of a study on percent coverage of biological communities on the *Triclinium* wall, trying to identify the most affected areas. The analysis has been carried out on the left part of the *Mithraeum* face of the *Triclinium* wall (x = 4-8 m and z = -0.7 m in **Fig. 2b**), sheltered from the atmospheric agents, while it was unfeasible to investigate the right part of it due to the massive presence of *podia* in the lower part of the wall. Specifically, to estimate microbial concentrations, the calculation of the total biological coverage on the building's walls was applied. Anew assessment method consisting of a combination of Stage method and Braun-Blanquet scale, was designed, as described in a previous work (Scatigno and Ravera, 2015). A modular grid of 25x25 cm (quadrant value) has been created and mounted on the whole wall, facilitating in this sense the calculation of percent coverage and assigning a spatial number as instructed for both methodologies.

Early environmental studies (Scatigno et al., 2016b) conducted in several microclimate campaigns (temperature and relative humidity), brought to light some particularly critical areas, where humidity accumulates in correspondence of the corners of house and in correspondence of the lowest area, defining a less pronounced "cloud" of dispersion and describing a most humid and non-ventilated area.

RESULTS

Foundations

In **Figure 5** we show the two meshes, used for forward (**Figs. 5a, b**) and inverse (**Fig. 5c**) computation. The VEMI algorithm is able to give a mapping between two meshes in order to assign the correct value of resistivity to the coarser mesh once the forward solution has been achieved and vice versa.

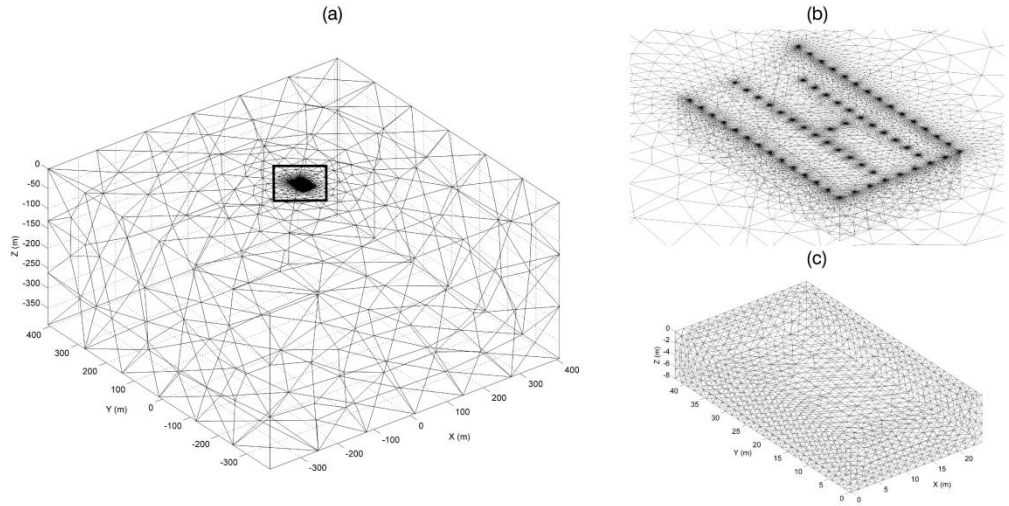

Figure 5. 3D ERT model of the "Casa di Diana" foundations. **a**) Model for forward computation; **b**) particular of the area within the black rectangle in **Fig 1a**, where the position of electrodes is highlighted; **c**) model for inversion.

This procedure is extremely important to save memory during inversion (we need to know resistivity only near the electrodes) without undermine the accuracy of the forward solver (we need to extend the external boundaries "far enough" the current source).

Results from the 3D inversion on ground array are displayed in **Figure 6** by means of horizontal sections drawn on the resistivity model at a depth of 1, 2.5, 4 and 6 m from the floor level. The model highlights in its shallower part (**Fig. 6a, b**) three resistivity anomalies elongated along the y-direction, linked to the presence of buried walls in these areas, acting as foundations. In fact, these bodies are located in the correspondence of the three load bearing elements: two external walls and one intermediate spine wall. However, at higher depths (**Fig. 6c, d**) only the two external walls keep high resistivity values due to the presence of foundations up to 6-7 m from the floor level. The background resistivity is about 30-50 Ωm up to a depth of 7 m, compatible with the presence of a shallow aquifer. Below resistivity decreases abruptly to 1-2 Ωm due to the presence of salt water, similarly to the results previously obtained by Cardarelli et al. (2016).

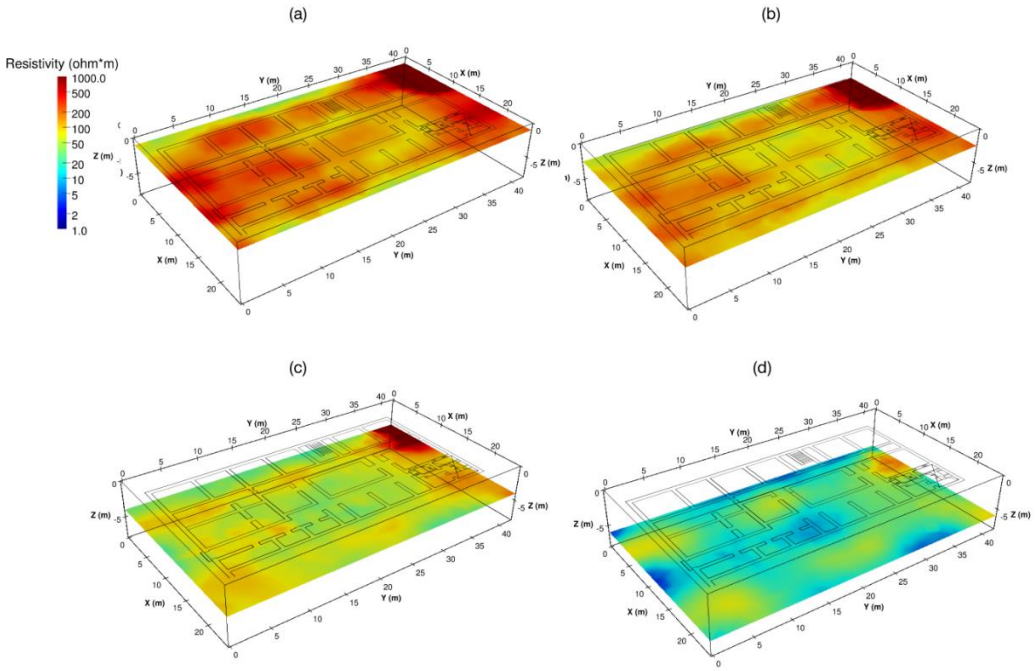

Figure 6. Inverted 3D ERT model of the "Casa di Diana" foundations. Horizontal sections are drawn at a depth of 1 (a), 2.5 (b), 4 (c) and 6 m (d) from the floor level. Images made using Kitware Paraview.

The shape of foundations is shown in **Figure 7**, by means of a volumetric image of the resistivity values higher than 50 Ωm, associable to the presence of anthropic elements.

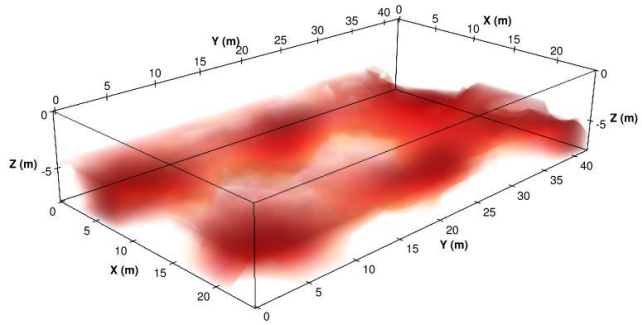

Figure 7. Volumetric image of the "Casa di Diana" foundation walls, obtained mapping only elements deeper than 4 m with resistivity values higher than 50 Ωm. Image made using Kitware Paraview.

The foundations seem to be strip footings built underneath the two main load bearing walls (as usually made for Roman buildings), even though we cannot exclude that the highest resistivity values (dark red areas) recovered both at the four corners of the building and in the middle part of it could be related to spread footings.

"Triclinium" wall

The three-dimensional reconstruction of the *Triclinium* wall is shown in **Figure 8** in terms of finite element mesh (**Fig. 8a**)

and inverted resistivity model (**Fig. 8b**). Owing to the particular boundary conditions discussed before, we use the same meshes for forward and inverse computations.

The inverted model is clearly divided into an upper resistive zone (h>0.7 m; Ω>500 Ωm) and a conductive lower zone. This lower area is expected to be more conductive as a result of the effect of the rising damp, evident after a visual inspection.

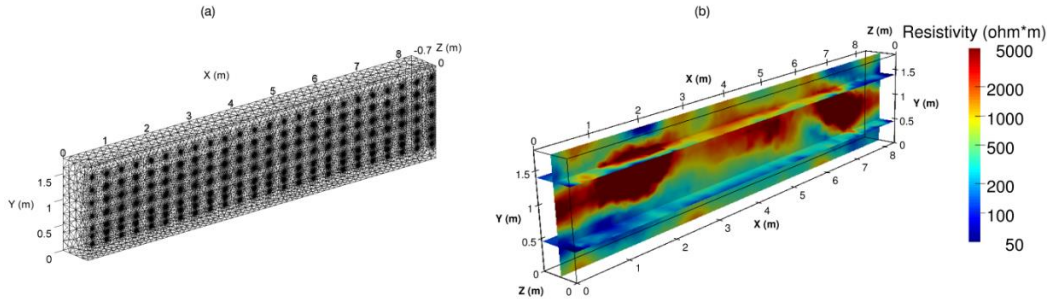

Figure 8. 3D ERT model of the "Triclinium" wall. (a) Mesh for forward and inverse computation. (b) Inverted model with horizontal slices drawn at 0.45 and 1.6 m from the floor level and vertical slice at a depth of 0.35 m from the outdoor face.

Among this layering, we can also identify another differentiation along the z-direction, directly correlated with the construction materials. In fact, we detect high resistivity in the inner part of the wall (high porosity of mortar), while the outer part of the wall is slightly conductive, due to the presence of bricks. Moreover, it is possible to observe, as the water is present mainly in the corners of the wall, as shown by the high values of relative humidity recorded (Scatigno et al. 2016). **Figure 9** enhances the layering of the *Triclinium* wall, by means of higher (> 500 Ωm, orange) and lower (< 500 Ωm, blue) resistivity volumes. It is clearly visible that the conductive zone pertains to the portion of the wall affected to rising damp (h< 0.7 m) while elsewhere the resistivity is higher.

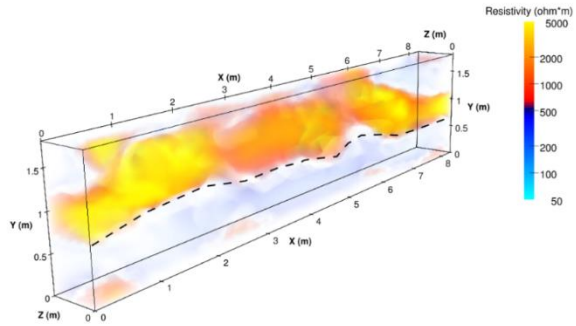

Figure 9. Volumetric image of the "Triclinium" wall obtained mapping in orange elements with resistivity values higher than 500 Ωm and in blue elements having resistivity lower than 500 Ωm. The interface between high and low resistivity values is indicated with a black dashed line. Image made using Kitware Paraview.

In **Figure 10** the results coming from seismic inversion of the S1 (**Fig. 10a**) and S2 (**Fig. 10b**) profiles acquired on the wall (height=1.6 and 0.45 m from the floor level) are presented in comparison with the respective slices extrapolated from the ERT model (**Figs. 10c, d**). Both seismic models are characterized by low RMSE values resulting from the last iteration (0.31 and 0.37 ms respectively).

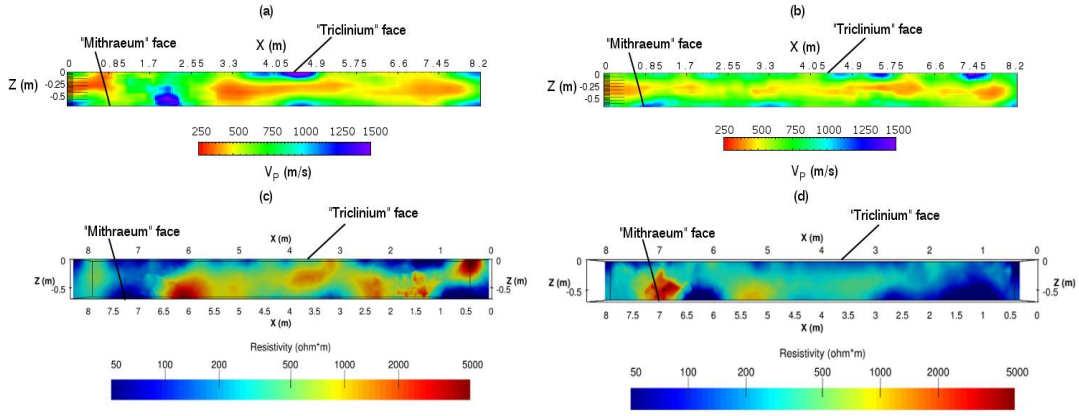

Figure 10. Inverted models of seismic profiles S1 (**a**) and S2 (**b**) at the "Triclinium" wall, compared with the respective slices of the 3D ERT model (**c, d**).

There is a good correlation among the two sections in terms of shape and position of the reconstructed anomalies. Mainly, the low resistivity zones (< 500 Ωm) correspond to high P-wave velocities (> 800 m/s), both located in the outer part of the wall, even though a high resistivity and P-wave velocity area was found for the S1 (**Fig. 10a**) at x=2 m and z=-0.6 m, probably related to the presence of an arch. On the contrary, low velocities (< 800 m/s), with a minimum of 250 m/s, are observed in correspondence to high resistivity values (> 500 Ωm) in the inner part of the section (due to the high porosity of the mortar). Therefore, geophysical models reflect the construction technique, where the outer bricklayer is less porous and more rigid than the inner mortar. The lower velocities and high resistivity values detected near the wall surfaces in both lines can be due to cracks and fractures visible on the wall.

Biological and environmental analysis

The results of the biological studies, shown in **Figure 11**, show that the damaged zone is extended up to 0.75 m from the floor level (the blank cells have a zero value), with a maximum stage level of 4. This height is similar to that shown by the ERT model in **Figure 9**. The most affected zone is concentrated on the left bottom part of the wall (height of 0-0.5 m) characterised by the highest values (4 in **Fig. 11** and **Tab. 1**). On the other hand, the lowest values (values of 0-1) are detected in the right part of the wall (close to the *Mithraeum* room).

Taking into account the Braun-Blanquet scale (**Tab. 2**), a mean coverage of 40% (level no.3 in **Tab. 2**) can been assigned to the investigated wall.

Figure 11. Backside of the investigated wall- Modular grid installation in the Mithraeum room, with the Stage method values assignation. The "x" indicates the frescos presence and so the no value assignation.

Table 1. Stage method.

Stage	Conservation treatment for biological colonisation	Biological colonisation type	
x	Not needed	-	
1	Superficial cleaning (mechanical suction)	Mosses, lichens and fungi	Shortly rooted
2	Deep cleaning (first chemical and after mechanical)		consolidated
3	Deep cleaning + consolidation		
4	Deep cleaning + consolidation due to rupture		
5	Deep cleaning + consolidation due to rupture by superior plants	Superior plants	

Table 2. Braun-Blanquet scale.

n.	Species coverage class [%]
+	Present, very scares cover
1	Well represented, < 5%,
2	Abundant, < 25%,
3	25-50%
4	50-75%
5	> 75%

Since the biological system pump water from the shallow aquifer, as demonstrated by the recorded low temperatures and the presence of levels of relative humidity close to saturation especially in the lower strata (height of 0-0.75 m), we can confirm that rising damp affects the *Triclinium* wall.

With reference to the five main points presented in the Introduction, we merge together the results after Cardarelli et al. (2016) and those obtained for the foundations in order to calibrate the resistivity range. Cardarelli et al. (2016) established that the resistivity of the geological formations is lower than 50-60 Ωm and at a depth of 8 m from the floor

level (5.5 m a.sl.) they detected the fresh water/salt water interface.

DISCUSSION

Results presented in this work are in agreement with these ranges and therefore we can relate resistivity values higher than 50 Ωm to anthropic features (pavement, foundations), both for the ground and for the wall surveys.

Foundations can interact with the fresh water, since they are extended up to 6-7 m from the floor level, favouring the rising damp on the investigated wall.

Electrical and seismic models, reconstructed at the *Triclinium* wall, are strongly heterogeneous in the three main directions. Overall, we can associate high resistivity to low velocity values, both due to the high porosity of mortar. On the contrary, high velocity, generally, is seen close to the faces of the wall, together with lower resistivity, linked to the more rigid and conductive bricks layer. However, geophysical models reflect also cracking and rising damp issues affecting the wall. The former is visible with a resistivity increase (and a velocity decrease) occurring at the faces of the wall (in particular at x=1-2 and 6-7 m and y=1-1.5 m), the latter is related with a conductive anomalous zone pointed out in **Figure 9**.

In this sense, the chemical analysis has validated geophysical results, where the rising damp hydrate the brick materials, favouring the attack from sulphate salts coming from a dry deposition. The materials present a high risk of sulphate and for this the geophysical surveys reveal a strong resistivity decrease in the lower zone of the wall.

With reference to a previous work where a laboratory sample of a Roman masonry wall was analysed using seismic tomography (Cardarelli and de Nardis, 1999), the bricks have velocity values compatible with a good state of conservation (optimal V_P=1500-1700 m/s, recovered V_P=1300-1400 m/s) only in few zones, even though there are many fractured zones where there is a substantial decrease of velocity. On the contrary, velocities globally obtained for mortar (optimal V_P=500 m/s, recovered V_P=250-600 m/s) can potentially represent an anomaly due to degradation phenomena.

Therefore, an experimental procedure for investigating the structural elements should comprehend the electrical method, being rapid and cost-effective, both in terms of acquisition (30 minutes for each line) and data processing, to be executed extensively for reconstructing a 3D model of the structure. Given the background layering of the wall (conductive-resistive-conductive), the anomalies enhanced by the ERT models could be related to changes in the moisture content (decrease of resistivity caused by the rising damp) or to the presence of weathering or fractures (increase of resistivity caused by an increase of porosity). However, the minimization of the contact resistances of the electrodes is still a major issue because the use of completely non-invasive electrodes (plates or cylinders only lean against the wall) is strictly recommended even though they often not ensured a good contact due to the surface roughness of the archaeological structures.

Whereas the ambiguity in the model interpretation still remain one can execute seismic lines (more time-consuming) focused on zones where uncertainty is higher. A preliminary quality factor can be given by the deviation between P-wave velocity and resistivity values recovered in field and the optimal values obtained in the laboratory, where bricks display higher

P-wave velocity and lower resistivity than the inner mortar. Moreover, any anomalies due to degradation should be visible as a velocity decrease for the two materials.
Finally, the biological analysis enabled to validate the geophysical results giving more explanation about the causes of the conductive anomalies in the lower zone of the wall. In fact, the interface detected by ERT between the conductive and the resistive zones is located at the same height (0.75) reached by the microbial communities (**Fig. 11**). In this zone and particularly in the left bottom part of the wall (x = 5.5-8, y = 0-0.5 m), where "stage" values are higher than 3, very deep restoration actions are needed, such as cleansing and consolidation (**Tab. 1**).

CONCLUSIONS

An integrated experimental procedure is presented in this work for assessing the current state of conservation of a wall, prone to cracking and affected by rising damp. Through a 3D survey performed around the building we detect deep anomalous bodies, related to the "Casa di Diana" foundation. Resistivity values higher than 50 Ωm can be related to anthropic features (pavement, foundations), since the resistivity range of the geological formations is lower. Foundations are probably strip footings located underneath the load bearing walls and extended up to a depth of 6-7 m. They can interact with the shallow aquifer, favouring the rising damp on the elevated walls.
The combined use of electrical and seismic tomography, validated with biological analysis, can be a reliable tool to obtain a high-resolution model of a masonry wall, as demonstrated on the *Triclinium* wall made in *opus caementicium*. In fact, the high resistivity and low P-wave velocity values revealed can be associated to the presence of the inner mortar, while higher velocity and low resistivity were observed for the existence of the outer brick component. These background values change in presence of degradation, due to cracking and rising damp. In the former case, we have an increase of resistivity in the bricks together with lower velocity values. The latter phenomenon affects the whole volume of the wall by means of a strong resistivity decrease. Overall, the wall is undergoing a noteworthy degradation process, proven by the massive presence of fractures (low velocity and high resistivity zones) and a significant volume where rising damp is present (low resistivity zone).
Validation of geophysical results has been given by biological studies. The presence of microorganisms, such as Cyanobacteria, green algae and lichens occurred mainly from the pavement up to 0.75 m, which corresponds to the height where a sharp variation of resistivity was observed in the geophysical model.
The integrated method described in this work can be used to reconstruct a three-dimensional model of a masonry structure: the interpretation of 3D ERT, integrated by a focused seismic survey and validated through biological analysis can remove the ambiguity arising on interpretation of a single non-invasive technique. Based on these results, we make available to archaeologists a high-resolution tool useful to plan restoration activities at the study site.
Future works could be focused on the individuation of a non-invasive way to stop the rising damp and reduce the high values of relative humidity, which represents a key parameter for safeguarding this site of great historical importance.

ACKNOWLEDGEMENTS

The project was founded by "Sapienza" University of Rome - Ateneo Grant 2015. Francesco Pugliese ("Sapienza" University of Rome) is thanked for his technical support on field survey. Claudia Scatigno is grateful to the University of the Basque Country (UPV/EHU), and in particular to PhD Nagore Prieto-Taboada, for the grant for study sojourns by trainee researchers from foreign universities engaged in a jointly supervised doctoral thesis.

REFERENCES

Adler A. and Lionheart W.R. 2006. Uses and abuses of EIDORS: an extensible software base for EIT. Physiological Measurement 27, S25.

Cardarelli E., De Donno G., Scatigno C., Oliveti I., Martinez M.P. and Prieto-Taboada N. 2016. Geophysical and geochemical techniques to assess the origin of rising damp of a Roman building (Ostia Antica archaeological site). Microchemical Journal 129, 49-57.

Cardarelli E. and De Nardis R. 1999. The use of 3-D and 2-D seismic tomography for assessing the physical integrity of building panels. European Journal of Environmental and Engineering Geophysics 3, 131-142.

Cardarelli E. and De Nardis R. 2001. Seismic refraction, isotropic anisotropic seismic tomography on an ancient monument (Antonino and Faustina temple AD 141). Geophysical Prospecting 49, 228-240.

Cardarelli E and Cerreto A. 2002. Ray-tracing in elliptical anisotropic media using linear travel time seismic interpolation (LTI) method applied to travel time seismic tomography. Geophysical Prospecting 50, 55–72.

Cardarelli E. and Cerreto A. 2015. Staggered Grids as a Tool to Improve the Model Resolution in Seismic Tomography for Elliptical Anisotropic Media. 21st European Meeting of Environmental and Engineering Geophysics, Turin, 6-10 September.

Cardarelli E. and Di Filippo 2009. Integrated geophysical methods for the characterisation of an archaeological site (Massenzio Basilica—Roman forum, Rome, Italy). Journal of Applied Geophysics 68(4), 508-521.

Cataldo R, D'Agostino D, Leucci G. 2012. Insight into the buried archaeological remains at the Duomo of Lecce (Italy) using ground penetrating radar surveys. Archaeological Prospection 19(3), 157–165.

Conyers L.B. 2013. Ground penetrating Radar for Archaeology, 3rd edn. Rowman and Littlefield Publishers, Alta Mira Press, Latham, Maryland.

Crispim C.A. and Gaylarde C.C. 2005. Cyanobacteria and biodeterioration of Cultural Heritage: a review. Microbial Ecology 49 (1), 1-9.

Daniels DJ. 2009. Ground Penetrating Radar, 2nd edn. IET: London; 734.

D'Aranno, P.J., De Donno, G., Marsella, M., Orlando, L., Renzi, B., Salviani, S., Santarelli, M.L., Scifoni, S., Sonnessa, A., Verri, F. and Volpe, R., 2016. High-resolution geomatic and geophysical techniques integrated with chemical analyses for the characterisation of a Roman wall. Journal of Cultural Heritage 17(1), 141-150.

De Donno G. 2013. 2D tomographic inversion of complex resistivity data on cylindrical models. Geophysical Prospecting 61(Suppl.1), 586-601.

De Donno G. and Cardarelli E. 2014. 3D complex resistivity tomography on cylindrical models using EIDORS. Near Surface Geophysics 12(5), 587-598.

De Donno G. and Cardarelli E. 2015. A Flexible Interface for Tomographic

Inversion of Real and Complex Resistivity Data in EIDORS. 21st European Meeting of Environmental and Engineering Geophysics, Turin, 6-10 September.

Franzoni E. 2014. Rising damp removal from historical masonries: A still open challenge. Construction and Building Materials 54, 123-136.

Gaffney C. 2008. Detecting trends in the prediction of the buried past: A review of geophysical techniques in archaeology. Archaeometry 50, 313-36.

Gomez-Laserna O., Olazabal M. A., Morillas H., Prieto-Taboada N., Martinez-Arkarazo I., Arana G., Madariaga J. M. 2013. In-situ spectroscopic assessment of the conservation state of building materials from a Palace house affected by infiltration water. Journal of Raman Spectroscopy 44, 1277-1284.

Goodman D. and Piro S. 2013. GPR Remote Sensing in Archaeology. Springer, Berlin, 233.

Gentilini C., Franzoni E., Bandini S., Nobile L. 2012. Effect of salt crystallisation on the shear behaviour of masonry walls: an experimental study. Construction and Building Materials 37, 181- 189.

Merello Giménez P., Pérez García, María Del Carmen, García Diego FJ, Fernández Navajas Á, Pérez Miralles J, Baró Zarzo JL, Curiel Esparza, J., D'Antoni, P., Ribera i Lacomba, A. and Ferrazza, L., 2013. Ariadne's house (Pompeii, Italy) wall paintings: A multidisciplinary study of its present state focused on a future restoration and preventive conservation. Materiales de Construcción 63, 449-67.

Mikhalova M.V., Bellotti P., Valeri P. and Tortora P. 1999. Intrusion of Seawater into the River Part of the Tiber Month. Water Resources 26(6), 679-686.

Mol L. and Preston P.R. 2010. The writing's in the wall: a review of new preliminary applications of electrical resistivity tomography within archaeology. Archaeometry 52, 1079–1095.

Morillas H., Maguregui M., Gómez-Laserna O., Trebolazabala J., Madariaga J. M. 2013. Could marine aerosol contribute to deteriorate building materials from interior areas of lighthouses? An answer from the analytical chemistry point of view. Journal of Raman Spectroscopy 44, 1700-1710.

Mustafa K. 2013. Deterioration of different stones used in historical buildings within Nigde province, Cappadocia. Construction and Building Materials 48, 789-803.

Neubauer W, Eder-Hinterleitner A, Seren S, Melichar P. 2002. Georadar in the Roman civil town Carnuntum, Austria: an approach for archaeological interpretation of GPR data. Archaeological Prospection 9(3) 135–156.

Orlando, L., Cardarelli, E., Cercato, M. and De Donno, G., 2015. Characterisation of a Pre-Trajan wall by integrated geophysical methods. Archaeological Prospection, 22(3), 221-232.

Orlando L. and Slob E., 2009. Using multicomponent GPR to Monitor Cracks in a Historical Building. Journal of Applied Geophysics, 67, 327-334.

Perez-Gracia V., Caselles J.O., Clapes J., Martinez G., Osorio R. 2013. Non-destructive analysis in Cultural Ceritage buildings: evaluating the Mallorca cathedral suparcporting structures. NDT & E Int. 59, 40–47.

Piro S, Goodman D, Nishimura Y. 2003. The study and characterisation of Emperor Traiano's villa (Altopiani di Arcinazzo, Roma) using high-resolution integrated geophysical surveys. Archaeological Prospection 10(1), 1–25

Polymenakos L., Papamarinopoulos S., Miltiadou A. and Charkiolakis N. 2005. Investigation of the foundations of a Byzantine church by three-dimensional

seismic tomography. J Appl Geophys 57, 81-93.

Sass O. 2005. Rock moisture measurements: techniques, results, and implications for weathering. Earth Surf Process Landforms 30, 359-374.

Scatigno C. and Ravera S. 2015. Characterisation of the biological proliferation on Roman masonry Case study: "Casa di Diana" Mithraeum (Ostia Antica, Rome – Italy). XXVIII Convegno Nazionale della Società Lichenologica Italiana in Lanciano (IT).

Scatigno C., Prieto-Taboada N., Martinez M. P., Conte A. M., García-Diego F. J. and Madariaga, J. M. 2016a. Analytical techniques for the characterisation of historical building materials: case study "Casa di Diana" Mithraeum (Archaeological site in Ostia Antica, Italy). Advances in Materials Science Research, 31.

Scatigno C., Gaudenzi S., Sammartino M.P., Visco G. 2016b. A microclimate study on hypogea environments of ancient roman building. Science of the Total Environment 566-567.

Soupios, P.M., Loupasakis, C. and Vallianatos, F., 2008. Reconstructing former urban environments by combining geophysical electrical methods and geotechnical investigations -an example from Chania, Greece. Journal of Geophysics and Engineering, 5(2), p.186.

Tsokas G.N., Diamanti N., Tsourlos P.I., Vargemezis G., Stampolidis A. and Raptis K.T. 2013. Geophysical prospection at the Hamza Bey (Alkazar) monument Thessaloniki, Greece. Mediterranean Archaeology and Archaeometry 13, 9-20.

Tsourlos PI, Tsokas GN. 2011. Non-destructive electrical resistivity tomography survey at the south walls of the Acropolis of Athens. Archaeological Prospection 18(3), 173–186.

Westley, K., Plets, R. and Quinn, R., 2014. Holocene Paleo-Geographic Reconstructions of the Ramore Head Area, Northern Ireland, Using Geophysical and Geotechnical Data: Paleo-Landscape Mapping and Archaeological Implications. Geoarchaeology, 29(6), pp.411-430.

6.3 Conclusions

The integration of ERT and ST techniques allowed us to obtain a geometrical characterisation of the building's foundations, as well as to analyse the current state of conservation of an inner wall, prone to cracking and additionally affected by the rising damp phenomenon. It was also found out that the groundwater vulnerability (hydro-geological setting) due to saline intrusion by Tyrrhenian sea found (5-13 m height - ERT) overreaching from mouth inwards [94] but which was proved to be independent from the freshwater aquifer identified at less depth. This last freshwater aquifer probably supplies the tanks and the well, but it seemed to have an enrichment with salts (cyclic salts) from the mineralization of subsoil connected with the salt marshes' production until the Twentieth Century. In this sense, the rising damp could lead from the freshwater aquifer.

The 3D survey performed around the building allowed to detect deep anomalous bodies, probably related to the "Casa di Diana" foundation walls, this is in agree with the building hypothesis of the archaeologist in charge. Although there is a few information in literature regarding the position of the foundations, it was possible to relate the resistivity values (higher than 50-60 Ωm) to anthropic features (pavement, foundations), since the resistivity range of the geological formations is lower.

The combined use of ERT and ST can be a reliable tool to obtain a high-resolution map of a wall made in *opus caementicium*. In fact, the low resistivity and P-wave velocity values revealed can be associated to the presence of an inner mortar, while higher values of both parameters were observed when the outer brick component was present. Overall, referencing a previous work where a laboratory sample of a Roman masonry wall was analysed using ST [17], the brick part seems to be in good conditions (optimal VP=1500 - 1700 m/s, recovered VP=1200 m/s), even though the low velocity values of the mortar (optimal VP=500 m/s, recovered VP=250 m/s) can potentially represent an anomaly due to the visible degradation phenomena that the building materials suffer (pulverisation, cracking, chromatic alteration and surface opacification).

Chapter 7 Analytical procedures. Petrographic-mineralogical and chemical analysis[32]

Nowadays, a broad range of analytical techniques is available and applied in the preservation of Cultural Heritage. However, to characterise the historical materials and to obtain quantitative and qualitative information regarding their composition and structure, it is necessary choose the appropriate analytical instruments.

First of all, destructive techniques should be avoided, wherever possible, to preserve the integrity of the historical buildings. Therefore, the development of non-invasive, non-destructive and *in-situ* analyses is extremely important. In this sense, in the last years, the growing interest in Cultural Heritage safeguard has given an impetus to the development of new non-invasive techniques, for the study of historical-artistic structures, with the aim to identify the state of conservation and to plan solutions for the restoration and maintenance of such structures [100].

However, in some cases, the use of non-destructive techniques still requires micro-sampling, which could be crucial to achieve the objective of the research. In this sense, non-destructive techniques (that not require a sampling consumption) are the key to obtain the maximum information with the smallest amount of sample, which is available to be measured by many different techniques. That is, these techniques allow the storing of samples for future additional examinations, avoiding the need of sampling the artwork again consuming more material [101]. Amongst them, the spectroscopic instruments seem to be the most useful in the field of Cultural Heritage [100, 102-108].

Taking all of these into account, and in order to investigate more the building materials of the "Casa di Diana", a multi-analytical methodology was adopted. Precisely, a multidisciplinary approach was designed to characterize the original materials and to understand the chemical decaying processes that they are subjected evaluating, in this sense, their conservation state.
Thus, a primary overview on stone materials conserved in the *Mithraeum* (bricks, mortars, and furniture materials included) by petrographic-mineralogical analyses was initially performed.

[32] An adapted version was published in:
Scatigno, C., N. Prieto-Taboada, M. Preite Martinez, A. M. Conte, F. J. García-Diego, and J. M. Madariaga. "Analytical techniques for the characterisation of historical building materials: case study "Casa di Diana" Mithraeum (Archaeological site in Ostia Antica, Italy)." Advances in Materials Science Research (2016): 31.

Article 6

Petrographic-mineralogical characterisation of stone materials from a *Mithraeum* building sited in an open museum. Article submitted to Construction and Building Materials.

PETROGRAPHIC-MINERALOGICAL CHARACTERISATION OF STONE MATERIALS FROM A *MITHRAEUM* BUILDING SITED IN AN OPEN MUSEUM

C. Scatigno[a,b]*, A.M. Conte[c], M. Preite Martinez[a], N. Prieto-Taboada[b] and J.M. Madariaga[b]

[a] Department of Earth Science, University of Rome "La Sapienza", Piazzale Aldo Moro 5, 00185, Rome, Italy
[b] Department of Analytical Chemistry, University the Basque Country, (UPV/EHU), Barrio Sarriena s/n, 48940, Leioa, Spain
[c] Institute of Geosciences of Earth Resources - National Research Council (IGG- CNR), University of Rome "La Sapienza", Piazzale Aldo Moro 5, 00185, Rome, Italy
*Corresponding author: Email: claudia.scatigno@uniroma1.it

Abstract
The characterisation of the archaeological materials is a priority issue particularly for open museums that are set in complex environmental scenarios. Polarized Optical Microscopy (PLM), X-ray Diffraction (XRD), Scanning Electron Microscope with Energy Dispersive X-ray (SEM-EDS) and isotopic analysis ($\delta^{13}C$, $\delta^{18}O$), were applied on the raw materials (bricks, mortars, furnishings and fittings) conserved in "Casa de Diana" *Mithraeum* (130 CE). The prevalence of siliciclastic or calcitic component discriminates the red and yellow bricks, as well as different accessory minerals classify the red ones. Black pozzolanic clasts distinguish the mortar samples. The altar material, catalogued as marble, revealed a carbonate based stone.

Keywords stone materials characterization; Petrographic Polarizing Microscope (PLM); X-ray diffraction (XRD); Scanning Electron Microscope with energy dispersive X-ray (SEM-EDS); X-ray maps; stable isotopes (oxygen and carbon).

Highlights

- *Mithraeum* raw materials characterisation by mineralogical-petrographic analyses
- Different microstructure and aggregate type found into the red and yellow bricks
- Pozzolanic mortar typical of the Roman buildings

1 INTRODUCTION

Europe has a particularly rich and diversified Cultural Heritage, including buildings, monuments and artefacts of all sizes, characterised by a great variety of materials. Their conservation and safeguard represents an important economic effort but culturally, a fundamental need in its own right [1].

In particular, the Built Heritage, which represents the history and culture of a location and its communities [2], collects a wide variety of historical architectures (i.e. masonries, churches, castles and fortifications). These last represent, thanks to its historical-artistic value, a unique and irreplaceable expression of the human traces, which as the rest of Cultural Heritage, merits to be conserved. In this sense, stony building materials are often considered as being the most resistant building material, however they can suffer the impact of different weathering processes that can transform their original composition [3], due to direct exposure to environmental stressors (than can be either

repetitive or persistent). Thus, its conservation is extremely necessary.

A large number of ancient structures characterises Italy, including Roman and religious examples. Among them, Cultural Heritage sites, also called "open museums" represent a consistent group [4]. The definition of "open museum" includes all historical structures, monuments (such as ancient palaces, churches, masonries, open-air exhibitions, etc.) which are not located in closed environments and, therefore, directly exposed to outdoors and environmental stressors. These sites are set in a complicated scenario due to the numerous conservative problems that they face and because their preventive conservation is particularly complex due to the particular environmental features.

Focusing on the Roman buildings, *Mithraea* are ones that usually are found in open museums. The *Mithraeum* term identifies a place dedicated to the cult of the Persian god Mithra, being a sanctuary of this Indo-European god, whose cult expanded rapidly in the 1st-century Roman Empire. Sixteen *Mithraea* (only one of which is set in a *hypogeum*, the "Terme di Mitra" *Hypogeum*) have been found in the archaeological complex of Ostia Antica (Italy, Rome) which represents one of the best-known examples of open museum present in Italy, together with Pompeii and Herculaneum [5]. Most of the other *Mithraea* are completely exposed to macroclimate and therefore, very few structures were found in relatively good state of conservation thanks to the presence of protective structures (roofs) built in modern days. One of the best examples of these *Mithrae* is the "Casa di Diana" *Mithraeum*, a Roman building that dates back to 130 CE sited in Ostia Antica, that is the studied area in this work. Unfortunately, until now, neither conservative actions (apart from direct and punctual recovery actions carried out by restores equips), nor detailed information on this site are available.

On the base of the conservation tools, the materials' characterisation represents a fundamental phase. In the archaeological context, scientific literature illustrates a wide variety of approaches applied in the study and characterisation of materials [2,6-15] which are often subjected to different kinds of damages as a consequence of the impacts due to the environmental conditions [4,6,11,16-27]. The importance of the characterisation of raw materials lies in the value of knowing decaying mechanisms in maintenance and restoration works, giving also crucial information for the archaeological knowledge of the cultural sites.

Thus, an integrated analytical approach represents a useful method for the evaluation of stony materials [6,11,28]. Amongst the analytical techniques, Petrographic Polarizing Microscope (PLM) and X-Ray Diffraction (XRD) are usually applied [14,29,30]. In this sense, the petrographic study is the preliminary step of this type of analytical approaches to characterize the textural properties and mineralogy of materials, the amount and type of cement, percentage and type of clay matrix, porosity, extent of weathering, etc [31].

XRD represents a rapid analytical technique used for the identification of mineral phases. Rapidity, easiness and the requirement of small amounts of material are the principles advantages of this method. It can be used also to perform semi-quantitative analyses of poly-mineralic mixtures in given rocks and stones [32]. Therefore, phase identification may be a very complicated process,

requiring optimized measuring techniques and substantial experience for data interpretation [33]. For all of this, the XRD is one of the most common techniques to identify the main crystallized phases and decaying compounds in the field of Cultural Heritage [34].
In addition, other analytical techniques as Scanning Electron Microscope coupled with energy dispersive X-ray Spectroscopy (SEM-EDS) and stable isotopes quantification (mainly oxygen and carbon), complement the mentioned PLM and XRD techniques in order to study in depth, the materials, like mortars employed, as well establishing the origin of certain materials (as in the case of travertine artefacts).
Thus, these all mentioned techniques were used to remedy the lack of information about the ancient materials kept inside the "Casa de Diana" *Mithraeum* to understand the building construction (wall-building materials as bricks and mortars), and to assess the state of conservation, giving crucial information about this site (historical, archaeological and for restoration purposes).

2 MATERIALS AND METHOD

2.1 Site description

The Roman building under study, named "Casa di Diana" (Region I, Insula III), it had originally five floors, where the ground floor hosted shops and the upper floors apartments [35]. Nowadays, only the ground floor and traces of the projecting part of the continuous balcony of the first floor still survive. Regarding the two rooms (*pre-Mithraeum* and *Mithraeum*), they remain as in the past, with dark rooms, shadows, wet and cold, an altar illuminated by a natural spotlight, everything set to recreate a particular atmosphere for the tauroctony: the killing of the bull.

The bricks and mortars constitute the principal studied wall-building materials, being the major ones, together with other materials that comprise the furniture found inside like the *dolium*, an earthenware vase or container used during the sacred rite and the altar. The latter was investigated in all its parts (apse, corbels, aedicule made up by different materials) because it represents the most important decorative element in the Mithraism rite.

2.2 Sampling and analytical procedure

In order to classify, where it is possible, the majority of the materials and taking into account the preciousness and uniqueness of the materials, a selection of them were carried out, collecting and archiving a total of 20 micro-samples. Sampled materials and sampling sites are listed in **Table 1**, along with the analytical methodology applied.
Petrographic observations were carried out by Olympus Optical BX60 equipped with a MegaPixel Firewire- Vitana Corporation (PL-A6xx Capture 3.1) camera. The samples were reduced in thin-sections, following the same procedure as for rock fragments. After a flat surface is obtained, the polished surface is cut to obtain the thinnest slice possible. The sample is trimmed until it reaches a thickness of about 30 microns.

Table 1. Sampling collection. The analytical methodologies are listed with abbreviations. PLM: Polarized Light Microscope; XRD: X-Ray Diffraction; SEM: Scanning Electron Microscope.

Sample n.	Material typology	Sampling area	Analytical methodology
1	Brick	Wall *Mithraeum* at east side (corner wall)	PLM, XRD
2	Brick	Wall *Mithraeum* at east side (height: 0.38 cm, corner)	PLM, XRD
3	Brick	Wall *Mithraeum* at east side (height: 1.54 cm, corner)	PLM, XRD
4	Brick	*Mithraeum* at north side. Altar (aedicule)	PLM, XRD
5	Brick	*Mithraeum* at north side. Altar (aedicule)	PLM, XRD
6	Brick	*Mithraeum* at north side. Altar (corbel)	PLM, XRD
7	Mortar	Wall *Mithraeum* at north side (height: 1.54 cm, oppose corner)	PLM, XRD
8	Mortar	*Mithraeum* at north side. Altar (aedicule)	PLM, XRD
9	Mortar	*Mithraeum* at north side. Altar (aedicule)	PLM, XRD
10	Mortar	*Mithraeum* at north side. Altar (aedicule)	PLM, XRD, SEM
11	Pumice	*Mithraeum* at north side. Altar (apse)	PLM, XRD
12	Pumice	*Mithraeum* at north side. Altar (apse)	PLM, XRD
13	Pumice	*Mithraeum* at north side. Altar (apse)	PLM, XRD
14	Travertine	*Mithraeum* at north side. Altar (corbel)	PLM, XRD, stable isotopes ($\delta^{13}C$, $\delta^{18}O$)
15	Limestone	*Mithraeum* at north side. Altar (block)	PLM, XRD
16	Limestone	*Mithraeum* at north side. Altar base (grooved block at the base of the altar)	PLM, XRD
17	Marble	*Mithraeum* at north side. Altar support (slab resting on top of sample 20)	PLM, XRD
18	Ceramic	*Dolium. pre- Mithraeum* (right side inside)	PLM, XRD
19	Plaster	*Mithraeum* at north side. Altar (aedicule)	PLM, XRD
20	Plaster	*Mithraeum* at north side. Altar (apse)	PLM, XRD

The identification of both predominant and accessory mineral phases [9,30], was carried out by a Siemens D500 X-ray Powder Diffractometer using a monochromatic X-ray beam (Cu–Kα1 X-radiation, 1.54 λ, 40 kV and 20 mA). All the samples were finely grounded and homogenized through manual milling in an agate mortar until a grain size < 0.053 mm and drying cabinet (60 °C) until constant weight was obtained (24h).

Scanning Electron Microscope (SEM) analysis was also performed on the thin-section of one mortar sample, coated with a conductive layer of graphite. Back-scattered-electron images (BSE), energy dispersive X-ray (EDS) spectra and X-ray maps were acquired using a FEI-Quanta 400 (SEM–EDAX), combining a high-quality imaging and qualitative elemental analysis.

Finally, for isotopic analyses of oxygen and carbon were carried out with a Finnigan Delta Plus mass spectrometer, after preparation in accordance with the procedure of McCrea, 1950 [36] were acquired for the travertine sample. Results are expressed in terms of δ‰ and referred to the PDB standard [37]. The CO_2 was extracted from travertine by reaction with 100% phosphoric acid following the procedures described in [36] and then introduced in the mass spectrometer.

3 RESULTS AND DISCUSSION

3.1 Bricks

The nature, shape and size of different types of embedded grains and the brick

matrix obtained by petrographic and diffractometric analyses (**Fig. 1, Tab. 2**) indicated that sample 1 (**Fig. 1, a1-2**) presented a quite fine matrix with a dark brown colour and a prevalent siliciclastic aggregate made of quartz and feldspar grains, subordinate opaque grains and rare crystals of clinopyroxene. Some small black lumps were also present.

The sample 2 (**Fig. 1, b1-2**) presented a finer and more homogenous matrix than sample 1, with a pale brown colour. Moreover, the matrix seemed to have suffered evident firing stress (**Fig. 1b2** - red arrows); it also contained small amounts of calcite and gypsum. The aggregate was very scarce and composed essentially by crystals of quartz and occasional black lumps, which include several mineral grains (**Fig. 1, b 1-2**) and an isolated carbonate shell (**Fig. 1b2** – white circle).

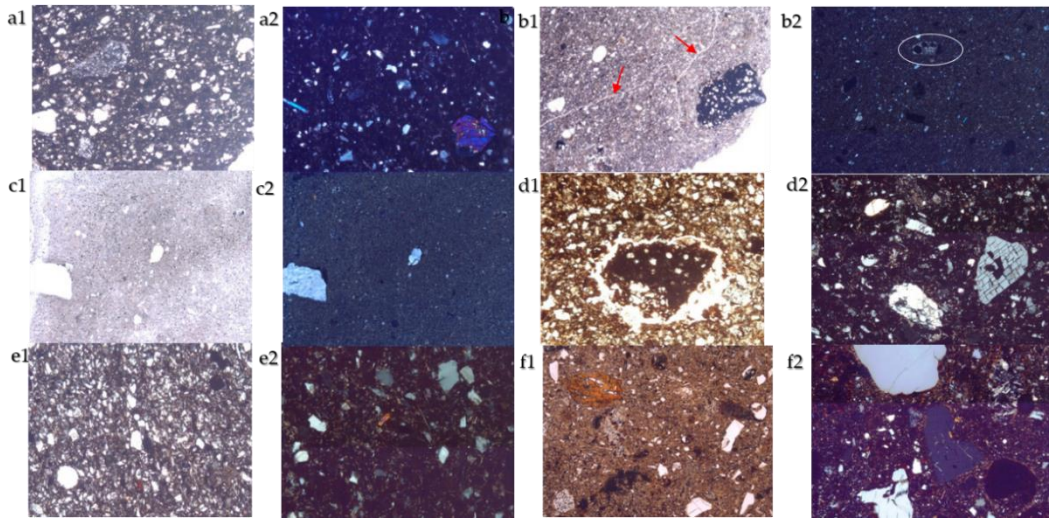

Figure 1. Microphotographs of brick samples. **a**) sample 1; **b**) sample 2; **c**) sample 3; **d**) sample 4; **e**) sample 5; **f**) sample 6. **a1** - f1 plane polarized light; **a2-f2** crossed polarized light. All microphotographs are at 4x magnifications.

Sample 3, the only one collected from the yellow bricks, displayed a microstructure similar to sample 2 with a very scarce aggregate fraction and an even finer matrix (**Fig. 1**). The pale ochre colour of the matrix, more visible under crossed polarized light (**Fig. 1c2**) was likely due to the abundant calcite fraction present in the matrix and revealed by XRD analyses. Small amount of gypsum was recognised also in this sample. Exclusively crystals of quartz composed the scarce aggregate fraction.

Sample 4 presented a medium-grained matrix with a pale brown-reddish colour, constituted prevalently by siliciclastic minerals, i.e., numerous quartz and feldspars crystals and subordinate Fe-oxides. Some prismatic white crystal of orthopyroxene with orthogonal cleavage, as well as occasional black lumps were also present (**Fig. 1d2**) as an aggregate fraction.

Table 2. Main mineralogical phases revealed by XRD in the analysed six bricks. ◊Indicates that this sample corresponds to the unique yellow brick measured. +++ Abundant, ++ Present, + Small amount, Tr. Traces, - Undetected.

	Samples					
Compound (name)	**1**	**2**	**3◊**	**4**	**5**	**6**
Amorphous stuff	+	++	+	++	+	+++
Quartz	+++	+	++	++	+++	+/Tr
Calcite	Tr	+/++	+++	+	++	-
Dolomite	-	-	-	-	+	-
Albite	++	+	+	+	+/Tr	++
Pyroxene	-	-	-	+	-	Tr
Mica	-	+/Tr	+	-	+++	+
Analcite	-	Tr	-	-	-	-
Sanidine	++	-	+	++	+/Tr	++
Hematite	Tr	-	-	Tr	-	-
Gypsum	-	+	+	-	-	-

Sample 5 presented a matrix of brown colour similar to sample 1 but a different mineral composition of the aggregate fraction: in sample 5 the prevalent grains of quartz were in association with mica instead of feldspars. Isolated black lumps, including mineral grains, were also present (**Fig. 1e**).

Finally, sample 6 presented a fine matrix like 1, 2, 4 and 5, with a pale brown-reddish colour, like the one found in sample 4. Numerous big quartz crystals and numerous small black lumps were found (**Fig. 1f**).

In general, the matrix colour goes from dark brown to brown-reddish. A separate case is represented by sample 3 (yellow brick) with pale ochre colour. In comparison with the red bricks, which presented more blacks lumps and rough minerals, the yellow one display fewer and smaller siliciclastic minerals and a more homogeneous mixture.

3.2 Mortars

The nature, shape and size of different types of clasts observed suggest that the pozzolan and their mineral phases, as analcite and clinopyroxene, are the principal constituents of the mortar samples (**Fig. 2, Tab. 3**).

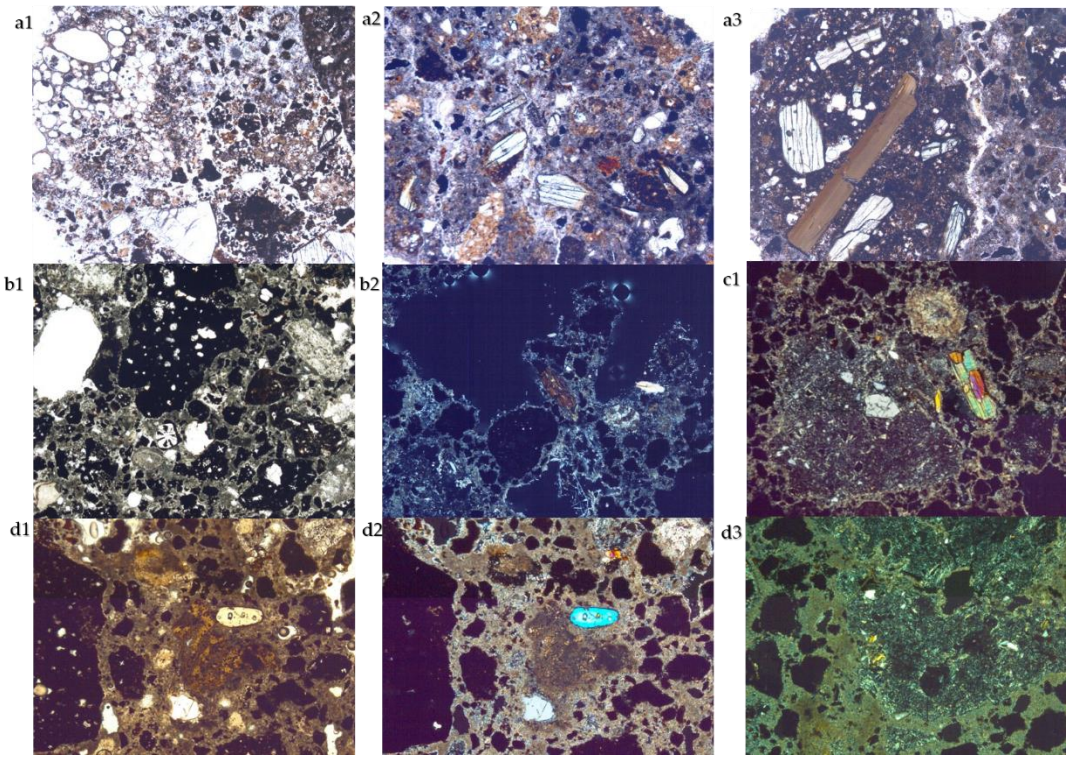

Figure 2. Microphotographs of mortar samples. **a**) Sample 7 (**a1**: plane polarized light, **a2**, -**a3** crossed polarized light; **b**) sample 8 (**b1**: plane polarized light, **b2**: crossed polarized light); **c**) sample 9 (**c1**: crossed polarized light); **d**) sample 10 (**d1**: plane polarized light, **d2**-**d3**: crossed polarized light). All microphotographs are at 4x magnifications.

Specifically, sample 7 had an aggregate displaying heterogeneous size and shape of fragments; the larger clasts were formed mainly by black pozzolan having some phenocrysts of mica and pyroxene (**Fig. 2a**), and subordinately of pumice. Smaller fragments were represented by pozzolan clasts and single crystals (mainly pyroxene and analcite-leucite) derived from the crush of pozzolan lumps. Occasionally mica and quartz were also presented. The binder-aggregate ratio was low, approximately 1:3. The binder was of carbonate nature with a microsparitic texture and included lumps of CaO, not blended in the mixture, due to defect of carbonation or heterogeneity of the lime itself. The fragments interface characterized binder/pozzolan by reaction phenomena (**Fig. 2a3**).

Sample 8 presented an aggregate with very heterogeneous particle size. Pozzolanic fragments of different size and crystals of clinopyroxene and leucite (both in pozzolanic fragments and as isolated crystals) represented the main clasts in the aggregate. Some lava fragments and occasional quartz were found. Cooking residues consisted of calcic lumps. The binder -aggregate ratio was low and the matrix presents a heterogeneous colour (**Fig. 2, b1-2**).

Sample n.9 presented an aggregate with pozzolanic fragments, rarer fragments of lava containing plagioclase crystals, few large crystals of mica and occasional

quartz. The matrix was heterogeneous due to the presence of numerous carbonatic relicts caused by cooking and mixing. The binder -aggregate ratio was low (**Fig. 2, c1**).

Table 3. Main mineralogical phases revealed by X-ray diffraction (XRD) in the four analysed mortars. +++ Abundant, ++ Present, + Small amount, Tr. Traces, - Undetected.

	Samples			
Compound (name)	**7**	**8**	**9**	**10**
Amorphous stuff	+++	++	++	+++
Quartz	Tr	Tr	-	-
Calcite	+++	++	+++	++/+++
Clinopyroxene	++	++	+/++	+/++
Mica	++	-	+	-
Analcite	+++	+++	++	+++
Chlorite	Tr	-	-	-
Hematite	-	Tr	-	-

Finally, sample 10 presented an aggregate that had a grain size with a bimodal distribution; the larger fragments were formed principally of pozzolanic clasts, rare fragments of lava and of reused mortar displaying shrinkage fractures (**Fig. 2d**). The fine fraction was constituted by rare minerals resulting from crushed pozzolanic materials (essentially pyroxene and analcite - leucite), smaller lava fragments and occasionally crystals of quartz (**Fig. 2d**). A binder-aggregate ratio higher than in sample 7 was found. The matrix was homogeneous with micritic texture, but rare marl lime residues caused to incomplete decarbonation can be observed (**Fig. 2d**). A probable presence of reaction edges it also observed.

The XRD results (**Tab. 3**) were in accordance with the optical microscope observations. The aggregate mainly consisted of black pozzolans, since the mineral phases that predominate were analcite and clinopyroxene typical for this vulcanite. The amorphous material, likely referable to the glass fraction in the pozzolanic fragments, is more abundant in sample n.10, indicating that the pozzolanic fragments were more rich in glass. Moreover, XRD results showed that sample n. 7 presented the highest content of mica crystals, representing an exception for this group of investigated mortars (**Tab. 3**).

In order to investigate the mortars further, a SEM-EDS (ES and BSD detectors for SEM) analysis and X-ray mapping was performed on sample n.10, obtaining an elemental characterisation/distribution of both binder and aggregate (punctual and area information) (**Fig. 3-6**). Regarding the aggregate, spectral results confirmed the presence of analcite (**Fig. 3a1**) and pyroxene (**Fig. 3a2**) inside the pozzolanic fragments (**Fig. 3a**), as well as the presence of Fe and Ti oxides (**Fig. 3a** - red circles). Regarding the binder (**Fig. 4**), it was possible to observe a mixed carbonate-

aluminosilicate matrix (**Fig. 4b2** - EDS right spectrum) with diffuse analcite microcrystals having amoeboid appearance (**Fig. 4b2, points 3**) and some carbonate lumps (CaO grains not hydrated during the extinguishing, with different appearance and dimensions (30-60 μm)) (**Fig. 4b2, points 1**, left spectrum). Further details of the binder composition were observed at higher magnification as reported in **Figure 5**.

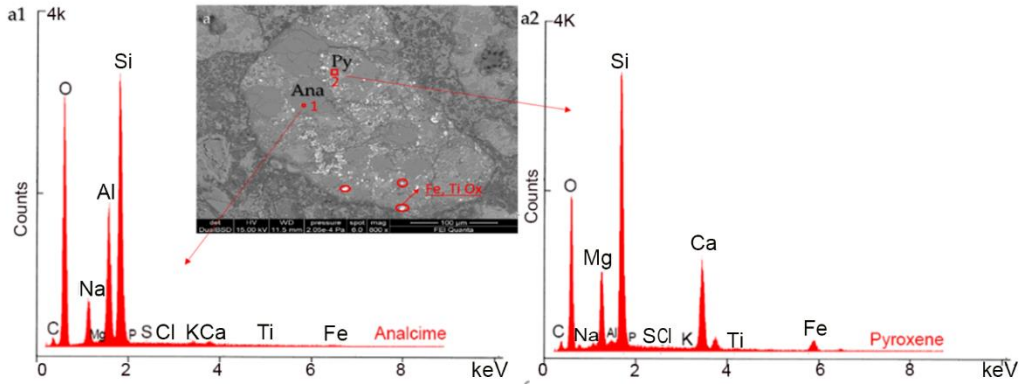

Figure 3. Aggregate, pozzolana fragment. **a**) BSD image, 100μm. **a1**): EDS spectrum "point 1" that identify the analcite mineral; **a2**): EDS spectrum "area 2" that identify the pyroxene mineral.

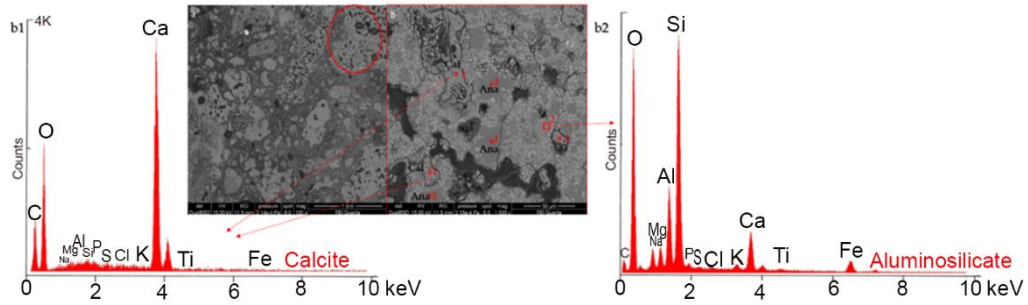

Figure 4. Binder. **a**) BSD image 1 mm; **b**) zoom 50 μm. **b1**) EDS spectrum "point 1"; **b2**) EDS spectrum "area 2".

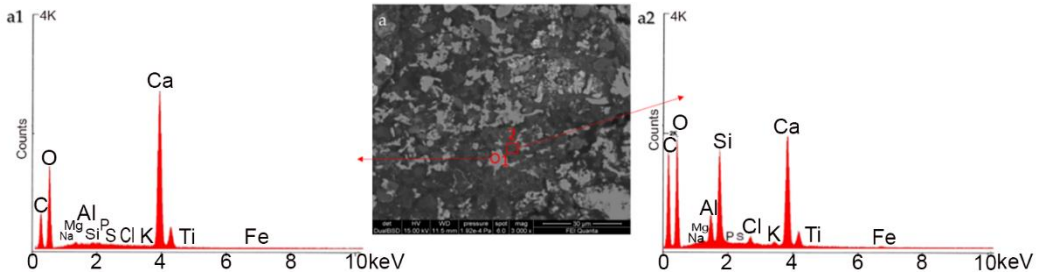

Figure 5. Binder at higher magnification. **a**) BSD image 30 μm; **a1**) EDS spectrum "point 1"; **a2**) EDS spectrum "area 2".

Furthermore, a reaction layer linked to hydraulic reactivity [38] was identified between the binder and the aggregate (**Fig. 6**) [38,39].

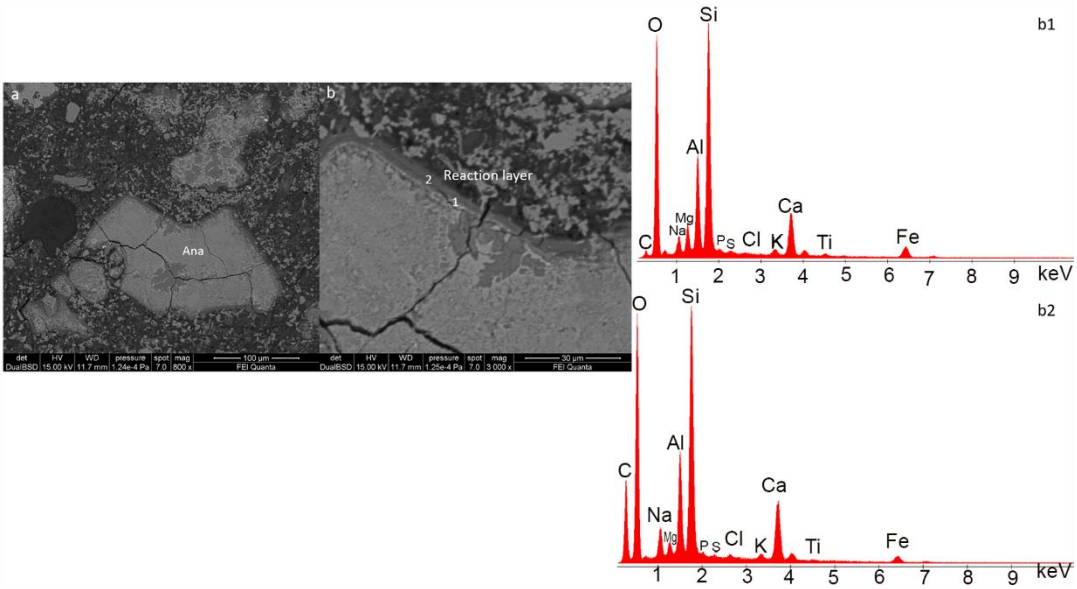

Figure 6. Reaction layer composition. **a**) Analcite crystal. BSD at 50 μm; **b**) Zoom at 30 μm; **b1-2**) layer at contact with the carbonate binder.

In particular, it was possible to observe this in isolated analcite crystals (**Fig. 6**) and in others minerals, such as the quartz (the aggregate was poor of quartz), in which the carbonatic component of the binder reacted with the external layer of the mineral (**Fig. 6b2**).

Regarding the elemental distributions maps obtained by the EDS detector on the sample n. 10 (**Figure 7),** two relevant areas were observed in the sample (**Fig. 7a, c**). It is possible to conclude that Si and Al were the most abundant components, along with Ca, validating the point-by-point EDS spectra and the petrographic results. The detection of Si was strongly linked to aluminosilicate minerals such as analcite (aggregate) and to the aluminosilicate fraction of the binder (the carbonate fraction is evidenced by the Ca map). The quartz was a rare behaviour (as can be seen in the **Fig. 7, c1**). The Cl presence could be related to the possible input of the marine aerosol coming from the nearby coastline.

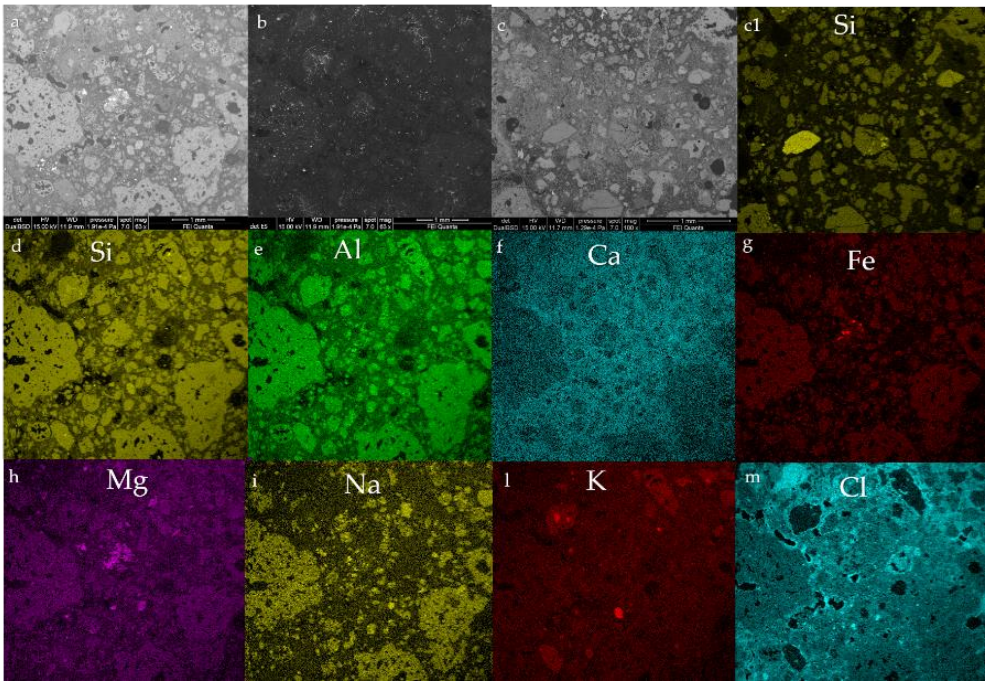

Figure 7. X-ray maps on two areas of the sample n.10. **a**) First area revealed at BSD detector (1 mm); **b**) first area revealed at ES detector (1 mm); **c**) second area at BSD detector (1 mm); **c1**) Si map of the second area investigated; **d-m** Si, Al, Ca, Fe, Mg, Na, K, Cl of the first area investigated.

3.3 Other materials

Regarding the other sampled materials (pumice, travertine, limestone, marble, ceramic and plasters), petrographic observation and XRD analysis are reported on **Figure 8 and Table 4**, respectively.

The microstructures of the samples n.11-13 were characterised by a marked vesicularity, leading to the identification of such samples as pumice. To better imitate the cave where the Mithra was born, the pumice (applied on a layer of gypsum – as was found by XRD analysis – **Tab. 4**) was also painted with a blue pigment (as can be observed on a pumice piece – **Fig- 8c**). Indeed, it is well-known that the god Mithra is linked to the sky and in particular to astronomy (as the Twins' constellation, *cautes* and *cautopates*, the torch-bearers, which with their torch raised up and downward, represent the day and night, the spring and autumn equinox, respectively, linked to Mithra rite, to Tauroctony) [40].

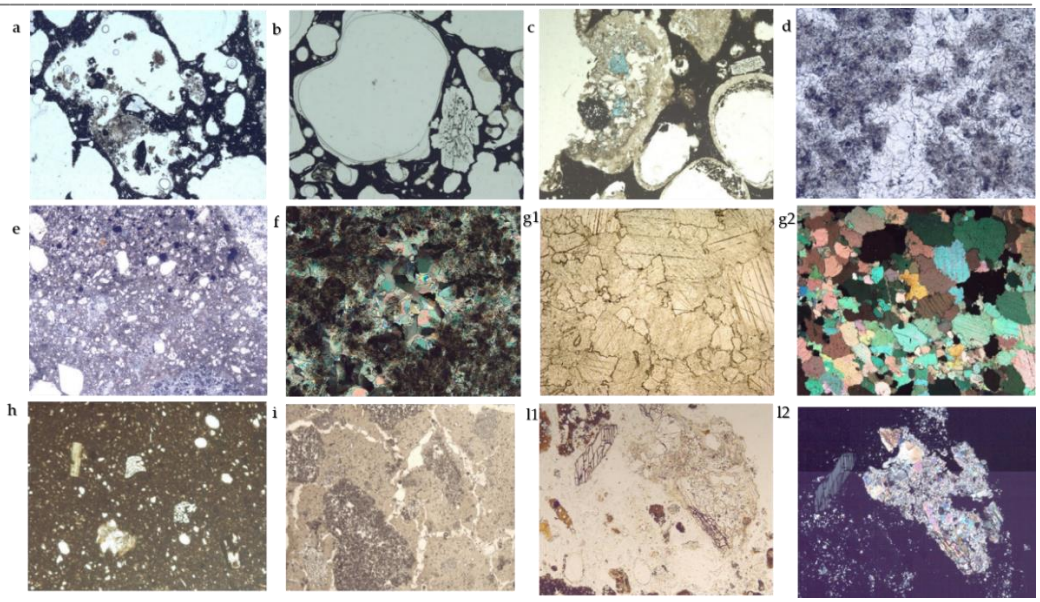

Figure 8. Microphotographs of the "others materials". **a**) Sample 11; **b**) sample 12 (parallel nicols); **c**) sample 13; **d**) sample 14; **e**) sample 15; **f**) sample 16; **g**) sample 17; **h**) sample 18; **i**) sample 19; **l**) sample 20. All the microphotographs are at plane polarized light, except than f, g2 and l2 that are at crossed polarized light. All the samples are investigated at 4x magnifications, except the l2, observed at 10x.

Sample n.14 (**Fig. 8d – Tab. 4**) was identified as travertine basing on petrographic observation and by XRD analysis (calcite). Isotopic results (expressed in terms of δ‰ and referred to PDB stand) were $\delta\ ^{13}C_{PDB}$= 10.08 and $\delta\ ^{18}O_{PDB}$= -6.34, typical values for the travertine of Tivoli [41,42].

Sample n.15 had an inventory number corresponding to "marble altar". Petrographic analysis of its thin-section, showed a heterogeneous fine matrix with scattered crystals of calcite and other minerals (**Fig. 8e**). XRD analysis revealed the presence of lanarkite ($Pb_2(SO_4)$ O) and putoranite, (Cu (Fe, $Ni)_2S_2$). These observations suggested that the material was not a marble, but probably a limestone coated with a white pigment.

Regarding sample 16, XRD analysis showed the presence of calcite as the only mineral phase. Microscopic observation revealed a microcrystalline structure, presenting vugs surrounded by larger crystals aggregates consisted of recrystallized calcite. The appearance of the matrix pointed toward the identification of the sample as a carbonaceous limestone (**Fig. 8f**).

Sample 17 was a medium-grained marble that exhibited a typical grey colour banding and emitted a distinct sulphur odour when scraped or grinded. The combination of these three features is strongly indicative of a Proconnesian provenance [43]. Observations at PLM revealed a granoblastic texture with the typical rhombohedral cleavage of calcite crystals, which did not show any preferred orientation. Grain size varied from medium to fine (0.1–5 mm) and contacts between grains formed 120° triple junctions. Micas represented accessory minerals (**Fig. 8g**).

Table 4. Main mineralogical phases revealed by XRD in the analysed "others materials". +++ Abundant, ++ Present, + Small amount, Tr. Traces, - Undetected. *Preparation layer of pumice.

Compound (name)	Pumice			Travertine	Limestone		Marble	Ceramic	Plaster	
	11	12	13	14	15	16	17	18	19	20
Amorphous stuff	++	++	+++	-	-	+	+	+	-	-
Calcite	-	Tr	+	+++	+++	+++	+++	+	+++	+++
Quartz	-	-	-	-	-	-	-	+	-	-
Dolomite	-	-	-	-	-	-	Tr	-	-	-
Albite	+++	++	+	-	-	-	-	++	-	-
Augite	+++	++	++	-	-	-	-	+	-	-
Muscovite	+	+	Tr	-	-	-	-	+	-	-
Analcite	Tr	-	-	-	-	-	-	-	-	-
Hematite	+	Tr	Tr	-	-	-	-	-	-	-
Sanidine	-	++	++	-	-	-	-	++	-	-
Putonarite	-	-	-	-	Tr	-	-	-	-	-
Lanarkite	-	-	-	-	Tr	-	-	-	-	-
Gypsum*	Tr	Tr	Tr	-	-	-	-	Tr	-	-

Sample n. 18 was a ceramic characterised by a compact microstructure with low aggregate/binder ratio. The aggregate was made of plagioclase and feldspar minerals, with small amount of siliciclastic minerals (**Fig. 8h – Table 3**).

For the last samples, n. 19 and 20, XRD revealed the presence of calcite as the only crystalline phase. The microscopic observation on thin-sections, however, showed some differences in the structure and texture (**Fig. 8, i-l**).

4 CONCLUSIONS

The combined use of PLM, XRD, SEM-EDS and stable isotopes analytical techniques, represent a powerful approach in the materials' characterisation point of view, in that it enabled to bring to light some important issues.

First, differences in the microstructure and aggregate type, between the red and yellow bricks investigated, as well as amongst the red bricks, were found. Regarding the first highlight, although the only one yellow bricks investigated, the petrographic-mineralogical result gives a response that should be deserved an in-depth study. Actually, the difference between the red and the yellow brick was also macroscopically observed at first sight on feature walls and during some preliminary tests [44], where the red bricks appeared to be more compact and in a better state of conservation and with a predominance of the first one than the yellow ones. This last consideration, linked to the results obtained by seismic tomography conducted on one wall-building [45] suggested the awareness in the use of two different types of bricks (red and yellow), in terms of resistance and their strategic accommodation during the walls' construction. Therefore, it could be interesting, for a next study, to design a specific analytical protocol, in order to establish the origin of these differences,

studying the bricks' behaviour, extracting information of raw materials and deterioration products. Indeed, small amount of gypsum was recognised also in these two typologies, pointed out a sulphate attack.

Regarding the differences found amongst the red bricks, PLM and XRD results pointed out that it consists in the matrix colour (from dark brown to brown-reddish, this latter due to Fe-oxides) and in the homogeneity of matrix (with evident firing stress found in one sample). Moreover, a siliciclastic aggregate (with different quartz/feldspar ratio) and variable of amount of small black lumps characterise this type of bricks, with the only exception of one sample in which mica replaced the feldspars in the aggregate. These aspects represent an interesting clue, perhaps related to the nature of the clay, kiln environment, temperature of the firing process, nature and amount of temper.

Second, it was possible to establish the nature of mortars also thanks to SEM-EDS and X-ray maps. That is a pozzolanic mortar characterised by pozzolanic fragments and mineral phases as analcite and clinopyroxene, typical of these vulcanite, which result from crushed pozzolan. Moreover, reaction phenomena were observed in silicate minerals (analcite and quartz), underling the well-known hydraulic property of this kind of materials. The binder-aggregate ratio was low (approximately 1:3); the binder results a mixing between aluminosilicate and carbonate components. Cooking residues consisting of calcic lumps were also found.

Finally, the mithraic altar, with an inventory number classified as marble, actually is a limestone coated with a white pigment. Thanks to stable isotopes results, the travertine constituting the corbel, came as expected from nearby Tivoli deposits.

In conclusion, this study has given a crucial information regarding the wall-building construction, as well the state of conservation of bricks (not good due to the SOx attack that reflects in the continuous presence of gypsum) and some important issues linked to manufacturing processes and the quarries.

ACKNOWLEDGEMENTS

The authors would like to thank the staff of the archaeological area of Ostia Antica, especially the director Dr. Cinzia Morelli, the security company, and the technical staff (Drs. Paola Germoni, Flora Panariti, Orietta Mantovani) for the permission to work in this house. The authors also gratefully acknowledgements to Marco Albano (Department Earth Science, University of Rome "Sapienza") to carried out the SEM analysis, to Stefano Stellino (Department Earth Science, University of Rome "Sapienza") for the XRD analysis and Dr. Mauro Brilli (CNR-IGAG Rome) for the isotopic analysis.

The work was developed in the University of the Basque Country (UPV/EHU) and has been partially supported by the project DISILICA-1930 (ref. BIA2014-59124-P) funded by the Spanish Ministry of Economy and Competitiveness (MINECO) and the European Regional Development Fund (FEDER). Finally, Claudia Scatigno is grateful to University of the Basque Country (UPV/EHU) for her grant for study sojourns by trainee researchers from foreign universities engaged in a jointly supervision doctoral thesis.

REFERENCES

[1] Korka, E. (Ed.). (2015). The Protection of Archaeological Heritage in Times of

Economic Crisis. Cambridge Scholars Publishing.

[2] Borges, C., Silva, A. S., & Veiga, R. (2014). Durability of ancient lime mortars in humid environment. Constr. Build. Mater., 66, 606-620.

[3] Smith, B. J., & Turkington, A. (Eds.). (2016). Stone Decay: Its Causes and Controls. Routledge.

[4] Laurenti, M. C. (Ed.). (2012). Le coperture delle aree archeologiche: museo aperto. Gangemi Editore spa.

[5] Gaudenzi S, Preite Martinez M, Bernardini ML, Imperi F, De Bianchi S, Guiso M et al. Studio multidisciplinare sui mitrei di ostia Antica. 2012.

[6] Scatigno, C., Prieto-Taboada, N., Martinez, M. P., Conte, A. M., García-Diego, F. J., & Madariaga, J. M. (2016). Analitycal techniques for the characterisation of historical building materials: case study "Casa di Diana" Mithraeum (Archeological site in Ostia Antica, Italy). Adv.in Mater. Sci. Res., 31.

[7] Colombini, M. P., Giachi, G., Modugno, F., Pallecchi, P., & Ribechini, E. (2003). The characterization of paints and waterproofing materials from the shipwrecks found at the archaeological site of the Etruscan and Roman harbour of Pisa (Italy). Archaeometry, 45(4), 659-674.

[8] Scalenghe, R., Barello, F., Saiano, F., Ferrara, E., Fontaine, C., Caner, L., ... & Petit, S. (2015). Material sources of the Roman brick-making industry in the I and II century AD from Regio IX, Regio XI and Alpes Cottiae. Quaternary International, 357, 189-206.

[9] Aloise, P., Ricca, M., La Russa, M. F., Ruffolo, S. A., Belfiore, C. M., Padeletti, G., & Crisci, G. M. (2014). Diagnostic analysis of stone materials from underwater excavations: the case study of the Roman archaeological site of Baia (Naples, Italy). Appl. Phys. A, 114(3), 655-662.

[10] Barone, G., La Russa, M. F., Giudice, A. L., Mazzoleni, P., & Pezzino, A. (2008). The Cathedral of S. Giorgio in Ragusa Ibla (Italy): characterization of construction materials and their chromatic alteration. Environ. Geol., 55(3), 499-504.

[11] Brai, M., Casaletto, M. P., Gennaro, G., Marrale, M., Schillaci, T., & Tranchina, L. (2010). Degradation of stone materials in the archaeological context of the Greek–Roman Theatre in Taormina (Sicily, Italy). Appl. Phys. A, 100(3), 945-951.

[12] Cardinale, N., & Ruggiero, F. (2002). A case study on the environmental measures techniques for the conservation in the vernacular settlements in Southern Italy. Build. Environ., 37(4), 405-414.

[13] Cataldo, R., De Donno, A., De Nunzio, G., Leucci, G., Nuzzo, L., & Siviero, S. (2005). Integrated methods for analysis of deterioration of cultural heritage: the Crypt of "Cattedrale di Otranto". J. Cult. Herit., 6(1), 29-38.

[14] Özkaya, Ö. A., & Böke, H. (2009). Properties of Roman bricks and mortars used in Serapis temple in the city of Pergamon. Mater. Charact., 60(9), 995-1000.

[15] Vola, G., Jackson, M., Oleson, J. P., Brandon, C., & Hohlfelder, R. L. (2010). Mineralogical and petrographic characterisation of ancient Roman maritime concretes from Mediterranean Harbours. In J. Válek, C. Groot, & J. J. Hughes (Eds.), Proceedings of the 2nd Historic Mortars Conference and RILEM TC (pp. 381-388).

[16] Cardell, C., Benavente, D., & Rodríguez-Gordillo, J. (2008). Weathering of limestone building material by mixed sulfate solutions. Characterization of stone microstructure, reaction products and decay forms. Mater. Charact., 59(10), 1371-1385.

[17] Cennamo, P., Montuori, N., Trojsi, G., Fatigati, G., & Moretti, A. (2016). Biofilms in churches built in grottoes. Sci. Total Environ., 543, 727-738.

[18] Charola, A. E. (2013). Salts in the deterioration of porous materials: an overview. Journal of the American institute for conservation.

[19] Charola, A. E., Pühringer, J., & Steiger, M. (2007). Gypsum: a review of its role in the deterioration of building materials. Environ. Geol., 52(2), 339-352.

[20] Dragovich, D., & Grose, J. (1990). Impact of tourists on carbon dioxide levels at Jenolan Caves, Australia: an examination of microclimatic constraints on tourist cave management. Geoforum, 21(1), 111-120.

[21] Elert, K., Cultrone, G., Navarro, C. R., & Pardo, E. S. (2003). Durability of bricks used in the conservation of historic buildings—influence of composition and microstructure. J. Cult. Herit., 4(2), 91-99.

[22] Sanchez-Moral, S., Luque, L., Cuezva, S., Soler, V., Benavente, D., Laiz, L., ... & Sáiz-Jiménez, C. (2005). Deterioration of building materials in Roman catacombs: the influence of visitors. Sci. Total Environ., 349(1), 260-276.

[23] Sanchez-Moral, S., Luque, L., Cuezva, S., Soler, V., Benavente, D., Laiz, L., ... & Sáiz-Jiménez, C. (2005). Deterioration of building materials in Roman catacombs: the influence of visitors. Science of the Total Environment, 349(1), 260-276.

[24] Scatigno, C., & Ravera, S. (2015). Characterisation of the biological proliferation on Roman masonry. Case study: "Casa di Diana" Mithraeum (Ostia Antica, Rome–Italy).

[25] Scatigno, C., Gaudenzi, S., Sammartino, M. P., & Visco, G. (2016). A microclimate study on hypogea environments of ancient roman building. Science of The Total Environment, 566, 298-305.

[26] Scatigno, C., Moricca, C., Tortolini, C., & Favero, G. (2016). The influence of environmental parameters in the biocolonization of the Mithraeum in the roman masonry of casa di Diana (Ostia Antica, Italy). Environmental Science and Pollution Research, 1-10.

[27] Videla, H. A., Guiamet, P. S., & de Saravia, S. G. (2000). Biodeterioration of Mayan archaeological sites in the Yucatan Peninsula, Mexico. International biodeterioration & biodegradation, 46(4), 335-341.

[28] Miriello, D., Barca, D., Bloise, A., Ciarallo, A., Crisci, G. M., De Rose, T., ... & La Russa, M. F. (2010). Characterisation of archaeological mortars from Pompeii (Campania, Italy) and identification of construction phases by compositional data analysis. Journal of Archaeological Science, 37(9), 2207-2223.

[29] Korkanç, M. (2013). Deterioration of different stones used in historical buildings within Nigde province, Cappadocia. Construction and Building Materials, 48, 789-803.

[30] Yaseen, I. A. B., Al-Amoush, H., Al-Farajat, M., & Mayyas, A. (2013). Petrography and mineralogy of Roman mortars from buildings of the ancient city of Jerash, Jordan. Construction and Building Materials, 38, 465-471.

[31] Madariaga, J. M. (2015). Analytical chemistry in the field of cultural heritage. Analytical Methods, 7(12), 4848-4876.

[32] Pouyet, E., Fayard, B., Salomé, M., Taniguchi, Y., Sette, F., & Cotte, M. (2015). Thin-sections of painting fragments: opportunities for combined synchrotron-based micro-spectroscopic techniques. Heritage Science, 3(1), 1.

[33] Artioli, G. (2013). Science for the cultural heritage: the contribution of X-ray diffraction. Rendiconti Lincei, 24(1), 55-62.

[34] Cultrone, G., & Sebastián, E. (2008). Laboratory simulation showing the influence of salt efflorescence on the weathering of composite building materials. Environmental geology, 56(3-4), 729-740.

[35] Gering, A. (2014). Le ultime fasi della monumentalizzazione del centro di Ostia tardoantica. Attività della missione della Humboldt-Universität di Berlino tra il 2009 e il 2013. Mélanges de l'École française de Rome-Antiquité, (126-1).

[36] McCrea, J. M. (1950). On the isotopic chemistry of carbonates and a paleotemperature scale. The Journal of Chemical Physics, 18(6), 849-857.

[37] Craig, H. (1957). Isotopic standards for carbon and oxygen and correction factors for mass-spectrometric analysis of carbon dioxide. Geochimica et cosmochimica acta, 12(1), 133-149.

[38] Moropoulou, A., Bakolas, A., & Bisbikou, K. (2000). Investigation of the technology of historic mortars. Journal of Cultural Heritage, 1(1), 45-58.

[39] Moropoulou, A., Bakolas, A., & Bisbikou, K. (2000). Physico-chemical adhesion and cohesion bonds in joint mortars imparting durability to the historic structures. Construction and Building Materials, 14(1), 35-46.

[40] Hannah, R. (1996). The image of Cautes and Cautopates in the Mithraic tauroctony icon. Religion in the Ancient World (Amsterdam), 177-92.

[41] Manfra, L., Masi, U., & Turi, B. (1976). La composizione isotopica dei travertini del Lazio. Geol. Rom, 15, 127-174.

[42] Minissale, A., Kerrick, D. M., Magro, G., Murrell, M. T., Paladini, M., Rihs, S., ... & Vaselli, O. (2002). Geochemistry of Quaternary travertines in the region north of Rome (Italy): structural, hydrologic and paleoclimatic implications. Earth and Planetary Science Letters, 203(2), 709-728.

[43] Attanasio, D., Brilli, M., & Rocchi, P. (2008). The marbles of two early Christian churches at Latrun (Cyrenaica, Libya). Journal of Archaeological Science, 35(4), 1040-1048.

[44] Scatigno, C., Sammartino, M. P., & Gaudenzi, S. (2014). Non-invasive analysis of soluble salts. Preliminary results on the case study of Casa di Diana Mithraeum (Achaeological site of Ostia Antica-Italy).

[45] Cardarelli, E., De Donno, G., Oliveti, I., & Scatigno, C. (2016, September). Assessing the State of Conservation of a Masonry Building through the Combined Use of Electrical and Seismic Tomography. In Near Surface Geoscience 2016-22nd European Meeting of Environmental and Engineering Geophysics.

This overview on stone materials brought to light a difference, in the texture and aggregate type, between the red and the only yellow brick investigated. Due to this uniqueness, the study was not representative. Therefore, albeit partial, this petrographic-mineralogical result deserved an in-depth study.

Moreover, this difference was also macroscopically observed at first sight on feature walls, and during some preliminary tests [9]. Actually, the red bricks appeared to be more compact and in a better state of conservation and with a predominance of the first one then the yellow ones (**Chapter 1.2**). This last consideration, linked to the results obtained by ST (**Chapter 6.2**), suggested the awareness in the use of two different types of bricks (red and yellow), in terms of resistance, and their strategic accommodation during the walls' erection.

Finally, taking into account, that the observed difference in colour could be related to many factors (nature of the clay, kiln environment an operator, temperature of the firing process, nature and amount of temper), it was necessary to design an analytical protocol, in order to establish the origin of these differences.

Considering the relevance of the bricks in ancient build heritage (favourite building material in the Roman Empire) and the wide bricks industry, which played an important role in Rome (Ostia Antica) than any of other industry in antiquity from here onwards, the materials' characterisation must to be taken into consideration the red and yellow bricks.

Furthermore, in the literature, although the availability of studies on Roman brick's characterisation [113, 109-129] was wide, it not focused on these two typology of bricks [130, 131].

In this sense, a combination as (micro) energy dispersive X-ray fluorescence (μ-EDXRF), Raman spectroscopy, X-ray diffraction (XRD) and ion chromatography (IC) was selected, in order to study the bricks' behaviour, extracting information of raw materials and deterioration products.

7.1 Non-destructive spectroscopic analysis[33]

Several years ago, the sampling of a small number of samples was the critical step to perform analyses in the field of Cultural Heritage. The development of the portable devices allows these analyses to be performed *in-situ* with successful

[33] An adapted version was published in:
Scatigno, C., N. Prieto-Taboada, M. Preite Martinez, A. M. Conte, F. J. García-Diego, and J. M. Madariaga. "Analytical techniques for the characterisation of historical building materials: case study "Casa di Diana" Mithraeum (Archaeological site in Ostia Antica, Italy)." Advances in Materials Science Research (2016): 31.

results, avoiding the sampling and therefore ensuring the integrity of the Built Heritage [132]. Moreover, the sampling can be assisted by *in-situ* analyses to avoid unnecessary damage, which is essential in the Built Heritage field. Hence, the use of portable spectroscopic techniques is growing over traditional methods and, in the last years, many works that can be found in the literature were carried out *in-situ* using several portable spectroscopic devices [99, 100, 107, 133-138].

Among them, X-ray fluorescence spectrometry (XRF) is a well-established analysis technique for rapid and simple determination of the elemental composition of a material. This method is non-destructive, multi-elemental, fast and cost-effective. It can be applied in a non-vacuum environment directly on the sample without any preparation [135, 138-141]. Moreover, the development of the technology has allowed *in-situ* and non-invasive analysis with a good analytical signal [114].

Another *in-situ* analytical technique to take into account is Raman spectroscopy. During the last decade, Raman spectroscopy has become an established analytical technique for the study of art and antiquities [101, 142]. This is because Raman spectroscopy technique used on historical objects to characterize and survey artworks (qualitatively and semi quantitatively), offers the possibility of non-destructive, non-invasive and *in-situ* analyses [143]. Moreover, the samples can be analysed without any pre-treatment, simply by placing them under the laser beam. Furthermore, Raman spectroscopy is one of the most used techniques for the study of these kinds of systems due to its high sensitivity to small structure variations, which allows polymorphic compounds to be distinguished [144]. In fact, it permits to differentiate compounds such as calcite and aragonite which are characterized by the same molecular formula ($CaCO_3$) but a different crystal system (trigonal and rhombic, respectively). In addition, Raman spectroscopy distinguishes different numbers of hydration water, as in the case of gypsum ($CaSO_4 \cdot 2H_2O$), hemihydrate ($CaSO_4 \cdot 0.5H_2O$) and anhydrite ($CaSO_4$) [144]. In the particular case of building materials, the Raman spectroscopic technique allows to characterize both original and decaying compounds [99, 100, 138].

Taking all of this into account, both techniques were performed on bricks, by an *in-situ* screening, in order to study the compounds and the elements that describe their colours, avoiding the direct sampling.

Article 7

Combination of *in-situ* spectroscopy and chemometric techniques to discriminate different types of Roman bricks and the influence of microclimate environment. Article submitted to Analytical and Bioanalytical Chemistry. Ms. Ref. No.: ABC-00005-2017.

COMBINATION OF *IN-SITU* SPECTROSCOPY AND CHEMOMETRIC TECHNIQUES TO DISCRIMINATE DIFFERENT TYPES OF ROMAN BRICKS AND THE INFLUENCE OF MICROCLIMATE ENVIRONMENT

C. Scatigno[a,b]*, N. Prieto-Taboada[b], C. García-Florentino[b], S. Fdez-Ortiz de Vallejuelo[b], M. Maguregui[b], J.M. Madariaga[b]

[a] Department of Earth Science, University of Rome "La Sapienza", Piazzale Aldo Moro 5, 00185, Rome, Italy.
[b] Department of Analytical Chemistry, University the Basque Country, (UPV/EHU), Barrio Sarriena s/n, 48940, Leioa, Spain
*Corresponding author: claudia.scatigno@uniroma1.it
Phone: (+ 39) 0649914156, Fax: (+39) 064454729

Abstract
Red and yellow bricks are wall-building materials generally used in Roman masonries. The reasons for the different coloration are not always understood, causing a loss of crucial information both for the conservation and for the archaeological knowledge of the cultural sites. In this work, a combination of *in-situ* analyses, employing portable Raman spectroscopy and handheld energy dispersive X-ray fluorescence (HH-ED-XRF) spectroscopy along with chemometric analysis, was carried out on ancient Roman bricks of the "Casa di Diana" building (Ostia Antica, Italy-130 CE). Specifically, the compounds and the characteristic elements, which describe each brick type (red and yellow), were studied avoiding destructive or invasive sampling. The molecular analysis allowed us to identify the major and minor compounds that characterise the bricks (anatase, hematite, quartz, calcite and silicates). However, the elemental analysis gave more useful information. Thus, the HH-ED-XRF complex data matrix generated, was treated by a Principal Component Analysis (PCA) to identify behavioural differences of the coloured bricks. The results revealed that Ca and Fe were the discriminatory elements for the two types of bricks. The PCA outcomes suggested that the contribution of certain elements was different in the bricks (mainly Ca, P, Sr, As and S, for yellow bricks), which could indicate different raw materials. Even among bricks with the same apparent red colour (Al, Si, Ti, K, Fe, Cr, Mn, Ni, Zn, Cu, Rb and Zr, seemed to be the elements linked to raw materials), as a function of the surface impacts (orientation and microclimate affect the salts' formation) a distinction was made. Furthermore, the PCA pointed out towards yellow bricks being more affected by decaying processes (related with Ca, P and S), complying with the Raman spectroscopy results where the efflorescences (gypsum) were identified especially in these type of bricks 'surface.

Keywords Roman bricks; Raman spectroscopy; handheld energy dispersive X-ray fluorescence (HH-ED-XRF); Principal component analysis (PCA); environmental stressors; *in-situ* analysis.

Highlights

- A combined approach with portable Raman and handheld HH-ED-XRF spectroscopy to study the Roman coloured bricks.
- An *in-situ* screening to distinguish among different types of Roman bricks: red and yellow.
- A PCA steps procedure to perform a discriminant analysis using the data matrix obtained by HH-ED-XRF spectroscopy.
- The microclimate as an important issue in the materials' conservation.

1 INTRODUCTION

Bricks, ceramic materials obtained by firing raw clay at temperatures ranging between 650 and 1100 °C, are the most ancient manmade building materials [1] comprising masonry structures of the old civilizations, developed around the Mediterranean basin [2]. Bricks were the favourite building material in Rome between the middle of the first century (Emperor Nero) and the beginning of the fourth century (Emperor Constantine) [3]. In fact, the brick industry played an important role in Rome, representing the most advanced manufacture sector compared with any other industrial process in antiquity. Because of the importance of Roman manufactory, bricks often presented an imprinted seal, as a trade mark on bricks stamps [3]. Regarding these ancient bricks' composition, especially the ones developed in areas close to rivers (where alluvial deposits and argillaceous plastic soils were abundant), the fired bricks were produced through the process of mixing sifted raw materials containing quartz, feldspar and clay with water and then shaping, drying and baking [4]. Clays constitute the basic raw material of bricks and are the result of natural deterioration of igneous stones and schist. They consist of mixtures of aluminate, silicate and aluminosilicate compounds of calcium, iron and alkali metals [2].

Taking into account the relevance of these materials in the ancient built heritage, several studies on Roman bricks' characterisation have been conducted in order to study their mechanical properties and the construction phases [5], as well as the chemical characterisation within multidisciplinary investigations [1, 6]. In this sense, it is established that, commonly, Roman bricks were produced from calcium-poor raw materials fired at 750-850°C [4]. The ceramic body is at first glance homogeneous, without inclusions, often yellow in colour, indicating either low iron content or high amounts of calcium [6]. However, not only the colour differences could be attributed to different raw materials (nature of the clay) but also to differences in the temperature of the firing process, as well as to the nature and amount of temper [1]. In a study conducted on fired bricks, evaluating the different physic-mechanical properties, the red colour (light red and reddish brown) was attributed to Roman bricks and the yellow colour (reddish yellow) to Byzantine bricks [2].

Therefore, the bricks' study and their classification seem to be essential, giving crucial information on the cultural site's properties, both from a conservative and archaeological point of view. Indeed, with such knowledge it could be possible, during the restoration processes, to define how to integrate the gaps, choosing the best type of brick, identifying which colour of bricks is preferentially attacked during the damage processes (causing a decrease in the resistance level), as well as understanding the reason for the different type of coloration, and acquiring important archaeological information of the cultural site. Moreover, the importance of develop a discriminating methodology of the different types of bricks resides also in the identification of different parts of the same Roman buildings constructed with yellow and red bricks, that appear even

mixed, being impossible to distinguish the two coloured bricks on the walls at first sight due to severe decaying. What is more, the presence of natural mixtures containing smaller amounts of aluminosilicates in comparison to other common silicates could generate some variation in colour tones, increasing the colour tones as the concentration increases. For that reason, the identification of the different type of brick and the reasons for the colour differences becomes more abstruse without the use of appropriate analytical techniques [7].

A wide range of *in-situ* and non-destructive analytical techniques are available and applied in the preservation of built heritage [8, 9]. These kinds of techniques minimize the damage generated to the built heritage during the analytical study avoiding unnecessary sampling if the *in-situ* analysis does not justify them. Obviously, sometimes the sampling is unavoidable but in such cases, the *in-situ* analysis represents the key to minimize them thanks to appropriate conclusions derived from the screening performed in the field [10-14]. Among the *in-situ* analytical techniques used to study ancient bricks, the spectroscopic ones are the most relevant [13, 15-22].

Considering the relevance of the bricks in ancient built heritage, the wide variety of bricks industries, the absence of a clear spectroscopic differentiation between the red and yellow bricks and the possible influence of chemical composition on the formation of white subeffloresences and patinas on the most outer exposed areas of the bricks, we developed a methodology to clarify such unresolved issues. Furthermore, in literature, the studies on Roman brick's characterisation [1-6] are widespread but they do not focus on these red and yellow bricks [23, 24]. For that reason, Raman spectroscopy and handheld energy dispersive X-ray fluorescence (HH-ED-XRF) techniques were selected to study the Roman bricks of a particular Roman building ("Casa di Diana" *Mithraeum*), located in the ancient archaeological city of Ostia Antica (Italy), in order to distinguish the two bricks typology (red and yellow) and to study the bricks' behaviour, extracting information in terms of raw materials and deterioration products by chemometric analysis.

1.1 Site description

In Italy, there are many archaeological evidences of Roman houses. The best-known examples are Pompeii, Herculaneum and Ostia Antica. The present study takes into consideration the latter, Ostia Antica that was Rome's first *colonia* and played an important role as a port to supply the city of Rome. Amongst Roman masonries, we focused on a particular building, called "Casa di Diana" (Rome, Italy), and dated 130 CE. It is a building that housed most of the urban citizen population of ancient Rome (*insula*), particularly rich in decorations (mosaic floors) and furniture, as a large marble fountain, signs of example of aristocratic luxury of the wealthiest the upper-middle class (the *equites*). The house originally had five floors, where the ground floor hosted shops, while the upper floors had the apartments; nowadays only the ground floor and traces of the projecting part of the continuous balcony of the first floor still survive. On the northern side, two inter-communication rooms (*Mithraeum*

and *pre-Mithraeum*) are found. On the western side, a room, without a roof (*Triclinium*), communicates with them by openings of different dimensions. The two rooms are completely different in terms of microclimatic environment. Previous works pointed out towards the presence of both semi-confined and *hypogeum* environments in a single volume [25]. In particular, high relative humidity values close to saturation (98%) were recorded on the wall-building materials up to 1 m [25].

The building of "Casa di Diana" was essentially erected using Roman bricks. Two principal colours, red and yellow are identified [26], but a mattifying veil on the inner wall (**Fig. 1a**) makes difficult to distinguish the mid-tones between them. Furthermore, the tone variability is not homogeneous in the whole building, groups of different red and yellow tone bricks are found in the walls, from dark red to light yellow, visible both on the inside and the outside of the structure (**Fig.1**). The walls of the building present a different feature: the red ones seem to be more numerous than the yellow ones, although the mattifying veil affected more the interior walls (**Fig. 1a**). The bricks suffer several conservative problems, in particular salt efflorescence and biological proliferation [25-28]. The latter concerns the lower strata (0-1 m) of the building. Actually, the materials in correspondence of major biological presence appear to be in an advanced state of damage. Both mentioned decaying products are linked to the complex scenario (microclimate environment) in which the building is found [25, 27], due to a specific hydro-geological setting of the area [28, 29].

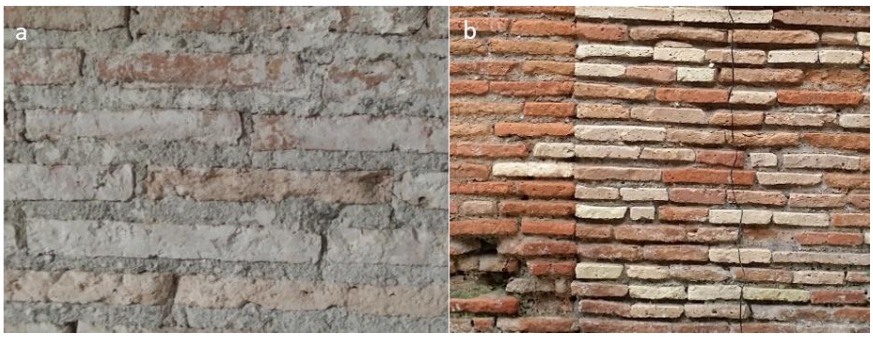

Figure 1. Appearance of the wall-building. **a**) With the mattifying veil; **b**) without an intense veil.

Until now, conservative actions (apart from direct and punctual recovery actions carried out by restores equips) were not applied in the building under study.

2 METHODS AND MATERIALS

2.1 *In-situ* measurements

Before starting the analysis with portable Raman spectroscopy and HH-ED-XRF, the area selection strategy was adopted to guarantee the representativeness of the whole building. After a close examination on the wall-building features, some walls seemed to present only red bricks (as it happened on the west wall of the *pre-Mithraeum*). Among red tone, 4-5 tones (not present on each wall) are observable. In order to measure these shades and taking into

account the rising damp level and some inaccessible areas (presence of wall paintings, mosaic flooring and artworks such as *podia*) that were not possible to be measured, 9 areas along the walls surface (southern wall and northern wall for the *pre-Mithraeum* and *Mithraeum*, respectively) were considered in this study (**Fig. 2b**). Specifically, three areas in the *Mithraeum* (16, 19 and 20), five areas in the *pre-Mithraeum* (15, 17, 18, 21 and 23) and one area from the *Triclinium* room (22) (**Fig. 2**) were selected. For each area, two kinds of bricks (red and yellow without considering their different tonalities) were analysed and for each colour measured, an abbreviation "R" (red) or "Y" (yellow) was assigned (**Tab. 1**). In this sense, 16 bricks (red and yellow) were selected (0-1 m from the ground floor). To simplify the terminology, a letter was assigned to each room (A, B, C, as *pre-Mithraeum*, *Mithraeum* and *Triclinium*, respectively) where the bricks were measured.

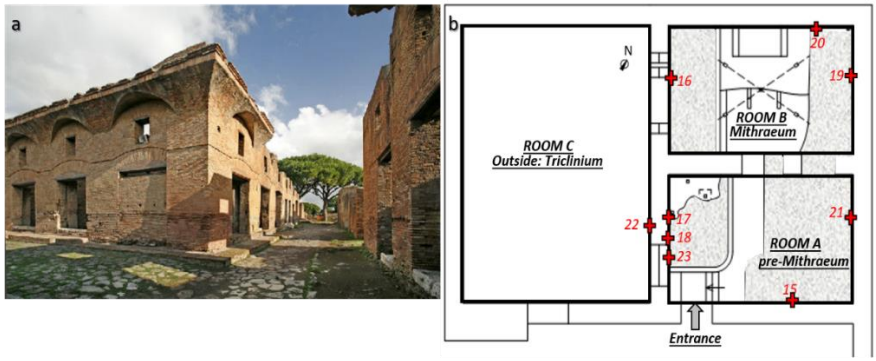

Figure 2. Image of "Casa di Diana" building (**a**) and plan of measurement strategy (**b**). The (+) red symbols indicate selected areas in which Raman spectroscopy and HH-ED-XRF analyses were performed.

Therefore, for each area and type of brick, two measurements were carried out, in order to evaluate any eventual difference, distinguishing in this way surface and inner measurements when possible. Indeed, as it is possible to observe in the Table 1, the areas selected are not always characterised by the same measurements (surface and inner). In some cases, when the salts crust was too thick (causing difficulties with its removal), the measurements were performed only in the inner part of the bricks (broken zones), analysing the original compounds of the bricks.

Thus, a total of 34 analysed points were obtained (**Tab. 1**). In this way, a new ID (identification number) assignation was created (**Tab. 1** – last column).

Table 1. ID Assignation of the points measured on the "Casa di Diana" walls.

Area	Room	Colour	Orientation	Measurements	New ID
15	A	Y	S	Inner	AYSI-1
				Inner	AYSI-2
		R	S	Surface	ARSS-1
				Inner	ARSI-2
16	B	Y	W	Surface	BYWS-1
				Inner	BYWI-2
		R	W	Inner	BRWI-1
				Inner	BRWI-2
17	A	Y	W	Surface	AYWS-1
				Inner	AYWI-2
		R	W	Surface	ARWS-1
				Inner	ARWI-2
18	A	R	W	Surface	ARWS-3
				Inner	ARWI-4
23	A	R	W	Surface	ARWS-5
				Inner	ARWI-6
19	B	Y	E	Inner	BYEI-1
				Inner	BYEI-2
		R	E	Surface	BRES-1
				Inner	BREI-2
20	B	Y	N	Surface	BYNS-1
				Inner	BYNI-2
		R	N	Inner	BRNI-1
				Inner	BRNI-2
21	A	Y	E	Surface	AYES-1
				Inner	AYEI-2
				Inner	AYEI-3
		R	E	Surface	ARES-1
				Inner	AREI-2
22	C	Y	E	Surface	CYES-1
				Inner	CYEI-2
		R	E	Surface	CRES-1
				Surface	CRES-2
				Inner	CREI-3

2.2 Raman spectroscopy

The molecular characterization was carried out by Raman spectroscopy, using a portable InnoRam spectrometer (B&WTEKINC., USA) provided with a 785 nm excitation laser with a nominal laser power of 225 mW and a CCD detector (Peltier cooled). All the spectra were obtained with a resolution of 3 cm^{-1} in a spectral range of 125–2500 cm^{-1}. The measurements were carried out in a continuous mode in order to scan the samples entirely. When an optimum response was obtained, the measurement point was fixed to improve and to collect the spectrum. The integration times and the spectra accumulations were set to obtain the better signal-to-noise ratio. Following this procedure, more than 100 spectra were recorded. The acquisition of data was carried out with BWSpec software (B&WTEKINC, USA) and the analysis, treatment and interpretation of the results were made with the Omnic Version 7.2 software Thermo Nicolet (Madison, WI, USA) and with e-VISART [30] e-VISARCH dispersive Raman and FT-Raman spectra databases, as well as the RRUFF online database [31].

2.3 HH-ED-XRF system

To detect elemental differences between colour group members, a handheld energy dispersive X-ray fluorescence spectrometer X-MET5100 (Oxford Instruments, UK) equipped with a rhodium anode X-ray tube (operating at 45 kV) was used. The diameter of the X-ray beam in the instrument used is 9 mm. The analyzer has a high-resolution silicon drift detector (SDD), with a spectral resolution of 20 eV and an energy resolution around 150 eV (calculated for Mn-K_α at 20°C). The instrument is also equipped with a Personal Digital Assistant (PDA) that allows an easier management of the instrument and the storage process of the results. In order to improve the limit of detection, the measurements were acquired for 100 seconds (real time). The analyses were performed directly by placing the sampling interface in the wall-building. Although the software is based on the use of Fundamental Parameters quantification methods, in this work, the net counts of K_α lines of each detected element in the spectrum were considered following a previous normalization process [32]. See elsewhere for further details [33]. The spectra obtained were transferred from the PDA to the computer in .txt format and were transformed into binary files in order to be treated with the EZData (ChemiLab, USA) program, which allows us to analyse the net areas of the XRF lines of the elements present in each spectrum.

The final data matrix obtained by XRF, in the form of normalized net counts of each element. Principal Component Analysis (PCA) was performed by PLS-Toolbox v.7.0.2 (Eigenvector Research, USA) implemented in MATLAB 2010 software (The Mathworks, MA, USA). Data were also treated with the OriginPro 8.5 software (OriginLab® Corporation, Northampton, Massachusetts, USA) for the descriptive statistical analysis of the data matrix.

3 RESULTS AND DISCUSSION

3.1 Raman spectroscopy results

The Raman spectra pointed out some compounds that characterise the two colours of bricks in terms of raw materials. Anatase (TiO_2, identified by its Raman band at 145 cm^{-1}), hematite (Fe_2O_3, easily identified by its characteristic bands at 227, 294 and 416 cm^{-1}), quartz (SiO_2, identified by its band at 466 cm^{-1}), calcite ($CaCO_3$, characterized by the main band at 1087 cm^{-1}) (**Fig. 3a-d**) and undetermined silicates (fluorescence bands observed in the range of 1200-1900 cm^{-1} of the Raman spectrum) [34, 35], represent the compounds which characterise the red bricks (**Fig. S1**).

Regarding the yellow bricks, calcite (observed Raman bands at 282, 713 and 1087 cm^{-1}), hematite (identified by 227, 294, 415, 502 and 612 cm^{-1} Raman bands) and quartz (mean Raman band at 465 cm^{-1}) were detected (**Fig. 4a-c**). The typical bands promoted by some silicates, were not so clearly observed in this case, probably due to the different nature of the raw material (minor amount of silicates). Furthermore, gypsum ($CaSO_4 \cdot 2H_2O$, Raman bands at 416, 449, 621, 672, 1010 and 1137 cm^{-1}), which covered most of the surface in practically all yellow bricks was often observed (**Fig. 4d**) [18].

Apart from measuring the bricks, additional measurements were carried out on the mattifying veil obtained after its scraping from the surface of the bricks. All the Raman spectra acquired showed the typical Raman feature of gypsum. Even if these efflorescences are present indistinctly in red and yellow bricks, this phenomenon is particularly evident on the latter. Although, the Raman spectra highlighted some compounds that characterise one brick typology rather than the other, as in the case of anatase, which could represent a colour marker, as well as an indicator of the temperature reached in the firing process [35], exclusive for the red one, a substantial difference of the two coloured bricks was not clear. In particular, both kinds of bricks contain hematite so this pigmented mineral phase cannot be the only factor responsible of the different shades of the bricks.

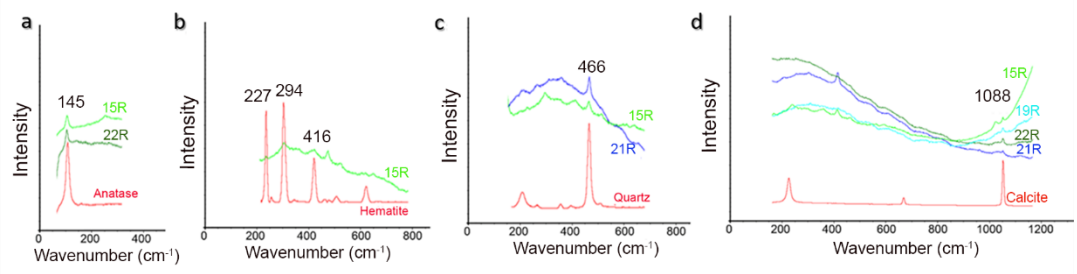

Figure 3. Raw Raman spectra of red bricks. **a**) Anatase; **b**) hematite; **c**) quartz and **d**) calcite.

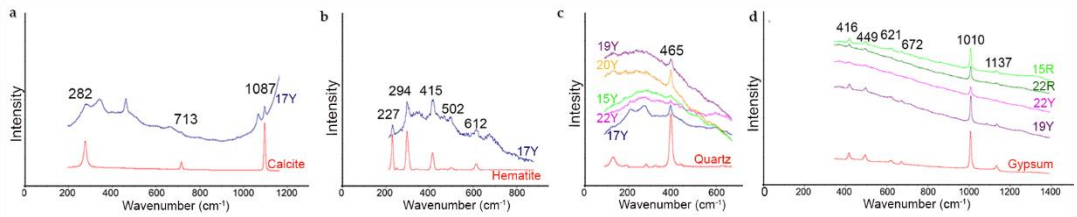

Figure 4. Raw Raman spectra of yellow bricks. **a**) Calcite and additional bands which were not possible to assign; **b**) hematite; **c**) quartz and **d**) gypsum Raman spectra for the red and yellow bricks.

The lack of clear differences in the molecular characterization between bricks could be related with the mattyfing veil, which, although it was tried to avoided it, it could difficult the deep characterisation of the bricks taking into account also the gypsum identification. In this sense, HH-ED-XRF analysis could be more appropriate to discriminate among bricks thanks to its capacity to penetrate deeper into the materials.

3.2 HH-ED-XRF results

The HH-ED-XRF spectra revealed a clearer distinction of the two types of coloured bricks (**Fig. 5**). Indeed, it was possible to observe that the Fe and Ca seemed to be the key elements to discriminate between the two types of bricks. In fact, the red bricks presented more iron than the yellow bricks. On the contrary, Ca was the element that is peculiar for the yellow bricks. Moreover, the red bricks seemed to have more Si and

Al, which suggested a different composition in terms of aluminosilicates.

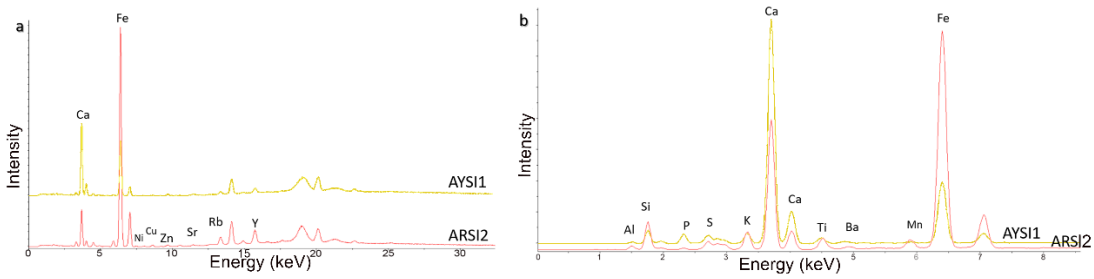

Figure 5. HH-ED-XRF spectra. **a**) AYSI1 and ARSI2 samples (FP); **b**) AYSI1 and ARSI2 samples (spectra showing elements with Z ≤ 29).

Other important information emerged observing the HH-ED-XRF spectra for each type of brick and according to the area measured (inner or surface). In the inner areas or on the surface of the yellow bricks, the major elements (Fe and Ca) did not change and only a small peak area difference was visible for the others elements (Rb, Sr, Zr, and Br). Contrarily, in the red ones, a marked difference was observed within the same type of brick, between Fe, Ca and the others elements (Rb, Sr, Zr, and Br), where the peak area changed considerably.

For all of that, HH-ED-XRF provided interesting information for studying the differences between bricks. Thus, the data matrix was treated also employing chemometric tools, exploring the possible relationship between the discriminatory chemical elements of Roman coloured bricks.

3.3 HH-ED-XRF data analysis

Firstly, the data set consisted of an initial matrix with 34 analyses on the selected areas, in rows, and the normalized net counts of 20 elements (Al, Si, P, S, K, Ca, Ti, Ba, Cr, Mn, Fe, Ni, Cu, Zn, Br, Pb, Rb, Sr, Zr, and Y) in columns. It is important to underline that the HH-ED-XRF spectrometer does not allow us to perform deconvolution of acquired spectra. Therefore, it is not possible to affirm the presence of As in the analyzed bricks because of its interference with Pb.

The data set considers both inner and surface measurements. First, a descriptive statistical analysis with Box plot, Scatter plot and Correlation graphs, was performed. The Box plot representation (**Fig. 6**) revealed important results regarding the variable (elements) distribution in the points/areas, pinpointing the influence of certain elements. As can be observed in the **Figure 6,** the elements with major range were Fe, Ca, Sr (**Fig. 6a, c**) together with Sr (**Fig. 6c**). Their amplitudes revealed the Ca and Fe influence considerably in the selected areas of the walls. However, for the red bricks, Fe presented an asymmetrical distribution, which indicated a different contribution in the different points/areas, maybe related with the wide colour range of this type of bricks. Contrarily, the yellow bricks showed a symmetrical distribution for the first two elements (Fe, Ca – **Fig. 6a, b**). In this sense, it is interesting to note that the Ca presented a smaller range in the yellow bricks than in the red ones. Performing others Box plots considering the same measured typology between the two types

of bricks, the major range of Ca were confirmed for both the inner part and surface. Furthermore, Pb, Ba, Br and Y were not always found in some areas analysed.

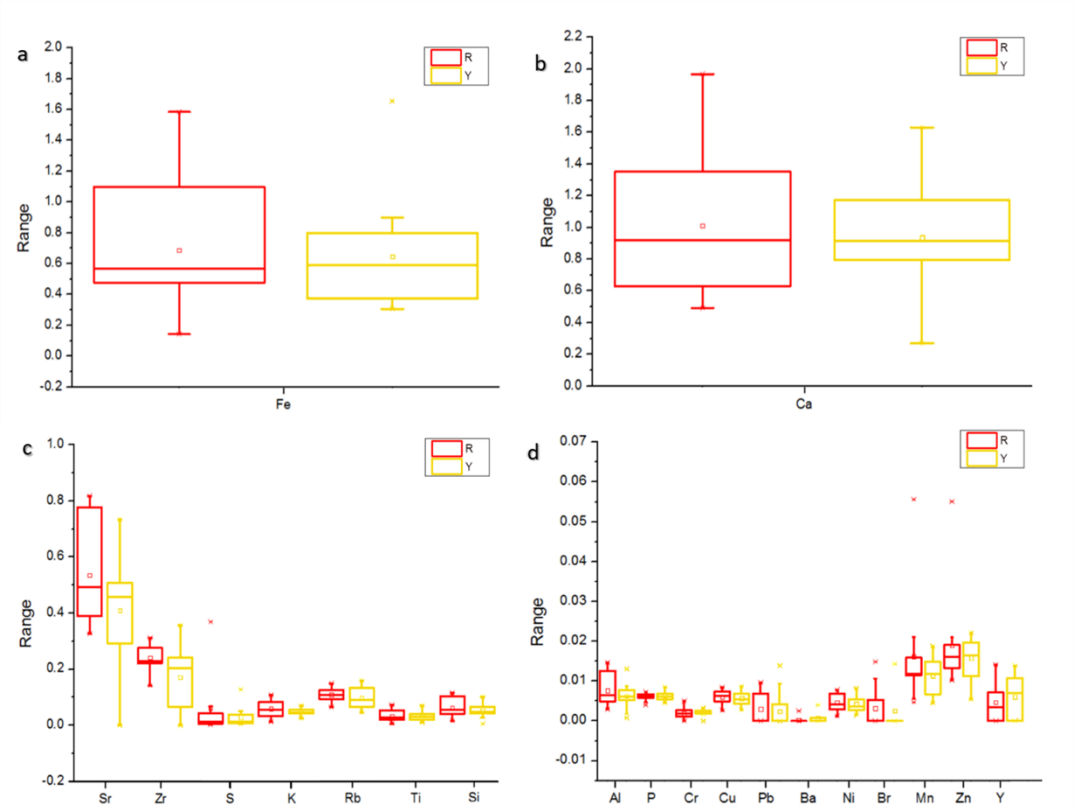

Figure 7. Box plots considering the data set of (34 x 21), red and yellow bricks. The Box are calculated according Whisker: the box displays the maximum and minimum values (two crosses outside the box), the median domain (the middle line inside the box) and the lower and the upper quartile (the ends of the box).

Cross correlation analysis was also performed using all available data. Al/Si had a high factor of correlation (0.99), as well as K and Si (0.92), indicating the presence of aluminosilicates for both types of bricks, as shown by Raman spectroscopy.

3.4 PCA analysis of the HH-ED-XRF data

According to the previous results, it was made possible to simplify the matrix, discarding some elements, in the data set for the Principal Component Analysis (PCA). Pb, Ba, Br and Y were discarded from the data matrix, obtaining a first new data set with 34 analyses in rows and of 16 elements in columns, which was centred and scaled. Three PCAs were carried out, explaining 73% of the total variance (PC1: 49 %, PC2: 16 %, and PC3: 8 %) as can be seen in **Figure 7a, b**. At first sight, a separation of the red and yellow bricks was observed, although it was not very clear. In more detail, considering the scores plot (**Fig. 7a**), it was observed that the yellow bricks were characterised by a positive value of PC1 (except from CYES1

and AYWI2), while the red bricks were characterised by dispersion between PC1 and PC2 axes. Ca and Fe appeared to be the key elements to discriminate between the two types of bricks. In this sense, the most important difference between the two typologies of bricks seemed to be the composition and the level of damage. In fact, the red bricks, and in particular the measurements in the inner of the bricks (**Fig. 7a**), were characterised by elements linked to the original composition (raw materials), such as Al, Si, Ti, K, Fe, Cr, Mn and Ni. Moreover, others elements (Cu, Rb, Zr and Zn) were related particularly with the points measured on the surface (**Fig. 7a, b**). It is interesting to observe that Ti was clearly related with the red bricks (**Fig. 7a, b**), as previously highlighted in the Raman spectroscopy results.

On the other hand, the yellow bricks seemed to be linked to Ca, P, Sr, and S, three of which (Ca, P and S) were probably associated to decaying products (soluble salts formation as carbonatation and sulphatation phenomena [27]), which describe both external (surface) and internal measurements. In this way, the positive value of PC1 could be related to decaying processes. Nonetheless, S had negative PC2 value, contrarily to Ca and P, both linked to positive PC1. Moreover, red bricks were more correlated to raw elements (aluminosilicates and aluminosilicates characterised by high oxides content), while the yellow ones corresponded mostly to decaying elements (SOx impact). This evaluation is coherent with the results obtained in previous studies, which evidenced a smaller resistance of the yellow bricks to the salts attacks [26].

It was also possible to see some tendencies related to the room's belonging. Concretely, room C (**Fig. 7a**) seemed to fall in the centre of PCA (except for the CREI2). For such reason, the existence of another external factor that could affect the system is plausible. Considering the presence of different microclimates in this historical building, demonstrated in previous studies, and particularly for every single room [25], the logical step seemed to be the analysis of the data separately for the different rooms, taking into account the different micro-environments (Room A, B and C).

Taking into consideration that the *Mithraeum* (Room B) and the *Triclinium* (Room C) had a lower number of measured points, we have considered the room A, the *pre-Mithraeum*, as a representative example of the indoor behaviour. Thus, a second data matrix was studied. Specifically, a data set of 17 analyses in rows and of 16 elements in columns was carried out, obtaining a PCA model with three first PCs explaining the 85% (PC1: 58 %, PC2: 19 %, and PC3: 8 %) of the total variance (**Fig. 7c, d**). In this case, the separation of the colours was clearer (**Fig. 7c**).

Furthermore, another tendency correlated to the wall orientation seemed to appear. The scores representation showed a weak tendency for the east wall (**Fig. 7c**) characterised by a positive value of PC1 and in the red bricks of west wall orientation (except ARWS3) with positive value of PC2. Among the walls, the east side is linked to an important environmental issue. It is the only one wall where the outdoor exchanges are frequent due to the presence of the main entrance and a window of considerable dimension.

That is, not only the yellow bricks seemed to suffer from macroclimate conditions (environmental stressors). The feature of this specific wall affected also the red bricks (one part, relative to surface measurements), which were influenced by Ca, P and S (**Fig. 7d**). To sum up, such red bricks were visually more affected by salts than in the other walls.

In summary, clearer tendencies per colour, composition, decaying products and orientation were observed. Taking all of this into account, the hypothesis of the influence of the microclimate was supported. Another step was necessary, regarding the east wall and the 12 variables with major range (matrix with 14 x 12), three first PCs explained the 74% of the total variance (**Fig. 8**).

The scores representation pointed out a little separation based on the room of belonging. It is important to highlight that the east wall confines with the room C, a room without roof (unreal outdoor). It is evident that the measurements belonging to this room follow their own tendency, more closed (except for the CYEI2) without any differences according to the colour of the bricks.

The positive PC1 may be related to the indistinct attack by efflorescences and sub-efflorescences (the areas are measured on both inner and surface). The other two rooms seem to follow a unique tendency, underling an indoor environment.

Furthermore, the east wall which confines with the triclinium is a particular wall, where several openings are present in both rooms (even if the room A is more exposed to macroclimate). The bricks analysed on the surface presented positive PC2 values (except AYES1) and the inner present negative PC2 values (except CYEI2).

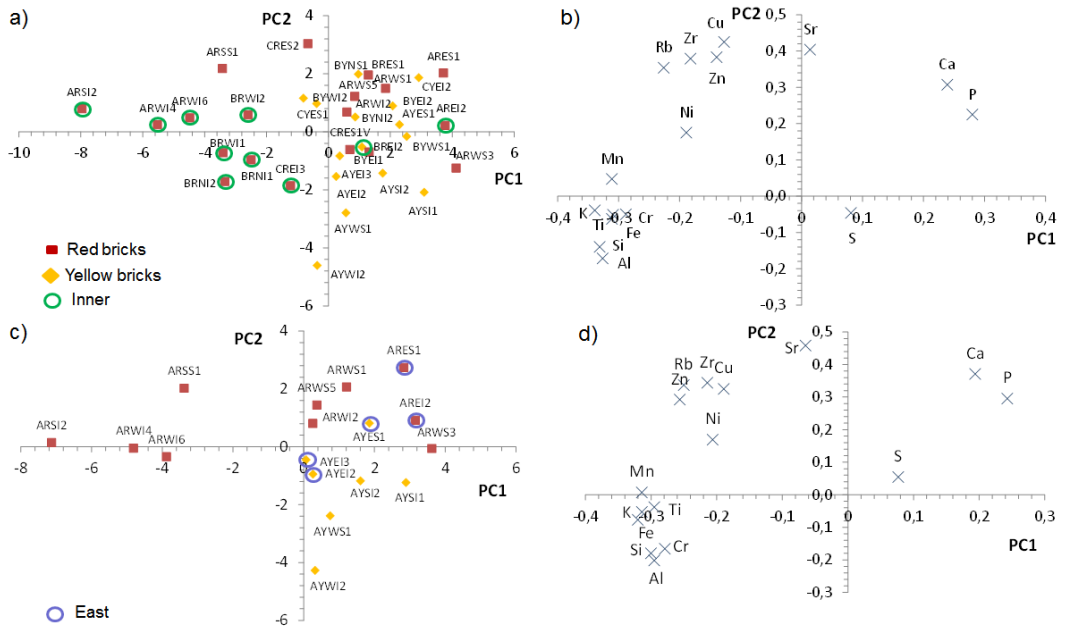

Figure 7. **a**) Scores (34 x 16 matrix), **b**) Loadings (34 x 16 matrix), **c**) Scores room "A" (34 x 16 matrix) and **d**) Loadings room "A" (34 x 16 matrix) in the bi-dimensional space defined by the two first principal components (PC1 and PC2). The blue circled measuring points belong to the east wall and the green the inner red bricks.

Taking all of these into account, the room and orientation of the walls seemed to be linked, as well as the environmental stressor (CO_2, SOx) that affected differently the two types of bricks.

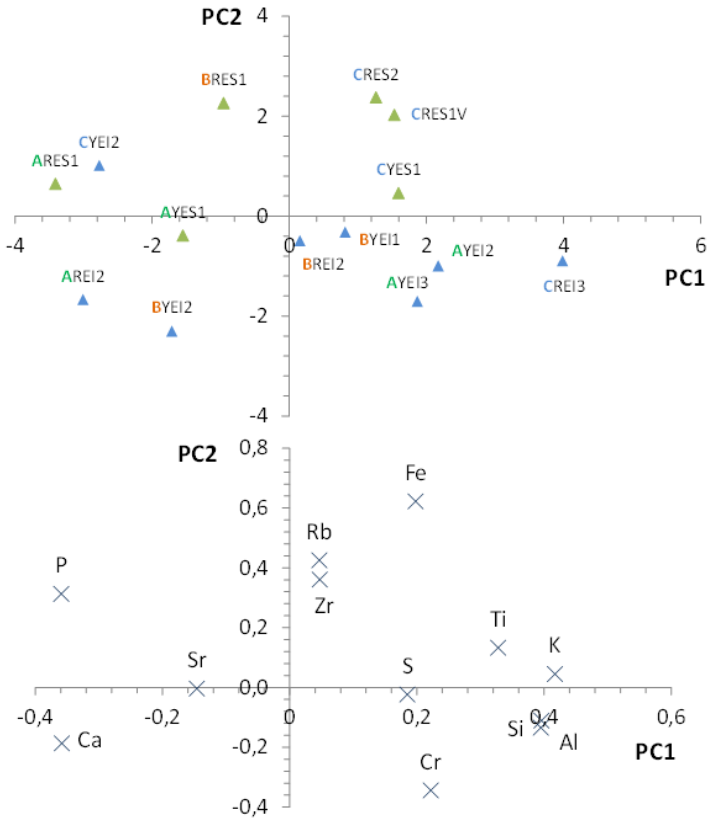

Figure 8. Scores and loading representation in the bi-dimensional space defined by the two first principal components (PC1 and PC2) using the dataset of the east walls.

4 CONCLUSIONS

HH-ED-XRF spectroscopy represents a powerful technique, particularly suitable for the study of coloured bricks. Indeed, the colour changes in materials are, in many cases, a consequence of small variations of elements concentration and, therefore, the molecular analysis could lead to less useful results in order to discriminate the bricks. However, the combination of two non-destructive spectroscopy techniques, has allowed the identification of behavioural differences between the two types of coloured bricks, defying some compounds (anatase, gypsum and silicates) and some elements (Ca, Fe) that discriminate and characterise the red and yellow bricks.

These analyses, with the combination of an appropriate PCA chemometric data treatment, pointed out that the yellow bricks were more damaged than the red bricks (affecting both the inner part and

surface). This fact could be related to the different raw material because it was observed that it was not the same in both case. In fact, also the different coloration seemed to be defined by different composition. Moreover, it is important to underline how the microclimate seemed to play an important role in the conservation state of materials, as well as the orientation and feature of walls. In fact, there is a close relationship between environmental stressors and particular areas or walls of building. The speed and the direction of the wind (airflow) play an important role in the transport of air pollutants, like sulphates or carbon dioxide. The *pre-Mithraeum* presents some openings, which represent the passage of long-range transports of pollutants too. Thus, the more affected wall is the one exposed to the east side, where also the more resistant red bricks are damaged.

Furthermore, the results obtained represent a helpful starting point for restoration actions. For example, knowing which kind of material, according its resistance (keeping in time) it is required for gaps. Therefore, although important issues have emerged, a deeper analysis for the study of the raw materials, manufacturing processes and decaying products that can affect the colour of bricks in different way is recommended. In this sense, this work highlights the need of preliminary *in-situ* analyses as a step sampling procedure, to justify the sampling and minimize it, something that is crucial in the field of cultural heritage.

ACKNOWLEDGEMENTS

The authors would like to thank the staff of the archaeological area of Ostia Antica, especially the director Dr. Cinzia Morelli, the security company, and the technical staff (Drs. Paola Germoni, Flora Panariti, Orietta Mantovani) for the permission to work in this house. The work was developed in the University of the Basque Country (UPV/EHU) and has been partially supported by the project DISILICA-1930 (ref. BIA2014-59124-P) funded by the Spanish Ministry of Economy and Competitiveness (MINECO) and the European Regional Development Fund (FEDER). Claudia Scatigno is grateful to University of the Basque Country (UPV/EHU) for her grant for study sojourns by trainee researchers from foreign universities engaged in a jointly supervision doctoral thesis.

REFERENCES

[1] Cardiano, P., Ioppolo, S., De Stefano, C., Pettignano, A., Sergi, S., & Piraino, P. (2004). Study and characterization of the ancient bricks of monastery of "San Filippo di Fragalà" in Frazzanò (Sicily). *Analytica Chimica Acta*, *519*(1), 103-111.

[2] Stefanidou, M., Papayianni, I., & Pachta, V. (2015). Analysis and characterization of Roman and Byzantine fired bricks from Greece. *Materials and Structures*, *48*(7), 2251-2260.

[3] Bloch, H. (1941). The Roman Brick Industry and Its Relationship to Roman Architecture. *Journal of the American Society of Architectural Historians*, *1*(1), 3-8.

[4] Özkaya, Ö. A., & Böke, H. (2009). Properties of Roman bricks and mortars used in Serapis temple in the city of Pergamon. *Materials characterization*, *60*(9), 995-1000.

[5] Miriello, D., Barca, D., Bloise, A., Ciarallo, A., Crisci, G. M., De Rose, T., ... & La Russa, M. F. (2010). Characterisation of archaeological mortars from Pompeii (Campania, Italy) and identification of

construction phases by compositional data analysis. *Journal of Archaeological Science*, *37*(9), 2207-2223.

[6] Calliari, I., Canal, E., Cavazzoni, S., & Lazzarini, L. (2001). Roman bricks from the Lagoon of Venice: a chemical characterization with methods of multivariate analysis. *Journal of Cultural Heritage*, *2*(1), 23-29.

[7] Bikiaris, D., Daniilia, S., Sotiropoulou, S., Katsimbiri, O., Pavlidou, E., Moutsatsou, A. P., & Chryssoulakis, Y. (2000). Ochre-differentiation through micro-Raman and micro-FTIR spectroscopies: application on wall paintings at Meteora and Mount Athos, Greece. *Spectrochimica Acta Part A: Molecular and Biomolecular Spectroscopy*, *56*(1), 3-18.

[8] Gallello, G., Ghorbani, S., Ghorbani, S., Pastor, A., & de la Guardia, M. (2016). Non-destructive analytical methods to study the conservation state of Apadana Hall of Persepolis. *Science of The Total Environment*, *544*, 291-298.

[9] Ismail, Y., Abdrabou, A., & Abdallah, M. (2016). A non-destructive analytical study and the conservation processes of Pharaoh Tutankhamun's painted boat model. *International Journal of Conservation Science*, *7*(1).

[10] Huntley, J., Westaway, K. E., Gore, D. B., Aubert, M., Ross, J., & Morwood, M. J. (2016). Non-Destructive or Noninvasive? The Potential Effect of X-Ray Fluorescence Spectrometers on Luminescence Age Estimates of Archaeological Samples. *Geoarchaeology*.

[11] Gómez-Laserna, O., Arrizabalaga, I., Prieto-Taboada, N., Olazabal, M. Á., Arana, G., & Madariaga, J. M. (2015). In situ DRIFT, Raman, and XRF implementation in a multianalytical methodology to diagnose the impact suffered by built heritage in urban atmospheres. *Analytical and bioanalytical chemistry*, *407*(19), 5635-5647.

[12] Arrizabalaga, I., Gómez-Laserna, O., Aramendia, J., Arana, G., & Madariaga, J. M. (2014). Applicability of a Diffuse Reflectance Infrared Fourier Transform handheld spectrometer to perform in situ analyses on Cultural Heritage materials. *Spectrochimica Acta Part A: Molecular and Biomolecular Spectroscopy*, *129*, 259-267.

[13] O Gómez-Laserna, O., Olazabal, M. Á., Morillas, H., Prieto-Taboada, N., Martinez-Arkarazo, I., Arana, G., & Madariaga, J. M. (2013). In-situ spectroscopic assessment of the conservation state of building materials from a Palace house affected by infiltration water. *Journal of Raman Spectroscopy*, *44*(9), 1277-1284.

[14] Prieto-Taboada, N., Ibarrondo, I., Gómez-Laserna, O., Martinez-Arkarazo, I., Olazabal, M. A., & Madariaga, J. M. (2013). Buildings as repositories of hazardous pollutants of anthropogenic origin. *Journal of hazardous materials*, *248*, 451-460.

[15] Čtvrtníčková, T., Cabalín, L. M., Laserna, J., & Kanický, V. (2008). Comparison of double-pulse and single-pulse laser-induced breakdown spectroscopy techniques in the analysis of powdered samples of silicate raw materials for the brick-and-tile industry. *Spectrochimica Acta Part B: Atomic Spectroscopy*, *63*(1), 42-50.

[16] Bitossi, G., Giorgi, R., Mauro, M., Salvadori, B., & Dei, L. (2005). Spectroscopic techniques in cultural heritage conservation: a survey. *Applied Spectroscopy Reviews*, *40*(3), 187-228.

[17] Morillas, H., Maguregui, M., Trebolazabala, J., & Madariaga, J. M. (2015). Nature and origin of white efflorescence on bricks, artificial stones, and joint mortars of modern houses evaluated by portable Raman spectroscopy and laboratory analyses. *Spectrochimica*

Acta Part A: Molecular and Biomolecular Spectroscopy, *136*, 1195-1203.

[18] Prieto-Taboada, N., Gómez-Laserna, O., Martínez-Arkarazo, I., Olazabal, M. Á., & Madariaga, J. M. (2014). Raman Spectra of the Different Phases in the CaSO4–H2O System. *Analytical chemistry*, *86*(20), 10131-10137.

[19] Prieto-Taboada, N., Maguregui, M., Martinez-Arkarazo, I., Olazabal, M. A., Arana, G., & Madariaga, J. M. (2011). Spectroscopic evaluation of the environmental impact on black crusted modern mortars in urban–industrial areas. *Analytical and bioanalytical chemistry*, *399*(9), 2949-2959.

[20] Maguregui, M., Knuutinen, U., Castro, K., & Madariaga, J. M. (2010). Raman spectroscopy as a tool to diagnose the impact and conservation state of Pompeian second and fourth style wall paintings exposed to diverse environments (House of Marcus Lucretius). *Journal of Raman Spectroscopy*, *41*(11), 1400-1409. [21] Maguregui, M., Sarmiento, A., Escribano, R., Martinez-Arkarazo, I., Castro, K., & Madariaga, J. M. (2009). Raman spectroscopy after accelerated ageing tests to assess the origin of some decayed products found in real historical bricks affected by urban polluted atmospheres. *Analytical and bioanalytical chemistry*, *395*(7), 2119-2129.

[22] Sarmiento, A., Maguregui, M., Martinez-Arkarazo, I., Angulo, M., Castro, K., Olazábal, M. A., ... & Madariaga, J. M. (2008). Raman spectroscopy as a tool to diagnose the impacts of combustion and greenhouse acid gases on properties of Built Heritage. *Journal of Raman Spectroscopy*, *39*(8), 1042-1049.

[23] Cultrone, G., Sebastián, E., Elert, K., De la Torre, M. J., Cazalla, O., & Rodriguez–Navarro, C. (2004). Influence of mineralogy and firing temperature on the porosity of bricks. *Journal of the European Ceramic Society*, *24*(3), 547-564.

[24] Cultrone, G., Sidraba, I., & Sebastián, E. (2005). Mineralogical and physical characterization of the bricks used in the construction of the "Triangul Bastion", Riga (Latvia). *Applied Clay Science*, *28*(1), 297-308.

[25] Scatigno, C., Gaudenzi, S., Sammartino, M. P., & Visco, G. (2016). A microclimate study on hypogea environments of ancient roman building. *Science of The Total Environment*, *566*, 298-305.

[26] Scatigno, C., Prieto-Taboada, N., Martinez, M. P., Conte, A. M., García-Diego, F. J., & Madariaga, J. M. (2016). Analytical techniques for the characterisation of historical building materials: case study "Casa di Diana" Mithraeum (Archeological site in Ostia Antica, Italy). *Advances in Materials Science Research*, 31

[27] Scatigno, C., Moricca, C., Tortolini, C., & Favero, G. (2016). The influence of environmental parameters in the biocolonization of the Mithraeum in the roman masonry of casa di Diana (Ostia Antica, Italy). *Environmental Science and Pollution Research*, 1-10.

[28] Cardarelli, E., De Donno, G., Scatigno, C., Oliveti, I., Martinez, M. P., & Prieto-Taboada, N. (2016). Geophysical and geochemical techniques to assess the origin of rising damp of a Roman building (Ostia Antica archaeological site). *Microchemical Journal*.

[29] Cardarelli, E., De Donno, G., Oliveti, I., & Scatigno, C. (2016, September). Assessing the State of Conservation of a Masonry Building through the Combined Use of Electrical and Seismic Tomography. In *Near Surface Geoscience 2016-22nd European Meeting of Environmental and Engineering Geophysics*.

[30] Castro, K., Pérez-Alonso, M., Rodriguez-Laso, M. D., Fernández, L. A., & Madariaga, J. M. (2005). On-line FT-Raman and dispersive Raman spectra database of artists' materials (e-VISART database). *Analytical and bioanalytical chemistry*, *382*(2), 248-258.

[31] Downs, R. T. (2006, July). The RRUFF Project: an integrated study of the chemistry, crystallography, Raman and infrared spectroscopy of minerals. In *Program and abstracts of the 19th general meeting of the international mineralogical association in Kobe, Japan* (Vol. 3).

[32] Daniel, F., Mounier, A., Pérez-Arantegui, J., Pardos, C., Prieto-Taboada, N., Fdez-Ortiz de Vallejuelo, S., & Castro, K. (2016). Hyperspectral imaging applied to the analysis of Goya paintings in the Museum of Zaragoza (Spain). *Microchemical Journal*, *126*, 113-120.

[33] García-Florentino, C., Maguregui, M., Morillas, H., Marcaida, I., Madariaga, J.M. (2016) Spectral data treatment methodology to avoid the use of hand-held Energy Dispersive X-ray fluorescence spectrometers as black boxes. *Spectrochimica Acta Part B (under review).*

[33] Maguregui, M., Prieto-Taboada, N., Trebolazabala, J., Goienaga, N., Arrieta, N., Aramendia, J., ... & Martinez-Arkarazo, I. (2010). CHEMCH 1st International congress chemistry for cultural heritage. *Ravenna, 30th June–3rd July.*

[34] Gómez-Nubla, L., Aramendia, J., Fdez-Ortiz de Vallejuelo, S., Castro, K., & Madariaga, J. M. (2011). Relations Between Leachated Compounds and Raman Spectrum of Black Slags from EAF in Order to Characterize Them. *LPI Contributions*, *1616*, 36.

[35] Hanaor, D. A., & Sorrell, C. C. (2011). Review of the anatase to rutile phase transformation. *Journal of Materials science*,*46*(4), 855-874. 74.

The *in-situ* measurements seemed to point out differences between the two types of bricks. Both bricks have different raw materials and decaying behaviour. Moreover, this last work represented the confirmation of the relationship between environment and materials. Actually, thanks to PCAs designed to steps, with the use of different data matrices it was possible to come to light that the bricks showed a particular tendency linked to the room belonged, as well as to the orientation.

However, although the above-mentioned important issues the results were not clear, being more tendencies than affirmations. For that reason, it would be recommended a deeper analysis for the study of the raw materials, manufacturing processes and decaying products that can affect the colour of bricks in different ways. In this sense, although in general, the sampling is avoided, thanks to this work a micro-sampling was justified to improve the *in-situ* results.

Article 8

A non-destructive spectroscopic study to evaluate the technological differences and conservation state of two types of Roman coloured bricks. Article submitted to MicroChemical Journal. Ms. Ref.MICROC_2016_321.

A NON-DESTRUCTIVE SPECTROSCOPIC STUDY TO EVALUATE THE TECNOLOGICAL DIFFERENCES AND CONSERVATION STATE OF TWO TYPES OF ROMAN COLOURED BRICKS

C. Scatigno[a,b]*, N. Prieto-Taboada[b], J.M. Madariaga[b], M. Preite Martinez[a], A. M. Conte[c]

[a,b*] University of Rome "Sapienza" - Department of Earth Science, Piazzale Aldo Moro 5, 00185 Rome, Italy. Phone: + 39 0649914156, Fax: +39 064454729

[b] University the Basque Country, (UPV/EHU), Department of Analytical Chemistry, Barrio Sarriena s/n, 48940, Leioa, Spain

[c] National Research Council (CNR) - Institute of Geosciences of Earth Resources (IGG), Piazzale Aldo Moro 5, 00185 Rome, Italy

*Corresponding author: claudia.scatigno@uniroma1.it

Abstract

The study of both original and decaying compounds is relevant in understanding the chemistry behind the deterioration processes, above all in open museum contexts, where artefacts are exposed to many environmental stressors. In this sense, a combination of non-destructive spectroscopy techniques (Raman spectroscopy, micro-X-ray fluorescence and X-ray diffraction) was applied on a Roman building (130 CE), the "Casa di Diana" *Mithraeum* (Ostia Antica archaeological site), in order to study the raw materials, manufacturing and decaying products of the two observed types of Roman fired bricks (red and yellow) that compose the building.

The joint use of non-destructive spectroscopy techniques allowed to identify differences in the raw materials, firing temperature (manufacturing processes), as well as in the conservation state, for each typology of bricks. In particular, one clay contains argillaceous minerals (illite clay), while another one is of carbonate rocks derivation (kaolinite clay), describing the red and yellow colours respectively. Furthermore, the compounds identified, which act as temperature markers (anatase and muscovite), indicate that the firing temperature of the red bricks was below 900°C. Contrarily, in the yellow bricks, albite and diopside were identified, indicating a firing temperature over 900°C. Moreover, it was possible to establish if the bricks were made in the same lot or in different processes. Regarding the decaying products, the gypsum covers most of the surface of most bricks, both of the red and the yellow ones, but these latter are more susceptible to environmental stressors. Therefore, this work points out for first time, that the difference in the colour of bricks could not only be derived from the use of different raw materials, but also from a different manufacturing process or, even, different historical periods.

Keywords red and yellow bricks; raw materials and decaying products characterisation; manufacturing processes; micro-X-ray fluorescence technique (μ-EDXRF); Raman spectroscopy; X-ray diffraction technique (XRD).

Highlights

- A joint non-destructive spectroscopy technique was performed on roman coloured bricks
- A study of both original and decaying compounds was carried out on Roman walls
- Temperature markers to trace back the temperature of the firing processes
- Different manufacturing process identified depending on colour

1 INTRODUCTION

Nowadays, a broad range of analytical techniques is available and applied in the preservation of Cultural Heritage [1-3]. In this context, destructive and/or invasive techniques should be avoided, whenever possible, to preserve the integrity of the studied artefacts [4, 5]. Therefore, the

development of non-destructive and *in-situ* analysis is extremely important [6-10] substituting invasive methods and minimizing the risk of damage. However, in some cases, the use of non-destructive techniques still requires micro-sampling, which could be crucial to achieve the objective of the research. In this sense, non-destructive techniques are the key to obtain the maximum information with the smallest amount of sample, which is available to be measured by many different techniques. This is one of the most important reasons for the huge development of these kinds of techniques in the last years. Amongst them, the spectroscopic instruments seem to be the most useful in the field of Cultural Heritage [11-21].

Nevertheless, not only the selection of the best complementary non-destructive techniques is important, but also the study of both original and decaying compounds to understand the chemical behaviour of the artefacts under study. In this sense, numerous studies can be found in the literature that span over a wide range of useful analytical techniques carried out to identify the decaying products [22-25] as well as to characterize the chemical and mineralogical changes in building materials [16-29]. However, the study of both original and decaying compounds seems to be more relevant to understand the chemistry behind the deterioration processes [14, 30-33]. Thus, in the case of Built Heritage, to evaluate its conservation state, the knowledge of the original compounds should be the first step to understand the decay processes, above all in the open museum contexts, where they are exposed to many environmental stressors. The recognition of the original compounds is fundamental for a future conservation plan, not only for filling of gaps (plasterwork) during the restoration processes, but also for the identification, where possible, of the originality of the building materials and their period of manufacture, giving important archaeological information regarding the cultural site. In this sense, in archaeological sites, where buildings are subjected to harsh climatic conditions, the relationship between the content and container, within the environment and the raw materials, is also fundamental.

In this regard, Ostia Antica, and in particular the "Casa di Diana" *Mithraeum* (130 CE), represents a particularly complicated scenario due to the numerous conservative problems that it is affected [25,30, 34-36]. Regarding construction materials, the masonry was build using two different coloured bricks, red and yellow. Bricks, which are ceramic materials widely used in the manmade building material history [37], are obtained by firing raw clay at temperatures ranging between 650 and 1100° C [38, 39], producing series of mineralogical, textural and physical changes [40] that depend on several factors [40]. Thus, the observed difference in colour could be related to many factors. In particular, colour, composition and mechanical properties are dependent on the nature of the clay (kaolinite, illite, and smectite), kiln environment (oxidative or reductive), kiln operator, temperature of the firing process, nature and amount of temper (quartz, carbonates, grounded fired clays) [41]. Although in proper conditions primary clay minerals may survive, calcite tempered clays are subjected to two main thermic processes: clay dehydroxylation (ca. 400–600° C) and decarbonation of the calcareous materials

(750–850° C). Higher firing temperatures lead the calcite decomposition products to react with fired clays to form new calcium silicate phases such as gehlenite, anorthite or diopside (wollastonite). In addition to possible mineral phases, formation and mineralogical changes during the firing and heating, respectively, and others changes related to environmental stressors might occur. In this sense, marine aerosol, air pollution and acid gases cause the formation of new compounds, i.e. the migration and crystallization of soluble salts. For these reasons, a deep study of the bricks is crucial to understand the factors resulting in colour differences.

On the other hand, this masonry has been subjected to several studies, based on electrical and seismic tomography investigations, as well as geochemical analyses [24,25] and environmental monitoring [34, 35], which have allowed to characterise the decay processes and their origin. One of these has been the determination and characterisation of salts weathering formation (CO_2, SO_2, NO_x), attacking through a dry deposition mechanism, as well as the determination of the fresh water aquifer as the most probable factor responsible for the rising damp (and of the high RH) and as the key step of the salt formation mechanism. However, both types of bricks present a different behaviour to the mentioned environmental stressors and thus, it is important to have a deep knowledge of the raw material, to understand whether this behavioural difference can be correlated to other factors, such as differences in the manufacturing process, firing temperature, or raw materials. In this sense, although in previous works it was possible to observe some differences in the composition of the bricks and their interaction with the environment, the *in-situ* analysis did not result in enough data to determine the reason for these differences. Thus, the reason of the different coloration is still unknown. With this premise, a micro-sampling can be justified, as it allows obtaining an improvement of the results thanks to laboratory analysis.

For all of these, in this work, two types of Roman bricks (red and yellow), which form the wall-building of "Casa di Diana" *Mithraeum*, were studied in order to understand the differences between them through the use of non-destructive techniques (μ-EDXRF, Raman spectroscopy and XRD), maximizing the information with a minimum amount of sample.

2 MATERIALS AND METHOLOGY

2.1 Site description and sampling design

The ancient city of Ostia, sited at the mouth of the Tiber River, 15 km downstream from Rome, is built mainly of brick-faced conglomeratic concrete structures that have remained largely intact for nearly 2000 years. The "Casa di Diana" *Mithraeum* is a *domus* that dates back to 130 CE, remaining partly in use until the early fourth century, while the whole archaeological site was inhabited until the 9th century CE [30, 42].

The entire house is mainly composed of bricks and pozzolanic mortar aligned with the "*opus caementicium*" technique. Focusing on bricks, as has been previously mentioned, it is possible to identify two main typologies: red and yellow, with a predominance of the first one. In both the red and yellow bricks, a wide range of tones is present, varying from dark red to

light yellow. The red bricks appear more compact and in a better state of conservation than the yellow bricks [30]. The building is completely affected by efflorescences, displayed throughout the entire year, both on internal and external walls, producing a mattifying veil on the bricks. A recent study has determined that acid gases, probably the main source of salt weathering, come from the nearby Leonardo da Vinci airport (also known as Fiumicino) and that the mechanism of the acid attack involves the dry deposition of the atmospheric acid gases.

In this sense, taking into consideration the results obtained by the previously conducted *in-situ* analysis [30], a total of 16 micro-samples (red and yellow bricks) were collected from the wall-building using a scalpel. First, 9 sampling points were defined, 5 in the *pre-Mithraeum*, 3 from the *Mithraeum* and one in the adjacent *Triclinium*, a room without roof (**Fig. 1**).

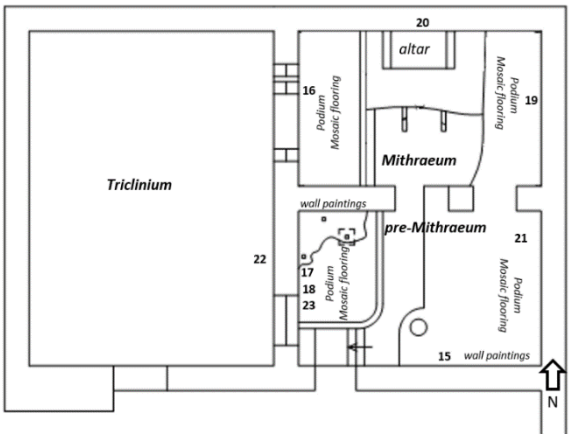

Figure 1. Sampling design of "Casa di Diana" building.

These sampling points correspond to the wall where the bricks were accessible. Moreover, when it was possible, one micro-sample for each colour was collected. That is, a micro-sampling based on colour, orientation and room was carried out. As can be observed in **Figure 1**, not all of the walls were possible to sample because they were inaccessible (southern wall and northern wall for the *pre-Mithraeum* and *Mithraeum*, respectively) due to the presence of wall paintings, mosaic flooring and/or artworks such as *podia*. It is necessary to mention that the collected samples, due to the size (micro-samples) and the level of decaying, were almost powdered, nevertheless, it was possible to measure the mattifying veil, and therefore, to differentiate between the supposed raw material and the formed salts.

2.2 Spectroscopic techniques

Firstly, all the micro-samples were investigated with non-destructive μ-EDXRF by a TORNADO M4 X-ray spectrometer (Bruker Nano, Berlin, Germany) in order to differentiate the elemental composition of the coloured bricks, as well as the mattifying veil (efflorescences) present in both types of bricks. The system was equipped with an X-ray tube working at a voltage of 50 kV and an anode current of 599 μA. Tungsten was used as the anode material. The emitted X-ray photons were detected with

a silicon drift detector (SDD). To increase the sensitivity for the Ag L-line, an Al filter (12.5 μm) was used. Additionally, the sample chamber was operated under vacuum conditions (20 mbar), in order to avoid signal overlap of the Ag line and argon from the surrounding air. The samples were mapped with a spot size of 15 μm and an acquisition time of 20 ms for each spot. The spectra were acquired and analysed using ESPRIT 1.9 software (Bruker Nano GmbH Corporation, Germany). For each samples, multipoint analyses were carried out.

The determination of the molecular composition of the samples was performed using two different spectrometers, with the purpose of analysing the original composition and the degradation products formed on Roman bricks. The first Raman spectrometer was a handheld InnoRaman-ultramobile spectrometer (B&WTEKINC, USA) provided with a 785 nm excitation laser with a nominal laser power of 225 mW and a CCD detector (Peltier cooled). All the spectra were obtained with a resolution of 3 cm^{-1} in a spectral range of 125–2500 cm^{-1}. The integration times and the spectra accumulations were set to obtain a better signal-to-noise ratio. The measurements were carried out in a continuous mode in order to scan the samples entirely. When an optimum response was obtained, the measurement point was fixed to improve and to collect the spectrum. Following this procedure, more than 100 spectra were saved. The acquisition of data was carried out with BWSpec software (B&WTEKINC, USA). For samples with several compounds, where the resolution was critical to obtain good Raman spectra, a second spectrometer, a RA100 Raman Spectrometer, coupled to a fibre optic microprobe with a diode laser of785 nm excitation wavelength and a Peltier cooled CCD detector, was used. The laser has a maximum output power of 500 mW at the source. The microprobe was equipped with a 20× objective, resulting in a laser spot size of 5 μm, allowing also other magnifications like 4× and 50×. The spectrometer was also equipped with a micro-TV camera, allowing the user to focus on the sample and to view it in magnification. The spectra were collected in the same range and resolution of the previous spectrometer. Data acquisition was carried out with the Wire Version 3.2 software package of Renishaw (Gloucestershire, UK). In both cases, a daily calibration was performed using the band at 520.5 cm^{-1} of a silicon chip and the excitation power was controlled to avoid thermal decomposition or mineral phase changes of the measured surfaces (less than 50mW). Moreover, the integration times and accumulations of the spectra were modified to improve the signal-to-noise ratio.

The Raman spectra were processed with the Omnic Version 7.2 software Thermo Nicolet (Madison, WI, USA), and their interpretation was done using the e-VISART [43] e-VISARCH [44, 45] dispersive Raman and FT-Raman spectra databases as well as the RRUFF online database [46].

Finally, in order to characterise (qualitatively) the bricks according to their colour, X-ray Diffraction (XRD) carried out a mineralogical analysis of three powdered bricks (in order to minimize the destructiveness of the method). These three samples were chosen on the base of their representative tone, the darker red, the lighter yellow and one belonging to a middle tone, orange (15R, 22Y and 18O, respectively). It is necessary to remark that XRD must be defined as a destructive

technique because it requires the powdering of the sample. However, it does not require a sampling consumption, allowing for the sample to be reused for successive analyses. Thus, taking into account the powdery nature of the sampled bricks, for simplification purposes, in this work XRD is considered a non-destructive technique, as it does not involve the destruction of the collected samples. XRD patterns were recorded using Cu*Kα* radiation (*n*=1.5418 Å) on a Philips PANalytical X'Pert PRO diffractometer operating at 40 kV and 40 mA at a step size of 0.0260°. The programme used for qualitative analyses was WinPLOTR Programme (CDIFX UMR6226 Rennes/ILL Grenoble).

All data obtained by the three analytical techniques was treated with OriginPro 8.5.1 software (descriptive statistical analysis).

3 RESULTS AND DISCUSSION

3.1 μ-EDXRF

In order to highlight the differences between red and yellow bricks (among raw materials and decaying products from each colour of bricks), a descriptive statistical analysis was performed. For each one colour of brick, the raw material and the efflorescences were analysed separately (**Figs. 2-3, Tab. 1**). In this sense, regarding the raw material analysis, the Box & Whisker representations (**Fig. 2**) showed how Ca and Fe are the major elements for both bricks **(Fig. 2, ab**), indicating, in particular for the Ca (**Fig. 2a**), the probable derivation from carbonate rocks or the calcareous nature. On the other hand, the Fe could be linked to the colour of the bricks, more in the red bricks. However, the homogenous distribution (symmetrical distribution) found in the red bricks (**Fig. 2b**), indicates a homogeneous concentration of Fe, thus, the range tone of the red bricks seems to be linked with other factors. The different behaviour of both elements (Ca and Fe) could also indicate that the raw material is not the same for both types of bricks. Therefore, manufacturing (temperature, firing process and kiln environment) could not be the only factor responsible of the differences between both types of bricks, but the composition of the raw material could also play a role, indicating the use of different clay for each type of brick.

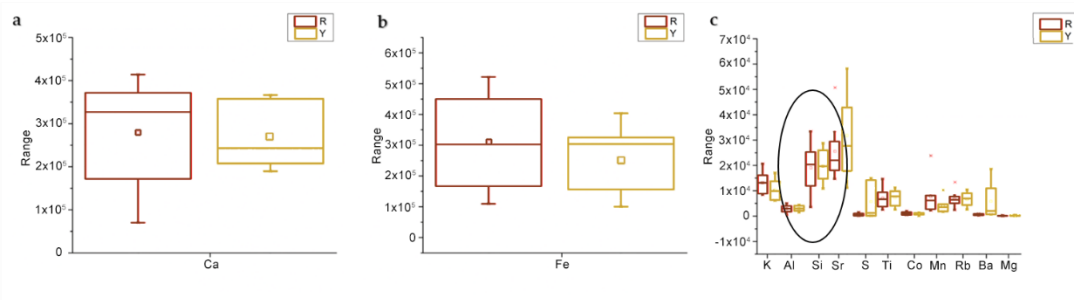

Figure 2. Box & Whisker of the results obtained from the raw material analysis for the red and yellow bricks. **a**) Calcium distribution; **b**) Iron distribution; **c**) all others elements.

The symmetrical distribution of other elements (**Fig. 2c**), in particular Al and Si, indicated, probably, the presence of aluminosilicates in both brick types. Moreover, it was possible to observe how the Si presents bigger amplitude for red bricks in comparison to the yellow ones and how, on the contrary, the Sr has a vaster distribution in the latter (**Fig. 2c**).

Performing a classical data correlation for each colour, the correlation between Al/Si was extremely high (r= 1, r= 98, for the red and yellow bricks, respectively). Thus, the presence of aluminosilicates in the bulk of both types of bricks was clear. In this sense, the ratio (Al/Si) was a little different for the red and yellow bricks, suggesting the use of different raw materials (**Fig. 2c – black circle**).

Other relevant observations were made in the correlation analysis. In particular, the negative correlation of Ca in the red bricks with the majority of others elements could indicate a production in which calcareous clays was not used [47], or a complete transformation into carbonate of the original calcium oxide, indicating calcite of secondary formation. The first hypothesis was the most probable, highlighting, in this sense, the possibility of the raw material not being the same for both bricks, because ongoing petrographic studies have remarked the presence of siliciclastic minerals (clastic, not carbonate, such as quartz and feldspar grains) as well as accessory minerals, such as pyroxene and hematite, in the matrix (dark brown colour). Thus, the red bricks were supposed to contain argillaceous mineral clays [47,48].

Moreover, the bricks based on such calcareous clay have a colour ranging from pink to light yellow that fits with the yellow bricks results [47]. In this sense, it is important to underline that Ca, Mg and Sr (which presents a major distribution in the yellow bricks – **Fig. 2c**), and specifically their oxides rate, generally describe calcareous clays [49]. Thus, the raw material of both types of bricks appears to be totally different.

Leaving these results aside, it is necessary to mention the decaying compounds may have affected the raw material analysis, making it difficult to guarantee the reliability of the analysis of the original bulk by this penetrating technique. In fact, the data for yellow bricks presented certain correlations, such as Ca/Cl and Ca/S, possibly indicating the formation of calcium chloride and calcium sulphate due to the known atmospheric attack. For that reason, these results must be confirmed with the results of the molecular analysis.
In order to survey more deeply the yellow bricks, a correlation according the samples was carried out (**Table 1**).

Table 1. Correlation analysis according the sample for yellow bricks (raw material)**.**

	15Y	***16Y***	*17Y*	*19Y*	*20Y*	*21Y*	*22Y*
15Y	1						
16Y	0.95	**1**					
17Y	0.88	**0.68**	1				
19Y	0.94	**0.79**	0.99	1			
20Y	0.98	**0.88**	0.93	0.98	1		
21Y	0.99	**0.90**	0.93	0.98	0.99	1	
22Y	0.85	**0.64**	1	0.98	0.91	0.91	1

It is possible to observe the high correlation between all of the yellow bricks, except for the 16Y sample. This high correlation could indicate that the same raw material was used and manufactured without many changes. Such phenomenon could be quite complicated in a manual manufacturing process. For this reason, it could be possible for this group of bricks to represent same production [48].

On the other hand, in the case of red bricks, it was possible to observe three different groups in the correlation analysis of the raw data. Thus, in the red bricks, other factors (different lots, raw materials, etc.) were involved (**Table 2**).

Leaving aside the raw material analysis, the results of the measured salts were also statistically evaluated (**Fig. 3**), allowing the observation of differences between red and yellow bricks.

Table 2. Correlation analysis according the sample for red bricks (raw material)

	15R	*16R*	*17R*	*18R*	*19R*	*20R*	*21R*	*22R*
15R	1							
16R	**1**	1						
17R	**1**	**0.99**	1					
18R	0.60	0.66	0.56	1				
19R	0.85	0.89	0.83	0.93	1			
20R	0.93	0.95	0.91	0.85	**0.98**	1		
21R	0.53	0.59	0.49	**1**	0.89	0.81	1	
22R	0.58	0.64	0.54	**1**	0.92	0.84	**1.00**	1

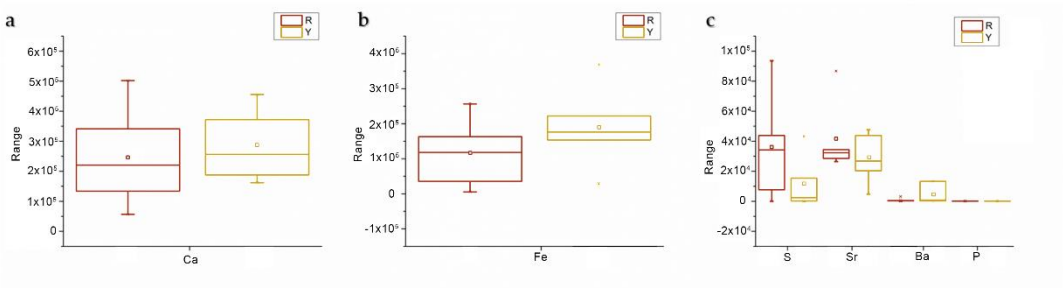

Figure 3. Box & Whisker of the results obtained from the decaying materials (salts) analysis for the red and yellow bricks for red and yellow bricks. **a**) Calcium distribution; **b**) Iron distribution; **c**) all others elements.

The most important results were correlated to the S identification, which was higher in the red bricks, along with calcium presence. This fact could indicate the formation of calcite and gypsum. It is surprising that these results were observed in the red bricks, which seem to be less degraded than the yellow ones. In any case, it was difficult to obtain significant conclusions about the decaying salts because of the thick layer of efflorescences, which also allowed the measurement of the raw material. In this sense, the Raman spectroscopy could be more useful.

Finally, the correlation analysis (on decaying products) was performed again. In this case, the yellow bricks presented the same groups as the raw material case, so the efflorescence affects all the yellow bricks. In the same way, in the case of the

red bricks the subgrouping observed in the raw material data was not repeated in this correlation analysis. This could indicate that the subgrouping observed in the raw material analysis was not correlated to the decaying processes (the raw material analysis was slightly affected by salts, as has been observed in the correlation analysis), leaving manufacturing as the most probably reason for the differences observed.

3.1 Raman spectroscopy

A distinction between the two colours of bricks was observed in terms of raw materials. In red bricks, in order of their relative presence (observed more times), anatase (TiO_2, identified by its Raman peaks at 145 cm^{-1}- **Fig. 4a**), hematite (Fe_2O_3, observed Raman bands at 227, 294 and 416 cm^{-1}), quartz (SiO_2, identified by its characteristic band at 466 cm^{-1}) and calcite ($CaCO_3$, characterized by a main band at 1088 cm^{-1}) were found as original compounds. The nature of calcite was difficult to assess, as it was difficult to assess, as it could be an original compound (indicating that the firing temperature was not high enough to allow its transformation into calcium oxide) or it could be a decaying compound of the carbonation of the mentioned oxide. Raman bands of typical silicates were also visible (main Raman bands observed at 1200-1900 cm^{-1}, **Fig. 5**) [20, 50].

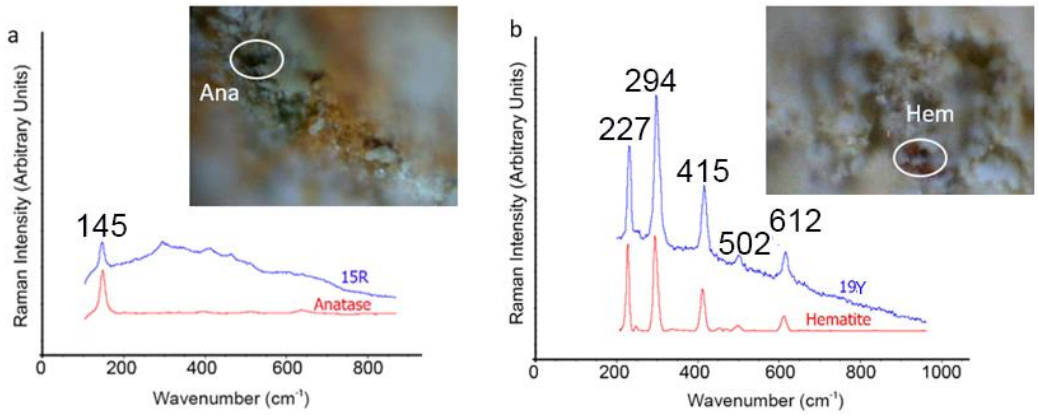

Figure 4. Raman spectra of raw materials. **a**) Spectra of anatase in a red brick (15R) mixed with hematite, image 20x magnifications (15R sample); **b**) Spectra of hematite in a yellow brick (19Y) spectra, image 20x magnifications (19Y sample).

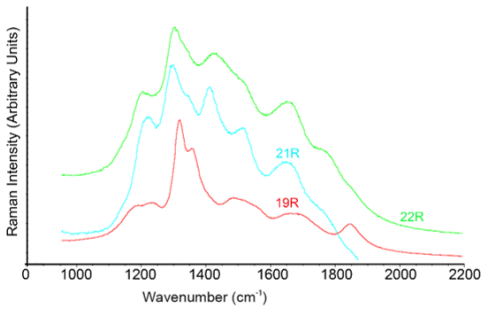

Figure 5. Raman spectra of some samples (typical silicates Raman bands).

Finally, it is necessary to remark that the presence of hematite, widely observed, which was probably linked to the colour of the bricks, as have been previously mentioned in terms of the identified iron in the μ-EDXRF analysis. Anatase also represents a colour marker (it was sometimes added to bricks as a colorant), as well as an indicator of the temperature reached in the firing process. The identification of anatase, instead of the other polymorphic forms (such as brookite and rutile), indicated that the heating temperature was below 900° [51]. This fact suggested that the calcite could be an original component of the clay in red bricks, not only a secondary compound, confirming what has been mentioned in the previous analysis, because it requires temperatures higher than 850-900° C for its transformation in calcium oxide [39, 48, 52].

Regarding the yellow bricks, calcite, quartz and hematite in correspondence of black or red points (observed Raman bands at 227, 294, 415, 502 and 612 cm^{-1} – **Fig. 4b**) were detected. Thus, the absence of titanium oxide it was remarkable, as well as the presence of hematite only as punctual grains, which pointed out again hematite as the factor responsible for the red colour of the bricks.

Concerning the degradation products, differences were not observed in terms of the identified compound, but in its relative presence. Calcite (1088 cm^{-1}) was present in form of efflorescence, indicating the carbonation of the calcium oxide. Such process was observed for all the yellow bricks, although some of the red ones were calcite-free (Fig. 6a). However, the major decaying compound observed was gypsum ($CaSO_4 \cdot 2H_2O$, detected Raman bands at 416, 449, 621, 672, 1010, 1137 cm^{-1}) [53], which covers most of the surface of most bricks, for both the red and yellow ones. Its presence was more evident in the yellow bricks (**Fig. 6b**). This corresponded to the results obtained in previous works, where gypsum was identified as the main salt that crystalizes in the bricks, especially in the yellow ones.

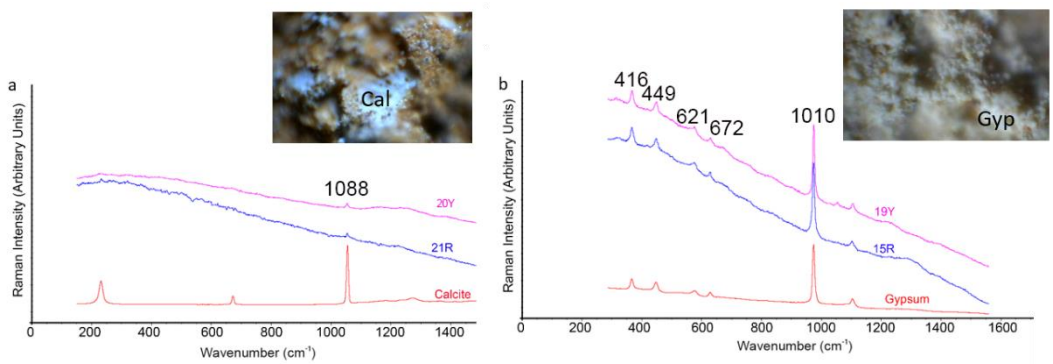

Figure 6. Calcite and gypsum Raman spectra. **a**) Image 20x magnifications (20R) and calcite spectra (20Y, 21R); **b**) Image 20x magnifications (19Y) and gypsum spectra (19Y, 15R).

3.2 X-Ray Diffraction

The results of the XRD analysis are reported in **Table 3**, while the patterns are showed in **Figure 7**. The mineralogical analysis revealed that the bricks were mainly composed of quartz, calcium carbonate, albite and analcite. The composition of red and orange bricks was

the same, except for the presence of wollastonite in the sample 18O. Diopside and gypsum were detected in yellow bricks. Focusing on **Figure 7**, significant peak intensity values of calcite are observed in the sample 18O. Moreover, the intensity of albite and analcite peaks increased for the yellow bricks (**Fig. 7**). Phyllosilicate (muscovite) was characteristic of the red and orange bricks.

Table 3. Identified phases list XRD.

Sample ID	Visible	Compound Name	Chemical Formula	Nature of the silicates	Max. Temperature	References
15R	*	Quartz	SiO_2	Tectosilicates	1050 °C	[178]
	*	Calcium carbonate	$Ca(CO_3)$	-	700-850 °C	[168, 177]
	*	Albite	$Na(Si_3Al)\ O_8$	Plagioclase/Feldspar	1050-1100 °C	[173, 178]
	*	Muscovite	$KAl_2(Si_3Al)O_{10}(OH)_2$	Phyllosilicate	800 – 900 °C	[130, 177]
	Minor	Analcite	$(Na_{0.92}Al_{0.84}\ Si_{2.16}\ O_6)(H_2O)$	Aluminosilicate/Zeolite	Crystallization secondary product (burial environment - weathering process	[179]
18O	*	Quartz	SiO_2	Tectosilicates	1050°	[178]
	*	Calcium carbonate	$Ca(CO_3)$	-	700-850 °C	[168, 177]
	*	Albite	$Na\ (AlSi_3O_8)$	Plagioclase/Feldspar	1050 -1100 °C	[173, 178]
	*	Muscovite	$KAl_2Si_3AlO_{10}\ (OH)_2$	Phyllosilicate	800– 900 °C	[130, 177]
	Minor	Analcite	$(Na_{0.92}Al_{0.84}\ Si_{2.16}\ O_6)(H_2O)$	Aluminosilicate/Zeolite	Crystallization secondary product (burial environment - weathering process	[179]
	Minor	Wollastonite	$CaSiO_3$	Inosilicates	900 – 1100 °C	[130, 177, 178]
22Y	*	Quartz	SiO_2	Tectosilicates	1050° C	[178]
	*	Calcium carbonate	$Ca(CO_3)_2$	-	700-850 ° C	[177]
	*	Albite	$Na(Si_3Al)\ O_8$	Plagioclase/Feldspar	1050° -1100	[178]
	*	Analcite	$(Na_{0.92}Al_{0.84}\ Si_{2.16}\ O_6)\cdot(H_2O)$	Aluminosilicate/Zeolite	Crystallization secondary product (burial environment - weathering process	[179]
	*	Diopside	$Ca(Mg,\ Al)\ (Si,\ Al\ )2O_6$	Inosilicates/Pyroxene	1000ºC	[177]
	Minor	Gypsum	$CaSO_4\cdot 2(H_2O)$	-	decaying product - weathering process	-

According to the absence or presence of a particular raw clay (new mineral phases or compositional variations), it was possible to make interesting considerations about the firing temperature of the examined samples (**Fig. 8, Table 2**). Even though, some reactions taking place when single phases form at high temperatures (T > 750° C) are well-known [40], the interactions between various phases that coexist, disappear, or form, are yet to be investigated [52]. Moreover, there were some compounds that could represent both original and decaying compounds, such as calcite. For such reason, these compounds could not be used as temperature markers because they could lead to incorrect conclusions. In any case, some of the identified compounds allowed to make interesting observations.

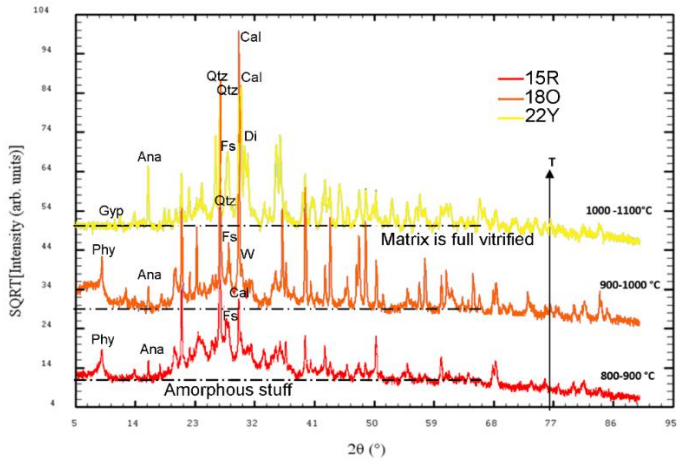

Figure 7. X-ray diffraction patterns.Symbols after Kretz [180]: Qtz=quartz; Phy=phyllosilicates; Fs=feldspar; Cal=calcite; Di= diopside. The dotted coloured lines indicate the amorphous stuff level.

Quartz grains do not undergo any appreciable morphological and chemical transformation until the temperature of 1050° C, similarly to the albite that retains its original morphology and optical characteristics [48, 54]. This indicated that the firing temperature of all bricks has not exceeded this value. In terms of the analcite mineral, some studies conducted on ceramic products revealed that its concentration increases proportionally to the firing temperatures, where the highest intensities can be found in the overfired samples (>1050° C) [55]. As can be seen in **Figure 7**, the higher intensity of analcite peak corresponded to the yellow bricks, suggesting higher temperatures. Similarly, phyllosilicates undergo significant changes based on the firing temperatures, disappearing around 800-900° C [39, 42]. The corresponding peak was reduced until it disappears in the yellow bricks, clearly indicating higher temperatures than the reddish bricks. Moreover, yellow bricks revealed a higher degree of vitrification than the red ones (**Fig. 7**), supporting the temperature observation.

Taking all of this into account, the red colour bricks presented compounds that indicated a firing temperature lower than 900° C. Similarly, the orange bricks (considered red in the μ-EDXRF correlation analysis) had the same composition of red bricks, with the exception of wollastonite. This compound indicated a slightly higher temperature than the one of the red bricks. Thus, these results confirmed that the red bricks were made of the same raw material, but with differences in the manufacturing, as can be observed in the wide tone variation. Finally, the yellow bricks presented a different composition, related to higher temperatures, around 1000° C. The quartz was also present in these bricks, but its amount decreases with increasing temperature, resulting in the formation of Ca-rich silicates, such as diopside, as a principal compound [40]. Moreover, the presence of gypsum indicated the subsequent attack of $CaCO_3$ by the atmospheric SO_2 [56] thus, the yellow bricks seemed to present behaviour more susceptible to acid gases attack. This implied that the yellow bricks seemed to be manufactured in a different way than the red bricks, using different raw materials, which has implications on the

conservation state. This was quite uncommon because, in literature, the use of temperatures above 900° C generally indicates a higher resistance to environmental stressors, as well as a lower number of open pores, etc. [57]. In this sense, although the yellow bricks have been probably fired at high temperature or with the use of binders (such a straw), during the manufacturing processes (mudbricks, unfired bricks), that reduce the plasticity [58] thanks to the increment of the amount of non-argillaceous minerals. These points appeared to be understandable in the context of the Roman imperia, where the manufacture of bricks was well developed [59, 61].

4 CONCLUSIONS

This work demonstrates that both types of studied bricks present completely different raw materials (nature of the clay) and manufacturing processes. Specifically, the use of argillaceous minerals (illite clay) in red bricks and of clay of carbonate rock derivation (kaolinite clay) for the yellow ones has also been confirmed.

Although the colour of red bricks is clearly linked to the presence of hematite and anatase, the range of tones is wider due to the range of temperatures used in the manufacture. This indicates that this type of bricks could be fired only in one lot, but, for example arranged on different levels (closer or further to the fire), or in more than one lot. In any case, it was evident that the temperature reached in the manufacture of yellow bricks (>900° C) was higher than that of the red bricks (<900° C).

On the other hand, the yellow bricks seem to be made in the same lot because of the stable firing temperature (>900° C) and colour. Moreover, the temperature was high enough to cause the decarbonation of calcite (presence of the secondary calcite) in all of the yellow samples, showing a noticeable decaying level of these bricks, distinguishable by the high presence of calcium sulphate.

Thus, taking into account the different raw materials used, the different manufacture and the scarce presence of the yellow bricks (which could be caused by the use of these bricks to fill the gaps, probably in a lead to the hypothesis that the yellow bricks could correspond to another historic period, for instance byzantine, rehabilitation procedure) which corresponds to the last period of utilization, of this house. This hypothesis must be studied deeply in future works.

ACKNOWLEDGEMENTS

The authors would like to thank the staff of the archaeological area of Ostia Antica, especially the director Dr. Cinzia Morelli, the security company, and the technical staff (Drs. Paola Germoni, Flora Panariti, Orietta Mantovani) for the permission to work in this house.

The work was developed in the University of the Basque Country (UPV/EHU) and has been partially supported by the project DISILICA-1930 (ref. BIA2014-59124-P) funded by the Spanish Ministry of Economy and Competitiveness (MINECO) and the European Regional Development Fund (FEDER). Claudia Scatigno is grateful to University of the Basque Country (UPV/EHU) for the grant for study sojourns by trainee researchers from foreign universities engaged in a jointly supervised doctoral thesis. Finally, the authors are grateful to SGIker service and the personal support of Aitor Larrañaga, from the University of the Basque Country and to Claudia Moricca for her English revision.

REFERENCES

[1] Janssens K, & Van Grieken R. Non-destructive micro analysis of Cultural Heritage materials. Elsevier, 2004.

[2] Pires J, Cruz A. J. Therm. Anal. Calorim. 2007;87:411.

[3] Madariaga JM. Anal. Methods 2015;7:4848.

[4] Moropoulou A, Labropoulos KC, Delegou ET, Karoglou M, Bakolas A. Constr.Build.Mater. 2013;48:1222.

[5] Binda L, Saisi A. Historical constructions. University of Minho, Guimarães, 2001.

[6] Adriaens A. Spectrochim. Acta, Part B. 2005;60:1503.

[7] Kandemir-Yucel A, Tavukcuoglu A, Caner-Saltik E. Infrared Phys.Technol. 2007;49:243.

[8] Papadopoulou D, Zachariadis G, Anthemidis A, Tsirliganis N, Stratis J. Talanta 2006;68:1692.

[9] Forster N, Grave P, Vickery N, Kealhofer L. X-Ray Spectrometry 2011;40:389.

[10] Gallello G, Ghorbani S, Ghorbani S, Pastor A, de la Guardia M. Sci.Total Environ.2016;544:291.

[11] Bitossi G, Giorgi R, Mauro M, Salvadori B, Dei L. Appl. Spectrosc. Reviews 2005;40:187.

[12] Laserna, OG, Taboada, NP, Ibarrondo, I, Arkarazo, IM, Dueñas, MÁO, Mota, JMM. 2011:195.

[13] Prieto-Taboada N, Maguregui M, Martinez-Arkarazo I, Olazabal M, Arana G, Madariaga J. Anal. Bioanal. Chem. 2011; 399:2949.

[14] Prieto-Taboada N, Ibarrondo I, Gómez-Laserna O, Martinez-Arkarazo I, Olazabal M, Madariaga J. J.Hazard.Mater. 2013; 248:451.

[15] Prieto-Taboada N, Gómez-Laserna O, Martinez-Arkarazo I, Olazabal MÁ, Madariaga JM. Anal.Chem. 2013;85:9501.

[16] Morillas H, Maguregui M, Trebolazabala J, Madariaga JM. Spectrochim. Acta, Part A 2015;136:1195.

[17] Sarmiento A, Maguregui M, Martinez-Arkarazo I, Angulo M, Castro K, Olazábal M et al. J.Raman Spectrosc. 2008;39:1042.

[18] Maguregui M, Sarmiento A, Martínez-Arkarazo I, Angulo M, Castro K, Arana G et al. Anal. Bioanal. Chem. 2008;391:1361.

[19] Čtvrtníčková T, Cabalín LM, Laserna J, Kanický V. Spectrochim. Acta, Part B 2008;63:42.

[20] Maguregui M, Sarmiento A, Escribano R, Martinez-Arkarazo I, Castro K, Madariaga J. Anal. Bioanal. Chem. 2009;395:2119.

[21] Maguregui M, Knuutinen U, Castro K, Madariaga JM. J.Raman Spectrosc. 2010;41:1400.

[22] Cardell C, Benavente D, Rodríguez-Gordillo J.Mater.Charact. 2008;59:1371.

[23] Akram K, Ahn J, Kwon J. Ionizing radiation: Applications, sources and biological effects 2012:1.

[24] Cardarelli E, De Donno G, Scatigno C, Oliveti I, Martinez MP, Prieto-Taboada N. Microchem. J. 2016

[25] Cardarelli, E, De Donno, G, Oliveti, I, Scatigno, C. 2016

[26] Vassilev SV, Tascón JM. Energy Fuels 2003;17:271.

[27] Iordanidis A, Garcia-Guinea J, Karamitrou-Mentessidi G. Mater. Charact. 2009;60:292.

[28] Serrano-Arnáez B, Compana J, Fernández-García M. J. Archaeol. Sci.: Reports 2016;7:60.

[29] Ferreira LV, Gomes MV, Pereira M, Santos L, Machado IF. J. Archaeol. Sci.: Reports 2016;6:182.

[30] Scatigno C, Prieto-Taboada N, Martinez MP, Conte A, García-Diego F, Madariaga J. Adv. in Materials Science Research 2016:31.

[31] Prati S, Bonacini I, Sciutto G, Genty-Vincent A, Cotte M, Eveno M et al. Appl. Phys. A 2016;122:1.
[32] La Nasa J, Orsini S, Degano I, Rava A, Modugno F, Colombini MP. Microchem. J. 2016;124:940.
[33] Gómez-Laserna O, Olazabal MÁ, Morillas H, Prieto-Taboada N, Martinez-Arkarazo I, Arana G et al. J.Raman Spectrosc. 2013; 44:1277.
[34] Scatigno C, Gaudenzi S, Sammartino M, Visco G. Sci.Total Environ. 2016; 566:298.
[35] Scatigno C, Moricca C, Tortolini C, Favero G. Environ Sci.Poll.Res. 2016:1.
[36] Scatigno, C, Cardarelli, E, De Donno, G, Oliveti, I, Preite Martinez, M. 2015.
[37] Özkaya ÖA, Böke H. Mater.Charact. 2009;60:995.
[38] Warren J. Conservation of brick. Butterworth Heinemann, 1999.
[39] Cultrone G, Sebastián E, Elert K, De la Torre, María José, Cazalla O, Rodriguez–Navarro C. J.Eur. Ceram.Soc. 2004;24:547.
[40] Peters T, Iberg R. Ceramic Bulletin 1978;57:503.
[41] Cardiano P, Ioppolo S, De Stefano C, Pettignano A, Sergi S, Piraino P. Anal.Chim.Acta 2004;519:103.
[42] Gaudenzi, S, Preite Martinez, M, Bernardini, ML, Imperi, F, De Bianchi, S, Guiso, M et al. 2012
[43] Castro K, Pérez-Alonso M, Rodriguez-Laso M, Fernández LA, Madariaga J.Anal.Bioanal.Chem. 2005;382:248.
[44] Pérez-Alonso M, Castro K, Madariaga JM. Anal.Chim.Acta 2006;571:121.
[45] Perez-Alonso M, Castro K, Madariaga JM. Curr. Anal. Chem. 2006;2:89.
[46] Downs, R.T. The RRUFF Project: an integrated study of the chemistry, crystallography, Raman and infrared spectroscopy of minerals. 2006;3
[47] Kornilov A. Glass and Ceramics 2005; 62:391.
[48] Fiori C, Vitali D, Camurri E, Fabbri B, Gualtieri S. Appl.Clay.Sci. 2011; 53:454.
[49] Negro Ponzi M. Edilizia residenziale tra V e VIII secolo".4 Seminario sul Tardoantico e l'Alto medioevo in Italia centrosettentrionale (Monte Barro-Galbiate, 2-4 settembre 1993) 1994:53.
[50] Gómez-Nubla L, Aramendia J, Fdez-Ortiz de Vallejuelo S, Castro K, Madariaga J. LPI Contributions 2011;1616:36.
[51] Hanaor DA, Sorrell CC. J.Mater.Sci. 2011; 46:855.
[52] Cultrone G, Rodriguez-Navarro C, Sebastian E, Cazalla O, De La Torre, Maria Jose. Eur. J. Mineral. 2001;13:621.
[53] Prieto-Taboada N, Gómez-Laserna O, Martínez-Arkarazo I, Olazabal MÁ, Madariaga JM. Anal.Chem. 2014;86:10131.
[54] Riccardi MP, Messiga B, Duminuco P. Appl.Clay.Sci. 1999;15:393.
[55] Schwedt A, Mommsen H, Zacharias N, Garrigós JBI. Archaeometry 2006;48:237.
[56] Lubelli B, van Hees RP, Groot CJ. Constr.Build.Mater. 2004;18:119.
[57] Karagiannis N, Karoglou M, Bakolas A, & Moropoulou A. Building Materials Capillary Rise Coefficient: Concepts, Determination and Parameters Involved. In: New Approaches to Building Pathology and Durability, Springer, 2016. p. 27.
[58] Quagliarini E, Lenci S. J.Cult.Herit. 2010; 11:309.
[59] DeLaine J. Exploring the economics of building techniques at Rome and Ostia. In: Economies Beyond Agriculture in the Classical World, Routledge Abingdon, 2001. p. 230.
[60] Fernandes FM, Lourenço PB, & Castro F. Ancient clay bricks: manufacture and properties. In: Materials, Technologies and Practice in Historic Heritage Structures, Springer, 2010. p. 29.
[61] KRBrz R. Symbols for rock-forming minerals. Am.Mineral. 1983;68:277.

The joint use of non-destructive spectroscopy techniques allowed to identify differences for each typology of bricks (raw materials, manufacturing process, behaviour and even, period of time), closing an important issue, even for the historical-artistic knowledge of the archaeological site under study (the probably different of two historical periods). Moreover, the last work allowed also diagnosing the gypsum as the principal compound that affect the wall-materials. Actually, gypsum covers most of the surface of the both type of bricks, although yellow bricks seemed to be the most affected.

On the other hand, taking into account the doubts leaved by hydro-geological setting and geochemical analysis about the rising damp original and, in particular, the possible aggressiveness of them on materials, it was important to establish its role in the building materials damage.

7.2 Quantitative soluble salts analysis[34]

Soluble salts represent one of the main conservation problems for building materials, because their presence within the capillary network causes the dissolution of building materials, material loss and cracks [9]. The water, carrying dissolved ions or promoting its, is a key step of the crystallisation of salts [1, 63, 81, 98, 105, 116, 169-170].

However, this phenomena is caused as a results of many factors such as thermo-hygrometric conditions (mainly their variation frequency), characteristics of the materials (mainly its porosity) and of the salts (mainly solubility, hygroscopy or hydration level in the crystalline structure) [9]. Moreover, not all salts are equally harmful and for this reason, the identification of their nature is crucial [171]. In fact, the possibility of dehydration–hydration processes plays a critical role in the deterioration mechanisms, as in the case of sodium sulphates, which are thoroughly studied [82]. Moreover, the nature of the salts is not the only important aspect, their concentration is also a crucial factor to evaluate the conservation state of a building [172]. Some studies analyse the action of marine aerosol on construction materials or historical monuments [173]. In coastal regions, as in the present case, the atmosphere could be enriched with particles that are naturally generated by the action of wind on the water surface [174, 175]. These particles compose the sea spray, which introduces ionic species into the atmosphere, principally chlorides and sulphates [82].

[34] An adapted version was published in:
Scatigno, C., N. Prieto-Taboada, M. Preite Martinez, A. M. Conte, F. J. García-Diego, and J. M. Madariaga. "Analitycal techniques for the characterisation of historical building materials: case study "Casa di Diana" Mithraeum (Archaeological site in Ostia Antica, Italy)". Advances in Materials Science Research (2016): 31.

In order to identify the nature of the salts and to quantify them, the most useful technique is ionic chromatography (IC) after the extraction of soluble salts. In this sense, this technique is widely used, even being regulated by a standardized protocol [176]. Moreover, this procedure is not only reliable for determining the damage of the soluble salts, but also to assess the effectiveness of salt removal methods in Cultural Heritage [4, 9, 117, 118, 127, 139, 171, 177-181].

In this sense, a quantitative characterisation (IC) and thermodynamic modelling (ECOS-RUNSALTS and Hydra-Medusa) of soluble salts were applied (taking advantage of the previous micro-sampling and the non-consumption of sample), to establish the mechanism and the origin of soluble salts' formation.

Article 9

Quantitative characterisation and thermodynamic modelling of soluble salts on Roman bricks as a tool to discriminate the origin of their formation. Article under review in Environmental Science and Pollution Research. Ms. Ref. No.: ESPR-D-16-04938.

QUANTITATIVE CHARACTERISATION AND THERMODYNAMIC MODELLING OF SOLUBLE SALTS ON ROMAN BRICKS AS A TOOL TO DISCRIMINATE THE ORIGIN OF THEIR FORMATION

C. Scatigno[a,b]*, N. Prieto-Taboada[b], J.M. Madariaga[b]

[a,b*] Department of Earth Science, University of Rome "La Sapienza", Piazzale Aldo Moro 5, 00185, Rome, Italy. Phone: (+ 39) 0649914156, Fax: (+39) 064454729
[b] Department of Analytical Chemistry, University the Basque Country, (UPV/EHU), Barrio Sarriena s/n, 48940, Leioa, Spain.
*Corresponding author: Email: claudia.scatigno@uniroma1.it

Abstract
This work aims to evaluate the processes driving to the formation of soluble salts on the surface of walls of the *Mithraeum* (a downstairs room with RH values are close to 96-99%) of "Casa di Diana", a brick made Roman building located in the famous archaeological site of Ostia Antica (Italy), the port of the old Rome town. To perform such evaluation, we suggest to combine ion chromatography analysis of the water extracts from brick and efflorescences to use such quantitative information (low chloride concentrations and medium to high dissolved sulphate and nitrates) to conduct thermodynamic modelling, using adequate software (ECOS-RUNSALT and Medusa-Hydra) to predict the formation of salts. The results give us the possibility to understand the formation mechanisms, allowing the identification of the source and the types of salts that can occur. Despite the proximity to the Tyrrhenian Sea, the contribution of the marine aerosol was discarded as well as the influence of the subterranean aquifers or the direct rainfall influence on the formations of the efflorescence salts. In contrast, it was possible to determine the atmospheric acidic gases (CO_2, SO_2, NO_x) as the most probable source of the weathering, attacking chemically to the bricks through a dry deposition mechanism (Fiumicino airport is quite close to the archaeological site). Finally, regarding the risk level of contamination, according to the total concentration of soluble salts, the surfaces of the materials should be considered mildly/very polluted with a medium/high risk of hygroscopic moisture, due to the high concentration of sulphates.

Highlights

- Not only a quantitative analysis of salt crystallization-dissolution processes gives a response
- Thermodynamics modelling software as essential tools to evaluate soluble salts
- The freshwater aquifer as the key step in the salt formation mechanism
- Atmospheric acid gases as the most probable source of salt weathering attack

Keywords soluble salts; ion chromatography; thermodynamic modelling and chemometric data treatment; atmospheric acid gases; building safeguard.

1 INTRODUCTION

Infiltration water is one of the main problems affecting historical masonry structures and it is surely the most widespread phenomenon leading to moisture presence in building structures (Franzoni 2014). Moisture plays a key role in the degradation of porous materials, being directly or indirectly responsible for several decay processes such as freeze-thaw cycles, soluble salts crystallisation cycles, biological growth, chemical attack by acid rain and wind erosion (Gentilini et al. 2012, Korkanç 2013). This phenomenon increases in coastal environments, which due to high levels of moisture and marine

aerosol, represents the principal source of deterioration of buildings located close to the sea (Morillas et al. 2013). Moreover, building are also affected by other types of external stressors such as acid atmospheric gases (especially CO_2, SO_2 and NO_x) which can impact on materials following either wet or dry processes (Morillas et al. 2015, Morillas et al. 2013). Considering these sources of deterioration, several types of degradation can be commonly observed, such as detachment of materials, biological proliferations or formation of soluble salts (Morillas et al. 2015). In fact, the latter is one of the most harmful problems in the conservation of built heritage, promoting cracks and loss of materials (Hossain et al. 2009). For such reason, the crystallization of soluble salts is not only an aesthetical problem in the form of efflorescence, but produces also a considerable decay when salts precipitate beneath the material as sub-efflorescence. Thus, the growth of salt crystals within the pores of a stone could generate stress (internal tensions), either by its crystallization or by changes in volume (expansion of crystals) according to the number of hydration waters due to relative humidity (RH) and temperature (T) (environmental parameters), among others (Brai et al. 2010, Gómez-Laserna et al. 2013). Solubility of the crystalline phases and the evaporation rate of water facilitate the mobility into the pores, representing factors to be taken into account. Therefore, the assessment of the critical environmental conditions of salt laden porous material and hence, potential risks of salt damage, requires the knowledge of the thermodynamics of the relevant chemical equilibria (Steiger 2005). Moreover, the processes of the salts formation are linked to the micro-environmental conditions. For this reason, quantitative analyses of salt crystallization–dissolution processes are not the only source of information regarding their formation, taking into account the knowledge about the salt behaviour, and if possible, the changes in T and humidity conditions, is crucial (Heinrichs and Azzam 2015). In this sense, the thermodynamic modelling represents an important tool to understand the salts' formation and, subsequently, the ways to avoid it, safeguarding historical buildings. For this reason, in literature the simulation of salt damage on porous materials is well disseminated (Espinosa et al. 2008, Espinosa-Marzal and Scherer 2010, Heinrichs and Azzam 2015, Nicolai 2008), as well as the use of particular thermodynamic software (Aramendia et al. 2014, Godts et al. 2012). In this sense, there are two interesting thermodynamics modelling software, the ECOS-RUNSALT (Heinrichs and Azzam 2015, Maguregui et al. 2008, Price 2007) and Medusa-Hydra (Kubiak et al. 2012, Stelzner and Eggert 2008), whose usefulness in cultural heritage is widely demonstrated. The first program utilises a thermodynamic model to predict which solid minerals (salts) exist in equilibrium taking into account the T and RH interval (Bala'awi and Prokos 2011, Godts et al. 2012, Larsen 2007). However, this software has problems when gypsum is involved in the process, as well as in the situation of the RH values exceeding 98%. On the other hand, the second program allows predicting the chemical equilibria in dissolution with less limitations than ECOS-RUNSALT, but considers a fixed T value of 25° C. Despite these tools, the processes and pathways of salt damage are still incompletely understood (Godts et al. 2012, Heinrichs and Azzam 2015).

Taking all this information into account, the present work introduces a quantitative analytical technique (IC) combined with thermodynamic data analyses (ECOS-RUNSALT, Medusa-Hydra) and chemometric (PCA) as a tool to understand the behaviour of the soluble salts that affect the "Casa di Diana" *Mithraeum*, an important house located in a famous archaeological area of Rome (Ostia Antica, Italy). Thus, the aim of this work was to determine and characterise the soluble salts, evaluating their impact on Roman bricks, identifying the origin and the mechanism for their formation, in order to improve the conservation plan of this cultural site.

2 MATERIALS AND METHODS

2.1 The building under study

The "Casa di Diana" *Mithraeum* (130 CE) is a Roman masonry located in a famous archaeological site (Ostia Antica), near to the Tyrrhenian sea (at least around 5 km south) also in the proximity of Ciampino (around 30 km east) and Leonardo da Vinci airports, commonly known as Fiumicino airport (around 7 km northwest) (**Fig. 1**). The *Mithraeum,* a place dedicated to the cult of the Persian god Mithra during the Roman times, consists of two intercommunicating rooms, the "*Mithraeum*" and "*pre-Mithraeum*", each of which measures approximately 27 m^2 (**Fig. 2a**) and has several openings (windows and main door) exposing small areas to sunlight and outer air. A roofless room named *Triclinium* (Fig. 2b), neighbouring with the *pre-Mithraeum* and *Mithraeum,* is also present. Regarding the building materials, the structure of the house (wall thickness of 0.6 m) was constructed using bricks and pozzolanic mortar aligned with the "*opus caementicium*" technique. Focusing on bricks, it is possible to identify two typologies, distinguished by their colour: red and yellow (Scatigno et al. 2016c). The masonry has also its own well of a depth of 4.20 m, located between the *latrina* and the courtyard, from which it was possible to draw water, as well as an external tank, adjacent to the house.

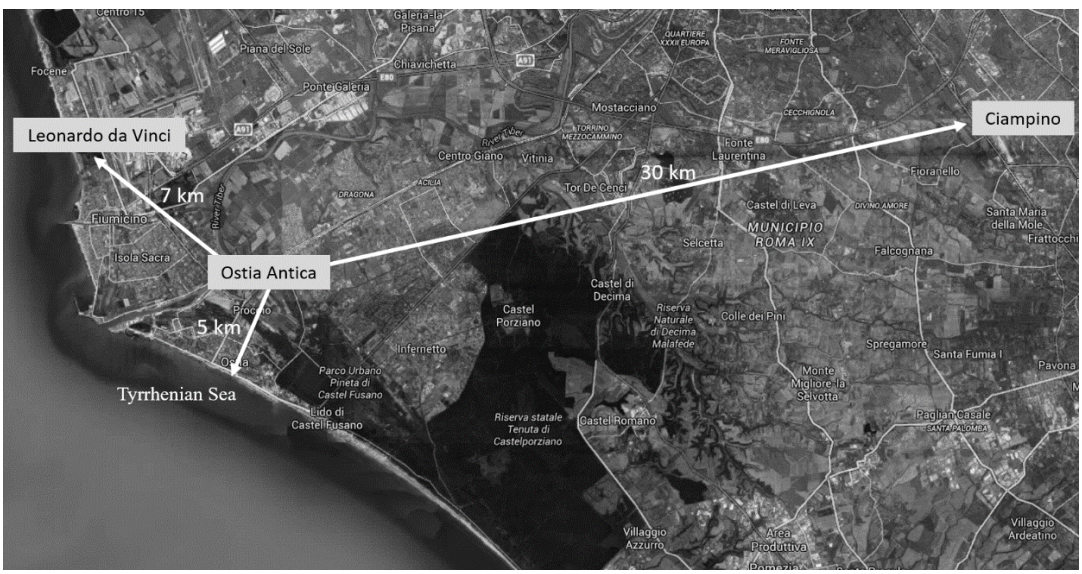

Figure 1. Ostia Antica map which allows observing the distances and orientation in comparison to the two airports and Tyrrhenian Sea.

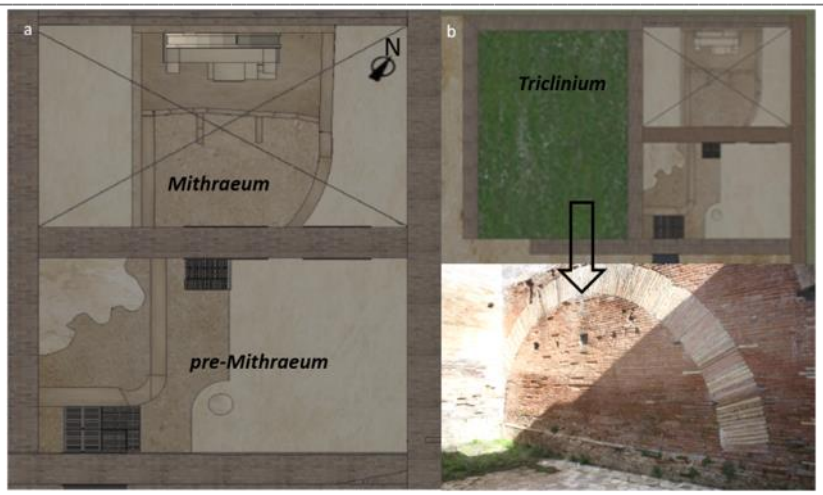

Figure 2. Plan of the building. **a**) *Pre-Mithraeum* and *Mithraeum* rooms; **b**) *Triclinium* room (zoom of the northeast wall of *Triclinium*).

Regarding the conservation problems, the structure suffers several decaying, such as biocolonization, salts formation on the surface of the bricks, material detachment, among others. Focusing on salts, the building is affected by efflorescence, displayed throughout the entire year, both on internal and external walls (**Fig. 3**). In this sense, one of the most important decaying factors to take into account is the indoor environment, defined as *hypogeum*, which is characterised by RH up to 98% (García-Diego et al. 2016, Scatigno et al. 2016a, Scatigno et al. 2016b). Thanks to previous studies, it seems that the origin of this *hypogeum* environment is the rising damp generated by a subterranean aquifer characterized by two types of waters depending on the depth (freshwater with piezometric level at about 2.5 m and salt water from 8-10 m) (Cardarelli et al. 2016). Although it is believed that a possible impermeable stratum (sand alluvial deposits) separates the two "water pockets", the initial hypothesis was that, at least one of these waters masses, influences the salt formation (probably the deeper water mass because of its salt concentration) (Cardarelli et al. 2016). However, there is another possible source to be taken into consideration. The rainfall (mixed with atmospheric acid gases and/or marine aerosol) that could be also the responsible of the salt formation by infiltration from the roof, the *Triclinium* room towards the bricks detachments or even through the openings (i.e. window of considerable size sited at west side of *pre-Mithraeum* room).

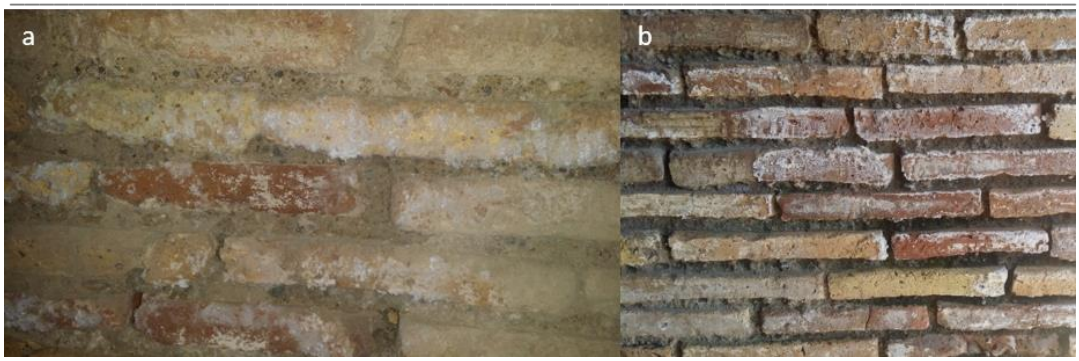

Figure 3. Examples of the soluble salts formation on walls. **a**) The mattifying veil and the efflorescences on south wall of *pre-Mithraeum* (indoor); **b**) The opacifying and the efflorescences on south wall of *Triclinium* (outdoor).

The diversity of sources that could be affecting to the building is important and thus, the clarification of the proper source that promotes the formation of the soluble salts is essential to the conservation plan of the building.

2.2 Sampling and analytical procedure

The sampling methodology was designed to evaluate all factors that could have influence the salt formation. In this sense, two different typology of bricks (red and yellow) were sampled on different walls (building orientation), as they are subjected to different environmental conditions (García-Diego et al. 2016). In any case, to assure the significance of the data collected, a reasoned non-probabilistic sampling design has been implemented (**Tab. 1**). 18 solid samples were selected to identify and to characterise the observed soluble salts. Specifically, 16 bricks were sampled

taken into account the orientation and the kind of brick (one for red and another for yellow). Other two samples of salts efflorescence were also taken from two walls with different orientation and found in different rooms (24S and 25S). Furthermore, a water sample was also obtained (W) from the well, in order to characterise the type of water and, indirectly, also of the freshwater aquifer(probably into communication). The rainwater sample (T1) was collected during a geochemical study conducted in November 2015 (Cardarelli et al. 2016).
Finally, despite the sampling of the deepest water mass was not possible, it has been classified in previous studies as marine water (Cardarelli et al. 2016).

Table 1. Samples collected (name, colour, room appurtenance and wall orientation). In the case of T1, the sample was collected in a previous study.

SAMPLE ID	TYPE OF BRICK	ROOM	ORIENTATION
15R	Red	*pre-Mithraeum*	South
15Y	Yellow	*pre-Mithraeum*	
16R	Red	*Mithraeum*	West
16Y	Yellow	*Mithraeum*	
17R	Red	*pre-Mithraeum*	West
17Y	Yellow	*pre-Mithraeum*	
18R	Red	*pre-Mithraeum*	West
18R2	Red	*pre-Mithraeum*	West
19R	Red	*Mithraeum*	East
19Y	Yellow	*Mithraeum*	
20R	Red	*Mithraeum*	North
20Y	Yellow	*Mithraeum*	
21R	Red	*pre-Mithraeum*	East
21Y	Yellow	*pre-Mithraeum*	
22R	Red	*Triclinium*	East
22Y	Yellow	*Triclinium*	
24S (salt 1)	-	*Mithraeum*	West
25S (salt 2)	-	*pre-Mithraeum*	East
W (well water)	-	*Latrinium - inside*	East
T1 (rain water)	-	*Tank -outside*	[28]

Regarding the analytical method, all the samples were crushed in an agate mortar and dried in a drying cabinet (60° C) until constant weight was obtained (24h). The soluble salts were extracted by an ultrasound-assisted procedure with water (100 mg of sample in 100 mL of Milli-Q water), following an optimized methodology based on European standards (Prieto-Taboada et al. 2012). This pre-treatment was replicated four times for each analysed sample. After the extraction, the obtained solutions were characterised by a Dionex ICS 2500 ionic chromatograph with an ED50 suppressed conductivity detector. An IonPac AS23 (4×250 mm)column and IonPac AG23 (4×50 mm) precolumn from Dionex were used for the separation of anions. The quantification of cations was conducted using an IonPac CS12A (4×250 mm) column and IonPac CG-12A (4×50 mm) precolumn from Dionex. The chromatographic conditions used in the anion quantification were 5 mM Na_2CO_3/0.8 mM $NaHCO_3$, 25 mA and 1 ml/min as mobile phase, suppression current and flow, respectively. In the case of cations, 20 mM CH_4SO_3 as mobile phase, 59 mA of suppression current and 1 ml/min flow were used. Prior to the analysis, the samples were passed through a 0.45 μm nylon syringe filters and brought to a final volume.

In order to estimate the carbonate concentration, the pH values of the extracted soluble salts were measured. Thus, the pH measurements were conducted with SOILSTIK pH meter item#2105 (Spectrum Technologies, Inc.) and were replicated three times.

Data was treated with OriginPro version 8.5.1 (OriginLab© Massachusetts, USA) and the Principal Component Analysis (PCA) was performed using the Unscrambler X version 10.4 (chemometric software package - Camo, Woodbridge, NJ, USA) package (cross validation method and Singular Value Decomposition algorithm).

Regarding the environmental monitoring, the thermo-hygrometric data, deriving from a wide microclimatic campaign conduced from 2012 to 2015, were inserted in the computer program ECOS-RUNSALT (v. 1.9) (Bionda and Storemyr 2002, Price 2000, Price 2007), according to the allowed range configured, to predict the soluble salts formation at the micro-environmental conditions (annual average) established by several monitoring campaigns (García-Diego et al. 2016, Scatigno et al. 2016a, Scatigno et al. 2016b). Unfortunately, ECOS-RUNSALT does not consider gypsum, reason for which another software, the Medusa-Hydra program (v. 2010) (Puigdomenech 2010), was used. The latter does not consider the environmental conditions nor predicts chemical equilibria in dissolution, but fills the gap left by the other program. For such reason, a combination of both programs was used.

3 RESULTS AND DISCUSSION

Thanks to the quantitative analysis, F^-, ClO_2^-, Cl^-, NO_2^-, NO_3^-, PO_4^{3-} and SO_4^{2-} anions and Na^+, K^+, Mg^{2+} and Ca^{2+} cations, were quantified. The soluble salt results are shown in Table 2. Because of the nature of the mobile phase used, it was not possible to analyse the concentration of the dissolved bicarbonate. It was then theoretically determined through the completion of the mass balance and electroneutrality in the liquid extracts after performing the soluble salt tests (Prieto-Taboada et al. 2011, Veneranda et al. 2014).

$$\Sigma \text{ (valence*cation conc.)} - \Sigma \text{ (valence*anion conc.)} = \text{Bicarbonate concentration}$$

In order to estimate the carbonate or bicarbonate presence, pH measurements were required. All the bricks samples presented a pH below 8, as can be seen in **Figure 4**, thus, bicarbonate was estimated (Prieto-Taboada et al. 2011). In the case of water and salts samples, also bicarbonate was assumed.

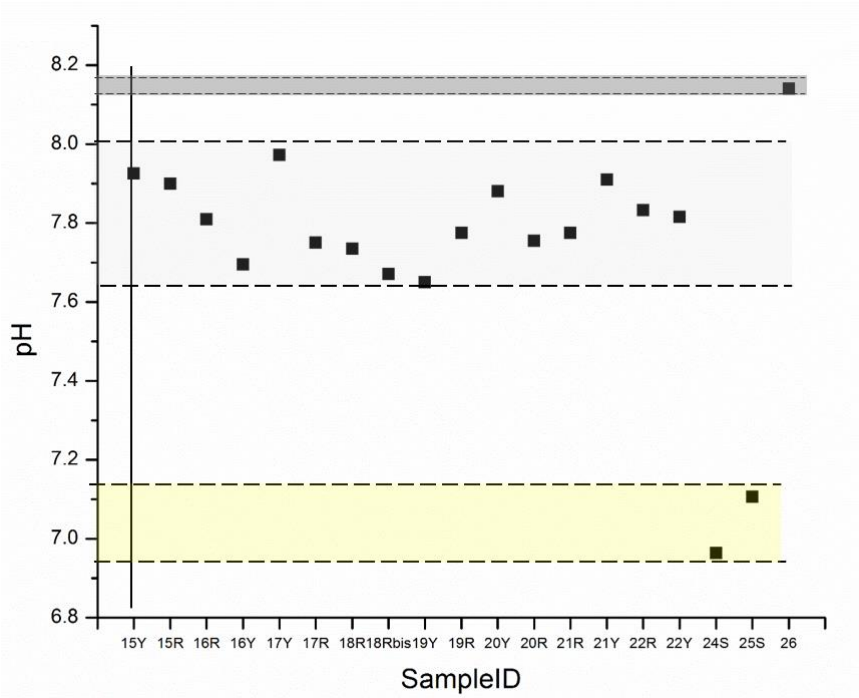

Figure 4. pH measurement scatter plot. The salts samples (24S and 25S) were represented in the yellow rectangle and the water sample in the by grey rectangle.

To better understand the origin of these salts, a correlation diagram, normally used in hydro geochemical studies (Chebotarev 1955), was plotted using the results shown in **Table 2 (Fig. 5**). Really, the diagram visualises and classifies the hydro-geochemical facies (one or more) and the dominant among them, identifying a genetic classification (Cardarelli et al. 2016). Taking into account that the water extraction decreases the ion concentration in the solution but not the ionic ratio, the use of this diagram could help to identify the type of water that mobilises the salts. Thus, the diagram reveals carbonate species such as $Ca^{2+}$and Mg^{2+}, that is, of carbonate origin. Nevertheless, extracting more information about the origin of these carbonates was difficult because the results could indicate freshwater but also, the dissolution of the building materials by the action of the rainwater. However, the quantitative results and this diagram excluded the deepest mass of water of the know aquifer (salt water) as responsible of the rising damp because of the absence of a high concentration of anions as Cl^-, Na^+ or K^+. In this sense, one of the three possible salt sources could be discarded.

Table 2. Chemical composition of sampled bricks (mmol/kg) and water (mmol/l). The bicarbonate value was theoretically determined. The obtained RSD was below 5% in all cases.

Sample ID	Na^+	K^+	Mg^{2+}	Ca^{2+}	F^-	ClO_2^-	Cl^-	NO_2^-	NO_3^-	PO_4^{3-}	SO_4^{2-}	HCO_3^-
15R	13.1	20.8	18.6	201.4	7.8	0.053	9.0	1.7	5.6	8.1	7.4	410.6
15Y	41.5	20.7	38.7	227.8	7.5	0.045	66.5	1.2	87.6	14.9	8.9	370.0
16R	24.9	27.5	20.3	230.6	10.5	0.053	2.0	1.8	10.4	5.1	37.5	439.3
16Y	31.8	30.3	24.6	273.9	29.1	0.050	3.9	2.7	3.7	6.5	62.2	475.5
17R	79.6	32.1	32.0	444.2	27.8	0.048	13.3	1.0	17.9	26.1	342.3	241.2
17Y	42.3	19.7	26.4	246.1	3.7	0.046	71.6	1.8	35.8	17.5	45.2	351.1
18R	33.0	28.7	19.7	238.0	27.1	0.042	4.9	3.8	6.5	9.7	43.0	419.8
18R2	84.6	27.4	42.6	384.1	35.3	0.053	29.5	1.7	38.1	53.8	249.7	200.0
19R	15.0	25.2	11.2	223.6	13.2	0.038	1.0	1.3	<LOD	<LOD	39.6	414.8
19Y	35.0	23.2	34.8	431.0	41.1	0.042	68.0	1.2	21.0	30.3	244.7	278.3
20R	24.9	22.3	20.5	230.7	7.5	0.057	32.9	2.2	18.9	27.4	39.0	328.0
20Y	13.0	24.3	12.1	242.9	18.0	0.042	12.7	1.1	10.5	14.9	13.8	432.6
21R	34.2	26.3	14.6	229.9	10.7	0.050	14.9	1.3	4.2	6.6	19.5	459.6
21Y	19.8	26.5	14.2	194.2	7.6	0.064	3.9	1.7	<LOQ	<LOQ	2.7	444.5
22R	88.9	66.8	38.2	253.5	12.0	0.042	16.4	0.74	9.3	12.6	131.6	399.6
22Y	31.3	18.2	15.1	284.3	5.1	0.042	3.0	1.3	4.9	5.8	125.3	365.7
24S	19.4	14.9	15.1	2831.5	<LOQ	0.327	16.9	<LOD	<LOD	<LOQ	3254.7	-◊
25S	55.4	19.4	26.8	1194.9	<LOQ	0.090	7.6	<LOD	<LOD	<LOQ	924.5	661.4
W	2.7	1.1	0.76	1.1	0.034	n.d.	2.8	n.d.	0.20	0.40	0.33	2.5
T1	2.5	1.0	0.58	0.74	0.022	n.d.	2.1	n.d.	n.d.	n.d.	0.23	3.5

To find possible relationships among the concentration of the different ions collected in **Table 2,** a Correlation Analysis was performed using only the data from bricks (16 samples). The results are summarised in **Table 3** showing that the correlation between Ca^{+2}/SO_4^{2-} was likely (r=0.96). Thus, also in the brick samples, the gypsum formation had a high possibility of occurring. That is, a source of sulphates is affecting to the whole volume of *Mithraeum* because even the bricks at the highest level in the walls are partially sulphated in their surfaces.

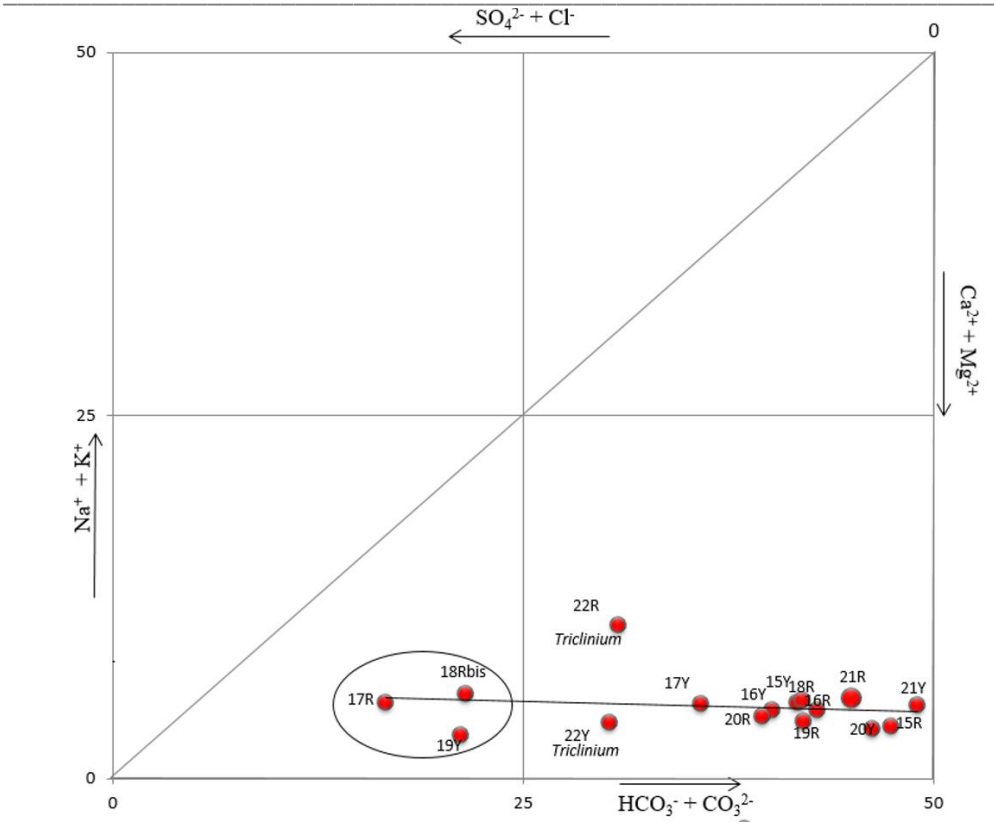

Figure 5. Anion and cations diagram (visualisation and classification of hydro chemical data) which excludes the marine water as origin of salts.

Table 3. Ions Correlation Analysis for brick samples.

	Na+	*K+*	*Mg2+*	***Ca 2+***	*F-*	*ClO2-*	*Cl-*	*NO2-*	*NO3-*	*PO43-*	*SO42-*	*HCO3-*
Na+	*1*											
K+	*0.63*	*1*										
Mg2+	*0.78*	*0.35*	*1*									
Ca 2+	*0.55*	*0.02*	*0.59*	*1*								
F-	*0.36*	*0.11*	*0.44*	*0.75*	*1*							
ClO2-	*-0.09*	*-0.13*	*-0.09*	*-0.22*	*-0.18*	*1*						
Cl-	*0.16*	*-0.24*	*0.58*	*0.30*	*0.07*	*-0.17*	*1*					
NO2-	*-0.27*	*-0.21*	*-0.18*	*-0.21*	*0.18*	*0.16*	*-0.17*	*1*				
NO3-	*0.27*	*-0.22*	*0.66*	*0.18*	*-0.03*	*-0.11*	*0.77*	*-0.15*	*1*			
PO43-	*0.54*	*-0.06*	*0.69*	*0.71*	*0.54*	*0.03*	*0.51*	*-0.06*	*0.47*	*1*		
SO42-	*0.70*	*0.20*	*0.61*	***0.96***	*0.66*	*-0.18*	*0.18*	*-0.27*	*0.10*	*0.67*	*1*	
HCO3-	*-0.42*	*0.16*	*-0.41*	*-0.58*	*-0.02*	*0.10*	*-0.38*	*0.39*	*-0.36*	*-0.51*	*-0.66*	*1*

Concerning the different salts that can be formed, the quantitative and correlation analyses identified gypsum and calcite as the main salts. In order to confirm this hypothesis, a first thermodynamic modelling was carried out using the RUNSALT software, because it has the possibility to introduce the RH as one input parameter, a very important factor in of this specific indoor environment: the average RH value is of 95.6%; but in the lowest strata (0-1.1 m) the recorded

RH values are very close to saturation (96-99%) (Scatigno et al. 2016a). Moreover, a previous monitoring campaign revealed that the T is stable (average annual temperature T_{my} 16° C) throughout the entire year and the daily T variations are not significant (García-Diego et al. 2016).

However, ECOS-RUNSALT has also some restrictions concerning the input of data, as the program does not consider carbonates. Moreover, in some occasions, the prediction of gypsum crystallisation might cause problems, since the program is unable to calculate the crystallisation of other salts in its presence, and gypsum must therefore be removed from the system. Finally, the program runs only within a certain thermo-hygrometric range. In particular, it does not allow maximum value relative humidity (RH_{max}) values exceeding 98%. Due to these restrictions, the model could be applied only to some of the described cases (15R, 16R, 18R, 21R, 21Y), due to the abundant presence of calcium in the materials under study. Furthermore, this program only considers the following ions: Na^+, K^+, Mg^{2+}, Ca^{2+}, Cl^-, NO_3^- and SO_4^{2-}.

Leaving these considerations aside, the ECOS-RUNSALT simulation was run considering a T_{my} of 16°C, a RH_{max} of 98%, a minimum value relative humidity (RH_{min})of 77% and the ionic concentrations obtained in the quantitative analysis. Within these thermo-hygrometric ranges, the program predicted specific sulphate minerals formation that indicated again a strong attack deriving from SO_4^{2-}(**Fig. 6**). In particular, the 16R and 18R red bricks presented the same phases (**Fig. 6**): aphthitalite ($(K,Na)_3Na(SO_4)_2$), picromerite ($K_2Mg(SO_4)_2{\cdot}6(H_2O)$), mirabilite ($Na_2SO_4{\cdot}10H_2O$), bloedite ($Na_2Mg(SO_4)_2{\cdot}4H_2O$). In the samples 21R and 21Y, aphthitalite and picromerite were suggested to be present by the simulation. Finally, picromerite was the only phase predicted in 15R.

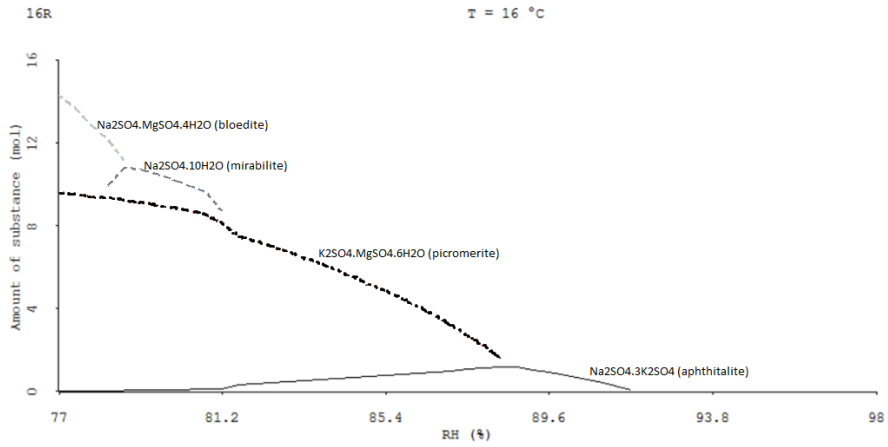

Figure 6. ECOS-RUNSALT output (16°C, RH 98-77%) for the sample 16R in which is possible to observe the formation of different sulphates.

If we take into account the limitation of ECOS-RUNSALT concerning the gypsum formation, which is a principal salt in this study, the predicted salts cannot be

considered major solid species, but its formation implies that saturation is reached somewhere. In order to find such saturation conditions, the second simulation strategy was performed using the Medusa-Hydra software. In a first attempt, the ionic concentrations of rainwaters (T1 taken from (Cardarelli et al. 2016)) were studied. In a second attempt, the ionic concentration of the freshwater, of the shallow aquifer (26W), were used as input data for the program. Both types of water presented a low concentration of dissolved ions (max. 0.029%) and a pH around 8.

Figure 7 shows the distribution diagram of calcium (**Fig. 7a**) and sulphate (**Fig. 7b**) considering that rainwater interacts with a calcite substrate. As seen, the calcite starts to be dissolved at pH<7, but the rainwater has a pH~8, not acid enough to attack calcite (**Fig. 7a**). Furthermore, considering the sulphate species, the rainwater does not explain the formation of any solid sulphates like gypsum, aphthitalite, picromerite, mirabilite or bloedite (**Fig. 7b**).

On the other hand, for the simulation using the concentrations of the well water sample (W), the results were the same: any solid sulphate species was formed from the calcite substrate. Thus, the ground and rainwaters are not enough to degrade the calcite and promote the formation of the predicted solid sulphate species.

The different simulations suggested the need of an extra sulphate concentration in solution. To verify this, **Figure 8** shows the sulphate distribution diagram of the species using the concentration conditions of the rainwater, at pH=7, as a function of the total dissolved sulphate concentration. As seen gypsum is formed when the saturation condition is reached. Thus, the formation of sulphate in bricks requires another input that cannot be explained with the ions dissolved in the rainwater or well in contact with freshwater aquifer. Taking this into account, the unique input for sulphates could be the atmospheric acid gases (SO_2) (Charola et al. 2007).

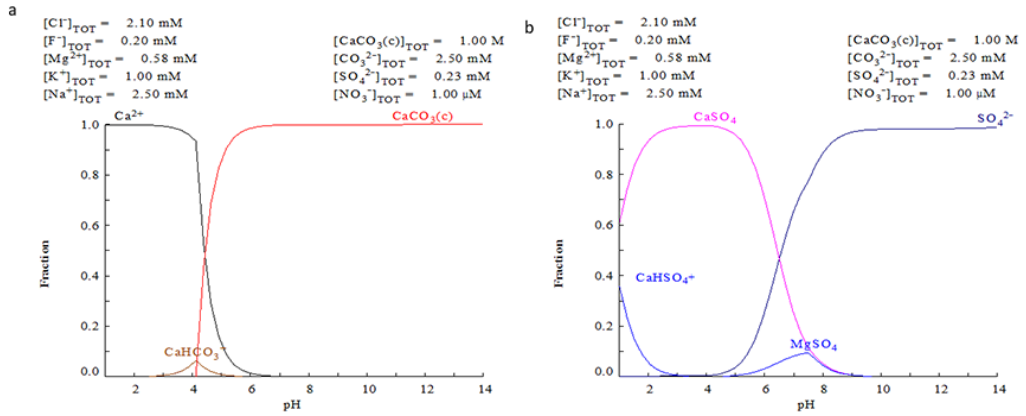

Figure 7. Medusa-Hydra output for rainwater (T1) interaction with calcium carbonate. **a**) Calcium species distribution vs. pH; **b**) sulphate species vs. pH. In both cases, the observed salt formation is not explained.

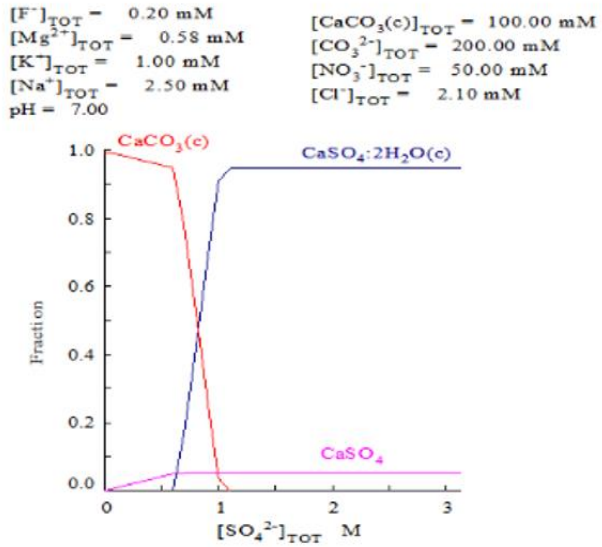

Figure 8. Medusa-Hydra modelling of the rainwater (W1) with sulphate input, probably from the atmospheric acid gases.

Taking all this into account, the effect of atmospheric acid gases seems to be clear. However, when it occurs, the presence of higher concentration of sulphates and a lower pH of the rainwater are expected, but in this case, this fact was not observed. This fact suggests that the acid attack of the atmospheric SO_2 occurs as a dry deposition mechanism. Moreover, taking into account the *hypogeum* environment and the extremely high humidity (above all in the lower strata of masonry) (Scatigno et al. 2016a), the dry deposition of acid gases into surface, involves also the acidification of the porous net water, which allows also the dissolution of carbonates despite the original water not having the required pH.

Thanks to all these observations, it was possible to propose a mechanism for the formation of the salts: (1) hydration process of the original oxides by H_2O to form reactive hydroxides. (2) Dry deposition of CO_2 in wet bricks to form carbonates and acid net water. (3) Dissolution of the carbonates and SO_2 attack to form sulphates. Considering the proposed mechanism, the porosity of the materials and the salts' mobility, the formation of subefflorescences is possible, but the phenomena is expected to be more intense on the interface with the atmosphere (efflorescences), as is the case studied. Nonetheless, it is clear that the key step is the hydration of the original compounds, because without this, the attack of the acid gases by dry deposition is unlikely.

Once the mechanism is understood, the definition of the origin of the pollution is crucial in order to try to contain it. It is noticeable that Ostia Antica is set at a distance of about 5 km from the seacoast in the south direction, so marine aerosol is expected to play a considerable role. However, the results did not support this hypothesis. Moreover, studies on the relationship between the salinity and

distance from the coast reveal an exponential decrease of the marine aerosol correlated to the increase of the distance from the coast. In fact, it was observed that five kilometres seem to be enough to minimize the contribution of the marine aerosol (Chico et al. 1998). Leaving this aside and focusing on the acid gases, their main sources are probably the nearby airports (Ciampino and Leonardo da Vinci). It is known that the wind direction changes, but the prevailing winds come from the northwest, that is, from the direction of the Leonardo da Vinci airport (around 7 km away from the site). Therefore, the diffuse pollution coming from the Leonardo da Vinci airport seems to be the most important source of atmospheric acid gases. For conservative purposes, the effort to diminish the negative influence of them is extremely difficult.

Another important gaseous acid is CO_2 that attacks the calcium carbonate dissolving calcium (and bicarbonate) ions. In this sense, the extra CO_2 can be controlled in terms of visitors' affluence (Scatigno et al. 2016b), but an airport proves to be a less controllable source. From this perspective, the proposed mechanism is very important, as it makes it possible to identify the step that plays the greatest role in the salt formation, in this case was the hydration process. Thus, if this step does not occur, the mechanism could be stopped. Considering this, the identification of the origin of such a high RH of the building must be studied in depth, although all previous studies of the house seem indicate that it is the freshwater aquifer (Scatigno et al. 2016b).

Leaving aside the origin of salts, the evaluation of their impact of them on the materials was also important. In order to establish a critical level of damage, the obtained concentrations (expressed as a percentage) (**Table 4**) were compared with the maximum levels marked by European standards (**Table 5**) for each anion. In this sense, all brick samples present a low risk of chlorine contamination, and only some of the samples present a medium risk deriving from nitrates. However, this indicates some nitrate input that could likely come also from the acid gases. Finally, there were some samples with medium and high risk of sulphate contamination, as expected taking in consideration the previous observations.
After the individual comparison, the total soluble salt content of the different bricks of the walls was around 1.0-5.9% (w/w), indicating that the materials were medium/very polluted which a medium/high risk of hygroscopic moisture and damage of the materials. This fact pointed out the real need to find a solution to the problem of soluble salts in order to preserve the archaeological site under study.

Table 4. Summary of the soluble salt results on bricks expressed in weight percentage (w/w%). The ionic concentrations considered dangerous by European standards are highlighted, despite other salts being present. The samples that exceed the risk levels are coloured in light grey box (low risk), medium grey box (middle risk) and dark grey box (high risk).

Sample ID	Cl^-	NO_3^-	SO_4^{2-}	Total*
15R	0.03%	0.03%	0.07%	**1.2%**
15Y	0.2%	**0.5%**	0.09%	**2.2%**
16R	0.007%	0.06%	0.4%	**1.7%**
16Y	0.01%	0.02%	0.6%	**2.1%**
17R	0.05%	0.1%	**3.3%**	**5.9%**
17Y	0.3%	**0.2%**	0.4%	**2.3%**
18R	0.02%	0.04%	0.4%	**1.8%**
18Rbis	0.1%	**0.2%**	**2.4%**	**5.3%**
19R	0.004%	<LOD	0.4%	**1.5%**
19Y	0.2%	0.1%	**2.4%**	**5.1%**
20R	0.1%	0.1%	0.4%	**2%**
20Y	0.05%	0.07%	0.1%	**1.6%**
21R	0.05%	0.03%	0.2%	**1.5%**
21Y	0.01%	<LOQ	0.03%	**1%**
22R	0.06%	0.06%	**1.3%**	**3.1%**
22Y	0.01%	0.03%	**1.2%**	**2.6%**

LOD Limit of Detection

*The sum of the analysed ions, so, the percentage is a lower approximation

Table 5. Degree of contamination by dangerous soluble salts expressed in weight percentage (w/w%) according to WTA (International Association for Science and Technology of Building Maintenance and the Preservation of Monuments).

RISK	$[Cl^-]$	$[NO_3^-]$	$[SO_4^{2-}]$	Total
Low	<0.30%	<0.12%	<0.80%	<1.2%
Middle	0.30-0.80%	0.12-0.50%	0.80-1.6%	1.2-2.9%
High	>0.80%	>0.50%	>1.6%	>2.9%

Finally, to obtain further information about the evident salt damage, chemometric analyses based on principal component analysis (PCA) were carried out using leverage validation method, after a previous auto scaling of the dataset. At first sight, the PCA with three principal components explains 72% of the total variance (**Fig. 9**).

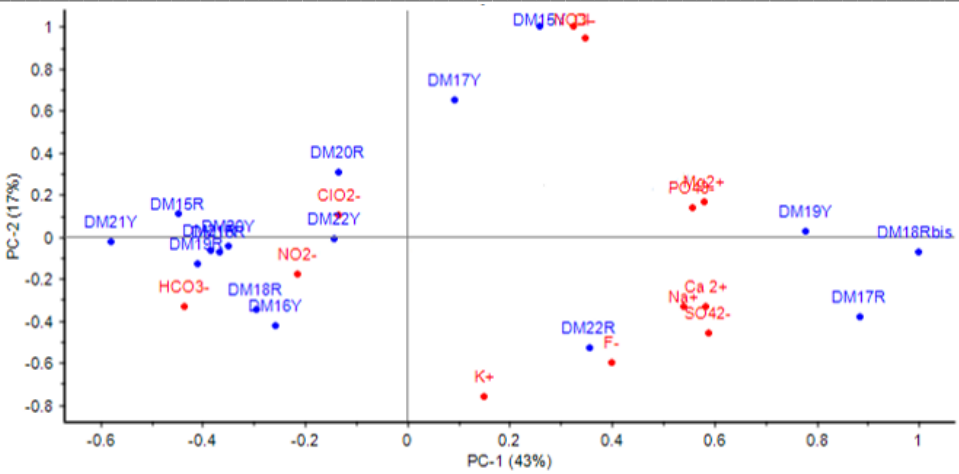

Figure 9. Bi-plot of the quantitative analyses of soluble salts in which it is not possible to observe differences between orientation, rooms or type of brick.

Apart from some clusters, such as Ca^{2+}, SO_4^{2-}, Na^{+}, related probably with gypsum formation, no distinction was found related to bricks' colour or to the rooms of belonging. It was possible to deduce that the soluble salts affect indistinguishably, from a general perspective on the whole house, without any correlation with the orientation of the wall or colour, despite the different environments (rooms and orientation) or original composition (type of brick). This fact could indicate that the high RH and the hydration of the materials could be caused by a general common factor affecting to the house, as an aquifer is found below the entire house. This excludes the rainfall, as because it could have a different effect in different levels depending on the holes, openings, roofs...etc.

4 CONCLUSIONS

Thanks to the proposed methodology that combines ion chromatography and thermodynamic modelling software (ECOS-RUNSALT and Medusa-Hydra) together with chemometric analysis, it was possible to understand the formation mechanism, identify the source and the types of salts that were formed in the studied building. In detail, it was possible to establish that the salt contribution does not come from the salt water found at greater depths (8 m) or any of the other water sources (freshwater aquifer or rainfall). Additionally, it was possible to discard the marine aerosol, despite the proximity to the Tyrrhenian Sea. In contrast, it was determined that the acid gases, probably the main source of salt weathering, come from the Leonardo da Vinci airport, and that the mechanism of the acid attack involves the dry deposition of the atmospheric acid gases.

On the other hand, the hydration process of the materials seemed to be crucial in the salt formation mechanism. In this way, taking into account also previous studies, the origin of rising damp, responsible of the high RH, was identified as the freshwater aquifer at shallower depths. Actually, the hydration of the materials represents the first step of a damage process, making them more favourable to salt attack. However, some uncertainly about the contribution of the freshwater aquifer, combined or not with rainwater still remains. In any case, it is clear that the

conservative plan to stop the formation of soluble salts should be focused on controlling the RH of the building, despite of the source of atmospheric acid gases not being possible to modulate.

Finally, regarding the risk level of contamination, the majority of brick samples were medium/very polluted which a medium/high risk of hygroscopic moisture and damage of the materials, due to the high sulphate presence, that attack indistinctly the red as the yellow bricks, without any difference caused by the orientation of the walls. This fact points out a real need to solve the problem of formation of the soluble salts in order to preserve the studied archaeological site.

ACKNOWLEDGEMENTS

The authors thank the archaeological area of Ostia Antica, in particular the director Dr. Cinzia Morelli, the security company, and the technical staff (Drs. Paola Germoni, Flora Panariti, Orietta Mantovani) for the permission to work in this house. Claudia Scatigno is grateful to the University of the Basque Country (UPV/EHU) for the grant for study sojourns by trainee researchers from foreign universities engaged in a jointly supervised doctoral thesis. Moreover, she is also grateful to Dr. Angela Nigro for her help with the Chebotarev diagram. The work developed in the University of the Basque Country (UPV/EHU) has been partially supported by the project DISILICA-1930 (ref. BIA2014-59124-P) funded by the Spanish Ministry of Economy and Competitiveness (MINECO) and the European Regional Development Fund (FEDER). Claudia Scatigno is grateful to Claudia Moricca for the English revision of the manuscript.

REFERENCES

Aramendia J, Gómez-Nubla L, Castro K, Madariaga JM (2014) Spectroscopic speciation and thermodynamic modelling to explain the degradation of weathering steel surfaces in SO 2 rich urban atmospheres. Microchemical Journal

Bala'awi F, Prokos P (2011) Salt mixtures phase equilibria: a tool of preventive conservation against salt weathering. Journal of Fauclty of Art, Ain Shams University

Bionda D, Storemyr P (2002) Modelling the behaviour of salt mixtures in walls: a case study from Tenaille von Fersen. The study of salt deterioration mechanisms. Decay of brick walls influenced by interior climate changes. Suomenlinnan hoitokunta, Helsinki

Brai M, Casaletto M, Gennaro G, Marrale M, Schillaci T, Tranchina L (2010) Degradation of stone materials in the archaeological context of the Greek–Roman Theatre in Taormina (Sicily, Italy). Applied Physics A

Cardarelli E, De Donno G, Scatigno C, Oliveti I, Martinez MP, Prieto-Taboada N (2016) Geophysical and geochemical techniques to assess the origin of rising damp of a roman building (Ostia Antica archaeological site). Microchemical Journal

Charola AE, Pühringer J, Steiger M (2007) Gypsum: a review of its role in the deterioration of building materials. Environ Geol

Chebotarev I (1955) Metamorphism of natural waters in the crust of weathering—1. Geochim Cosmochim Acta

Chico B, Otero E, Mariaca L, Morcillo M (1998) La corrosión en atmósferas marinas. Efecto de la distancia a la costa. Revista de Metalurgia

Espinosa R, Franke L, Deckelmann G (2008) Model for the mechanical stress due

to the salt crystallization in porous materials. Constr Build Mater

Espinosa-Marzal RM, Scherer GW (2010) Advances in understanding damage by salt crystallization. Acc Chem Res

Franzoni E (2014) Rising damp removal from historical masonries: A still open challenge. Constr Build Mater

García-Diego FJ, Scatigno C, Merello P (2016) Discrete and continuous monitoring to characterised the thermo-hygrometric state of wall-building materials in Ostia Antica archaeological site

Gentilini C, Franzoni E, Bandini S, Nobile L (2012) Effect of salt crystallisation on the shear behaviour of masonry walls: an experimental study. Constr Build Mater

Godts S, De Clercq H, Hayen R, De Roy J (2012) Risk assessment and conservation strategy of a salt laden limestone mausoleum and the surrounding funeral chapel in Boussu, Belgium.

Gómez-Laserna O, Olazabal MÁ, Morillas H, Prieto-Taboada N, Martinez-Arkarazo I, Arana G, Madariaga JM (2013) In-situ spectroscopic assessment of the conservation state of building materials from a Palace house affected by infiltration water. J Raman Spectrosc

Heinrichs K, Azzam R (2015) Quantitative Analysis of Salt Crystallization–Dissolution Processes on Rock-Cut Monuments in Petra/Jordan. In: Engineering Geology for Society and Territory-Volume 8. Springer, pp 507-510

Hossain KMA, Easa SM, Lachemi M (2009) Evaluation of the effect of marine salts on urban built infrastructure. Build Environ

Korkanç M (2013) Deterioration of different stones used in historical buildings within Nigde province, Cappadocia. Constr Build Mater

Kubiak JJ, Khankhane PJ, Kleingeld PJ, Lima AT (2012) An attempt to electrically enhance phytoremediation of arsenic contaminated water. Chemosphere

Larsen PK (2007) The salt decay of medieval bricks at a vault in Brarup Church, Denmark. Environ Geol

Maguregui M, Sarmiento A, Martínez-Arkarazo I, Angulo M, Castro K, Arana G, Etxebarria N, Madariaga J (2008) Analytical diagnosis methodology to evaluate nitrate impact on historical building materials. Analytical and bioanalytical chemistry

Morillas H, Maguregui M, Trebolazabala J, Madariaga JM (2015) Nature and origin of white efflorescence on bricks, artificial stones, and joint mortars of modern houses evaluated by portable Raman spectroscopy and laboratory analyses. Spectrochimica Acta Part A: Molecular and Biomolecular Spectroscopy

Morillas H, Maguregui M, Gómez-Laserna O, Trebolazabala J, Madariaga JM (2013) Could marine aerosol contribute to deteriorate building materials from interior areas of lighthouses? An answer from the analytical chemistry point of view. J Raman Spectrosc 44:1700-1710

Nicolai A (2008) Modelling and numerical simulation of salt transport and phase transitions in unsaturated porous building materials. ProQuest

Price CA (2007) Predicting environmental conditions to minimise salt damage at the Tower of London: a comparison of two approaches. Environ Geol

Price CA (2000) An expert chemical model for determining the environmental conditions needed to prevent salt damage in porous materials. European Commission Research Report 11, (Protection and Conserv

Prieto-Taboada N, Gómez-Laserna O, Martinez-Arkarazo I, Olazabal M, Madariaga J (2012) Optimization of two methods based on ultrasound energy as

alternative to European standards for soluble salts extraction from building materials. Ultrason Sonochem

Prieto-Taboada N, Maguregui M, Martinez-Arkarazo I, Olazabal M, Arana G, Madariaga J (2011) Spectroscopic evaluation of the environmental impact on black crusted modern mortars in urban–industrial areas. Analytical and bioanalytical chemistry

Puigdomenech I (2010) Hydra/Medusa Chemical Equilibrium Database and Plotting Software 2004. KTH Royal Institute of Technology, freely downloadable software at http://www.kemi.kth.se/medusa.accessed in March

Scatigno C, Gaudenzi S, Sammartino M, Visco G (2016a) A microclimate study on hypogea environments of ancient roman building. Sci Total Environ

Scatigno C, Moricca C, Tortolini C, Favero G (2016b) The influence of environmental parameters in the biocolonization of the Mithraeum in the roman masonry of Casa di Diana (Ostia Antica, Italy). Environ Sci Pollut Res. doi: 10.1007/s11356-016-6548-x

Scatigno C, Prieto-Taboada N, Preite Martinez M, Conte AM, García-Diego FJ, Madariaga JM (2016c) Analitycal techniques for the characterisation of historical building materials: Case study "Casa di Diana" Mithraeum (Archaeological site in Ostia Antica, Italy). In: Wythers MC (ed) Advances in Materials Science Research, Nova Science Publishers, Inc. edn, New York

Steiger M (2005) Crystal growth in porous materials—I: the crystallization pressure of large crystals. J Cryst Growth

Stelzner J, Eggert G (2008) Calcium Carbonate on Bronze Finds. Studies in conservation

Veneranda M, Irazola M, Díez M, Iturregui A, Aramendia J, Castro K, Madariaga JM (2014) Raman spectroscopic study of the degradation of a middle age mural painting: the role of agricultural activities. J Raman Spectrosc

7.3 Conclusions

On the whole, the correct selection of a multi-analytical methodology allowed to achieve the required specific targets of the chapter. Specifically, the analytical techniques allowed to characterise the wall-building materials, decaying compounds and the manufacturing process (firing temperature), as well as the conservation state for each typology of bricks.

In fact, both categories of bricks suffer the same decaying processes (carbonation and sulphation) due to the atmospheric acidic gases from the close Fiumicino airport through dry deposition. Despite the proximity of the Tyrrhenian Sea, the efflorescence salts' formation is not clearly dependent on it (neither marine aerosol, nor subterranean saline aquifer). Moreover, the subterranean fresh aquifer causes the hydration process that is the first and key step of the salt formations mechanism.

The orientation of the walls has influenced the conservation state of the bricks. In particular, the results pointed out that the most critical wall for both types of bricks was east wall of the *pre-Mithraeum*, the only real semi-confined wall, which is more influenced by macroclimate or environmental stressors (CO_2 and SO_2 acid gases). However, despite the same environmental stressors, the multi-analytical techniques employed pointed out that each type of brick present a different response, due to a different nature of materials and manufacturing process used.

Finally, the hypothesis that the yellow bricks date back to the Byzantine period was proposed for the first time, which will have to be proved or disproved in future works.

All these results showed the interaction with the surrounding environment, both the microenvironment and the hydro-geological setting.

Chapter 8 Integrated conclusions: conservation tools and final pyramid

In this PhD work, an experimental diagnostic approach has been presented, sustained by three main methodologies based on the study of the environment, the materials and their interface.

First of all, the diagnostic model designed is remarkable due to these features: (1) the use of traditional or widely used techniques, combined with other more recently developed techniques/software, applied to completely new contexts (**Article 4**, **Articles 7-8**), (2) the design and validation of new techniques (**Articles 2-3**), (3) the use of modern techniques applied for the first time in an archaeological context (**Chapter 6.2**) and (4) the application of innovative software and sensors experimented on *hypogea* environment (**Chapter 6.4**). Thus, this PhD work presents novel methodologies and/or innovative applications of existing protocols, which leads to an important scientific contribution.

Regarding the results of the developed environmental methodology, it was possible to identify different microclimates within a single building because of the unreal connection between the two rooms and the inadequate air movement, all of which make the environment uncomfortable for the visitors. In fact, for the first time, a *hypogeum* environment was identified in a semi-confined structure. Moreover, the RH values close to saturation, in the lower strata, have suggested the presence of rising damp.

Regarding materials' characterisation, it was possible to identify differences linked to the nature of raw materials (kaolinite and illite clay) and manufacture of the bricks, which present different behaviour to the environmental stressors (CO_2 and SO_2). Moreover, a different behaviour of the bricks was also observed according to the building orientation (walls exposition) and to the presence of different microclimates. Furthermore, the results led to the hypothesis that the yellow bricks could correspond to a different historic period.

The relationship between "content and container" was evident, for example from the **carbonation phenomena** and the **soil mineralisation**. The former is produced by the very high concentrations of CO_2 (of biological and anthropogenic origin) throughout the whole day (night cyclic emission and day emission in correspondence of the high turnout). This last issue, combined with the presence of vapour, activates the process of carbonation of materials (normally, a production of 750 ppm is necessary to activate it [199-202]).

The cyclic input of CO_2, caused by a lack of air ventilation, acts in way that its concentrations are higher than those allowed by norms (though there is a lack of

information on this matter in the field of cultural heritage), causing for it to be considered as a real pollutant. In contrast, the soil mineralisation was the result of the exploitation of the salt marshes over the centuries, but it was possible to discretise the real ground water vulnerability from the saline intrusion from the Tyrrhenian Sea.

Thus, the three analytical methodologies have allowed identifying the **sources of decay processes** that can be summarised as the rising damp from the freshwater aquifer and the atmospheric acids gasses. In this sense, the state of conservation of the "Casa di Diana" *Mithraeum* is bad, despite its apparent "integrity". For this, a rescue intervention of this important house of Ostia Antica is highly suggested.

Being aware of the lack of funding, small but essential actions have been suggested. First of all, taking into account the Stage Method (**Tab. 3 – Chapter 5.3**), the green film and the **biological apparatus** must be removed. The mechanical and chemical interventions are only a temporary remedy, so natural light must be controlled through the installation **of filters on the window**, in order to create less favourable conditions for the biological proliferation. As far as the artificial lighting is concerned, a substitution of the halogen **lamps** with **LED** (i.e. light-emitting diodes or, alternatively, fluorescent compact lamps with low thermal infrared emissions, lamp technology equipped with appropriate emission spectra), which would provide a good compromise between conservation and human comfort, is recommended. To erase completely the biological deterioration and the origin of decay, in addition to the change in E (both natural and artificial), it is important to act on the RH parameter. Its values, very close to saturation, can be reduced by applying an easy and cheap method. This consists in the positioning of a small ball of **expanded clay** or similar (changing them at necessary) on the floor. In this way, the high value of RH may be controlled. In order to facilitate the passage, a platform can be a good solution.

The reduction of CO_2 input during the day is easily obtainable with a **turnout control**, as the current system allows uncontrolled tourism. This fact derives because the "Casa di Diana" *Mithraeum* is subjected to guided tours only on Sunday (1 day per week), and so the guided tours are concentrated during such day. In addition to the official list, other people join without having booked the visit (taking advantage of the house is opened this day), and therefore their presence is not recorded. Another observation is that the crowd is concentrated in the first room (*pre-Mithraeum*) due to the inaccessibility of the Mitraic altar (an iron stepladder and a handrail are present at the centre of the two inter-communicating rooms). For this reason, the concentrations of CO_2 reach the highest values in that specific area. In this sense, a **turnout control** could consist in the reduction of the number of visitors per visit, forming smaller groups, reducing the CO_2 inputs, and

increasing the number of guided tours (to be carried out at least twice a week). In this sense, extending the guided tours, but performing them in a more organised and controlled way, could also result in an increase of the **usability** of the site, consequently increasing its "artistic value".

It is important to highlight that the elimination of the biological apparatus, acting directly on the parameters that regulate it, represents an alternative solution to HVAC (heating, ventilation and air conditioning) systems, more expensive and problem-free. Several studies discuss the role of these technical or other in historical buildings. Some works question the installation of these systems in particular cases [199-202], because, despite it being a common practice, HVAC systems modify indoor microclimatic conditions and create "microclimatic stress" for both the artefacts and the building, being an element foreign to the original building [199-202]. These critiques also involve the discussion of the concept of "historical climate". Indeed, their application on Goods' preservation is inadvisable. It makes no sense to speak of "optimal conditions" in this typology of buildings.
Nonetheless, the reduction of both CO_2 and RH has a direct consequence on the acidification of the water vapour [199-202] and, consequently, also on the carbonation phenomena.

Finally, the last point concerns the solution to the lack of air ventilation and the poor exchange of air, thanks to a system of air changing. It is necessary to check the results periodically, identifying and achieving the optimal conditions for the conservation of the materials.

Taking all of these into account, the pyramidal protocol structured, thanks to a solid analytical procedure, was fully developed (**Fig. 38**). Its final structure is the result of the initial hypothesis based on the "content and container" axiom (**Chapter 4 – Fig. 18**). **The final pyramid** shows all the actions (**analysis – Chapters 5-7**) developed based on the macroscopic observations (**anamnesis – Chapter 1.2**), until the final step (**conservation – Chapter 8**) is reached. All the actions are interconnected, proving that the basic relationship between the environment and the materials stored within it is the key to solve any scientific issue in the field of Cultural Heritage.

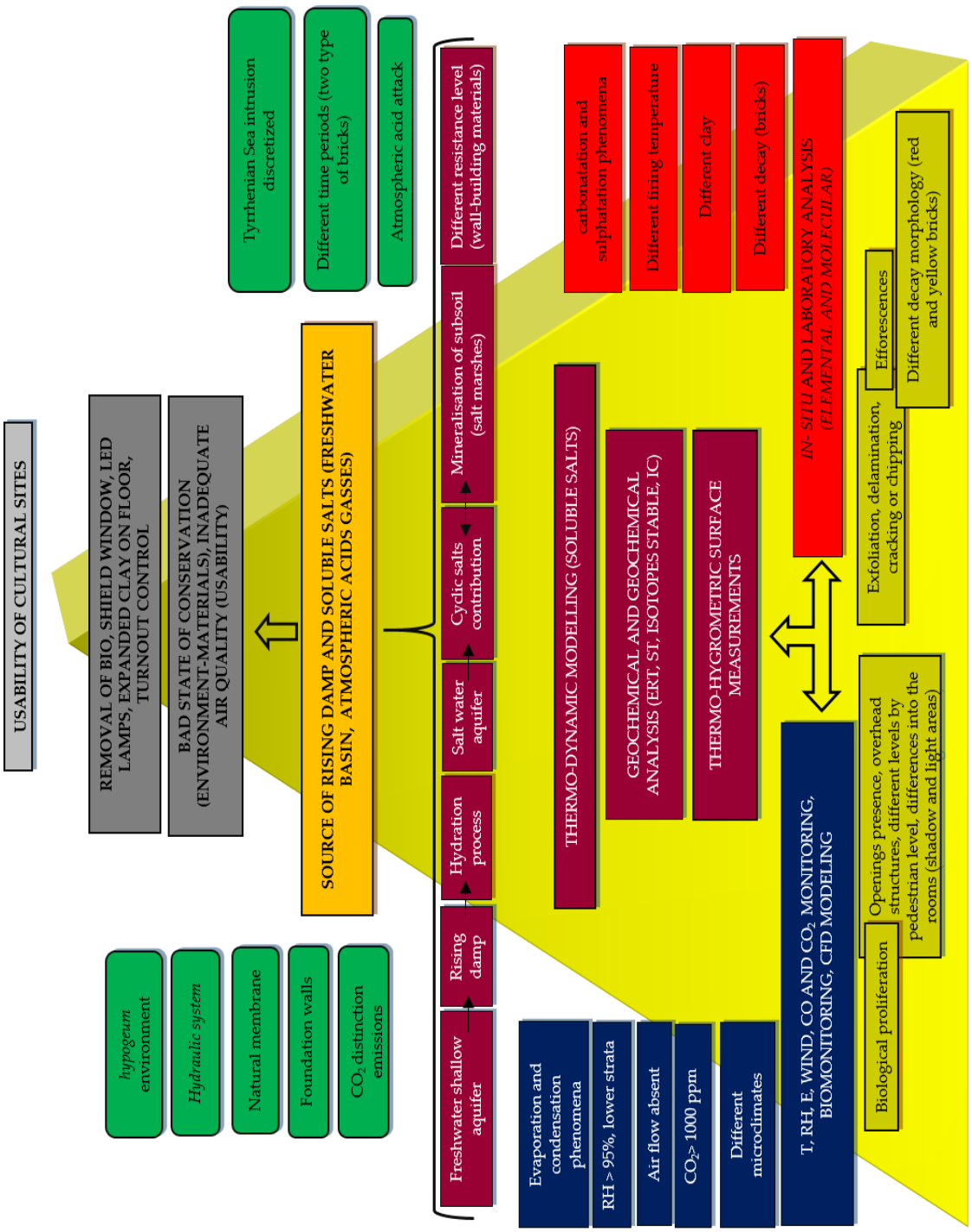

Figure 38. Schematic representation of the final diagnostic protocol.

Starting from the lowest level (yellow boxes), macroscopic observations represent a powerful tool to plan the successive actions (to focus the economic-instrumental resources), despite their obvious macroscopic character. Thus, on the base level of the pyramid, all the decay morphologies described in **Chapter 1.2** have been reported. Successively, on the first level there are the three spheres (the study of environment, materials and the interface between them, **Chapter 4 – Fig. 18**), which are the base of the pyramid's growth.
The blue boxes represent all the analyses (in capital letters) derived from the environmental characterisation and the obtained results (lower case letters). Contrarily, the red boxes represent all the analyses (in capital letters) derived by the analytical characterisation of the materials and the obtained results (lower case letters). The purple boxes (in capital letters) are the analyses carried out through physical and geophysical methods, applied in order to solve issues linked to the interaction between environment and materials, and the obtained results (lower case letters). As it has been observed, despite having been separated in the pyramid, the obtained results from these spheres are interconnected, giving the keys to identify the most important sources of damage (orange box). Thanks to it, it has been possible to define the conservation state of the "Casa di Diana" *Mithraeum* and to lay the "ad-hoc designing" for a conservative plan (grey boxes). Finally, the most important discoveries are also summarized in the pyramid (green circles).
Thus, the pyramid is now completed by the specific actions carried out during the procedure. Taking all of this into account, we consider that the objectives of this PhD work have been achieved.

Finally, it is important to underline that this diagnostic protocol can be adapted to other cultural heritage sites, such as open or closed museums. Many actions performed in this dissertation can be useful in other cultural sites or artefacts, as this investigation is related to all aspects of environmental science and engineering, technologies and integrated systems for high performance buildings, representing an improvement to preventive conservation.

Leaving aside the results, it is necessary to remark that although the different analysis done were conducted to achieve specific objectives and derived from different scientific areas, the information obtained in all of them was interconnected. Thus, the novelty of the protocol is essentially the multidisciplinary approach, the coordination and coherence of each survey and, finally, the demonstration of the usefulness of the multidisciplinary approach in the field of Cultural Heritage.

Chapter 9 Future works

Although the protocol was mostly completed taking into account the initial objectives, other aspects requiring consideration have appeared in the curse of this PhD work.

First of all, the air velocity study must be completed, in order to create a suitable model to complex terrains as archaeological sites. The measurements for the validation of the air turbulence method can be carried out also during days characterised by adverse meteorological conditions. In this sense, during the biomonitoring study, in these days (even if rare), the trend of the parameters (CO and CO_2) was subjected to a change (improving the AQ).

Secondly, a monitoring of the other acid gases' concentration should be carried out. In particular, on SO_2 and NOx, both found on the efflorescences, defining in this sense a full knowledge on the acid gases that attack the stone materials. Moreover, the evaluation of the gases coming from long-range transport would be recommended.

A study on the microbial volatile organic compounds (MVOCs) is also necessary. In this sense, microbial growth affects the whole building, not only the *Mithraeum*. Moreover, all the buildings of the studied archaeological site present this problem and mechanical removal action is impossible for the structures that are completely exposed to the outdoor environment. A possible connection to the formation of sulphate crusts and nitrate salts in stone monuments was attempted in the past for the presence of bacteria emitting sulphur and nitrogen based compounds.

Remaining on the topic of emissions, a further study on CO_2 is necessary. Indeed, one aspect to consider is the surface manifestation of CO_2-rich gases in the area surrounding the archaeological site (fumarole). Actually, in the coastal area of Fiumicino, leaks of natural gases (putting at risk the population) have manifested themselves for a long while [204]. Therefore, the high CO_2 concentration recorded could also be caused by this (as well as by the Fiumicino airport). In this sense a new project (Sapienza Ateneo, grant 2016) based on a combined study of geophysical techniques (ERT and IP – induced polarization) and geochemical analysis (CO_2 monitoring, isotopic analysis on water and soil samples) was proposed, in order to identify and reconstruct the natural gases' (CO_2 and CH_4) pocket geometry, redacting a map of the area affected.
Finally, following the hypothesis of the different historic periods of the bricks, a deeper study regarding them should be considered.

Chapter 10 Bibliography

1. Borges, C., A. Santos Silva, and R. Veiga. "Durability of ancient lime mortars in humid environment." *Construction and Building Materials* 66 (2014): 606-620.
2. Smith, Bernard J., and A. Turkington, eds. *Stone Decay: Its Causes and Controls*. Routledge, (2016).
3. Gallico, Sonia, and Maria Grazia Turco. "Il sito archeologico di Ostia Antica: tecniche costruttive, materiali, restauri." (2009).
4. Vittori, Cecile, Ilaria Mazzini, Ferréol Salomon, Jean-Philippe Goiran, Simona Pannuzi, Carlo Rosa, and Angelo Pellegrino. "Palaeoenvironmental evolution of the ancient lagoon of Ostia Antica (Tiber delta, Italy)." *Journal of Archaeological Science* 54 (2015): 374-384.
5. Marano, Federica, Federico Di Rita, Maria Rita Palombo, Neil Thomas William Ellwood, and Laura Bruno. "A first report of biodeterioration caused by cyanobacterial biofilms of exposed fossil bones: A case study of the middle Pleistocene site of La Polledrara di Cecanibbio (Rome, Italy)." *International Biodeterioration & Biodegradation* 106 (2016): 67-74.
6. Thorn, Andrew, and Valerie Magar. "An assessment of the condition of nine engraved sites in the Hong Kong Special Administrative Region." *Studies in Conservation* 61, no. sup1. (2016): 118-126.
7. Musei, Monumenti e Aree Archeologiche Statali. http://www.statistica.beniculturali.it/rilevazioni/musei/Anno%202014/MUSEI_TAVOLA8_2014.pdf
8. Gering, Axel. "Le ultime fasi della monumentalizzazione del centro di Ostia tardoantica. Attività della missione della Humboldt-Universität di Berlino tra il 2009 e il 2013." *Mélanges de l'École française de Rome-Antiquité* 126-1 (2014).
9. Scatigno, C., M. P. Sammartino, and S. Gaudenzi. "Non-invasive analysis of soluble salts." *Preliminary results on the case study of Casa di Diana Mithraeum (Achaeological site of Ostia Antica-Italy)* (2014).
10. Scatigno, C., and S. Ravera. "Characterisation of the biological proliferation on Roman masonry." *Case study: "Casa di Diana" Mithraeum (Ostia Antica, Rome–Italy)* (2015).
11. Adriaens, Annemie. "European actions to promote and coordinate the use of analytical techniques for cultural heritage studies." *TrAC Trends in Analytical Chemistry* 23, no. 8 (2004): 583-586.
12. García-Diego, Fernando-Juan, and Manuel Zarzo. "Microclimate monitoring by multivariate statistical control: The renaissance frescoes of the Cathedral of Valencia (Spain)." *Journal of Cultural Heritage* 11, no. 3 (2010): 339-344.
13. Merello, Paloma, Fernando-Juan García-Diego, and Manuel Zarzo. "Microclimate monitoring of Ariadne's house (Pompeii, Italy) for preventive conservation of fresco paintings." *Chemistry Central Journal* 6, no. 1 (2012): 1.

14. Bustamante, Eliseo, Enrique Guijarro, Fernando-Juan García-Diego, Sebastián Balasch, Antonio Hospitaler, and Antonio G. Torres. "Multisensor system for isotemporal measurements to assess indoor climatic conditions in poultry farms." *Sensors* 12, no. 5 (2012): 5752-5774.
15. De Donno, G., and E. Cardarelli. "A Flexible Interface for Tomographic Inversion of real and complex resistivity data in EIDORS." In *Near Surface Geoscience 2015-21st European Meeting of Environmental and Engineering Geophysics*. 2015.
16. Adler, Andy, and William RB Lionheart. "Uses and abuses of EIDORS: an extensible software base for EIT." *Physiological measurement* 27, no. 5 (2006): S25.
17. Cardarelli, Ettore, and Rita De Nardis. "Seismic refraction, isotropic anisotropic seismic tomography on an ancient monument (Antonino and Faustina temple AD 141)." *Geophysical Prospecting* 49, no. 2 (2001): 228-240.
18. Cardarelli, E., and A. Cerreto. "Staggered Grids as a Tool to Improve the Model Resolution in Seismic Tomography for Elliptical Anisotropic Media." In *Near Surface Geoscience 2015-21st European Meeting of Environmental and Engineering Geophysics*. 2015.
19. Fernández-Navajas, Ángel, Paloma Merello, Pedro Beltrán, and Fernando-Juan García-Diego. "Software for storage and management of microclimatic data for preventive conservation of cultural heritage." *Sensors* 13, no. 3 (2013): 2700-2718.
20. Epstein, Samuel, and Toshiko Mayeda. "Variation of O 18 content of waters from natural sources." *Geochimica et cosmochimica acta* 4, no. 5 (1953): 213-224.
21. McCrea, John Morden. "On the isotopic chemistry of carbonates and a paleotemperature scale." *The Journal of Chemical Physics* 18, no. 6 (1950): 849-857.
22. Aderohunmu, Femi A., Davide Brunelli, Jeremiah D. Deng, and Martin K. Purvis. "A data acquisition protocol for a reactive wireless sensor network monitoring application." *Sensors* 15, no. 5 (2015): 10221-10254.
23. Varas-Muriel, M. J., M. I. Martínez-Garrido, and R. Fort. "Monitoring the thermal–hygrometric conditions induced by traditional heating systems in a historic Spanish church (12th–16th C)." *Energy and Buildings* 75 (2014): 119-132.
24. Varas-Muriel, M. J., R. Fort, M. I. Martínez-Garrido, Ainara Zornoza-Indart, and Paula López-Arce. "Fluctuations in the indoor environment in Spanish rural churches and their effects on heritage conservation: Hygro-thermal and CO 2 conditions monitoring." *Building and Environment* 82 (2014): 97-109.
25. Merello Giménez, Paloma, María Del Carmen Pérez García, García Diego, Fernando Juan, Ángel Fernández Navajas, J. U. A. N. PÉREZ MIRALLES, José Luis Baró Zarzo et al. "Ariadne's house (Pompeii, Italy) wall paintings: A multidisciplinary study of its present state focused on a future restoration and preventive conservation." In *Materiales de Construcción*, vol. 63, no. 311, pp. 449-467. Consejo Superior de Investigaciones Científicas (CSIC), 2013.

26. Valero, Miguel Ángel, Paloma Merello, Ángel Fernández Navajas, and Fernando-Juan García-Diego. "Statistical Tools Applied in the Characterisation and Evaluation of a Thermo-Hygrometric Corrective Action Carried out at the Noheda Archaeological Site (Noheda, Spain)." *Sensors* 14, no. 1 (2014): 1665-1679.
27. Ramos, Luis F., Leandro Marques, Paulo B. Lourenço, Guido De Roeck, A. Campos-Costa, and J. Roque. "Monitoring historical masonry structures with operational modal analysis: two case studies." *Mechanical Systems and Signal Processing* 24, no. 5 (2010): 1291-1305.
28. Visco, Giovanni, Susanne Heidi Plattner, Patrizia Fortini, and Maria Pia Sammartino. "Second campaign of microclimate monitoring in the carcer tullianum: temporal and spatial correlation and gradients evidenced by multivariate analysis." *Chemistry Central Journal* 6, no. 1 (2012): 1.
29. Visco, Giovanni, Susanne Heidi Plattner, Patrizia Fortini, Serena Di Giovanni, and Maria Pia Sammartino. "Microclimate monitoring in the Carcer Tullianum: temporal and spatial correlation and gradients evidenced by multivariate analysis; first campaign." *Chemistry Central Journal* 6, no. 2 (2012): 1.
30. Maciejewska, Monika, Andrzej Szczurek, Grzegorz Sikora, and Agnieszka Wyłomańska. "Diffusive and subdiffusive dynamics of indoor microclimate: A time series modelling." *Physical Review E* 86, no. 3 (2012): 031128.
31. Thomas, Bertil, and Mohsen Soleimani-Mohseni. "Artificial neural network models for indoor temperature prediction: investigations in two buildings." *Neural Computing and Applications* 16, no. 1 (2007): 81-89.
32. Bertolin, Chiara, Dario Camuffo, and Isabella Bighignoli. "Past reconstruction and future forecast of domains of indoor relative humidity fluctuations calculated according to EN 15757: 2010." *Energy and Buildings* 102 (2015): 197-206.
33. Corgnati, Stefano Paolo, and Marco Perino. "CFD application to optimise the ventilation strategy of Senate Room at Palazzo Madama in Turin (Italy)." *Journal of Cultural Heritage* 14, no. 1 (2013): 62-69.
34. Balocco, Carla, Giuseppe Petrone, Oriana Maggi, Giovanna Pasquariello, Roberto Albertini, and Cesira Pasquarella. "Indoor microclimatic study for Cultural Heritage protection and preventive conservation in the Palatina Library." *Journal of Cultural Heritage* (2016).
35. Grau-Bové, Josep, Luca Mazzei, Liora Malkii-Ephstein, David Thickett, and Matija Strlič. "Simulation of particulate matter ingress, dispersion and deposition in a historical building." *Journal of Cultural Heritage* 18 (2016): 199-208.
36. D'Agostino, Delia, Paolo Maria Congedo, and Rosella Cataldo. "Ventilation control using computational fluid-dynamics (CFD) modelling for cultural buildings conservation." *Procedia Chemistry* 8 (2013): 83-91.
37. D'Agostino, Delia, and Paolo Maria Congedo. "CFD modelling and moisture dynamics implications of ventilation scenarios in historical buildings." *Building and Environment* 79 (2014): 181-193.

38. Nabizadeh Shahrebabak, Ebrahim, Soha Golafshan, and Mohammad R. Chamani. "Simulation of Air Flow through Skylight in Historical House, Case Study: Historic House of Mosavar-al-Molki." *Iran University of Science & Technology* 26, no. 1 (2016): 39-46.
39. Pagliaro, F., F. Nardecchia, F. Gugliermetti, and F. Bisegna. "CFD analysis for the validation of archaeological hypotheses–The indoor microclimate of ancient storage-rooms." *Journal of Archaeological Science* 73 (2016): 107-119.
40. Hussein, Ashraf S., and Hisham El-Shishiny. "Wind flow modelling and simulation over the Giza Plateau cultural heritage site in Egypt." *Journal on Computing and Cultural Heritage (JOCCH)* 2, no. 2 (2009): 6.
41. Hussein, Ashraf S., and Hisham El-Shishiny. "Influences of wind flow over heritage sites: A case study of the wind environment over the Giza Plateau in Egypt." *Environmental Modelling & Software* 24, no. 3 (2009): 389-410.
42. Hussein, Ashraf S., and Hisham El-Shishiny. "Modelling and simulation of low speed wind over the Great Sphinx." In *Computers and Communications, 2007. ISCC 2007. 12th IEEE Symposium on*, pp. 1027-1034. IEEE, 2007.
43. Flaga-Maryanczyk, Agnieszka, Jacek Schnotale, Jan Radon, and Krzysztof Was. "Experimental measurements and CFD simulation of a ground source heat exchanger operating at a cold climate for a passive house ventilation system." *Energy and buildings* 68 (2014): 562-570.
44. Xu, Guang, Kray D. Luxbacher, Saad Ragab, and Steve Schafrik. "Development of a remote analysis method for underground ventilation systems using tracer gas and CFD in a simplified laboratory apparatus." *Tunnelling and Underground Space Technology* 33 (2013): 1-11.
45. Version G 2.0 User's Guide (2001). FLUENT Inc
46. Allegrini, Jonas, Viktor Dorer, and Jan Carmeliet. "Analysis of convective heat transfer at building façades in street canyons and its influence on the predictions of space cooling demand in buildings." *Journal of wind engineering and industrial aerodynamics* 104 (2012): 464-473.
47. Crispim, C. A., and C. C. Gaylarde. "Cyanobacteria and biodeterioration of cultural heritage: a review." *Microbial ecology* 49, no. 1 (2005): 1-9.
48. Bhatnagar, Preeti, Abdul Arif Khan, Sudhir K. Jain, and M. K. Rai. ". Biodeterioration of Archaeological Monuments and Approach for Restoration." *Geomicrobiology* (2016): 255.
49. Salvadori, Ornella, and Annalaura C. Municchia. "The Role of Fungi and Lichens in the Biodeterioration of Stone Monuments." In *The Open Conference Proceedings Journal*, vol. 7, no. 1. 2016.
50. Caneva, G., O. Salvadori, S. Ricci, and S. Ceschin. "Ecological analysis and biodeterioration processes over time at the Hieroglyphic Stairway in the Copán (Honduras) archaeological site." *Plant Biosystems-An International Journal Dealing with all Aspects of Plant Biology* 139, no. 3 (2005): 295-310.

51. DeAraujo, Alice, Archana Vasanthakumar, Marcela Sepulveda, Vivien Standen, Bernardo Arriaza, and Ralph Mitchell. "Investigation of the recent microbial degradation of the skin of the Chinchorro mummies of Ancient Chile." *Journal of Cultural Heritage* (2016).
52. Tiano, Piero. "Biodeterioration of Stone Monuments a Worldwide Issue." In *The Open Conference Proceedings Journal*, vol. 7, no. 1. 2016.
53. Villa, Federica, Philip S. Stewart, Isaac Klapper, Judith M. Jacob, and Francesca Cappitelli. "Subaerial Biofilms on Outdoor Stone Monuments: Changing the Perspective toward an Ecological Framework." *BioScience* 66, no. 4 (2016): 285-294.
54. Zhang, Binsheng, Humayun Reza, Shiyan Gu, and Naren Gupta. "Investigations of physical and chemical characteristics of masonry stones and bricks during building cleaning: Part 1. Physical testing." *Journal of Physical Science and Application* 4, no. 4 (2014).
55. Zurakowska, Marta, and John J. Hughes. "Visual assessment of sandstone building façades: condition factors related to cleaning." *Quarterly Journal of Engineering Geology and Hydrogeology* 46, no. 4 (2013): 459-467.
56. Webster, R. G. M., C. A. Andrew, S. Baxter, J. MacDonald, M. Rocha, B. W. Thomson, K. H. Tonge, D. C. M. Urquhart, and M. E. Young. "Stone cleaning in Scotland-Research Report to Historic Scotland and Scottish Enterprise by Masonry Conservation Research Group." *Gilcomston Litho, Aberdeen* (1992).
57. May, Eric. "Microbes on building stone: for good or ill?." *Culture* 24, no. 2 (2003): 5-8.
58. Creer, Simon, Kristy Deiner, Serita Frey, Dorota Porazinska, Pierre Taberlet, W. Kelley Thomas, Caitlin Potter, and Holly M. Bik. "The ecologist's field guide to sequence-based identification of biodiversity." *Methods in Ecology and Evolution* (2016).
59. Green, Jessica L., Brendan JM Bohannan, and Rachel J. Whitaker. "Microbial biogeography: from taxonomy to traits." *Science* 320, no. 5879 (2008): 1039-1043.
60. Singh, Dhananjaya Pratap, Harikesh Bahadur Singh, and Ratna Prabha, eds. *Microbial Inoculants in Sustainable Agricultural Productivity: Vol. 1: Research Perspectives*. Springer, 2016.
61. Göthe, Emma, Allan Timmermann, Kathrin Januschke, and Annette Baattrup-Pedersen. "Structural and functional responses of floodplain vegetation to stream ecosystem restoration." *Hydrobiologia* 769, no. 1 (2016): 79-92.
62. Moropoulou, A., A. Bakolas, and S. Anagnostopoulou. "Composite materials in ancient structures." *Cement and concrete composites* 27, no. 2 (2005): 295-300.
63. Sandrolini, Franco, and Elisa Franzoni. "An operative protocol for reliable measurements of moisture in porous materials of ancient buildings." *Building and environment* 41, no. 10 (2006): 1372-1380.

65. Al-Homoud, Mohammad S. "Performance characteristics and practical applications of common building thermal insulation materials." *Building and environment* 40, no. 3 (2005): 353-366.
66. Korjenic, Azra, Vít Petránek, Jiří Zach, and Jitka Hroudová. "Development and performance evaluation of natural thermal-insulation materials composed of renewable resources." *Energy and Buildings* 43, no. 9 (2011): 2518-2523.
67. Singh, Manoj Kumar, Sadhan Mahapatra, and S. K. Atreya. "Thermal performance study and evaluation of comfort temperatures in vernacular buildings of North-East India." *Building and Environment* 45, no. 2 (2010): 320-329.
68. Woloszyn, Monika, Targo Kalamees, Marc Olivier Abadie, Marijke Steeman, and Angela Sasic Kalagasidis. "The effect of combining a relative-humidity-sensitive ventilation system with the moisture-buffering capacity of materials on indoor climate and energy efficiency of buildings." *Building and Environment* 44, no. 3 (2009): 515-524.
69. Valentino, Antonio, Adriana Bernardi, Nigel Blades, David Shooter, Kristin Gysels, Felix Deutsch, Monika Wieser, Oliver Kim, and Ursula Ulrych. "Environmental monitoring in four European museums."
70. European Committee for Standardisation (CEN) (2010) Conservation of cultural property – procedures and instruments for measuring temperatures of the air and the surface of objects.
71. European Committee for Standardisation (CEN) (2012) Conservation of cultural heritage – procedures and instruments for measuring humidity in the air and moisture exchanges between air and cultural property.
72. S Scatigno, C., N. Prieto-Taboada, M. Preite Martinez, A. M. Conte, F. J. García-Diego, and J. M. Madariaga. "Analitycal techniques for the characterisation of historical building materials: case study "Casa di Diana" Mithraeum (Archaeological site in Ostia Antica, Italy)." *Advances in Materials Science Research* (2016): 31.
73. Scatigno, C., S. Gaudenzi, M. P. Sammartino, and G. Visco. "A microclimate study on hypogea environments of ancient roman building." *Science of The Total Environment* 566 (2016): 298-305.
74. Scatigno, C., C. Moricca, C. Tortolini, and G. Favero. "The influence of environmental parameters in the biocolonization of the Mithraeum in the roman masonry of casa di Diana (Ostia Antica, Italy)." *Environmental Science and Pollution Research* (2016): 1-10.
75. Scatigno C, Cardarelli E, De Donno G, Oliveti I, Preite Martinez M (2015) Geophysics and geochemistry methodologies: application and techniques to structural evaluation of a roman masonry (archaeological site in Ostia Antica).
76. Cardarelli, E., G. De Donno, I. Oliveti, and C. Scatigno. "Assessing the State of Conservation of a Masonry Building through the Combined Use of Electrical and

Seismic Tomography." In *Near Surface Geoscience 2016-22nd European Meeting of Environmental and Engineering Geophysics*. 2016.
77. McGill, Robert, John W. Tukey, and Wayne A. Larsen. "Variations of box plots." *The American Statistician* 32, no. 1 (1978): 12-16.
78. Lai, Celine. "Archaeological museums and tourism in China: a case study of the Sanxingdui Museum." *Museum Management and Curatorship* 30, no. 1 (2015): 75-93.
79. Sousa, Vitor, Nuno Almeida, Ines Meireles, and Jorge de Brito. "Anomalies in wall renders: Overview of the main causes of degradation." *International Journal of Architectural Heritage* 5, no. 2 (2011): 198-218.
80. Larsen, Poul Klenz. "The salt decay of medieval bricks at a vault in Brarup Church, Denmark." *Environmental geology* 52, no. 2 (2007): 375-383.
81. Lourenço, Paulo B., Eduarda Luso, and Manuela G. Almeida. "Defects and moisture problems in buildings from historical city centers: a case study in Portugal." *Building and Environment* 41, no. 2 (2006): 223-234.
82. Charola, A. Elena. "Salts in the deterioration of porous materials: an overview." *Journal of the American institute for conservation* (2013).
83. Lubelli, Barbara, Rob PJ van Hees, and Caspar JWP Groot. "The role of sea salts in the occurrence of different damage mechanisms and decay patterns on brick masonry." *Construction and building materials* 18, no. 2 (2004): 119-124.
84. Hossain, Khandaker M. Anwar, Said M. Easa, and Mohamed Lachemi. "Evaluation of the effect of marine salts on urban built infrastructure." *Building and Environment* 44, no. 4 (2009): 713-722.
85. Morillas, Héctor, Maite Maguregui, Olivia Gómez-Laserna, Josu Trebolazabala, and Juan Manuel Madariaga. "Could marine aerosol contribute to deteriorate building materials from interior areas of lighthouses? An answer from the analytical chemistry point of view." *Journal of Raman Spectroscopy* 44, no. 12 (2013): 1700-1710.
86. Korkanç, Mustafa. "Deterioration of different stones used in historical buildings within Nigde province, Cappadocia." *Construction and Building Materials* 48 (2013): 789-803.
87. Korka, Elena, ed. *The Protection of Archaeological Heritage in Times of Economic Crisis*. Cambridge Scholars Publishing, 2015.
88. Gaffney, Chris. "Detecting trends in the prediction of the buried past: a review of geophysical techniques in archaeology." *Archaeometry* 50, no. 2 (2008): 313-336.
89. Goodman, Dean, and Salvatore Piro. *GPR remote sensing in archaeology*. Vol. 9. New York: Springer, 2013.
90. Sass, Oliver. "Rock moisture measurements: techniques, results, and implications for weathering." *Earth Surface Processes and Landforms* 30, no. 3 (2005): 359-374.

91. Mol, L., and P. R. Preston. "The writing's in the wall: a review of new preliminary applications of electrical resistivity tomography within archaeology." *Archaeometry* 52, no. 6 (2010): 1079-1095.
92. Polymenakos, L., S. Papamarinopoulos, A. Miltiadou, and N. Charkiolakis. "Investigation of the foundations of a Byzantine church by three-dimensional seismic tomography." *Journal of applied geophysics* 57, no. 2 (2005): 81-93.
93. Tsokas, Gregory N., Nectaria Diamanti, Panagiotis I. Tsourlos, George Vargemezis, Alexandros Stampolidis, and Konstantinos T. Raptis. "Geophysical prospection at the Hamza Bey (Alkazar) monument Thessaloniki, Greece." *Mediterranean Archaeology and Archaeometry* 13, no. 1 (2013): 9-20.
94. Capelli, Giuseppe, Roberto Mazza, and Claudio Papiccio. "Intrusione salina nel Delta del Fiume Tevere. Geologia, idrologia e idrogeologia del settore romano della piana costiera." *Giornale di Geologia Applicata* 5 (2007): 13-28.
95. Goiran, Jean-Philippe, Ferréol Salomon, Ilaria Mazzini, Jean-Paul Bravard, Elisa Pleuger, Cécile Vittori, Giulia Boetto et al. "Geoarchaeology confirms location of the ancient harbour basin of Ostia (Italy)." *Journal of Archaeological Science* 41 (2014): 389-398.
96. Cutnell, John D., and Kenneth W. Johnson. "Physics. 4th Edi-tion." (1998).
97. Ciotoli, Giancarlo, Giuseppe Etiope, Fabio Florindo, Fabrizio Marra, Livio Ruggiero, and Peter E. Sauer. "Sudden deep gas eruption nearby Rome's airport of Fiumicino." *Geophysical Research Letters* 40, no. 21 (2013): 5632-5636.
98. Gentilini, Cristina, Elisa Franzoni, Simone Bandini, and Lucio Nobile. "Effect of salt crystallisation on the shear behaviour of masonry walls: an experimental study." *Construction and Building Materials* 37 (2012): 181-189.
99. Gómez-Laserna, Olivia, María Ángeles Olazabal, Héctor Morillas, Nagore Prieto-Taboada, Irantzu Martinez-Arkarazo, Gorka Arana, and Juan Manuel Madariaga. "In-situ spectroscopic assessment of the conservation state of building materials from a Palace house affected by infiltration water." *Journal of Raman Spectroscopy* 44, no. 9 (2013): 1277-1284.
100. Laserna, O. Gómez, N. Prieto-Taboada, I. Ibarrondo, Irantzu Martínez Arkarazo, María Ángeles Olazabal Dueñas, and Juan Manuel Madariaga Mota. "Raman spectroscopic characterisation of brick and mortars: the advantages of the non-destructive and in situ analysis." In *Brick and mortar research*, pp. 195-213. 2011.
101. Laserna, O. Gómez, N. Prieto-Taboada, I. Ibarrondo, Irantzu Martínez Arkarazo, María Ángeles Olazabal Dueñas, and Juan Manuel Madariaga Mota. "Raman spectroscopic characterisation of brick and mortars: the advantages of the non-destructive and in situ analysis." In *Brick and mortar research*, pp. 195-213. 2011.
102. Bitossi, Giovanna, Rodorico Giorgi, Marcello Mauro, Barbara Salvadori, and Luigi Dei. "Spectroscopic techniques in cultural heritage conservation: a survey." *Applied Spectroscopy Reviews* 40, no. 3 (2005): 187-228.

103. Čtvrtníčková, Tereza, Luisa M. Cabalín, Javier Laserna, and Viktor Kanický. "Comparison of double-pulse and single-pulse laser-induced breakdown spectroscopy techniques in the analysis of powdered samples of silicate raw materials for the brick-and-tile industry." *Spectrochimica Acta Part B: Atomic Spectroscopy* 63, no. 1 (2008): 42-50.
104. Prieto-Taboada, Nagore, Olivia Gómez-Laserna, Irantzu Martinez-Arkarazo, María Ángeles Olazabal, and Juan Manuel Madariaga. "Relevance of Cross-Section Analysis in Correct Diagnosis of the State of Conservation of Building Materials as Evidenced by Spectroscopic Imaging." *Analytical chemistry* 85, no. 20 (2013): 9501-9507.
105. Morillas, Héctor, Maite Maguregui, Josu Trebolazabala, and Juan Manuel Madariaga. "Nature and origin of white efflorescence on bricks, artificial stones, and joint mortars of modern houses evaluated by portable Raman spectroscopy and laboratory analyses." *Spectrochimica Acta Part A: Molecular and Biomolecular Spectroscopy* 136 (2015): 1195-1203.
106. Sarmiento, A., M. Maguregui, I. Martinez-Arkarazo, M. Angulo, K. Castro, M. A. Olazábal, L. A´ Fernández et al. "Raman spectroscopy as a tool to diagnose the impacts of combustion and greenhouse acid gases on properties of Built Heritage." *Journal of Raman Spectroscopy* 39, no. 8 (2008): 1042-1049.
107. Prieto-Taboada, N., M. Maguregui, I. Martinez-Arkarazo, M. A. Olazabal, G. Arana, and J. M. Madariaga. "Spectroscopic evaluation of the environmental impact on black crusted modern mortars in urban–industrial areas." *Analytical and bioanalytical chemistry* 399, no. 9 (2011): 2949-2959.
108. Maguregui, M., A. Sarmiento, R. Escribano, I. Martinez-Arkarazo, K. Castro, and J. M. Madariaga. "Raman spectroscopy after accelerated ageing tests to assess the origin of some decayed products found in real historical bricks affected by urban polluted atmospheres." *Analytical and bioanalytical chemistry* 395, no. 7 (2009): 2119-2129.
109. Cardiano, Paola, Salvatore Ioppolo, Concetta De Stefano, Antonello Pettignano, Sergio Sergi, and Pasquale Piraino. "Study and characterisation of the ancient bricks of monastery of "San Filippo di Fragalà" in Frazzanò (Sicily)." *Analytica Chimica Acta* 519, no. 1 (2004): 103-111.
110. Stefanidou, M., I. Papayianni, and V. Pachta. "Analysis and characterisation of Roman and Byzantine fired bricks from Greece." *Materials and Structures* 48, no. 7 (2015): 2251-2260.
111. Stefanidou, M., I. Papayianni, and V. Pachta. "Analysis and characterisation of Roman and Byzantine fired bricks from Greece." *Materials and Structures* 48, no. 7 (2015): 2251-2260.
112. Miriello, Domenico, Donatella Barca, Andrea Bloise, Annamaria Ciarallo, Gino M. Crisci, Teresa De Rose, Caterina Gattuso, Flavia Gazineo, and Mauro F. La Russa. "Characterisation of archaeological mortars from Pompeii (Campania,

Italy) and identification of construction phases by compositional data analysis." *Journal of Archaeological Science* 37, no. 9 (2010): 2207-2223.
113. Calliari, Irene, Ernesto Canal, Silvia Cavazzoni, and Lorenzo Lazzarini. "Roman bricks from the Lagoon of Venice: a chemical characterisation with methods of multivariate analysis." *Journal of Cultural Heritage* 2, no. 1 (2001): 23-29.
114. Cultrone, Giuseppe, Eduardo Sebastián, Kerstin Elert, María José De la Torre, Olga Cazalla, and Carlos Rodriguez–Navarro. "Influence of mineralogy and firing temperature on the porosity of bricks." *Journal of the European Ceramic Society* 24, no. 3 (2004): 547-564.
115. Cultrone, Giuseppe, Inese Sidraba, and Eduardo Sebastián. "Mineralogical and physical characterisation of the bricks used in the construction of the "Triangul Bastion", Riga (Latvia)." *Applied Clay Science* 28, no. 1 (2005): 297-308.
116. Arrizabalaga, Iker, Olivia Gómez-Laserna, Julene Aramendia, Gorka Arana, and Juan Manuel Madariaga. "Applicability of a Diffuse Reflectance Infrared Fourier Transform handheld spectrometer to perform in situ analyses on Cultural Heritage materials." *Spectrochimica Acta Part A: Molecular and Biomolecular Spectroscopy* 129 (2014): 259-267.
117. Martínez-Arkarazo, I., D. C. Smith, O. Zuloaga, M. A. Olazabal, and J. M. Madariaga. "Evaluation of three different mobile Raman microscopes employed to study deteriorated civil building stones." *Journal of Raman Spectroscopy* 39, no. 8 (2008): 1018-1029.
118. Castro, K., M. Pérez-Alonso, M. D. Rodriguez-Laso, L. A´Fernández, and J. M. Madariaga. "Online FT-Raman and dispersive Raman spectra database of artists' materials (e-VISART database)." *Analytical and bioanalytical chemistry* 382, no. 2 (2005): 248-258.
119. Castro, Kepa, Benito Abalos, Irantzu Martínez-Arkarazo, Nestor Etxebarria, and Juan Manuel Madariaga. "Scientific examination of classic Spanish stamps with colour error, a non-invasive micro-Raman and micro-XRF approach: The King Alfonso XIII (1889–1901 "Pelón") 15 cents definitive issue." *Journal of Cultural Heritage* 9, no. 2 (2008): 189-195.
120. Pérez-Alonso, Maite, Kepa Castro, and Juan Manuel Madariaga. "Investigation of degradation mechanisms by portable Raman spectroscopy and thermodynamic speciation: The wall painting of Santa Maria de Lemoniz (Basque Country, North of Spain)." *Analytica chimica acta* 571, no. 1 (2006): 121-128.
121. Veneranda, Marco, Mireia Irazola, Marta Díez, Ane Iturregui, Julene Aramendia, Kepa Castro, and Juan Manuel Madariaga. "Raman spectroscopic study of the degradation of a middle age mural painting: the role of agricultural activities." *Journal of Raman Spectroscopy* 45, no. 11-12 (2014): 1110-1118.
122. Gómez-Laserna, Olivia, Iker Arrizabalaga, Nagore Prieto-Taboada, María Ángeles Olazabal, Gorka Arana, and Juan Manuel Madariaga. "In situ DRIFT, Raman, and XRF implementation in a multi-analytical methodology to diagnose

the impact suffered by built heritage in urban atmospheres." *Analytical and bioanalytical chemistry* 407, no. 19 (2015): 5635-5647.
123. Gómez-Laserna, Olivia, Iker Arrizabalaga, Nagore Prieto-Taboada, María Ángeles Olazabal, Gorka Arana, and Juan Manuel Madariaga. "In situ DRIFT, Raman, and XRF implementation in a multi-analytical methodology to diagnose the impact suffered by built heritage in urban atmospheres." *Analytical and bioanalytical chemistry* 407, no. 19 (2015): 5635-5647.
124. Pessanha, S., A. Guilherme, and M. L. Carvalho. "Comparison of matrix effects on portable and stationary XRF spectrometers for cultural heritage samples." *Applied Physics A* 97, no. 2 (2009): 497-505.
125. Morgenstein, Maury, and Carol A. Redmount. "Using portable energy dispersive X-ray fluorescence (ED-XRF) analysis for on-site study of ceramic sherds at El Hibeh, Egypt." *Journal of Archaeological Science* 32, no. 11 (2005): 1613-1623.
126. Smith, Gregory D., and Robin JH Clark. "Raman microscopy in archaeological science." *Journal of Archaeological Science* 31, no. 8 (2004): 1137-1160.
127. Klisińska-Kopacz, Anna. "Non-destructive characterisation of 17th century painted silk banner by the combined use of Raman and XRF portable systems." *Journal of Raman Spectroscopy* 46, no. 3 (2015): 317-321.
128. Prieto-Taboada, Nagore, Olivia Gómez-Laserna, Irantzu Martínez-Arkarazo, María Ángeles Olazabal, and Juan Manuel Madariaga. "Raman Spectra of the Different Phases in the CaSO4–H2O System." *Analytical chemistry* 86, no. 20 (2014): 10131-10137.
129. Janssens, Koen, and René Van Grieken, eds. *Non-destructive microanalysis of cultural heritage materials*. Vol. 42. Elsevier, 2004.
130. Pires, J., and A. J. Cruz. "Techniques of thermal analysis applied to the study of cultural heritage." *Journal of thermal analysis and calorimetry* 87, no. 2 (2007): 411-415.
131. Madariaga, Juan Manuel. "Analytical chemistry in the field of cultural heritage." *Analytical Methods* 7, no. 12 (2015): 4848-4876.
132. Moropoulou, Antonia, Kyriakos C. Labropoulos, Ekaterini T. Delegou, Maria Karoglou, and Asterios Bakolas. "Non-destructive techniques as a tool for the protection of built cultural heritage." *Construction and Building Materials* 48 (2013): 1222-1239.
133. Binda, L., and A. Saisi. "Non-destructive testing applied to historic buildings: The case of some Sicilian Churches." *Historical constructions. University of Minho, Guimarães* (2001).
134. Adriaens, Annemie. "Non-destructive analysis and testing of museum objects: an overview of 5 years of research." *Spectrochimica Acta Part B: Atomic Spectroscopy* 60, no. 12 (2005): 1503-1516.

135. Kandemir-Yucel, A., A. Tavukcuoglu, and E. N. Caner-Saltik. "In situ assessment of structural timber elements of a historic building by infrared thermography and ultrasonic velocity." *Infrared Physics & Technology* 49, no. 3 (2007): 243-248.
136. Papadopoulou, D. N., G. A. Zachariadis, A. N. Anthemidis, N. C. Tsirliganis, and J. A. Stratis. "Development and optimisation of a portable micro-XRF method for in situ multi-element analysis of ancient ceramics." *Talanta* 68, no. 5 (2006): 1692-1699.
137. Forster, Nicola, Peter Grave, Nancy Vickery, and Lisa Kealhofer. "Non-destructive analysis using PXRF: methodology and application to archaeological ceramics." *X-Ray Spectrometry* 40, no. 5 (2011): 389-398.
138. Gallello, Gianni, Shervin Ghorbani, Sharona Ghorbani, Agustin Pastor, and Miguel de la Guardia. "Non-destructive analytical methods to study the conservation state of Apadana Hall of Persepolis." *Science of The Total Environment* 544 (2016): 291-298.
139. Prieto-Taboada, N., I. Ibarrondo, O. Gómez-Laserna, I. Martinez-Arkarazo, M. A. Olazabal, and J. M. Madariaga. "Buildings as repositories of hazardous pollutants of anthropogenic origin." *Journal of hazardous materials* 248 (2013): 451-460.
140. Maguregui, M., A. Sarmiento, I. Martinez-Arkarazo, M. Angulo, K. Castro, G. Arana, N. Etxebarria, and J. M. Madariaga. "Analytical diagnosis methodology to evaluate nitrate impact on historical building materials." *Analytical and bioanalytical chemistry* 391, no. 4 (2008): 1361-1370.
141. Maguregui, Maite, Ulla Knuutinen, Kepa Castro, and Juan Maunel Madariaga. "Raman spectroscopy as a tool to diagnose the impact and conservation state of Pompeian second and fourth style wall paintings exposed to diverse environments (House of Marcus Lucretius)." *Journal of Raman Spectroscopy* 41, no. 11 (2010): 1400-1409.
142. Cardell, C., D. Benavente, and J. Rodríguez-Gordillo. "Weathering of limestone building material by mixed sulphate solutions. Characterisation of stone microstructure, reaction products and decay forms." *Materials characterisation* 59, no. 10 (2008): 1371-1385.
143. Akram, Kashif, Jae-Jun Ahn, and Joong-Ho Kwon. "Analytical methods for the identification of irradiated foods." *Ionizing radiation: Applications, sources and biological effects* (2012): 1-36.
144. Cardarelli, E., G. De Donno, C. Scatigno, I. Oliveti, M. Preite Martinez, and N. Prieto-Taboada. "Geophysical and geochemical techniques to assess the origin of rising damp of a roman building (Ostia Antica archaeological site)." *Microchemical Journal* (2016).

145. Vassilev, Stanislav V., and Juan MD Tascón. "Methods for characterisation of inorganic and mineral matter in coal: a critical overview." *Energy & Fuels* 17, no. 2 (2003): 271-281.
146. Iordanidis, A., J. Garcia-Guinea, and G. Karamitrou-Mentessidi. "Analytical study of ancient pottery from the archaeological site of Aiani, northern Greece." *Materials Characterisation* 60, no. 4 (2009): 292-302.
147. Serrano-Arnáez, B., J. M. Compana, and M. I. Fernández-García. "Chemical and mineralogical characterisation of Roman Sigillata moulds from Andújar (Jaén, Spain)." *Journal of Archaeological Science: Reports* 7 (2016): 60-70.
148. Ferreira, LF Vieira, M. Varela Gomes, M. F. C. Pereira, L. F. Santos, and I. Ferreira Machado. "A multi-technique study for the spectroscopic characterisation of the ceramics from Santa Maria do Castelo church (Torres Novas, Portugal)." *Journal of Archaeological Science: Reports* 6 (2016): 182-189.
149. Prati, S., I. Bonacini, G. Sciutto, A. Genty-Vincent, M. Cotte, M. Eveno, M. Menu, and R. Mazzeo. "ATR-FTIR microscopy in mapping mode for the study of verdigris and its secondary products." *Applied Physics A* 122, no. 1 (2016): 1-16.
150. La Nasa, Jacopo, Sibilla Orsini, Ilaria Degano, Antonio Rava, Francesca Modugno, and Maria Perla Colombini. "A chemical study of organic materials in three murals by Keith Haring: a comparison of painting techniques." *Microchemical Journal* 124 (2016): 940-948.
151. Warren, John. *Conservation of brick*. Butterworth Heinemann, 1999.
152. Peters, T. J. E. R. K., and R. Iberg. "Mineralogical changes during firing of calcium-rich brick clays." *Ceramic Bulletin* 57, no. 5 (1978): 503-509.
153. Imperi, E., S. De Bianchi, M. Guiso, M. P. Sammartino, A. M. Siani, A. Congiu, S. Stellino et al. "Studio multidisciplinare sui mitrei di Ostia Antica."
154. Perez-Alonso, Maite, Kepa Castro, and Juan M. Madariaga. "Vibrational spectroscopic techniques for the analysis of artefacts with historical, artistic and archaeological value." *Current Analytical Chemistry* 2, no. 1 (2006): 89-100.
155. Downs, R. T. "The RRUFF Project: an integrated study of the chemistry, crystallography, Raman and infrared spectroscopy of minerals." In *Program and abstracts of the 19th general meeting of the international mineralogical association in Kobe, Japan*, vol. 3. 2006.
156. Kornilov, A. V. "Reasons for the different effects of calcareous clays on strength properties of ceramics." *Glass and Ceramics* 62, no. 11-12 (2005): 391-393.
157. Fiori, C., D. Vitali, E. Camurri, B. Fabbri, and S. Gualtieri. "Archaeometrical study of Celtic ceramics from Monte Bibele (Bologna, Italy)." *Applied Clay Science* 53, no. 3 (2011): 454-465.
158. Negro Ponzi, M. M. "L'analisi delle murature come mezzo diagnostico negli scavi archeologici: contributo allo studio di laterizi e calce, in "." *Edilizia residenziale tra V e VIII secolo". 4 Seminario sul Tardoantico e l'Alto medioevo in Italia centrosettentrionale (Monte Barro-Galbiate, 2-4 settembre 1993)* (1994): 53-65.

159. Gómez-Nubla, L., J. Aramendia, S. Fdez-Ortiz de Vallejuelo, K. Castro, and J. M. Madariaga. "Relations Between Leachated Compounds and Raman Spectrum of Black Slags from EAF in Order to Characterize Them." *LPI Contributions* 1616 (2011): 36.
160. Hanaor, Dorian AH, and Charles C. Sorrell. "Review of the anatase to rutile phase transformation." *Journal of Materials science* 46.4 (2011): 855-874.
161. Cultrone, Giuseppe, Carlos Rodriguez-Navarro, Eduardo Sebastian, Olga Cazalla, and Maria Jose De La Torre. "Carbonate and silicate phase reactions during ceramic firing." *European Journal of Mineralogy* 13, no. 3 (2001): 621-634.
162 Riccardi, Maria P., Bruno Messiga, and P. Duminuco. "An approach to the dynamics of clay firing." *Applied Clay Science* 15, no. 3 (1999): 393-409.
163. Schwedt, A., H. Mommsen, N. Zacharias, and J. Buxeda I. Garrigós. "Analcime crystallization and compositional profiles - comparing approaches to detect post-depositional alterations in archaelogical pottery." *Archaeometry* 48, no. 2 (2006): 237-251.
164. KRBrz, RupH. "Symbols for rock-forming minerals." *American mineralogist*68 (1983): 277-279.
165. Karagiannis N, Karoglou M, Bakolas A, Moropoulou A Delgado, João MPQ, ed. *New Approaches to Building Pathology and Durability*. Vol. 6. Springer, 2016.
166. Quagliarini, Enrico, and Stefano Lenci. "The influence of natural stabilizers and natural fibres on the mechanical properties of ancient Roman adobe bricks." *Journal of Cultural Heritage* 11, no. 3 (2010): 309-314.
167. Mattingly, David J., and John Salmon, eds. *Economies beyond agriculture in the classical world*. Routledge, 2002.
168. Fernandes Francisco, M. "Ancient Clay Bricks: Manufacture and Properties/Francisco M. Fernandes, Paulo B. Lourenço, Fernando Castro Materials, Technologies and Practice in Historic Heritage Structures. Part 1." (2010): 29-48.
169. D'Agostino, Delia. "Moisture dynamics in an historical masonry structure: The Cathedral of Lecce (South Italy)." *Building and Environment* 63 (2013): 122-133.
170. Rirsch, Eric, and Zhongyi Zhang. "Rising damp in masonry walls and the importance of mortar properties." *Construction and Building Materials* 24, no. 10 (2010): 1815-1820.
171. Prieto-Taboada, N., O. Gómez-Laserna, I. Martinez-Arkarazo, M. A. Olazabal, and J. M. Madariaga. "Optimization of two methods based on ultrasound energy as alternative to European standards for soluble salts extraction from building materials." *Ultrasonics sonochemistry* 19, no. 6 (2012): 1260-1265.
172. Guerra, Edgardo Pinto. "Risanamento di murature umide e degradate." *Ed. Dario Flaccovio Editore* (2011): 123-126.
173. Charola, A. Elena, Josef Pühringer, and Michael Steiger. "Gypsum: a review of its role in the deterioration of building materials." *Environmental geology* 52, no. 2 (2007): 339-352.

174. Silva, A. Santos, T. Cruz, M. J. Paiva, A. Candeias, P. Adriano, N. Schiavon, and J. A. P. Mirão. "Mineralogical and chemical characterisation of historical mortars from military fortifications in Lisbon harbour (Portugal)." *Environmental Earth Sciences* 63, no. 7-8 (2011): 1641-1650.
175. Paiva, H., A. Velosa, R. Veiga, and V. M. Ferreira. "Effect of maturation time on the fresh and hardened properties of an air lime mortar." *Cement and Concrete Research* 40, no. 3 (2010): 447-451.
176. Technical committee CEN/TC 346 "Conservation of cultural heritage" (2014) EN 16455/2014: Conservation of cultural heritage - Extraction and determination of soluble salts in natural stone and related materials used in and from cultural heritage.
177. Franklin, B. J., J. F. Young, and R. Powell. "Testing of Sydney dimension sandstone for use in the conservation of heritage buildings." *Australian Journal of Earth Sciences* 61, no. 3 (2014): 351-362.
178. Skoog, Douglas A., James F. Holler, Stanley R. Crouch, and Luigia Sabbatini. *Chimica analitica strumentale*. EdiSES, 2009.
179. Alvarez de Buergo, M., P. Lopez-Arce, and R. Fort. "Ion chromatography to detect salts in stone structures and to assess salt removal methods." In *EGU General Assembly Conference Abstracts*, vol. 14, p. 1757. 2012.
180. Jungbauer, Alois. "Preparative chromatography of biomolecules." *Journal of Chromatography A* 639, no. 1 (1993): 3-16.
181. Haddad, Paul R., Peter E. Jackson, and G. M. Greenway. "Ion chromatography: principles and applications". (Journal of Chromatography Library, Vol. 46), Elsevier, Amsterdam. (1991): 321.
182. Franzoni, Elisa. "Rising damp removal from historical masonries: a still open challenge." *Construction and Building Materials* 54 (2014): 123-136.
183. Steiger, Michael. "Crystal growth in porous materials—I: The crystallization pressure of large crystals." *Journal of crystal growth* 282, no. 3 (2005): 455-469.
184. Crosta, Giovanni, Daniele Giordan, Jordi Corominas, Giorgio Lollino, Nicola Sciarra, Janusz Wasowski, and Rafig Azzam. *Engineering Geology for Society and Territory-Volume 2: Landslide Processes*. Springer, 2015.
185. Nicolai, Andreas. *Modelling and numerical simulation of salt transport and phase transitions in unsaturated porous building materials*. ProQuest, 2008.
186. Espinosa, R. M., L. Franke, and G. Deckelmann. "Model for the mechanical stress due to the salt crystallization in porous materials." *Construction and Building Materials* 22, no. 7 (2008): 1350-1367.
187. Espinosa-Marzal, Rosa M., and George W. Scherer. "Advances in understanding damage by salt crystallization." *Accounts of chemical research* 43, no. 6 (2010): 897-905.

188. Godts, Sebastiaan, Hilde De Clercq, Roald Hayen, and Judy De Roy. " Risk assessment and conservation strategy of a salt laden limestone mausoleum and the surrounding funeral chapel in Boussu, Belgium."(2012).
189. Aramendia, Julene, Leticia Gómez-Nubla, Kepa Castro, and Juan Manuel Madariaga. "Spectroscopic speciation and thermodynamic modelling to explain the degradation of weathering steel surfaces in SO_2 rich urban atmospheres." *Microchemical Journal* 115 (2014): 138-145.
190. Price, Clifford A. "Predicting environmental conditions to minimise salt damage at the Tower of London: a comparison of two approaches." *Environmental geology* 52, no. 2 (2007): 369-374.
191. Stelzner, Jörg, and Gerhard Eggert. "Calcium Carbonate on Bronze Finds." *Studies in conservation* 53, no. 4 (2008): 264-272.
192. Kubiak, Jan J., Premraj J. Khankhane, Pieter J. Kleingeld, and Ana T. Lima. "An attempt to electrically enhance phytoremediation of arsenic contaminated water." *Chemosphere* 87, no. 3 (2012): 259-264.
193. Bala'awi, Fadi, and Petros Prokos. "Salt mixtures phase equilibria: a tool of preventive conservation against salt weathering." *Journal of Faculty of Art, Ain Shams University* 39 (2011): 361-374.
194. García-Diego FJ, Scatigno C, Merello P. "Discrete and continuous monitoring to characterised the thermo-hygrometric state of wall-building materials in Ostia Antica archaeological site". (2016).
195. Bionda, D., and P. Storemyr. "Modelling the behaviour of salt mixtures in walls: a case study from Tenaille von Fersen." *The study of salt deterioration mechanisms. Decay of brick walls influenced by interior climate changes. Suomenlinnan hoitokunta, Helsinki* (2002): 95-101.
196. Price, Clifford. "An expert chemical model for determining the environmental conditions needed to prevent salt damage in historic porous materials." (2002): p-156.
197. Puigdomenech, Ignasi. "Hydra/Medusa chemical equilibrium database and plotting software." *KTH Royal Institute of Technology* (2004).
198. Chebotarev, I. I. "Metamorphism of natural waters in the crust of weathering—3." *Geochimica et Cosmochimica Acta* 8, no. 4 (1955): 198-212
199. Bencs, László, Zoya Spolnik, Dionne Limpens-Neilen, Henk L. Schellen, Bernhard AHG Jütte, and René Van Grieken. "Comparison of hot-air and low-radiant pew heating systems on the distribution and transport of gaseous air pollutants in the mountain church of Rocca Pietore from artwork conservation points of view." *Journal of Cultural Heritage* 8, no. 3 (2007): 264-271.
200. Bonazza, Alessandra, Palmira Messina, Cristina Sabbioni, Carlota M. Grossi, and Peter Brimblecombe. "Mapping the impact of climate change on surface recession of carbonate buildings in Europe." *Science of the total environment* 407, no. 6 (2009): 2039-2050.

201. Camuffo, Dario. *Microclimate for cultural heritage: Conservation, restoration, and maintenance of indoor and outdoor monuments*. Elsevier, 2013.
202. Vuerich, E., F. Malaspina, M. Barazutti, T. Georgiadis, and M. Nardino. "Indoor measurements of microclimate variables and ozone in the church of San Vincenzo (Monastery of Bassano Romano—Italy): A pilot study." *Microchemical Journal* 88, no. 2 (2008): 218-223.
203. Fabbri, Kristian, and Marco Pretelli. "Heritage buildings and historic microclimate without HVAC technology: Malatestiana Library in Cesena, Italy, UNESCO Memory of the World." *Energy and Buildings* 76 (2014): 15-31.
204. Sella, Pio, Andrea Billi, Ilaria Mazzini, Luigi De Filippis, Luca Pizzino, Alessandra Sciarra, and Fedora Quattrocchi. "A newly-emerged (August 2013) artificially-triggered fumarole near the Fiumicino airport, Rome, Italy." *Journal of volcanology and geothermal research* 280 (2014): 53-66.
205. Tans, P. P. "NOAA Earth System Research Laboratory, Global Monitoring Division." (2014).
206. UNI, EN. "13779. Ventilazione degli edifici non residenziali-Requisiti di prestazione per i sistemi di ventilazione e di climatizzazione." *Ente Nazionale Italiano di Unificazione, Milano* (2008).
207. UNI, EN. "15251. Criteri per la progettazione dell'ambiente interno e per la valutazione della prestazione energetica degli edifici, in relazione alla qualità dell'aria interna, all'ambiente termico, all'illuminazione e all'acustica." *Ente Nazionale Italiano di Unificazione, Milano* (2008).
208. Heinzow, Birger, and Helmut Sagunski. "Evaluation of Indoor Air Contamination by Means of Reference and Guide Values: The German Approach." *Organic Indoor Air Pollutants: Occurrence, Measurement, Evaluation* 9 (2009): 1.
209. Kalamees, Targo, J. Kurnitski, J. Jokisalo, L. Eskola, K. Jokiranta, and J. Vinha. "Measured and simulated air pressure conditions in Finnish residential buildings." *Building Services Engineering Research and Technology* (2010).
210. Snow, Frank J. "American Society of Heating, Refrigeration, Air Conditioning Engineers (ASHRAE) Thermographic Standard 101 P." In *Thermal Infrared Sensing Applied to Energy Conservation in Building Envelopes*, pp. 94-98. International Society for Optics and Photonics, 1982.

ANNEX 1 - Index of Figures

ANNEX 2 - Index of Tables

ANNEX 3 - List of abbreviations and Symbols

3D	Three Dimensional
AQ	Air quality (connected with its parameters like CO and CO_2)
ASHRAE	American Society of Heating, Refrigerating, and Air Conditioning Engineers
BC	Boundary Conditions
BSE	Back-scattered-electron images
CAD	Computer-aided design
CFD	Computational Fluid Dynamics
CO	Carbon oxide
CO_2	Carbon dioxide
E	Illuminance
ECOS	Environmental Control of Salts
EDS	Energy Dispersive X-ray
ERT	Electrical Resistivity Tomography
FEM	Finite Element Method
GAMBIT	Geometry and Mesh Building Intelligent Toolkit
LTI	Linear travel time interpolation
MiBACT	Ministero Beni e Attività culturali e del Turismo
NDIR	Non-Dispersive Infrared Technology
NTC	Negative temperature coefficient
P	Pressure
PDB	Pee Dee Belemnite
PLM	Petrographic Polarizing Microscope
Qa	Air flow

RANS	Reynolds Averaged Navier-Stokes
RH	Relative humidity
RHCond	Relative humidity measured by conductive method
RHRF	Relative humidity measured by radio frequency method
SEM	Scanning Electron Microscope
ST	Seismic tomography
Ta	Air Temperature
Tc	contact temperature
T_{dm}/ RH_{dm}	Average daily temperature/relative humidity
TIR	Infrared ray temperature
T_{min}/T_{max}	Minimum and maximum temperature
Ts	superficial temperature
V&V	Verification and validation
Va	Air velocities
VEMI	Versatile interface for Electrical Modelling and Inversion
WSN	Wireless sensor network
XRD	X-Ray Diffraction
XRF	X-ray Fluorescence
ΔP	Differential pressure
μ-EDXRF	micro-Energy Dispersive X-ray fluorescence

ANNEX 4 - Glossary

A

Anamnesis

Recollection, especially of a supposed previous existence.

Aquiclude

An impermeable body of rock or stratum of sediment that acts as a barrier to the flow of water.

C

Castrum (pl. *castra*)

A Roman fortified camp, rectangular in plan, and standardized throughout the Empire. It had two main thoroughfares at right angles, the *cardo maximus* and *via decumana*, each of which joined two gates set in towers with walls and towers around the whole. An old Roman fortress. Ostia may have been Rome's first *colonia*. According to the legend, Ancus Marcius, the semi-legendary fourth king of Rome, first destroyed Ficana, an ancient town that was only 17 km (11 mi) from Rome and had a small harbour on the Tiber, and then proceeded with establishing the new colony 10 km (6 mi) further west and closer to the sea coast. An inscription seems to confirm the establishment of the old *castrum* of Ostia in the 7th century BCE. The oldest archaeological remains discovered so far date back only to the 4th century BCE. The most ancient building currently visible are from the 3rd century BCE, notably the *Castrum* (military camp); of a slightly later date is the *Capitolium* (temple of Jupiter, Juno and Minerva). The *opus quadratum* of the walls of the original *castrum* at Ostia provides important evidence for the building techniques that were employed in the Roman urbanization during the period of the Middle Republic.

D

Dolium (pl. *dolia*)

A large earthenware vase or container used in ancient Roman times for the storage or transportation of goods.

Domus

A large single-family residence. However, the two kinds of housing were intermingled in the city and not segregated into separate neighbourhoods. The

ground-level floor of the *insula* was used for *tabernae*, shops and businesses, with living space upstairs. Like modern apartment buildings, an *insula* might have a name, usually referring to the owner of the building.

H

Hypogeum (pl. *Hypogea*)

An underground room simulating a cave, used for mithraic rites (as initiations).

Holocene

A geological epoch relating to or denoting the present epoch, which is the second epoch in the Quaternary period, followed the Pleistocene, at approximately 9.700 BCE.

Horreum (pl. *Horrea*)

A type of public warehouse used during the ancient Roman period. Although the Latin term is often used to refer to granaries, Roman horrea were used to store many other types of consumables. The horrea of Rome and its port, Ostia, stood two or more stories high. They were built with ramps, rather than staircases, to provide easy access to the upper floors. Grain horrea had their ground floor raised on pillars to reduce the likelihood of damp getting in and spoiling the goods. Many horrea appear to have served as great trading areas with rows of small shops (*tabernae*) off a central courtyard; some may have been fairly elaborate, perhaps serving as the equivalent of modern shopping arcades. Others, such as those in Ostia, dispensed with the courtyard and instead had rows of *tabernae* standing back-to-back. In the Middle East, horrea took a very different design with a single row of very deep *tabernae*, all opening onto the same side; this reflects an architectural style that was widely followed in the region's palaces and temple complexes, well before the arrival of the Romans. A particularly well-preserved horreum in Ostia, the Horrea Epagathiana et Epaphroditiana, is known from an inscription to have been named after two freedmen (presumably its owners), Epagathus and Epaphroditus.

I

Insula

In architecture, a kind of apartment building that housed most of the urban citizen population of ancient Rome, including ordinary people of lower- or middle-class status (the *plebs*) and all but the wealthiest from the upper-middle class (the *equites*). The term was also used to intend a city block.

L

Latrina

A toilet or a simpler facility that was used as a toilet within a sanitation system. It is often found passing through the principal entrance of a Roman masonry.

M

Mithraeum (pl. *Mithraea*)

A place dedicated to the cult of the Persian god Mithra during Roman times.

O

Opus caementicium

Roman concrete, also called *opus caementicium*, based on a hydraulic-setting cement, was a material used in construction during the late Roman Republic until the fading of the Roman Empire. It consists of an aggregate and hydraulic mortar – a binder mixed with water that hardens over time. The aggregate varied, and included pieces of rock, ceramic tiles, and brick rubble from the remains of previously demolished buildings. Reinforcing elements, such as steel rebar, were not used. Gypsum and lime were used as binders. Volcanic dusts, called pozzolana or "pit sand", were favoured where they could be obtained. Pozzolana makes the concrete more resistant to salt water in comparison to modern-day concrete. The pozzolanic mortar used had a high content of alumina and silica.
Concrete and, in particular, the hydraulic mortar responsible for its cohesion, was a type of structural ceramic whose utility derived largely from its rheological plasticity in the paste state. The setting and hardening of hydraulic cements derived from the hydration of materials and the subsequent chemical and physical interaction of these hydration products. This differed from the setting of slaked lime mortars, the most common cements of the pre-Roman world. Once set, Roman concrete exhibited little plasticity, although it retained some resistance to tensile stresses.
The setting of pozzolanic cements has a lot in common with the setting of their modern counterpart, Portland cement. The high silica composition of Roman pozzolana cements is very close to that of modern cement, to which blast furnace slag, fly ash, or silica fume have been added.
Vitruvius distinguished the types of aggregate appropriate for the preparation of lime mortars in his work "Ten Books on Architecture", written around 25 BCE. For structural mortars, he recommended *pozzolana*, which are volcanic sands from sand-like beds of Pozzuoli, brownish-yellow-grey in colour near Naples and

reddish-brown at Rome. Vitruvius specifies a ratio of 1-part lime to 3 parts pozzolana for cements used in buildings and a 1:2 ratio of lime to *pulvis Puteolanus* for underwater work, essentially the same ratio applied today for concrete used at sea. By the middle of the 1st century, the principles of underwater construction in concrete were well-known to Roman builders. The city of Caesarea was the earliest known example to have made use of underwater Roman concrete technology on such a large scale. The new building code by Nero, used for the rebuilding of Rome after the fire in 64 CE, which destroyed large portions of the city, consisted of largely brick-faced concrete. This appears to have encouraged the development of the brick and concrete industries.

P

Pre-Mithraeum

A personal simplification adopted to distinguish it from the *Mithraeum* room.

Podium (pl. *Podiae*)

Seats for the Romans that assisted the sacrificial ritual of the killing the bull.

Paleo-lagoon

A body of water cut off from the open sea by coral reefs or sand bars. The suffix indicates the reference to the paleo environment.

Plio-pleistocenic (deposits)

The Pliocene and Pleistocene epochs, or the system of rocks deposited during them.

T

Taberna (pl. *Tabernae)*

A single room shop covered by a barrel vault within great indoor markets of ancient Rome. Each *taberna* had a window above it to let light into a wooden attic for storage and had a wide doorway.

Triclinium (pl. *Triclinia*)

A formal dining room in a Roman building. Dining was the defining ritual in Roman domestic life, lasting from late afternoon until late at night. Typically, 9-20 guests were invited, arranged in a prescribed seating order to emphasize divisions in status and relative closeness to the *dominus* (the owner). As static, privileged

spaces, dining rooms received extremely elaborate decoration, with complex perspective scenes and central paintings (or, in this case, mosaics). Dionysus, Venus, and still lives of food were popular, for obvious reasons. Middle class and elite Roman houses usually had at least two *triclinia*; it is not unusual to find four or more. Here, the *triclinium maius* (big dining room) would be used for larger dinner parties, which would typically include many clients of the owner.

U

Usability

A legally recognised concept (Cultural Heritage and Landscape Code – Title II), the usability or enjoyment is the reason of being of the protection; it identifies, protects, and preserves the Cultural Heritage so that it can be offered to knowledge and collective enjoyment. Therefore, use precedes valorisation, which it as the increase of the conservation state and the knowledge of the artefact for public use, and is normally applied to a good that it already safeguarded, meaning that it is already usable. Fruition, on one hand, is a public purpose (the enjoyment of the cultural value of an artefact), on the other hand, it is a set of material and juridical activities necessary for the accomplishment of such aim.

ANNEX 5 - National and International Congresses

- ✓ 5th CMA4CH Mediterranean Meeting. Employ the Multivariate Analysis and Chemometrics in Cultural Heritage and Environment Fields. Scatigno, C., M. P. Sammartino, and S. Gaudenzi. *Preliminary results on the case study of Casa di Diana Mithraeum (Archaeological site of Ostia Antica-Italy)* (2014).
- ✓ 18thNational Congress SLI (Italian Society of Lichens). Scatigno, C., and S. Ravera. *Characterisation of the biological proliferation on Roman masonry. Case study: "Casa di Diana" Mithraeum (Ostia Antica, Rome–Italy)* (2015).
- ✓ National Congress Geositi, Geomorfositi e Geoarcheositi patrimonio geologico-ambientale del Mediterraneo, Società Italiana di Geologia Ambientale (SIGEA). *Metodologie geofisiche e geochimiche: applicazione e tecniche per la valutazione strutturale di una casa romana (sito archeologico in Ostia Antica)* (2015);
- ✓ 8th International Congress on Archaeology, Computer Graphics, Cultural Heritage and Innovation. Arqueològica 2.0. *Preliminary data of CFD modelling to assess the ventilation in an archaeological building* (2016); *Discrete and continuous monitoring to characterise The thermo-hygrometric state of wall-building materials in Ostia Antica archaeological site* (2016);
- ✓ 22nd European Meeting of Environmental and Engineering Geophysics. Session: Archaeological Prospecting II. Near Surface Geoscience 2016. *Assessing the state of conservation of a masonry building through the combined used of electrical and seismic tomography* (2016);

ANNEX 6 - Publications

CHAPTER PUBLISHED

- ✓ Scatigno, C., N. Prieto-Taboada, M. Preite Martinez, A. M. Conte, F. J. García-Diego, and J. M. Madariaga. "Analitycal techniques for the characterisation of historical building materials: case study "Casa di Diana" *Mithraeum* (Archaeological site in Ostia Antica, Italy)." *Advances in Materials Science Research* (2016): 31.

RESEARCH PAPER

Published

- ✓ Scatigno, C., S. Gaudenzi, M. P. Sammartino, and G. Visco. "A microclimate study on hypogea environments of ancient roman building. *"Science of The Total Environment* 566 (2016): 298-305.
- ✓ Cardarelli, E., G. De Donno, C. Scatigno, I. Oliveti, M. Preite Martinez, and N. Prieto-Taboada. "Geophysical and geochemical techniques to assess the origin of rising damp of a roman building (Ostia Antica archaeological site)."*Microchemical Journal* (2016).
- ✓ Cardarelli, E., G. De Donno, I. Oliveti, and C. Scatigno. "Assessing the State of Conservation of a Masonry Building through the Combined Use of Electrical and Seismic Tomography." In *Near Surface Geoscience 2016-22nd European Meeting of Environmental and Engineering Geophysics*. 2016.
- ✓ Scatigno, C., C. Moricca, C. Tortolini, and G. Favero. "The influence of environmental parameters in the biocolonization of the Mithraeum in the roman masonry of casa di Diana (Ostia Antica, Italy)."*Environmental Science and Pollution Research* (2016): 1-10.
- ✓ Imperi, E., S. De Bianchi, M. Guiso, M. P. Sammartino, A. M. Siani, A. Congiu, S. Stellino et al. "Studio multidisciplinare sui mitrei di Ostia Antica."; *SIA Società Italiana di Archeoastronomia* (2014): 200-217.

Under review

- ✓ Scatigno, C., N. Prieto-Taboada, J. M. Madariaga **"**Quantitative characterisation and thermodynamic modelling of soluble salts on Roman bricks as a tool to discriminate the origin of their formation". Article under review in *Environmental Science and Pollution Research*. Ms. Ref. No.: ESPR-D-16-04938.
- ✓ Scatigno, C., N. Prieto-Taboada, J. M. Madariaga, M. Preite Martinez, A. M. Conte. "A non-destructive spectroscopic study to evaluate the technological differences and conservation state of two types of Roman coloured bricks". Article submitted to *MicroChemical Journal*. Ms. Rif. MICROC-2016-321.
- ✓ Scatigno, C., F. J. García-Diego, P. Merello. "Evaporation and condensation phenomena on roman wall-building of a *hypogeum* environment by a discrete

monitoring". Article submitted to *Construction and Building Materials*. Ms. Ref. No.: CONBUILDMAT-D-16-03967.

- ✓ Cardarelli, E., G. De Donno, I. Oliveti, and C. Scatigno. "Three-dimensional reconstruction of a masonry building through electrical and seismic tomography integrated by biological and environmental studies". Article submitted to *Near Surface Geophysic*s. Ms. Ref. No.: NSG-2016-1458.
- ✓ Scatigno, C., N. Prieto-Taboada, C. García-Florentino, S. Fdez-Ortiz de Vallejuelo, M. Maguregui, J. M. Madariaga. "Combination of *in-situ* spectroscopy and chemometric techniques to discriminate different types of roman bricks and the influence of microclimate environment"**.** Article submitted to Analytical and Bioanalytical Chemistry. Ms. Ref. No.: ABC-00005-2017.
- ✓ Scatigno, C., A. M. Conte, M. Preite Martinez, N. Prieto-Taboada, J. M. Madariaga. "Petrographic-mineralogical characterisation of stone materials from a *Mithraeum* building sited in an open museum"**.** Article submitted to Applied Clay Science. Ms. Ref. No.: CLAY-S-17-00047.

SAPIENZA
UNIVERSITÀ DI ROMA

Universidad del País Vasco
Euskal Herriko Unibertsitatea

Rome (Italy), February 2017